UNIVERSITEIT
GENT

Een ab initio studie naar de invloed van laag-energetische modes op moleculaire partitiefuncties en afgeleide grootheden

Influence of low vibrational modes on molecular partition functions and derived quantities from first principles

Peter Vansteenkiste

Promotoren: Prof. Dr. M. Waroquier
Dr. Ir. V. Van Speybroeck

Proefschrift ingediend tot het behalen van de graad van
Doctor in de Ingenieurswetenschappen

Academiejaar 2005-2006

Vooraf

Voor vele mensen is het afwerken van een doktoraatsthesis het eindpunt, en sluit het een periode van hun leven af. Niet voor mij! Ik zie het eerder als een bewijs van mijn kapaciteiten als onderzoeker, maar ook als mens. Jarenlang –tijdens mijn studies dus– liet ik mij leiden door het nastreven van snel en vluchtig plezier. Voor de mensen die mij niet kenden in die periode: laat uw fantasie niet op hol slaan, voor mij was dat plezier hetzelfde als kaarten, of meer algemeen, spellekes spelen. Het was een tijd zonder zorgen, maar ook zonder ambitie, zonder doel. Ondanks alles zijn mijn ouders (allemaal) mij blijven steunen, mijn moeder voorop.

Het keerpunt is er gekomen door de ontmoeting met een zeer speciaal madameke, tegenwoordig mijn vrouw. Het klinkt misschien als een cliché, maar door haar heb ik ingezien dat er meer bestaat dan gewoon maar plezier maken, namelijk simpelweg gelukkig zijn. En dat is een sterk verslavend gevoel. Het deed mij zoeken naar alles wat mij gelukkig zou kunnen maken bovenop mijn fantastische relatie met *Honeybaby*. Dit streven vorgde ervoor dat ik mijn echte passie kon ontdekken: toegepaste fysika. Altijd al was ik geïnteresseerd in hoe de wereld ineen zit, en hoe ik die zou kunnen beschrijven en manipuleren, maar mijn luiheid hield mij tegen om er dieper op in te gaan. Nu was ik echter bereid om er wat moeite voor te doen, en kon ik dus beginnen genieten van opbrengsten ervan: een begin aan inzicht in bepaalde delen van de fysica.
En plots studeerde ik af...

... en toen was er Prof. Michel Waroquier. Samen met Veronique Van Speybroeck gaf hij mij de kans om mij verder te ontplooien. Tot vandaag weet ik niet waarom ze toen beslist hebben mij op te nemen in hun onderzoeksgroep. Was ik niet iemand die pas na negen jaar door zijn vijf-jarige studies is gesukkeld? Hoe het ook zij, ik ben hen enorm veel verschuldigd. Ik laat het aan de lezer over om na het lezen van deze thesis te beslissen of ik hen hiermee de eer heb aangedaan die ze verdienen. In mijn ogen is het een verslag van het begin van mijn echte leven, en ik hoop dat iedereen er de passie in zal terugvinden die ik voor deze onderzoeksbranche heb.

Weet wel dat niet alleen bovenvermelde mensen een rol hebben gespeeld in het tot stand komen van deze thesis. Al mijn kollega's verdienen een welgemeende 'dank u wel', met een paar hoofdrolspelers in het bijzonder, elk met hun eigen rol. Die rol varieert van het bezorgen van zielerust (Karen H.), het oplossen van computerperikelen (Ewald, Toon), de wiskundige ondersteuning (Dimitri) tot het zorgen voor wetenschappelijke inspiratie en leiding (Veronique, Michel).

Buiten het werk zijn er natuurlijk de usual suspects (familie) die met z'n allen schuldig zijn bevonden aan het jarenlang geven van motivatie, kansen en veel liefde. Ondanks zijn prille leeftijd is Gerbrecht hierin koploper. De meeste mensen zien een lief ventje, terwijl hij voor mij in de eerste plaats een bundeltje geluk is.

Contents

List of Tables

List of Figures

Chapter 1

Nederlandstalige samenvatting

Doel van de thesis

Het onderzoek verricht in het kader van dit doctoraatswerk situeert zich binnen het domein van de moleculaire modellering en meer specifiek "ab-initio" modellering van fysische en chemische eigenschappen van moleculaire systemen. Centrale grootheid in deze thesis vormt de totale moleculaire partitiefunctie. Deze grootheid laat toe macroscopiche eigenschappen te bepalen die experimenteel toegankelijk zijn en dus een maat zijn voor de validatie van de bekomen partitiefunctie.

Het grootste deel van deze thesis is gewijd aan modelontwikkeling voor een accurate beschrijving van flexibele moleculen, meer specifiek van de interne modes met grote amplitude. Met flexibiliteit bedoelt men dat delen van de molecule zich min of meer gemakkelijk kunnen vervormen. Voor de meer rigide moleculen is de standaardprocedure gebaseerd op een beschrijving van de interne vibraties in de 'Harmonische Oscillator' benadering (HO). Deze methode is heel eenvoudig, en standaard geïmplementeerd in alle ab-initio software pakketten, maar genereert vele onnauwkeurigheden indien ze wordt toegepast op flexibele moleculen. Ze gaat er namelijk van uit dat de molecule slechts als één conformeer ($\equiv$ lokaal energie-minimum) voorkomt.

Sommige interne bewegingen in flexibele moleculen corresponderen niet met vibraties maar met interne rotaties (IR). Onder interne rotatie bedoelt men de relatieve rotatie van twee delen van de molecule rond een (enkelvoudige) binding. In tegenstelling tot vibraties, zorgen IR's ervoor dat de molecule zich kan vervormen, waardoor verschillende conformeren toegankelijk worden.
Na berekening van het vibrationeel spectrum van de molecule kunnen een aantal laag-energetische modes als een interne rotatie geïdentificeerd worden. Het is evident dat de Harmonische Oscillator benadering geen goede benadering is waanneer zulke IR's aanwezig zijn. Het is essentieel dat de invloed van alle mogelijke conformeren in acht wordt genomen, wat enkel mogelijk is door een correcte beschrijving van de interne rotaties.
Er zijn een aantal zulke methoden voorhanden in de literatuur die allen kunnen worden gecatalogeerd onder de noemer 'Hindered Rotor' (HR) aangezien ze gebaseerd zijn op hetzelfde basisidee [1]. Wezenlijk verschillen ze niet veel van elkaar.
Een eerste consequente implementering van zowel de kwantummechanische als klassieke HR-benadering is uitgewerkt in onze groep door Veronique Van Speybroeck [2, 3]. Het initieel model in deze thesis (1D-HR) is daarop gebaseerd.

Het uiteindelijke doel van dit onderzoek is het vinden van een algemene methode die de interne bewegingen en flexibiliteit van de molecule beschrijft, alsmede de overeenkomende moleculaire partitiefunctie zo nauwkeurig mogelijk bepaalt.

Deze Nederlandstalige samenvatting tracht enkel het globale beeld van het verloop van het onderzoek weer te geven, zonder in detail te treden. Voor een meer diepgaande bespreking wordt telkens verwezen naar de overeenkomstige hoofdstukken die de weergave zijn van de gepubliceerde werken: dit doctoraatswerk heeft geleid tot een zevental A1 publicaties (appendix B), en tot de ontwikkeling van het software programma 'HRpublic' dat vrij ter beschikking wordt gesteld voor academische onderzoeksgroepen. Het kan aangevraagd worden via de website van de CMM onderzoeksgroep [4].

1.1 Het 1D-HR model

Gezien de veelheid aan mogelijke HR beschrijvingen was een eerste doelstelling het uitwerken van een specifieke en efficiënte implementatie. Deze moet enerzijds zo accuraat mogelijk zijn, maar natuurlijk ook praktisch toepasbaar, zodat ze gemakkelijk geïmplementeerd kan worden in bestaande ab-initio software pakketten.
De meer-dimensionale potentiële energie in functie van n interne rotaties wordt hier benaderd als een som van één-dimensionale bijdragen:

$$V^{nD}(\phi_1, \ldots, \phi_n) = \sum_{i=1}^{n} V_i^{1D}(\phi_i) \tag{1.1}$$

Dit is een courante benadering. Elk van deze één-dimensionale functies wordt evenwel berekend op een zeer nauwkeurige manier: het potentiële energie oppervlak wordt geconstrueerd bij diverse waarden van de rotatiehoek (5 graden interval). In deze procedure worden **alle** andere vrijheidsgraden volledig geoptimalizeerd. Dit vergt wel een meer intensieve computationele inspanning, maar met de huidige generatie computers is deze zeer haalbaar en beduidend veel nauwkeuriger dan de vroegere, meer traditionele methodes die gebaseerd zijn op de berekening van enkele stationaire punten waardoor de potentiële energiefunctie gefit wordt op basis van een beperkt aantal Fouriertermen.

Partitiefuncties kunnen berekend worden zowel kwantummechanisch als klassiek. De **kwantummechanische** werkwijze vergt de berekening van energieniveau's. Binnen het één-dimensionaal beeld bijvoorbeeld worden deze bepaald door oplossing van volgende Schrödinger vergelijking:

$$\left[-\frac{\hbar^2}{2I_i^{red}}\frac{\partial^2}{\partial\phi_i^2} + V_i(\phi_i)\right]\psi_{ki}(\phi_i) = \epsilon_{ki}\psi_{ki}(\phi_i) \tag{1.2}$$

De eigenwaarden ϵ_{ki} vormen de basisgrootheden nodig voor de kwantummechanische bepaling van de partitiefunctie q_i corresponderend bij de i^e rotatie:

$$q_i = \frac{1}{\sigma_i}\sum_k g_k e^{-\frac{\epsilon_{ki}}{k_B T}} \tag{1.3}$$

waarbij σ_i het symmetriegetal van de interne rotatie voorstelt, en g_k de ontaardingsgraad van energieniveau k.
De **klassieke** berekeningswijze van de partitiefunctie is gebaseerd op een integratie in de faseruimte [1]:

$$q_i = \frac{1}{\sigma_i}\frac{\sqrt{2\pi k_B T I_i^{red}}}{h}\int e^{-\frac{V_i(\phi_i)}{k_B T}}\mathrm{d}\phi_i \tag{1.4}$$

Het is evident dat bij hoge temperaturen de resultaten in beide beelden moeten convergeren.

Een belangrijke grootheid ter bepaling van q_i is het gereduceerd traagheidsmoment I_i^{red}. Voor het initieel model volgen we een algemeen aanvaarde manier om deze te berekenen (gepresenteerd in de doctoraatsscriptie van Veronique Van Speybroeck [3]). De afleiding houdt rekening met de koppeling met de globale rotatie van de molecule, waardoor de uitdrukking van het gereduceerd IR-traagheidmoment een afhankelijkheid vertoont van de hoofdtraagheidsmomenten.
In de literatuur worden meer geavanceerde uitdrukkingen gegeven voor I_i^{red}, waarbij rekening wordt gehouden met de andere interne rotaties aanwezig in de molecule. Een overzicht van de verschillende berekeningsmethoden wordt gegeven door East en Radom [5].

Een accurate bepaling van de totale moleculaire partitiefunctie Q_{tot} vergt echter de behandeling van **alle** globale en interne vrijheidsgraden. Uitgangsmodel vormt de standaard HO methode. Het is evenwel niet evident om deze methode enkel toe te passen op de overblijvende niet-IR vrijheidsgraden [6]. Een voor de hand liggende methode is het wegdelen van de partitiefunctie $q_{1D,i}^{HO}$ voor elke interne rotatie i uit de totale Q_{tot}^{HO} en te vervangen door de corresponderende HR partitiefunctie. Een aandachtspunt is wel de correcte beschrijving van $q_{1D,i}^{HO}$, of met andere woorden de bepaling van de correcte vibrationele temperatuur $\Theta = \frac{h\nu}{k_B}$. Deze wordt gevonden uit de kennis van de tweede afgeleide van de potentiële energie naar de torsiehoek, en van het gereduceerd moment I_i^{red} (zoals gebruikt in q_i).
Aldus leidt deze procedure tot volgende uitdrukking voor de globale 1D-HR partitiefunctie:

$$\begin{aligned} Q_{tot}^{1D-HR} &= Q_{tot}^{HO} \prod_{i=1}^{n} \frac{q_i}{q_{1D,i}^{HO}} \\ &= Q_{tot}^{HO} \prod_{i=1}^{n} \kappa_{1D-HR,i} \end{aligned} \tag{1.5}$$

Men kan dit resultaat interpreteren als volgt: elke specifieke interne rotatie wordt herschaald met een factor $\kappa_{1D-HR,i} = q_i/q_{1D,i}^{HO}$. Bij uitbreiding naar een multi-dimensioneel model is het niet onredelijk te veronderstellen dat die schaalfactor ongewijzigd blijft. Dit is een *ad hoc* veronderstelling, maar, zoals

later zal blijken, wel fysisch gegrond.

Aangezien de partitiefunctie geen meetbare grootheid is, moeten we voor experimentele verificatie onze toevlucht nemen tot het vergelijken van afgeleide grootheden. In een eerste stap focuseren we op de reproductie van entropie S en warmtecapaciteit C. Deze worden uit de moleculaire partitiefunctie Q afgeleid als volgt:

$$S = R\left(\ln Q + T\left(\frac{\partial \ln Q}{\partial T}\right)\right) \tag{1.6}$$

$$C = RT\left(2\frac{\partial \ln Q}{\partial T} + T\frac{\partial^2 \ln Q}{\partial T^2}\right) \tag{1.7}$$

In eerste instantie werd geopteerd voor een testset van n-alkanen : van ethaan tot decaan. Voor deze gassen is een veelheid aan experimentele gegevens voorhanden. Voor deze set is het ook mogelijk om vrij nauwkeurige ab-initio potentiële energie waarden te berekenen met een relatief snelle "level-of-theory": B3LYP/ 6-311g** [7, 8]. Dit is een 'Density Functional Theory' of DFT-methode [9], gebaseerd op de basistheorema's van Hohenberg en Kohn [10]. Voor het verkrijgen van de gewenste energieën en structuren gebruiken we het softwarepakket Gaussian [11]. In de loop van dit doctoraatswerk zijn daarvan twee versies gebruikt: initieel Gaussian98 [12], in een later stadium Gaussian03 [13].
Voor meer diepgaande theoretische besprekingen van DFT verwijzen we naar de literatuur. In dit onderzoek staat de modelontwikkeling i.v.m. de beschrijving van "large-amplitude" interne modes centraal, en niet zozeer de manier om de benodigde data (energie en geometrie) te verkrijgen.

De resultaten van de entropie- en warmtecapaciteitsberekeningen op alkanen, en de bespreking ervan, worden uitgebreid uiteengezet in hoofdstuk 3 [14]. Ze worden samenvattend voorgesteld in Figuren 1.1 en 1.2. Op deze plots is duidelijk te zien dat een meer correcte behandeling van de IR (zowel kwantummechanisch als klassiek) leidt tot een bijna perfecte reproductie van de experimentele waarden, vooral voor de entropie. Daar genereert de HO-methode telkens te kleine waarden. Voor de warmtecapaciteit is de overeenkomst van de HR methodes met de referentiewaarden kwalitatief minder, maar toch beter dan de HO voorspellingen.

Deze vaststellingen doen besluiten dat de overeenkomst met het experiment zo goed is dat een verbetering (t.o.v. 1D-HR) in de beschrijving van de interne

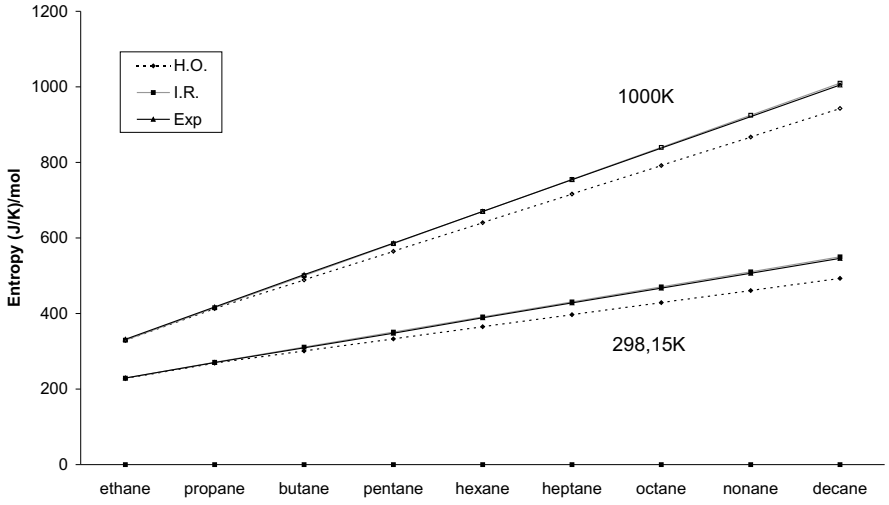

Figure 1.1: De entropie van n-alkanen bij 298,15K en 1000K volgens stijgende ketenlengte

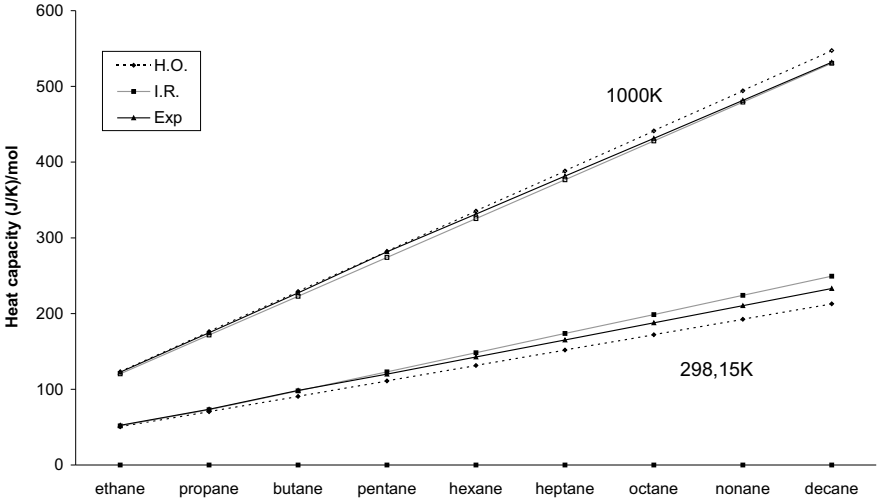

Figure 1.2: De warmtecapaciteit van n-alkanen bij 298,15K en 1000K volgens stijgende ketenlengte

modes slechts minimale correcties mag teweeg brengen. Deze verbeteringen zullen moeten voortvloeien uit puur theoretische overwegingen, want de reeds bevredigende experimentele overeenkomst geeft eigenlijk weinig ruimte om te suggereren wat nu beter zou kunnen. De enige aanwijzing is de wat mindere overeenkomst voor de warmtecapaciteit. Deze wordt ook bepaald door tweede afgeleiden van Q, in tegenstelling tot de entropie. Dit suggereert subtiele correcties in de reproductie van de totale partitiefunctie.
Concluderend kunnen volgende bedenkingen bij het huidige 1D-HR formalisme gemaakt worden:

- Een duidelijke optie voor verbetering ligt bij de beschrijving van de potentiële energie $V^{nD}(\phi_1, \ldots, \phi_n)$. Er moet onderzocht worden welke invloed de één-dimensionale benadering heeft op Q. Dit kan enkel door het berekenen van een volledig multidimensionaal energieoppervlak, en de corresponderende partitiefunctie.

- De inertiaalmomenten gebruikt voor de verschillende interne rotaties zijn eigenlijk ook één-dimensionale benaderingen. Indien men de correcte V^{nD} gebruikt, moeten de momenten natuurlijk ook in het gekoppelde (meer-dimensionale) beeld worden berekend.

- Meer nog, eigenlijk zou men de variatie van deze interne en ook van de globale traagheidsmomenten in acht moeten nemen. Het is fysisch moeilijk te verantwoorden om constante momenten te associëren aan een vervormende moleculaire structuur.

Deze bedenkingen liggen aan de basis voor de ontwikkeling van een accurater model dat in de volgende hoofdstukken wordt uiteengezet. Voor multidimensionale toepassingen wordt een kwantummechanische behandeling problematisch en beperken we ons in het verder verloop van deze studie tot een klassieke beschrijving van de partitiefunctie. Deze veronderstelling wordt ondersteund door de vaststelling dat bij temperaturen hoger dan 300 K de waarden voor de partitiefunctie uit beide benaderingen naar elkaar convergeren. Er wordt wel een correctiefactor toegevoegd voor een betere beschrijving bij lagere temperaturen: de Pitzer-Gwinn factor [15].

1.2 Het multi-dimensionale nD-HR model

In deze paragraaf wordt een eerste geavanceerde methode voorgesteld: het nD-HR model, waarin zowel de potentiële als de kinetische energie multi-dimensionale functies van de interne-rotatiehoeken worden: $V^{nD}(\phi_1, \ldots, \phi_n)$ en $\det A^{nD}(\phi_1, \ldots, \phi_n)$. De laatste functie is de determinant van de kinetische energie-matrix over de interne en globale rotatievrijheidsgraden. De theoretische afleiding van die matrix wordt uitvoerig behandeld in hoofdstuk 4 [16].
Numeriek wordt dit model toegepast op pentaan (2D-HR) en hexaan (3D-HR), waarbij de methyltoppen nog altijd volgens de één-dimensionale benadering worden beschreven. Meer dan drie dimensies is computationeel niet haalbaar. Om een idee te geven: de constructie van een één-dimensionale rotationele potentiaal vergt 72 punten; een twee-dimensionaal oppervlak 5184 punten, en tenslotte een drie-dimensionaal oppervlak 46656 punten, die allen op een ab-initio manier worden berekend.

Juist omdat de multi-dimensionale procedure zo rekenintensief is, kan die onmogelijk als standaardmethode worden gepromoot. Het multi-dimensionaal nD-HR model wordt in de verdere bespreking voorgesteld onder de verkorte benaming 'C1'. De zeer accurate C1 methode wordt beschouwd als het referentiekader om een aantal varianten van 1D-HR (C2,C3,C3',C4,C4') te kunnen evalueren. Deze gebruiken allen één-dimensionale potentiële energie-functie maar verschillen in de benadering voor de kinetische energiebijdrage. Meer bepaald de wijze hoe de traagheidsmomenten worden ingevoerd differentieert de diverse varianten.
We definiëren de geometriefactor $f^{nD}(\phi_1, \ldots, \phi_n)$ met behulp van

$$\det A(\phi_1, \ldots, \phi_n) = \det A_0 \cdot f^{nD}(\phi_1, \ldots, \phi_n) \tag{1.8}$$

waarbij A_0 de kinetische energie-matrix voorstelt horend bij de evenwichtsgeometrie van de molecule. Deze multi-dimensionale factor kan niet correct berekend worden op basis van enkel één-dimensionale berekeningen. We schetsen enkele benaderingsmethoden naar analogie met de opsplitsing van de multi-dimensionale potentiële energie.

- Een eerste optie is het factorizeren van de geometriefactor:

$$f^{nD}(\phi_1, \ldots, \phi_n) = \prod_{i=1}^{n} f_i^{1D}(\phi_i) \tag{1.9}$$

met elke f^{1D} berekend langs de één-dimensionele paden:

$$f_i^{1D}(\phi_i) = (\det A_0)^{-1} \cdot \det A(\phi_j^{ref}(\phi_i), \phi_i) \;\; \forall j \neq i \qquad (1.10)$$

waarbij alle interne rotatiehoeken functies worden van de torsiehoeken ϕ_i. Dit impliceert een optimalizatie van de molecule voor een vaste torsiehoek ϕ_i. Deze methode vormt de basis van de **C2** methode, en leidt tot een factorizatie van de partitiefuncties zoals voor de standaard 1D-HR, maar met een variabel traagheidmoment.

- Een tweede alternatief om f^{nD} te benaderen is geïnspireerd uit de observatie dat langsheen het interne rotatiepad de strukturen niet zoveel afwijken van de rigid-geroteerde referentiegeometrie (althans voor n-alkanen). Het zou dus een goede benadering kunnen zijn om de kinetische energiematrix te construeren op basis van de niet-gerelaxeerde geometrie. Nadeel van deze **C3** methode is dat het integrandum van de partitiefunctie niet gefactorizeerd kan worden en een multi-dimensionale numerieke integratie moet uigevoerd worden. Dit beperkt de toepassingsmogelijkheden van C3 tot zes dimensies, uitbreidbaar naar acht wanneer de methyltoppen zuiver één-dimensionaal worden behandeld (**C3'**).

- De eenvoudigste variant is uiteraard de voordien ingevoerde 1D-HR methode, in deze paragraaf voorgesteld door de verkorte notatie **C4'**. Daarin worden de momenten vast gehouden op hun gereduceerde waarden. Deze gereduceerde momenten zijn eigenlijk de diagonaalelementen van de kinetische energie-matrix. Door nu ook de niet-diagonale matrixelementen te beschouwen wordt het produkt van de traagheidsmomenten (intern en globaal) gelijk aan $\det A_0$. In de **C4** methode wordt deze waarde alweer constant gehouden op de referentiewaarde.

De verschillende benaderingen aangewend in deze methoden zijn schematisch weergegeven in Tabel 1.1 voor het geval van twee interne rotaties met hoeken ϕ_2, ϕ_3.

Zoals in de vorige paragraaf worden deze methoden toegepast op n-alkanen en op hun accuraatheid getest. De resultaten in functie van de ketenlengte zijn uitgezet in Figuur 1.3. Deel (a) toont de afwijkingen van de berekende entropie met referentiewaarden uit de literatuur. Op basis van hun divergerend gedrag kan men concluderen dat de C2 en C4 methoden falen. De drie andere benaderingen liggen in elkaars nabijheid. Merkwaardig is het goede resultaat bekomen met **C4'**, dat overeenkomt met het 1D-HR model. Deze benadering

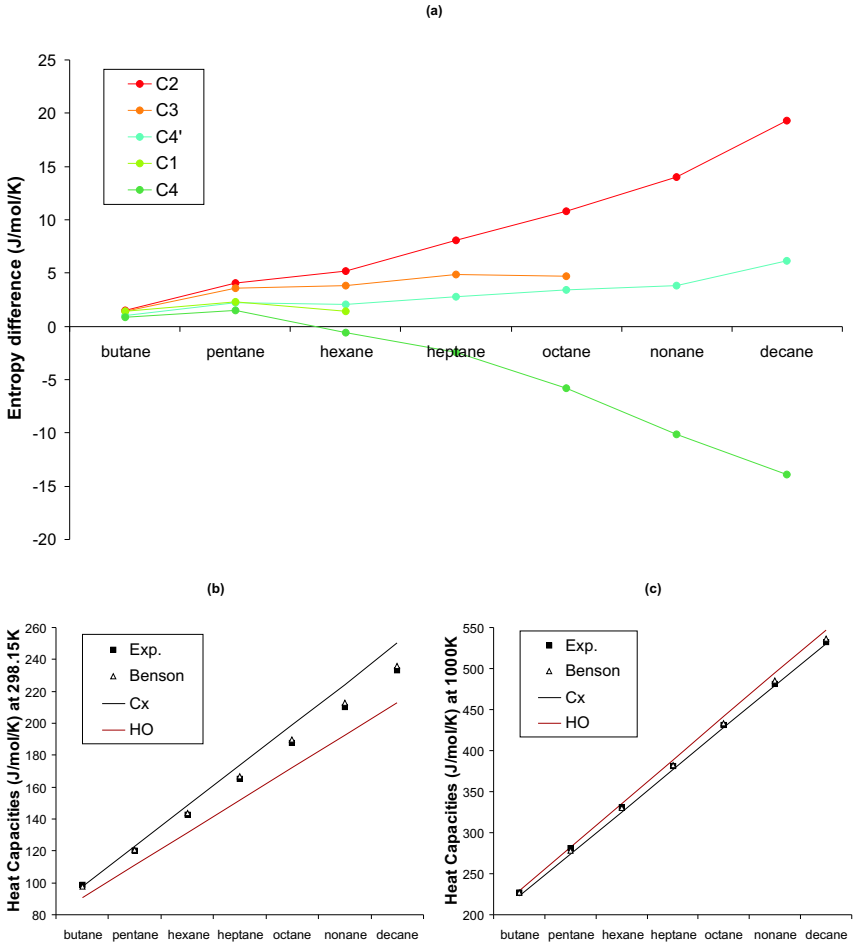

Figure 1.3: (a) Verschil in entropie tussen berekende en referentiewaarden in n-alkanen bij 298.15K. (b),(c) Warmtecapaciteit van n-alkanen op 298.15K and 1000 K

	$V(\phi_2,\phi_3)$	$A(\phi_2,\phi_3)$	$f^{2D}(\phi_2,\phi_3)$
C1=2D-HR	2D geometrie relaxatie	$\Rightarrow$ 2D geometrie relaxatie	$\Rightarrow$ 2D geometrie relaxatie
C2	1D geometrie relaxatie $V(\phi_2)+V(\phi_3)$	$\Rightarrow A(\phi_2,\phi_3(\phi_2))$ $\Rightarrow A(\phi_2(\phi_3),\phi_3)$	$\Rightarrow f_2^{1D}(\phi_2)$ $\Rightarrow f_3^{1D}(\phi_3)$
C3	1D geometrie relaxatie $V(\phi_2)+V(\phi_3)$	2D geen geometrie relaxatie	$\Rightarrow$ 2D geen geometrie relaxatie
C4	1D geometrie relaxatie $V(\phi_2)+V(\phi_3)$	A_0	1
C4'=1D-HR	1D geometrie relaxatie $V(\phi_2)+V(\phi_3)$	$I_x I_y I_z I_2^{red} I_3^{red}$	n.v.t.

Table 1.1: Overzicht van 1D-HR methodes vergeleken met 2D-HR.

heeft zonder twijfel de beste 'performantie/kwaliteit' verhouding. In tegenstelling tot de entropie, zijn de voorspelde waarden voor de warmtecapaciteit redelijk ongevoelig aan de gebruikte aanpak [Fig.1.3(b) en (c)].

1.2.1 Vertakte alkanen

Tot nog toe werd enkel een reeks van lineaire moleculen –n-alkanen– beschouwd. We pasten bovenstaande 1D-methodes ook toe op drie vertakte alkanen (2-methylbutaan, 2-methylpentaan, en 3,3-dimethylpentaan). Ook voor deze moleculen is de overeenkomst van de berekende entropiewaarden met de referentiewaarden zeer goed. De warmtecapaciteit evenwel kan niet gereproduceerd worden binnen de grenzen van het aanvaardbare: niet alleen zijn er grote afwijkingen van de experimentele waarden, maar ook de variatie van de waarden in functie van de temperatuur kent een volledig ander verloop. Vooral op hogere temperatuur falen alle HR-methodes, en is de HO-benadering te verkiezen.
De oorzaak hiervan moet gezocht worden in het feit dat de vertakte ketens sterk met elkaar gekoppeld zijn. In de vibrationele analyse (HO-benadering) is te zien dat een aantal laag-energetische modes overeenkomen met het bewegen van de verschillende ketens t.o.v. elkaar. Deze bewegingen zijn geen interne rotaties. Ze vertonen een treffende gelijkenis met een beweging die ook in de enkelvoudige ketens van n-alkanen voorkomen, waar ze evenwel geen laag-vibrationele modes zijn. We komen hierop terug bij de studie van sulfides, verder in deze samenvatting.

Eén van de doelen die we ons voor ogen moeten houden indien we de (1D)HR benadering willen verbeteren, is het incalculeren van deze bewegingen.

1.2.2 De 2D-HR beschrijving van pentaan

Het succes van 1D-HR in de meeste toepassingen blijft toch voor verrassing zorgen en kan moeilijk systematisch aan een toevalstreffer te wijten zijn. In de zoektocht naar mogelijke oorzaken, gaan we in deze paragraaf dieper in op de 2D-beschrijving van pentaan.
Vooreerst wordt het potentiële energie-oppervlak bestudeerd: in hoever wordt het 2D-oppervlak gereproduceerd door 1D-benaderingen? Minima en maxima van het oppervlak worden weergegeven in Tabel 1.2 in de twee modellen. Ten tweede wordt de geometriefactor in alle benaderingen berekend en met elkaar vergeleken (Tabel 1.3)

Deze vergelijkende studie leert dat de één-dimensionale benadering voor de potentiële energie V resulteert in een globale onderschatting van de energiebarrières, wat leidt tot een te grote Boltzmanfactor in het integrandum van de partitiefunctie. Om dit te compenseren moet de bijdrage van de kinetische energie, wat zich manifesteert in de grootte van de geometriefactor (bevat de traagheidsmomenten), iets onderschat worden. Dit gebeurt bij de twee benaderingen C4 en C4'. Uit de vergelijking met experiment kunnen we besluiten dat voor de C4' methode, die samenvalt met het 1D-HR model, de twee effecten elkaar nagenoeg opheffen waardoor de fouten die worden gegenereerd in het 1D-HR model in de beschrijving van de potentiële en kinetische energie worden gecompenseerd.
De gemiddelde waarden $< f(\phi_2, \phi_3) >$ uit Tabel 1.3 corresponderen duidelijk met de afwijkingen van de experimentele entropiewaarden in n-alkanen zoals weergegeven in Figuur 1.3(a). Merk op dat de rigide-rotatie benadering van C3 zeer goed is.

Samengevat:

Effect op q_{rot}	**C1**	**C2**	**C3**	**C4**	**C4'**
van de kinetische energie	=referentiewaarde	++	0	− −	−
van de potentiële energie	=referentiewaarde	+	+	+	+
Globaal effect	=referentiewaarde	+++	+	−	0

Een analoge studie op n-hexaan (m.b.v. 3D-HR) bevestigt bovenstaande resultaten.

Energie-Minima voor $V^{2D}(\phi_2, \phi_3)$

Type	Symmetrie	ϕ_1	ϕ_2	ΔE(kJ/mol)
tt	C_{2v}	0	0	0.00
tg-	C_1	0	115	3.62
tg-	C_1	115	0	3.62
tg+	C_1	0	245	3.62
tg+	C_1	245	0	3.62
g-g-	C_2	115	115	6.74
g-g+	C_1	115	270	13.96
g-g+	C_1	85	245	13.96
g+g-	C_1	245	85	13.96
g+g-	C_1	270	115	13.96
g+g+	C_2	245	245	6.74

Energie-Maxima voor $V^{2D}(\phi_2, \phi_3)$

(0,60),(60,0),(300,0),(0,300)	12.84
(0,180)(180,0)	23.70
(60,60)(300,300)	28.94
(180,60)(180,300),(60,180),(300,180)	39.30
(300,60)(60,300)	29.04
(180,180)	69.81

Energie-Minima voor $V^{1D}(\phi_2) + V^{1D}(\phi_3)$

(0,0)	0.00
(0,115)(115,0),(0,245),(245,0)	3.62
(115,115)(115,245),(245,115),(245,245)	7.24

Energie-Maxima voor $V^{1D}(\phi_2) + V^{1D}(\phi_3)$

(0,60),(60,0),(300,0),(0,300)	12.84
(0,180)(180,0)	23.70
(60,60),(300,60),(60,300),(300,300)	23.70
(180,60)(180,300),(60,180),(300,180)	36.54
(180,180)	47.40

Table 1.2: De minima en maxima op het potentiële-energie-oppervlak (1D en 2D) van de ethylrotaties in pentaan.

	C1	C2	C3	C4	C4'
Minima					
(85,0)	1.51	1.51	1.54	1.00	1.19
(275,0)	1.51	1.51	1.54	1.00	1.19
(0,85)	1.51	1.51	1.54	1.00	1.19
(0,275)	1.51	1.51	1.54	1.00	1.19
(85,85)	1.88	2.29	1.83	1.00	1.19
(275,85)	2.00	2.29	1.96	1.00	1.19
(85,275)	2.00	2.29	1.96	1.00	1.19
(275,275)	1.88	2.29	1.83	1.00	1.19
Maxima					
(180,0)	0.86	0.86	0.83	1.00	1.19
(0,180)	0.86	0.86	0.83	1.00	1.19
(180,180)	0.61	0.73	0.58	1.00	1.19
$< f(\phi_2, \phi_3) >$	1.36	1.46	1.34	1.00	1.19

Table 1.3: De geometriefactor in de potentiële energie minima en maxima van pentaan.

1.2.3 De 2D- en 3D-HR beschrijving van hexaan

De zeer accurate en computationeel intensieve C1-studie van n-pentaan (C1≡ 2D-HR) en n-hexaan (C1≡3D-HR) hebben ons geleerd dat de verschillen met de eenvoudige 1D-HR methode klein zijn. Toch mogen we hieruit niet besluiten dan 1D-HR altijd goede resultaten zal opleveren, zoals het falen van de methode voor vertakte alkanen aantoont. Voor validatie van benaderende modellen is het nuttig om te beschikken over een goede referentiemethode (zoals C1). Deze methode is evenwel niet altijd haalbaar door de hoge computationele kost en bovendien stelt zich de vraag of het n-dimensionale oppervlak niet accuraat kan gereproduceerd worden uit meerdere $(n-1)$-dimensionale oppervlakken met $n > 2$. Deze probleemstelling wordt gedetailleerd bestudeerd in hexaan: het 3D potentiële energie-oppervlak wordt exact geconstrueerd en er wordt nagegaan in hoever de 2D potentiële energie-oppervlakken in staat zijn het 3D-oppervlak correct te simuleren. Met dat doel voor ogen wordt volgende 2D-schatting van het m-dimensionaal energieoppervlak voorgesteld:

$$V^{mD}(\phi_1,...,\phi_m) \approx \sum_{i=1}^{m-1} V_{i(i+1)}^{2D}(\phi_i,\phi_{i+1}) - \sum_{i=2}^{m-1} V_i^{1D}(\phi_i) \tag{1.11}$$

We benadrukken dat de methyltoppen niet worden meegerekend in het aantal "echte" interne rotaties, weergegeven door de index m. Op analoge wijze wordt een 2D-benadering van de m-dimensionale geometrie factor voorgesteld:

$$f_A^{mD}(\phi_1,\ldots,\phi_m) \approx \frac{\prod_{i=1}^{m-1} f_{A,i(i+1)}^{2D}(\phi_i,\phi_{i+1})}{\prod_{i=2}^{m-1} f_{A,i}^{1D}(\phi_i)} \tag{1.12}$$

In hoofdstuk 5 [17] wordt aangetoond dat deze decomposities zeer betrouwbaar zijn. Dit is vermoedelijk het gevolg van het feit dat in de voorgestelde decomposities de koppelingen tussen naburige interne rotaties systematisch in rekening worden gebracht.
Als 2D-schattingen in staat zijn op correcte wijze 3D-grootheden te simuleren, kan men verwachten dat ze vrij goed afgeleide grootheden zoals entropie en warmtecapaciteit kunnen reproduceren. Een globaal beeld van de verschillen tussen de diverse 1D-, 2D- en 3D-HR benaderingen wordt weergegeven in Figuur 1.4. Het is duidelijk dat de 2D-benadering nagenoeg dezelfde waarden oplevert als 3D-HR, terwijl er toch nog duidelijke discrepanties voorkomen bij gebruik van 1D-HR.

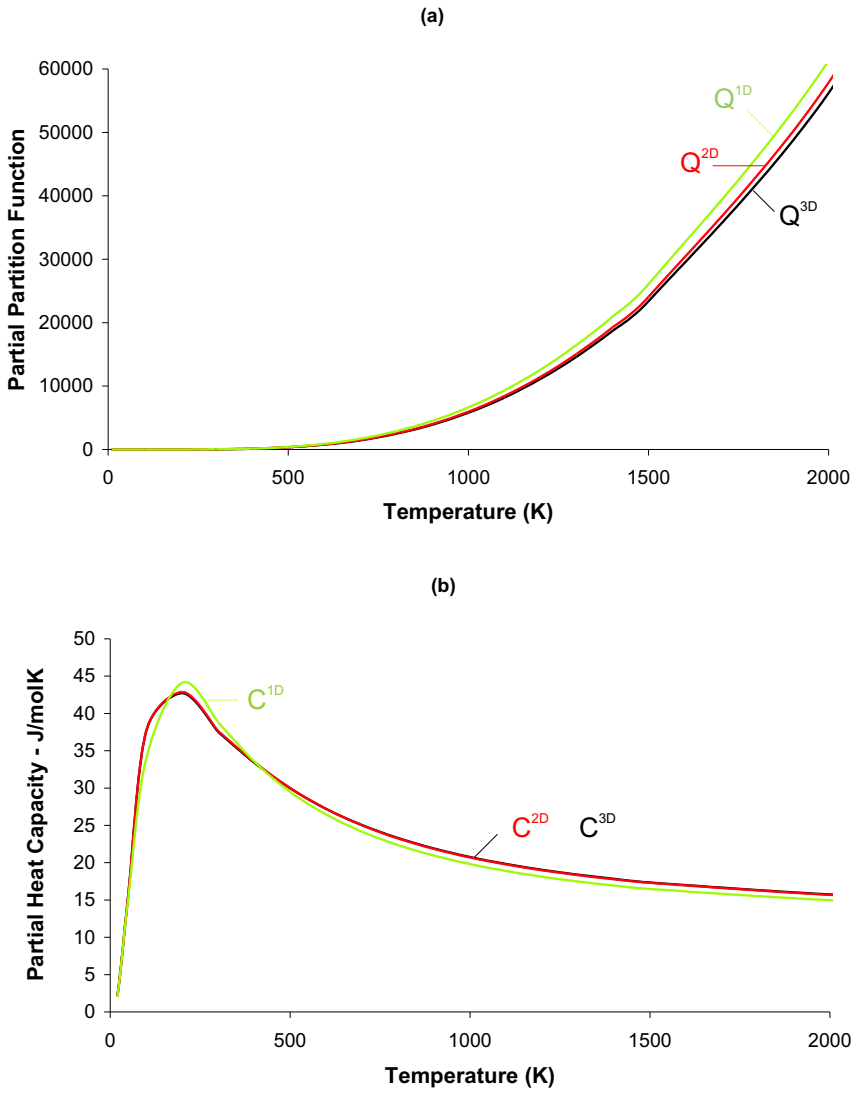

Figure 1.4: (a) Partitiefunctie en (b) warmtecapaciteit van de drie interne rotaties in hexaan volgens 1D-HR, 2D-HR en 3D-HR.

1.3 Ethers, alcoholen, sulfides en thiolen

Nu we hebben vastgesteld dat het vrij eenvoudig 1D-HR model zeer geschikt is voor een voldoende nauwkeurige beschrijving van lineaire alkanen, kunnen we onderzoeken in hoever men deze conclusie kan doortrekken naar andere lineaire moleculen. Een voor de hand liggende uitbreiding betreft het opnemen van ethers, alcoholen, sulfides en thiolen in de testset. Deze stellen n-alkanen voor met een heteroelement, m.a.w. waarbij een CH_2 fragment vervangen wordt door een zuurstof- of een zwavelatoom.

Door de aanwezigheid van een heteroelement dient eerst een korte level-of-theory analyse verricht te worden om na te gaan welke DFT-functionaal en basisset geschikt is voor een betrouwbare studie van deze klasse van moleculen. Deze studie leerde dat B3LYP/6-31+g(d) een goede level-of-theory is om de energieverschillen tussen verschillende conformeren van zowel alcoholen als ethers te voorspellen. Ook voor thiolen en sulfides is B3LYP/6-31+g(d) adequaat, maar voor deze moleculen blijkt B3LYP/6-311g** (gebruikt in de beschrijving van n-alkanen) evenzeer geschikt.
Dit wordt aangetoond in hoofdstuk 6 [18].

Alvorens de partitiefuncties voor deze n-alkanen met een heteroelement bekomen uit onze diverse modellen te valideren, is een voorafgaande conformationele studie van deze klasse van moleculen wenselijk gezien het belang van de energieminima van het potentiaal energie oppervlak op de numerieke waarde van de partitiefunctie. Deze conformationele analyse levert ook een bijkomend aspect op: als de ketenlengte groot wordt is het niet evident om alle conformaties op te zoeken, en is het aangewezen regels af te leiden die de verscheidene conformeren kunnen voorspellen. Voor n-alkanen gelden de Tasi-regels [19], en de vraag stelt zich of die regels verder kunnen worden toegepast op ethers, alcoholen, sulfides en thiolen, of dat er aanpassingen moeten worden aangebracht door de aanwezigheid van een heteroelement in de keten. Voor ethers en sulfides zijn de resulaten samengevat in Tabel 1.4. De conformaties tussen haakjes komen enkel voor in de kleinste moleculen.

Na de conformationele studie komen de energetische aspecten aan bod en meer bepaald de relatieve energieverschillen tussen de diverse minima. In welke mate kan een 1D-benadering deze afschatten? Conform met vorige conclusies is enkel een 2D-benadering (of hoger) van de potentiële energie [Vgl.(1.11)]

Twee opeenvolgende gauche conformaties:				
	$\phi_{s1}\phi_{l1}$	$\phi_{l1}\phi_{l2}$	$\phi_{l2}\phi_{l3}$	$\phi_{l3}\phi_{l4}$
Tasi	**Ethers:**			
g_-g_-	x_-Ox_-	Og_-g_-	Otg_-g_-	$Ottg_-g_-$
g_-x_+	(x_-Ox_+)		$Otg_-x'_+$	$Ottg_-x_+$
x_-g_+				$Ottx_-g_+$
Tasi	**Sulfides:**			
g_-g_-	g_-Sg_-	Sg_-g_-	Stg_-g_-	$Sttg_-g_-$
g_-x_+	g_-Sx_+		$Stx'_-x'_+$	$Sttg_-x_+$
x_-g_+	x_-Sg_+	Sx_-g_+		$Sttx_-g_+$

Drie opeenvolgende gauche conformaties:			
	$\phi_{s1}\phi_{l1}\phi_{l2}$	$\phi_{l1}\phi_{l2}\phi_{l3}$	$\phi_{l2}\phi_{l3}\phi_{l4}$
Tasi	**Ethers:**		
$g_-g_-g_-$	$x_-Ox_-g_-$	$Og_-g_-g_-$	$Otg_-g_-g_-$
$g_+x_-g_-$			
$x_+g_-g_-$			$Otx'_+g_-g_-$
$x_-g_+x_-$			$Otx'_-g_+x_-$
$g_-g_-x_+$		$Og_-g_-x'_+$	$Otg_-g_-x_+$
$g_-x_-g_+$			$Otg_-x_-g_+$
Tasi	**Sulfides:**		
$g_-g_-g_-$	$g_-Sg_-g_-$	$Sg_-g_-g_-$	$Stg_-g_-g_-$
$g_+x_-g_-$	$g_+Sx_-g_-$		$Stx'_+x'_-g_-$
$x_+g_-g_-$	$(x_+Sg_-g_-)$	$Sx_+g_-g_-$	
$x_-g_+x_-$		$Sx_-g_+g_-$	$Stx_-g_+x_-$
$g_-g_-x_+$		$Sg_-g_-x_+$	$Stg_-g_-x_+$
$g_-x_-g_+$	$g_-Sx_-g_+$	$Sg_-x_-g_+$	$Stg_-x_-g_+$
			$Stg_-x'_-x'_+$

Table 1.4: Aangepaste Tasi-regels voor ethers en sulfides.

in staat de energieverschillen met grote nauwkeurigheid te reproduceren. Het 1D-HR model genereert teveel conformationele afwijkingen (gedrag rond de g_-g_+ geometrie is totaal verschillend) maar ook het feit dat de energieën van de diverse minima heel dicht bij elkaar liggen, doet aanvoelen dat de 1D-HR partitiefunctie sterk zal kunnen afwijken van de 2D-HR schatting.

De bespreking van de 1D-HR en 2D-HR resultaten op deze n-alkanen met een heteroelement wordt uitvoerig uiteengezet in hoofdstuk 7 [20]. Entropiewaarden worden heel accuraat voorspeld. Vooral in ethers en alkoholen is de experimentele overeenkomst zelfs uitstekend te noemen. Voor diezelfde moleculen is de warmtecapaciteit ook goed gereproduceerd; voor thiolen en sulfides daarentegen faalt de theorie. Mogelijke oorzaken kunnen zijn dat andere invloeden een dominante rol beginnen te spelen, zo bijvoorbeeld het voorkomen van eigenmodes met een lage vibrationele temperatuur en niet corresponderend met een interne rotatie. Het voorkomen van zulke modes is karakteristiek aan sulfides, maar ook eigen aan vertakte alkanen waarvoor de HR-beschrijving ook tot een slechte voorspelling van de warmtecapaciteit leidt.

1.4 De HR-beschrijving van vier-ringen

Tot nog toe hebben we ons beperkt tot het behandelen van interne rotaties. Er bestaan echter ook andere laag-energetische modes die een analoge aanpak vergen, en waarvoor het (1D)HR model kan toegepast worden.
In cyclische moleculen (=ringen) komen de zogenaamde "ring-puckering" bewegingen voor die de structuur grondig kunnen vervormen. Het bekendste voorbeeld hiervan is de boot–stoel interconversie in cyclohexaan. In vierringen is er slechts één zulke beweging, waardoor dit type van moleculen zeer geschikt is voor het toepassen van het 1D-HR model.
Deze uitbreiding naar andere modes dan interne rotaties is nieuw en nog niet bestudeerd in de literatuur.

In eerste instantie onderzoeken we de meest eenvoudige vierring cyclobutaan en acht afgeleide moleculen. Oxetaan, thietaan, azetidine en phosphetaan zijn verkregen door het vervangen van een CH_2 fragment door respectievelijk O, S, NH en PH, dus door endo-substitutie. Cyclobutanoon, cyclobutaanthioon, cyclobutylideenamine en cyclobutylideenphosphine worden verkregen door een exo-substitutie: CH_2 vervangen door respectievelijk $C{=}O$, $C{=}S$, $C{=}NH$ en $C{=}PH$. In deze systemen is de ring-puckering verantwoordelijk voor de laagste vibrationele mode volgens de HO-analyse.

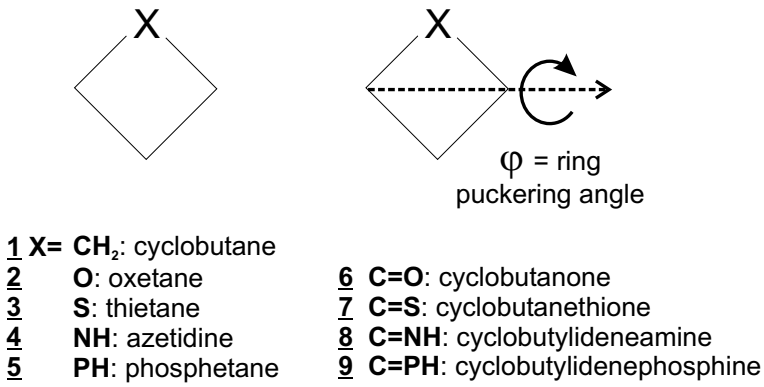

Figure 1.5: Definitie van de ring-puckering hoek in vierringen met een enkelvoudige substitutie.

Omdat de toepassing van het HR-model op deze specifieke interne mode nieuw is, werd ook de kwantummechanische methode aangewend en vergeleken

met de klassieke aanpak. Zoals bij de ontwikkeling van het 1D-HR model voor interne rotaties, zijn ook hier de verschillen tussen beide methoden verwaarloosbaar. Dit topic wordt uitvoerig behandeld in hoofdstuk 8 [21].
De invloed van het gebruik van het HR-model op de partitiefunctie en afgeleide thermodynamische grootheden is bijna volledig terug te brengen op een correkt gebruik van symmetriegetallen. Dit komt door de specifieke vorm van de puckering-potentialen (Fig.1.6).

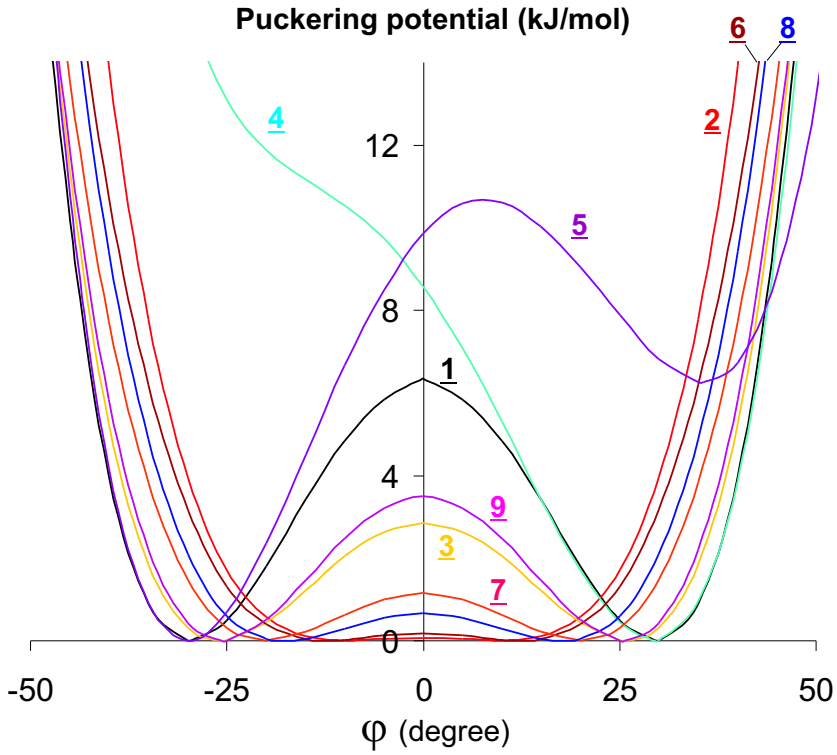

Figure 1.6: Potentiële energie-variatie van de ring-puckering in cyclobutaan **1**, oxetaan **2**, thietaan **3**, azetidine **4**, phosphetaan **5**, cyclobutanone **6**, cyclobutaanthione **7**, cyclobutylideneamine **8**, and cyclobutylidenephosphine **9**.

1.5 Het EHR-model

Uit het voorgaande blijkt dat het Hindered Rotor model niet altijd de gewenste resultaten geeft, en dat de mogelijke oorzaken waarschijnlijk te maken hebben met de aanwezigheid van andere laag gelegen vibrationale modes. Een bijkomende tekortkoming van het HR model is dat het slechts een deel van de coördinatenruimte in rekening wordt gebracht. Bijvoorbeeld bij moleculen waarin interne rotaties voorkomen beperkt het nD-HR model zich enkel tot de ruimte beschreven door de IR-coördinaten . De verantwoording voor deze beperking zit in aanname van de *ad hoc* veronderstelling (1.5).
Indien we nu een model kunnen opstellen waarin **alle** modes worden behandeld, hetzij als HR of als HO-vibratie, dan is a priori de koppeling tussen de verschillende bewegingen geïncorporeerd.

In hoofdstuk 9 [22] wordt het 'Extended Hindered Rotor' (EHR) model geïntroduceerd. Hierin worden alle coördinaten behandeld, zowel interne als globale. De globale translatie van de molecule kan eenvoudig afgescheiden worden aangezien deze automatisch onafhankelijk wordt van de overige bewegingen. De globale rotatie evenwel vertoont koppeling met de interne vrijheidsgraden door de Coriolis termen in de kinetische energie. In de bestaande kwantummechanische modellen worden die over het algemeen verwaarloosd. Aangezien we niet geïnteresseerd zijn in energieniveau's, maar enkel in de totale partitiefunctie, kunnen we de globale rotatie klassiek beschrijven. Dit geeft een grotere vrijheid in de keuze van de assenstelsels, en is het mogelijk te werken in een (variabel) stelsel waar de Coriolis termen systematisch verdwijnen. Op deze manier zijn de globale en interne vrijheidsgraden formeel gescheiden. Wel is het zo dat de hoofdtraagheidsmomenten, die de globale rotationele partitiefunctie bepalen, afhankelijk worden van de interne modes.
Het is aangewezen de interne coördinaten op te splitsen in twee groepen: de large-amplitude (zoals IR) en de vibrationele vrijheidsgraden. Vibrationele modes worden gekenmerkt door een (steile) kwadratische potentiaal, waardoor ze (snel) vibreren rond een evenwichtsgeometrie. We mogen er dus van uit gaan dat de beweging volgens die coördinaten de geometrie van de molecule nagenoeg niet verandert en dat deze vibrationele modes geen effect hebben op de traagheidsmomenten. Dit impliceert dat mag verondersteld worden dat de hoofdtraagheidsmomenten geen afhankelijkheid vertonen van deze specifieke vrijheidsgraden en dat ze kunnen worden berekend op basis van de evenwichtsgeometrie. Ze hangen echter wel af van de coördinaten behorend bij de laag-

energetische modes (large-amplitude bewegingen). Deze interne modes zijn gekenmerkt door een veel vlakker potentiaalverloop waarbij eventueel meerdere minima kunnen voorkomen, waardoor de structuur van de molecule sterk kan wijzigen. De traagheidsmomenten (intern en globaal) kunnen inderdaad sterk afhankelijk worden van deze large-amplitude modes. Deze afhankelijkheid zit ook ingebed in het nD-HR model, maar niet op dezelfde wijze: in $\det A_0$ zit geen kinetische koppeling met de vibrationele modes vervat terwijl in het EHR-model deze koppeling wel inbegrepen is. Verder is ook nieuw dat de kromming van de (kwadratische) potentiële energie in de vibrationele dimensies variabel wordt. De HO beschrijving voor de vibrationele niet-IR modes vertoont op die manier een afhankelijkheid van de IR modes.

Uiteindelijk komen we tot de situatie waarin de vibrationele en globale bewegingen formeel ontkoppeld zijn van de HR-vrijheidsgraden, waardoor het mogelijk wordt de partitiefunctie behorend bij deze bewegingen op te stellen voor elk punt in de HR-ruimte. De berekening van de HR-partitiefunctie gebeurt alweer klassiek, en de uitdrukking van de moleculaire partitiefunctie kan worden uitgeschreven als het produkt van de translationele partitiefunctie met een integraal over alle HR-variabelen. In het integrandum komen echter verschillende grootheden voor die functies zijn van de HR-variabelen, waaronder o.a. de vierkantswortel van het produkt van de HR-traagheidmomenten en de Boltzman factor zoals in de standaard HR beschrijving. De traagheidsmomenten zijn nu evenwel berekend met behulp van de kinetische energie-matrix over alle vrijheidsgraden, en zijn dus a priori verschillend van de (gereduceerde) momenten zoals gebruikt in het HR-model. Verder komen ook de vibrationele en globale rotatie partitiefuncties voor in het integrandum. Het geheel wordt best geschetst in het geval van één HR-dimensie φ. De totale partitiefunctie wordt nu:

$$\begin{aligned} Q_{tot}^{EHR} &= Q_{trans}(T)\; K(T) \\ &\quad \int_0^{2\pi} \mathrm{d}\varphi \, \sqrt{A_\varphi(\varphi)}\; e^{-\beta V^{HR}(\varphi)} \prod_{i=2}^{n} Q_i^{HO}(\varphi, T)\; Q_{rot}(\varphi, T) \end{aligned} \tag{1.13}$$

met $K(T) = \sqrt{\frac{2\pi k_B T}{h^2}}$.

Het is nu aangewezen om naar analogie met het multi-dimensionale nD-HR

model, een geometriefactor in te voeren, gedefinieerd als:

$$f_A(\varphi) = \sqrt{\frac{A_\varphi(\varphi)}{A_\varphi(0)} \frac{I_x(\varphi) I_y(\varphi) I_z(\varphi)}{I_x(0) I_y(0) I_z(0)}} \tag{1.14}$$

met als enig verschil dat de HR-momenten A_φ op een andere manier worden bepaald dan in voorgaande modellen. De invoering van de geometriefactor laat ons toe om de partitiefunctie van de globale rotatie (behorend bij de evenwichtsgeometrie) buiten de integraal te brengen.
Naar analogie met het voorgaande kan nu ook een vibrationele correctiefactor ingevoerd worden:

$$f_{vib}(\varphi, T) = \frac{\prod_{i=2}^{n} Q_i^{HO}(\varphi, T)}{\prod_{i=2}^{n} Q_i^{HO}(0, T)} \tag{1.15}$$

Deze factor is niet enkel een functie van φ, maar ook van de temperatuur T. De introductie van de factor $f_{vib}(\varphi, T)$ laat toe ook de vibrationele partitiefuncties behorend bij de evenwichtssituatie buiten de integraal te plaatsen.
Door het gebruik van de klassieke definitie van de partitiefunctie is het alweer aangewezen om de Pitzer-Gwinn correctie toe te passen. Aangezien in deze EHR-afleiding het φ-pad samenvalt met de vibrationele mode in de HO benadering, valt de teller van de PG-correctiefactor exact samen met de HO-partitiefunctie. Al deze overwegingen laten ons toe de totale EHR partitiefunctie uit te drukken als het product van de standaard HO-partitiefunctie met een schaalfactor $\kappa_{EHR}(T)$, wat een vergelijkende analyse tussen HR en EHR sterk vereenvoudigt:

$$\begin{aligned} Q_{tot}^{EHR}(T) &= Q_{tot}^{HO}(T) \sqrt{\frac{\beta}{2\pi}} \sqrt{\left.\frac{\partial^2 V}{\partial \varphi^2}\right|_0} \int_0^{2\pi} f_A(\varphi)\, f_{vib}(\varphi, T)\, e^{-\beta V^{HR}(\varphi)}\, \mathrm{d}\varphi \\ &= \kappa_{EHR}(T)\, Q_{rot,int}^{HO}(T) \end{aligned} \tag{1.16}$$

Een equivalente uitdrukking werd binnen het 1D-HR model reeds afgeleid:

$$\begin{aligned} Q_{tot}^{1D-HR}(T) &= Q_{tot}^{HO}(T) \sqrt{\frac{\beta}{2\pi}} \sqrt{\left.\frac{\partial^2 V}{\partial \varphi^2}\right|_0} \int_0^{2\pi} e^{-\beta V^{HR}(\varphi)}\, \mathrm{d}\varphi \\ &= \kappa_{HR}(T)\, Q_{rot,int}^{HO}(T) \end{aligned} \tag{1.17}$$

De gelijkenissen zijn groot maar er zijn wel fundamentele verschillen: de finale EHR-uitdrukking is het resultaat van een volledig fysisch en consistent model, wat niet kan beweerd worden van het HR-model.

De opvallende gelijkenis van de HR en EHR uitdrukkingen voor de partitiefunctie verklaart het goede resultaat van de 1D-HR beschrijving. Rond

de evenwichtsgeometrie is het produkt van de twee correctiefactoren $f_A f_{vib}$ per definitie gelijk aan één, en zijn beide HR en EHR resultaten equivalent. Voor alle andere geometrieën wordt de Boltzman-factor $e^{-\beta V^{HR}(\varphi)}$ de determinerende factor. Enkel bij geometrieën waar de waarden voor de potentiële energie zeer laag worden, of bij zeer grote waarden van de correctiefactor $f_A f_{vib}$ kunnen substantiële afwijkingen genoteerd worden.
Voor een 'normaal' energieverloop waar er slechts één dominant minimum is, zoals bij n-alkanen, zullen de HR en EHR-modelen quasi identieke resultaten geven. Voor een energieprofiel met meerdere laaggelegen minima zal $f_A f_{vib}$ wel een rol spelen. Dit kan een verklaring zijn voor de minder goede 1D-HR resultaten voor sulfides.

Situaties waarin grote $f_A f_{vib}$-waarden voorkomen, kunnen het resultaat zijn van twee oorzaken. Enerzijds kan een ingrijpende verandering van de structuur ervoor zorgen dat f_A groot wordt, zoals mogelijke repositionering van zware delen van de molecule (vertakkingen, delen met zware atomen zoals zwavel).

Anderzijds is het zeer waarschijnlijk dat f_{vib} groot wordt wanneer er laaggelegen vibrationele modes aanwezig zijn. Dit komt door de vorm van Q_i^{HO} die aanleiding geeft tot grote verschillen voor kleine variaties bij lage vibrationele temperaturen.
Deze overwegingen vormen een mogelijke verklaring voor het falen van HR voor de beschrijving van vertakte alkanen en van sulfides. Het moet evenwel nog onderzocht worden of EHR inderdaad betere resultaten geeft voor deze moleculen[1].

[1] De beperkte tijdsperiode van dit doctoraatswerk liet niet toe deze studie volledig af te werken. Er worden wel enkele eenvoudige toepassingen geschetst maar echt zware numerieke berekeningen met EHR zijn nog niet verricht geworden.

1.6 Eenvoudige toepassingen van het EHR-model

Het EHR-model wordt in eerste instantie toegepast op moleculaire systemen waarin slechts één EHR-variable optreedt. De numerieke implementatie van het één-dimensionaal EHR-model biedt geen problemen. Voor de validering met thermochemische grootheden wordt 1,3-butadieen als testvoorbeeld genomen, terwijl als validering voor de kinetiek de additiereactie van het vinylradicaal aan etheen beschouwd wordt. In dit voorbeeld wordt de rotatie om de vormende binding in de transitietoestand de enige EHR-vrijheidsgraad. Het één-dimensionaal EHR-model kan op een consistente wijze uitgebreid worden tot hogere dimensies wat de toepasbaarheid van de methode alleen maar ten goede komt. Vandaar dat ook 1-buteen in het testset opgenomen wordt met twee EHR-variabelen.

In Figuur 1.7 worden de schaalfactoren $\kappa(T)$ corresponderend bij de drie schema's: HO ($\kappa_{HO}(T) \equiv 1$), HR en EHR uitgezet voor de drie voorbeelden. Naargelang van het temperatuursgebied kunnen deze factoren oplopen tot 3. De onderlinge verschillen tussen 1D-HR en EHR zijn minder groot, wat doet besluiten dat de grootste correctie als gevolg van het voorkomen van large-amplitude interne modes reeds wordt gegenereerd door het eenvoudigste model: 1D-HR. Wat nu de invloed is van deze verschillen op afgeleide grootheden zoals entropie en warmtecapaciteit, wordt duidelijk weergegeven in Tabellen 1.5 en 1.6. Ten opzichte van de experimentele waarden is de gemiddelde RMS afwijking bij HO veel groter dan bij de twee Hindered-Rotor modellen. De kleinste afwijking wordt genoteerd bij EHR, wat het model ten goede komt. Inspectie van de resultaten leert ook dat vooral de warmtecapaciteit gevoelig is aan kleine correcties in de partitiefunctie. De EHR-predicties vertonen de beste overeenkomst en benaderen de referentiewaarden.

De validering van EHR met reactiekinetiek is nog in een beginfase. In dit werk worden de kinetische parameters (activeringsenergie E_a en pre-exponentiele factor A) voor de reactiesnelheid voor de beschouwde additiereactie gefit in het temperatuursgebied 300-600K. Maar er zijn voor deze reactie geen bruikbare experimentele data beschikbaar. In die context kan men deze applicatie hoogstens als een interessante oefening beschouwen om na te gaan in welke mate EHR predicties voor reactiekinetiek verschillen van HR. De resultaten zijn weergegeven in Fig.1.8. De verschillen manifesteren zich vooral in de pre-

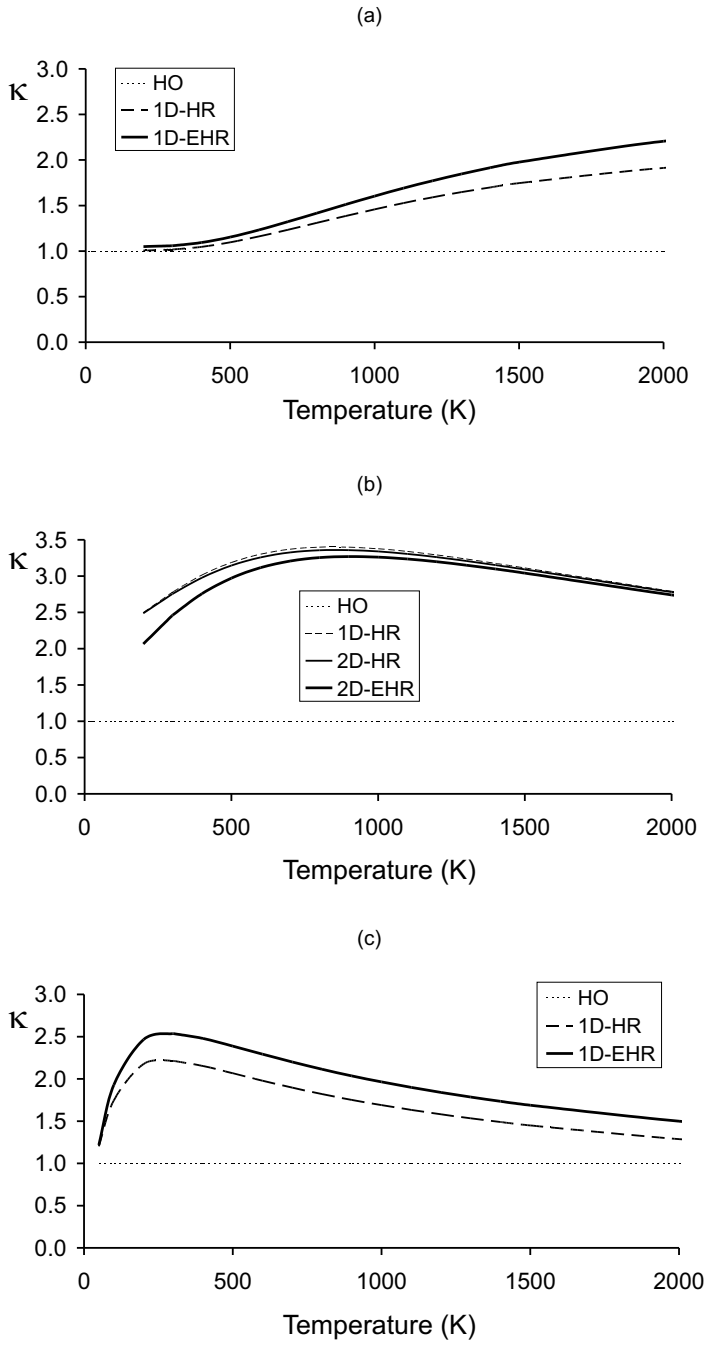

Figure 1.7: Schaalfactoren $\kappa(T)$ voor (a) 1,3-butadieen, (b) 1-buteen en (c) de additiereactie van het vinylradicaal aan etheen.

(a)	S(298.15K)	C(100K)	C(298,15K)	C(400K)	C(600K)	C(1000K)	C(1500K)
Ref.[23]	278.74	39.77	81.37	101.31	135.02	175.43	195.87
Ref.[24]		41.31	79.81	103.44	136.51	173.10	197.54
HO	276.42	40.88	74.33	94.87	127.63	167.79	194.52
1D-HR	277.06	40.98	76.57	99.82	134.69	171.27	194.38
1D-EHR	277.72	41.64	78.00	101.65	136.80	172.62	195.04

(b)	RMS van C(100K $\rightarrow$ 1500K)		MAD van C(100K $\rightarrow$ 1500K)	
	Ref.[23]	Ref.[24]	Ref.[23]	Ref.[24]
HO	6.11	5.90	5.40	5.31
1D-HR	2.84	2.35	2.30	2.17
1D-EHR	2.06	1.31	1.69	1.05

Level of theory: B3LYP/6-311g**.
Alle waarden in J/mol/K.

Table 1.5: Entropie en warmtecapaciteit in 1,3-butadieen: ab-initio versus experiment.

	S(298.15K)	C(200K)	C(298,15K)	C(400K)	C(600K)
Ref.[23]	307.83	67.55	88.41	109.22	145.84
Ref.[24]		65.19	85.56	108.48	146.75
HO	296.97	62.41	82.64	106.30	146.61
1D-HR	307.80	65.46	85.30	107.48	144.68
2D-HR	307.62	65.37	85.27	107.57	144.87
2D-EHR	308.12	66.20	85.93	108.08	145.21

Level of theory: B3LYP/6-311g**.
Alle waarden in J/mol/K.

Table 1.6: Entropie en warmtecapaciteit in 1-buteen: ab-initio versus experiment.

exponentiële factor: de EHR-waarde neemt met ongeveer 17% toe ten opzichte van de standaard HR waarde.

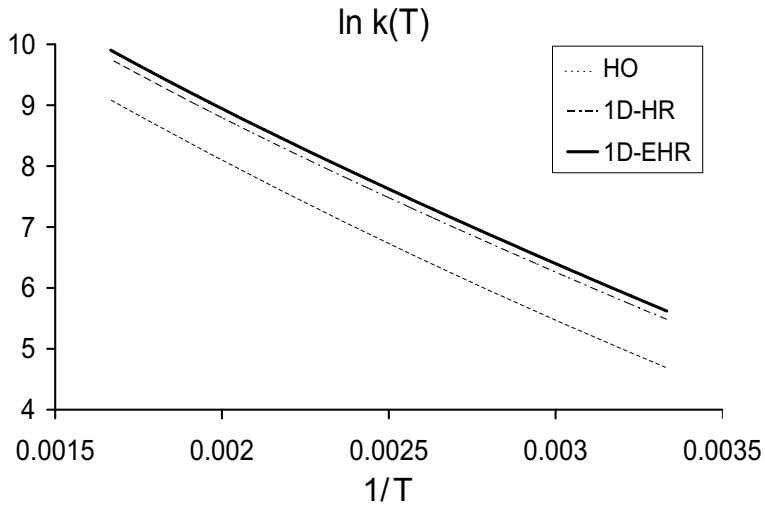

	HO	1D-HR	1D-EHR
E_a (kJ/mol)	21.98	21.40	21.46
A (m^3/mol/s)	6.48 E5	1.16 E6	1.36 E6

Figure 1.8: Arrhenius plot van k(T) voor de additiereactie van het vinylradicaal aan etheen.

1.7 Besluit en toekomstperspectieven

In dit doctoraatswerk zijn we erin geslaagd om een standaardmethode (1D-HR) te ontwikkelen voor een snelle en meestal accurate berekening van de totale moleculaire partitiefunctie rekening houdende met de diverse interne modes die in de molecule kunnen optreden. Reeds gedurende vijf jaar ongeveer werd de 1D-HR methode, of een variant ervan, in de literatuur aangewend als het referentiemodel om de invloed van interne rotaties op bv. de kinetiek van een chemische reactie in rekening te brengen. De correcties ten opzichte van de HO schattingen zijn meestal substantieel en zorgen in de meeste gevallen voor een beduidend betere experimentele overeenkomst. Zonder dat er een grondige studie werd verricht naar de oorzaken van deze goede overeenkomst ook voor moleculen met opeenvolgende IR's, werd 1D-HR langzamerhand als het standaard model erkend voor de behandeling van interne rotaties. Deze thesis heeft ertoe bijgedragen dat *de vraag naar het 'waarom'* beantwoord is geworden.

In moleculen met meerdere interne rotaties werd aangetoond dat afwijkingen in de beschrijving van de multi-dimensionele kinetische en potentiële energie als gevolg van de één-dimensionale benadering elkaar compenseren waardoor het nettoresultaat de fysische werkelijkheid benadert. Vraag blijft echter overeind of de opheffing van de twee bijdragen te wijten is aan toeval of het gevolg van een ingenieus mechanisme. Deze ultieme vraag wordt beantwoord door een in dit werk ontwikkeld nieuw model: het EHR-model, gebaseerd op een consistente behandeling van alle mogelijke koppelingen tussen de diverse bewegingsmodes in zowel de kinetische als de potentiële energie. De consistente procedure inherent aan EHR maakt dat deze methode nagenoeg exact is om verschillende laag-frequentie modes te beschrijven. Een nadeel van het EHR model is dat deze computationeel moeilijk haalbaar wordt bij hoge dimensie (> 2) van het aantal EHR-variabelen (aantal large-amplitude bewegingen) waardoor EHR nooit als een uniforme standaard methode aanzien kan worden, tenzij er hiervoor een soort ééndimensionale benadering kan ontwikkeld worden. Het kan echter wel als de referentiemethode beschouwd worden, waarmee alle andere benaderende methoden worden vergeleken.
De analytische uitdrukkingen voor de totale partitiefunctie in de twee modellen zoals weergegeven in Vgln.(1.13) en (1.17) hebben de oorzaken aangereikt waarom 1D-HR zo goed presteert en waarom beide modellen in vele gevallen dezelfde resultaten produceren. De vaststelling dat systematisch twee grote afwijkende contributies elkaar opheffen is dus geen toevalstreffer geweest. Het

zit structureel in het 1D-HR model vervat en de analytische uitdrukkingen laten ook toe te voorspellen in welke situaties men substantiële afwijkingen van het 1D-HR model kan verwachten.
Dit is o.a. het geval bij moleculen met zijketens, waar 1D-HR eerder faalt, althans wat betreft de reproductie van de warmtecapaciteit. Ook voor sulfides, die gekenmerkt worden door een veelvoud van laag-energetische conformationele toestanden, is de nauwkeurigheid bekomen met 1D-HR iets minder groot. Voor beide gevallen kunnen de afwijkingen geassocieerd worden aan de aanwezigheid van een aantal laag vibrationele modes, verschillend van interne rotaties.
Het EHR-model werd in eerste instantie getest op drie kleinere moleculaire systemen, voor de berekening van zowel thermodynamische als kinetische grootheden.

Op het vlak van theoretische ab-initio voorspelling van macroscopische grootheden die kunnen worden afgeleid op grond van statistische overwegingen uit kennis van microscopische partitiefuncties, mogen we stellen dat dit doctoraatswerk een essentiële bijdrage heeft geleverd.

Het werk is echter niet ten einde. Nog blijven er veel grote uitdagingen over. Het toepassingsgebied van EHR is veel groter dan in deze thesis voorgesteld. Vooral in moleculaire systemen waar men kan verwachten dat 1D-HR faalt kunnen uitgebreide EHR berekeningen van groot nut zijn, zelfs al vergen ze een hoge computationele prijs op grote workstations. Zo is verder onderzoek naar de invloed van sterk vertakte ketens op de partitiefunctie en afgeleide grootheden meer dan nodig. Ook uitbreiding van de large-amplitude bewegingen met "skeleton" vibraties in lineaire molecules en gekoppelde ring-puckering modes in cyclische moleculen vormen zeer nuttige toepassingsgebieden voor EHR en andere benaderingsmethoden. Al deze uitbreidingen kunnen in principe eenvoudig worden geïmplementeerd binnen de voor deze thesis ontwikkelde programmapakketten.

Het EHR-concept waarbij de lage vibrationele vrijheidsgraden gescheiden worden van de HO vrijheidsgraden, kan ook uitgebreid worden voor totaal

andere toepassingen. Zo zou het EHR-concept kunnen leiden tot de ontwikkeling van een methode ter bepaling van normale modes van het chemisch actief gedeelte van uitgebreide moleculaire systemen. Heterogene katalyse zoals zuur-base reacties die plaatsgrijpen over zeolieten, of andere enzymatische katalytische reacties over biomoleculen vergen hybride methoden zoals QM/MM omdat het moleculair systeem te groot is om een uniforme kwantummechanische beschrijving toe te laten. De invoering van een actief en een passief deel en de fundamenteel verschillende methoden om deze gebieden te beschrijven, leidt tot problemen ter bepaling van accurate eigenfrequenties van de modes ook in het actief deel van de molecule. Er is duidelijk een treffende gelijkenis tussen de invoering van twee gebieden in die grote moleculaire systemen en het opdelen van twee types van vibrationele modes inherent aan het EHR model.

Chapter 2

Model development and Applications: an outline

Aim and objectives

The general topic of this thesis is situated in the field of molecular modelling, with the principal aim to predict physical and chemical properties of molecules in an accurate way. The construction of an accurate total molecular partition function from first principles constitutes the most crucial step to achieve this goal.
Present-day methods for the description of molecules are developed for rigid molecules. Since most molecules are rather flexible –meaning they have several, structurally different conformers– this approach is not always suitable. To solve this problem, two approaches are possible.

- One may consider each of the conformers as a different molecule, and use the standard approach. The properties of an ensemble (gas) of these molecules is than derived from the average of the weighted properties of each conformer.
- A more advanced technique is to explicitly describe the internal dynamics –or at least part of it– responsible for the major structural changes of converting one conformer into an other.

The latter methodology was elaborated in this PhD thesis.
Until now, it is common practice to assign only a few internal coordinates to this description, and use the results as a correction on the basic (rigid) approach. No consistent model is available for the description of **all** coordinates, internal and global.
The development of such a method is the final goal of this work.

Structure of the thesis

In the next section a theoretical background of the concept of a partition function is given, along with the available approaches to calculate this function. The approximations and limitations are discussed, and suggestions for improvements are made.
Further sections deal with the various models which have been developed in the framework of this thesis, namely the description of internal modes (*e.g.* internal rotations) and their impact on the partition function.

The remaining part of the thesis is structured as follows: each chapter represents an article, published or in press, covering most of the work which has been done during the last four years within the scope of this PhD thesis. The full title of the paper, the list of (co)authors and the exact reference to the journal in which the paper has been published is given. As much as possible the contents of the paper is entirely retained. A central reference system is built in for the reader's convenience. Finally, in the last chapter a short conclusion is presented. All computations on geometries and binding energies of molecules in this thesis are performed within Density-Functional-Theory (DFT) and use is made of the Gaussian package [11] (Gaussian98 [12] and more recently Gaussian03 [13]).

2.1 Partition Function

The central quantity in this work is the total molecular partition function. It relates microscopic quantities –derived from first principles– with macroscopical properties basing upon statistical thermodynamics. Quantum-mechanically the partition function Q is constructed as a summation over all quantum-mechanical states with energy ϵ_k [1]:

$$Q = \sum_k g_k e^{-\frac{\epsilon_k}{k_B T}} \tag{2.1}$$

In principle these energies ϵ_k stand for the energy eigenvalues of the total Hamiltonian of the molecular system, containing kinetic energies of all atoms and electrons and all interactions among the different fragments of the entire system. An exact solution of this many-particle interacting system is unfeasible. Approximations should be made. We focus here on the usual assumptions made to construct the total partition function, and not to give schemes for calculating the energy levels.

The first assumption is that the electrons are always in their electronic ground-state, reducing the dependence of the Hamiltonian to the atoms only. This is called the Born-Oppenheimer approximation, and its justification is based on the very short relaxation time of the electronic state compared with the relatively slow atomic motions. The fast electronic relaxation is a result of the large separation of their energy levels. As a consequence, the high electronic energy levels will (in general) not contribute to the partition function for the temperatures considered ($\sim e^{-\frac{\epsilon_k}{k_B T}}$), and only the ground-state degeneracy will affect Q.

Even within the Born-Oppenheimer approximation, the Hamiltonian still depends on a large number of degrees of freedom: $3N$ for N atoms in the molecule. Three degrees of freedom are associated to the global translation (center-of-mass motion). The associated partition function Q_{trans} can be evaluated using the quantized energies for the center-of-mass system submitted to periodic boundary conditions [1]:

$$Q_{trans} = \left(m \frac{2\pi k_B T}{h^2} \right)^{3/2} V \tag{2.2}$$

where the volume V can be derived from the ideal gas law $PV = k_B T$.

Next to the global translation, also the global rotation can be separated relatively easy. Still, it requires the additional assumption that the molecule has a semi-rigid structure. Only then, the molecule can be treated as a solid object

with (fixed) principal moments of inertia $I_x I_y I_z$. For such an object, the global rotational partition function Q_{rot} can be elaborated classically, yielding:

$$Q_{rot} = \frac{1}{\sigma} 8\pi^2 \sqrt{\left(m \frac{2\pi k_B T}{h^2}\right)^3 I_x I_y I_z} \tag{2.3}$$

where σ is the symmetry number of the global rotation. It is a classical *ad hoc* factor to avoid over-counting in the underlying summation over energy levels [1].
Within the same assumption of a semi-rigid structure, the Harmonic Oscillator (HO) model is used to describe the $3N-6$ remaining (internal) variables θ_i. It assumes that only (very) small deviations of the reference structure are taking place, **and** that the potential energy variation is quadratic in all internal variables. This leads to a quadratic form of both potential and kinetic energy, where in the latter the moments of inertia are fixed (*i.e.* not θ_i-dependent) due to the rigid molecule approximation. Eigenvalues of the matrix representation of the Hamiltonian generate the vibrational temperatures $\Theta_i = \frac{h\nu_i}{k}$ of the various modes. The global partition function Q_{int} corresponding with the internal vibrational modes can be factorized as a product of individual partition functions q_i associated with each 'normal mode':

$$q_i = \frac{e^{-\Theta_i/2T}}{1 - e^{-\Theta_i/T}} \tag{2.4}$$

when Θ_i is expressed in Kelvin. **The HO model is the standard approach for the evaluation of the molecular partition function.**
This HO approach is implemented in most of the commercially available molecular modelling software packages such like Gaussian [12, 13] (more details are found on the website [25] of GAUSSIAN).

However, most molecules cannot be considered as rigid bodies, and hence the HO approach represents not the most appropriate way of describing some selective internal modes. Incorrect partition functions may lead to an inadequate reproduction of molecular properties. Still, even for flexible molecules, most of potential energy surface can be considered quadratic. Only for a few (combinations of) internal coordinates, the energy landscape is essentially non-quadratic, giving rise to large amplitude 'vibrations' with significant structural changes. The most common of these anharmonic motions are internal rotations (IRs). A textbook example is butane, characterized by two methyl rotations, and one ethyl rotation. The potentials are essentially anharmonic (see Chapter 3).

In the literature a multitude of approaches has been proposed to handle these modes. All of them can be cast under the label of the Hindered Rotor (HR) model, since they are all based on the same assumptions. They all differ in their specific implementation. All HR schemes rely on the potential energy variation along the large amplitude path(s). There exist various levels of theory to describe this potential energy function: in a very rude description it is constructed with the help of tabulated values [26, 27, 28, 29, 30]; in a more advanced model it can be described by means of spectroscopic energy levels; but the most accurate method relies on ab initio calculations. Next to the potential energy description the way of handling the kinetic energy contribution can largely differ in various models. A crucial ingredient in the kinetic energy term is the moment of inertia. It can vary under influence of the internal rotation, or it can be approximated as a constant derived from the equilibrium conformation. In a decoupled description (decoupled from other internal modes) each internal rotation can be handled separately and this approach is computationally very attractive and successful [5, 2]. For the specific internal rotation under consideration a more appropriate partition function can be constructed, instead of the incorrect HO prediction [6]. The internal modes differing from the large amplitude modes remain described in the HO approximation.
The specific implementation of the HR approach depends on the choices made in reproducing the potential energy, the moments of inertia and the way of correcting the HO results. An overview of the various schemes of the HR procedure is given in the introduction of chapter 9.

The improvement and standardization of the HR approach is the ultimate goal of this thesis. Numeric applications of the various HR schemes reveal a surprisingly satisfactory success of the most simple approach (with a 1D rotational potential surface from first principles indeed). In this thesis attempts are made to come up with physically relevant arguments why the most simple version of 1D-HR models succeed in a correct description of thermochemical properties.

2.2 The 1D-HR model

The primary task is to introduce a specific implementation of the HR approach, combining both efficiency and accuracy.
Since most molecules contain several internal rotations $\phi_1, \ldots, \phi_n$, the potential energy surface is multi-dimensional, increasing the complexity of the equation(s) to be solved.
In first instance, we may assume that the multi-dimensional potential energy V^{nD} is composed of one-dimensional contributions according to:

$$V^{nD}(\phi_1, \ldots, \phi_n) = \sum_{i=1}^{n} V_i^{1D}(\phi_i) \tag{2.5}$$

This approximation is still commonly used, and describes in a reasonable way the main features of the multi-dimensional surface, although a lot of conformations are missing. In our 1D-HR model we construct each of these one-dimensional potential functions by evaluating:

$$V(\phi_i) = \min_{\forall \theta_k \neq \phi_i} V(\theta_1, \ldots, \theta_{3N-6}) \tag{2.6}$$

on a one-dimensional grid in the specific torsional angle with grid increments of 5° (72 evaluations). This method is far more accurate than previous ab initio HR implementations, where 1D rotational potential energy curves are constructed on basis of some stationary points.

The calculation of the partition function can be performed either quantum mechanically or classically.

- Within the one-dimensional quantum-mechanical approach, the energy levels are obtained from the Schrödinger equation:

$$\left[-\frac{\hbar^2}{2I_i^{red}}\frac{\partial^2}{\partial\phi_i^2} + V_i(\phi_i)\right]\psi_{ki}(\phi_i) = \epsilon_{ki}\psi_{ki}(\phi_i) \tag{2.7}$$

  The energy levels ϵ_{ki} are used to evaluate the 1D partition function q_i of the i^{th} rotation:

$$q_i = \frac{1}{\sigma_i}\sum_k g_k e^{-\frac{\epsilon_{ki}}{k_B T}} \tag{2.8}$$

  where σ_i is the symmetry number of the internal rotation, and g_k the degeneracy of energy level k.

- The classical expression on the other hand is derived from an integration in phase space. The kinetic contribution is easily elaborated. The partition function is found after an one-dimensional integration of the potential energy contribution [1]:

$$q_i = \frac{1}{\sigma_i} \frac{\sqrt{2\pi k_B T I_i^{red}}}{h} \int e^{-\frac{V_i(\phi_i)}{k_B T}} \mathrm{d}\phi_i \tag{2.9}$$

The values resulting from both approaches should converge for increasing temperature [14].

Next to the potential energy, also the (reduced) moment of inertia I_i^{red} ($\sim$ kinetic energy) of the internal rotation is an important quantity. It is defined in Ref.[3], and includes coupling effects with the global rotation. For symmetric tops it reduces to

$$I_i^{red} = I_i \left(1 - \sum_{k=x,y,z} \gamma_k^2 \frac{I_i}{I_{gl,k}} \right) \tag{2.10}$$

with γ_k the direction cosines between the rotational axis and the axes of inertia of the global molecule, I_i the moment of the top, and $I_{gl,k}$ the moments of inertia of the global molecule. From this simple case of symmetric tops it becomes clear that the reduced moment has a unique value, while the 'raw' moment of inertia depends on which part of the molecule is kept fixed in space.

Once the HR partition function has been constructed, the next step is to determine the correct HO partition function which has to be replaced by the HR prediction. There is only one method which is correct: instead of using the eigenfrequency of the vibrational eigenmode, one needs the real frequency of the HO potential fitting the rotational potential at the equilibrium geometry. Its computation requires evaluation of the second derivative of the 1D potential energy at the minimum $\left.\frac{\partial^2 V_i^{1D}}{\partial \phi_i{}^2}\right|_{eq}$. Its frequency (or vibrational temperature $\Theta_i = \frac{h\nu_i}{k_B}$) is proportional to the ratio $\sqrt{\left.\frac{\partial^2 V_i^{1D}}{\partial \phi_i{}^2}\right|_{eq} / I_i^{red}}$ with the reduced moment of inertia I_i^{red}. With this vibrational temperature, the HO partition function $q_{1D,i}^{HO}$ is constructed, which has to be replaced by the corresponding HR partition function q_i.

Repeating this procedure for each internal rotation, we get the total partition function of the molecule within the 1D-HR model:

$$\begin{aligned} Q_{tot}^{1D-HR} &= Q_{tot}^{HO} \prod_{i=1}^{n} \frac{q_i}{q_{1D,i}^{HO}} \\ &= Q_{tot}^{HO} \prod_{i=1}^{n} \kappa_{1D-HR,i} \end{aligned} \tag{2.11}$$

Q_{tot}^{HO} represents the total HO partition function as resulting from most of the commonly used ab initio packages, while the scaling factor $\kappa_{1D-HR,i} = q_i/q_{1D,i}^{HO}$ stands for the ratio of HR over HO treatment of a one-dimensional rotation, following the procedure as mentioned above.
A potentially acceptable and conceivable extension is the transferability of this ratio to the total multi-dimensional treatment. This assumption offers an *ad hoc* solution for combining the one-dimensional HR results with the complete description, but with a strong physical motivation.

Partition functions are not directly measurable observables, but through use of mathematical expressions they are related to well-known thermodynamic quantities, such like the entropy S and heat capacity C:

$$S = R\left(\ln Q + T\left(\frac{\partial \ln Q}{\partial T}\right)\right) \tag{2.12}$$

$$C = RT\left(2\frac{\partial \ln Q}{\partial T} + T\frac{\partial^2 \ln Q}{\partial T^2}\right) \tag{2.13}$$

These observables are experimentally accessible and constitute an ideal test to validate the HR-model.

As initial test-set, a series of n-alkanes is used (from ethane to decane) for which experimental data are available. These hydrocarbons form linear chains with single C-C bonds about which internal rotations can take place. In addition, they are generally well-described within DFT [9, 10] and use of the hybrid functional: B3LYP/6-311g** [7, 8].
A detailed discussion of the application of 1D-HR on entropy and heat capacity results for n-alkanes is given in chapter 3. Figures 2.1 and 2.2 display some summarizing results. These plots show very clearly that a correct treatment of the IR leads to an almost perfect agreement between theoretical and experimental estimates, especially for the entropy. The HO predictions seem to underestimate systematically the experimental values. For the heat capacity, the discrepancy between 1D-HR predictions and experiment is somewhat

larger, but within acceptable range. On the contrary the HO model fails to reproduce the experimental reference values.

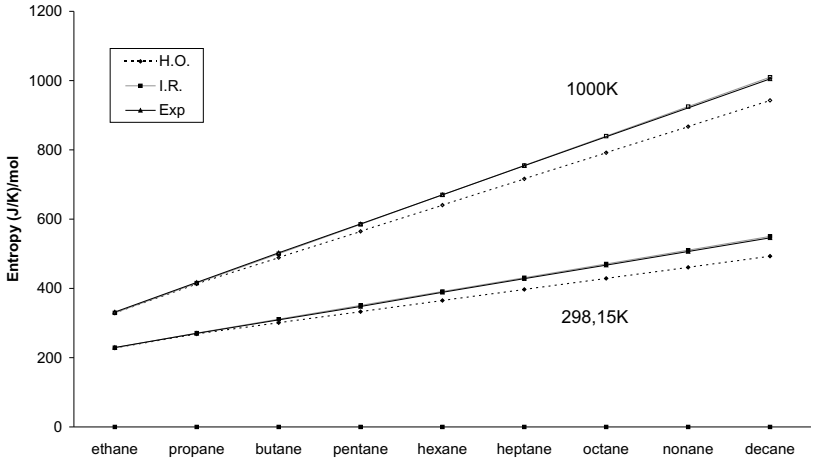

Figure 2.1: Entropy of n-alkanes at 298,15K and 1000K for increasing chain-length.

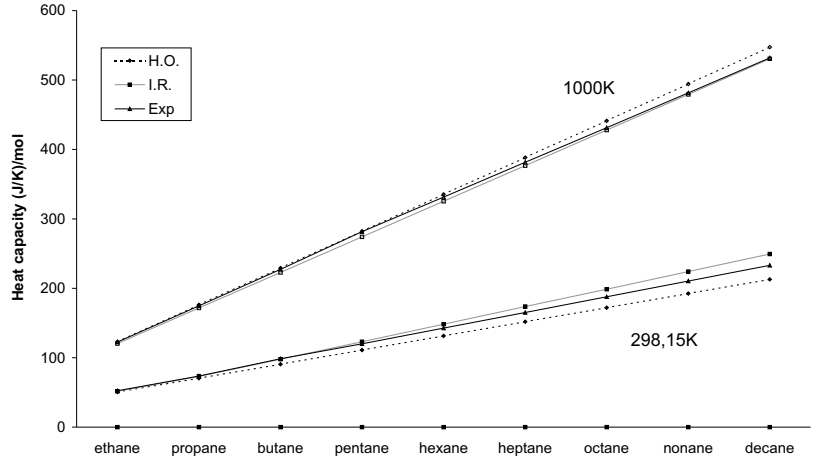

Figure 2.2: Heat capacity of n-alkanes at 298,15K and 1000K for increasing chain-length.

In chapter 8 results are given of 1D-HR calculations on n-alkanes with an hetero element (alcohols, ethers, thiols and sulfides), and the conclusions are not altered in the sense that the one-dimensional but correct treatment of internal rotations (1D-HR) yields thermochemical properties in a very satisfactory agreement with experiment. Larger discrepancies are noticed for the heat capacities, but their reproduction is very sensitive to changes of the partition functions. Second order derivatives of Q with respect to the temperature, present in the expression of the heat capacity, are submitted to larger uncertainties. A more advanced model that goes beyond the 1D-HR approximation is expected to generate only small additional corrections, leaving the reproduction of entropies unaltered but improving the curvature of the partition function with respect to the temperature.

Partition functions are also used to study the kinetics of a chemical reaction from first principles. The evaluation of macroscopical kinetic quantities such as the rate coefficient of a chemical reaction would in principle require the calculation of a large number of trajectories to create an appropriate ensemble (canonical,microcanonical,..). An averaging over all trajectories would then yield the required statistical quantities. For a better understanding of the reaction mechanism one needs a microscopic approach. This microscopic treatment requires the instantaneous evaluation of the potential energy surface in a fully ab-initio quantum mechanical way at each step on the trajectory of the reaction. Taken into consideration the number of different configurations that should be calculated with the computationally very expensive ab initio methods, this way of handling for deriving macroscopic quantities on a fully microscopic basis becomes prohibitive.
It is in this field of relating macroscopic concepts of chemical reactions with the microscopic picture of internal reorganisation of the individual molecules that *Transition State Theory* (TST) has made a decisive contribution. The concept of TST relies on static structure properties of three distinct states of the system: the reactants, the products and the transition state. Although rather old in its concept, the fundamental ideas of TST are still commonly used in chemical kinetics. Enormous progress is made in the microscopic description of the three relevant states, manifesting in a more reliable reproduction of the partition functions. Within TST the rate equation for a bimolecular reaction $A + B \rightarrow C$ is given by [31, 32]:

$$k(T) = \frac{k_B T}{h} K_C^{\ddagger} \tag{2.14}$$

$$with\ K_C^{\ddagger} = \frac{q_{\ddagger}}{q_A q_B} e^{-\frac{\Delta E_0}{k_B T}} \tag{2.15}$$

The rate constant is expressed per unit volume, per molecule and per time unit. k_B represents the Boltzmann's constant while T stands for the temperature and h is Planck's constant. The modified equilibrium constant $K_C^{\ddagger}$ is microscopically completely determined by the global partition functions of the reactants and transition state. ΔE_0 represents the molecular energy difference at $T = 0$ between the activated complex and reactants (determined in Hartree-Fock (HF) or DFT). If the zero point energies of the various vibrational modes are also taken up in ΔE_0, than the partition functions q_A, q_B and $q_{\ddagger}$ are referred to the lowest energy levels.
It is obvious that the accuracy of determining the kinetic parameters, and in particular the pre-exponential factor, is highly dependent on the quality of the partition functions obtained for the reactant(s) and transition state (for the forward reaction). Coupling with the overall rotation and/or mutual coupling with the other internal modes of the molecule are aspects which require a careful investigation.

All these considerations support a further study that goes beyond the 1D-HR approximation.
Following considerations may be valuable for further improvement of the 1D-HR formalism:

- The extension to the construction of a multi-dimensional potential energy $V^{nD}(\phi_1, \ldots, \phi_n)$ is an item to be studied attentively. This can only be accomplished by calculating the multi-dimensional partition function associated with V^{nD}, and to compare this quantity with the 1D results expressed as the product of individual 1D partition functions.

- In addition, also the (1D) reduced moments of inertia have to be upgraded to their nD equivalents. Next to the coupling with the overall rotation, also the coupling terms among the multiple internal rotation moments of inertia have to be considered.

- Since the internal rotations may induce a severe deformation of the original geometry of the molecule, the moments of inertia become highly varying functions of the various torsional angles. This feature should be incorporated in the model for calculating multi-dimensional HR partition functions, but also for an accurate evaluation of Q in the 1D-HR approach.

In the further course of this work, we will apply the classical expression for the partition function. A quantum-mechanical treatment becomes numerically almost unfeasible especially in the multi-dimensional case, or when the moments of inertia become functions of the torsional angles ϕ_i. It has been shown that for temperatures above 300 K both quantum-mechanical and classical values for the partition functions tend toward each other. If predictions are needed at lower temperatures, we will add the Pitzer-Gwinn factor [15]. This factor stands for the ratio of a quantum-mechanical HO partition function with its classical analogue. This leads to the following final expression for the 1D-HR partition function:

$$Q_{tot}^{1D-HR} = Q_{tot}^{HO} \prod_{i=1}^{n} \frac{q_i}{q_{1D,i}^{HO,Cl}} = Q_{tot}^{HO} \prod_{i=1}^{n} \kappa_{1D-HR,i} \tag{2.16}$$

2.3 The multi-dimensional nD-HR model

The most general version of the multi-dimensional nD-HR model involves the construction of both potential and kinetic energy terms as functions of all torsional angles under consideration: $V^{nD}(\phi_1,\ldots,\phi_n)$ and $\det A^{nD}(\phi_1,\ldots,\phi_n)$. The latter stands for the determinant of the kinetic energy matrix of the internal and global degrees of freedom. The construction of this matrix forms the subject of the extended 'theory section' of chapter 4 [16].
Since the calculation of the multi-dimensional energy surface V^{nD} is computationally not feasible for more than three dimensions, we limit ourselves to the calculation of V^{nD} in pentane ($n = 2$) and hexane ($n = 3$). The methyl tops are still treated in the one-dimensional approach.
We stress that a multi-dimensional approach can not be expected to become a standard method for the calculation of the molecular partition function. The computation times are too high. But a thorough study is needed to validate the various variants of the 1D-HR. We refer to this exact coupled multi-dimensional model as the reference method C1, while the 1D-HR variants are referred to as C2, C3(') and C4('). The last three methods differ in the way of calculating the moments of inertia appearing in the kinetic energy matrix.

We introduce the geometry factor $f^{nD}(\phi_1,\ldots,\phi_n)$ as the ratio of the determinants of the kinetic energy matrix A:

$$\det A(\phi_1,\ldots,\phi_n) = \det A_0 \cdot f^{nD}(\phi_1,\ldots,\phi_n) \tag{2.17}$$

where A_0 is evaluated at the equilibrium geometry of the molecule. This multi-dimensional factor cannot be determined using 1D calculations only. It is instructive to introduce some approximative schemes to describe this factor in analogy with the separation of the potential energy in several 1D contributions.

- One possibility is to propose a factorization of the geometry factor:

$$f^{nD}(\phi_1,\ldots,\phi_n) = \prod_{i=1}^{n} f_i^{1D}(\phi_i) \tag{2.18}$$

  where each f^{1D} is calculated along its specific one-dimensional large amplitude path:

$$f_i^{1D}(\phi_i) = (\det A_0)^{-1} \cdot \det A(\phi_j^{ref}(\phi_i), \phi_i) \;\; \forall j \neq i \tag{2.19}$$

  These paths are calculated according to Eq.(2.6). All variables, except ϕ_i, are allowed to relax to their equilibrium value ϕ_j^{ref} under the constraint

of fixed ϕ_i value, making them functions of this variable.
This factorization is the basic idea behind the **C2** method. The molecular partition function in this scheme retains the same form as for 1D-HR. Only the evaluation of the q_i functions is somewhat different, since a ϕ_i dependent function f_i^{1D} is added to the integrand.

- An other possibility to estimate the f^{nD} function, is the use of approximative geometries instead of ab initio calculated structures. This is possible, since (in n-alkanes) the relaxed ϕ_j^{ref} appear to vary only slightly from their values in the equilibrium geometry. We may therefore apply rigid rotations to obtain the desired geometries, and the calculation of the kinetic energy matrix is now based on these unrelaxed geometries.
A major drawback for this **C3** method, is that the integrand of the nD partition function can no longer be factorized into 1D contributions as for C2. This restricts the method's applicability to six coupled rotations, or eight when the methyl tops are treated one-dimensionally (C3').

- The most simple variant of the 1D-HR method is referred to **C4**. In this method the geometry factor turns out to be unity for all angles. We stress that the C4 method slightly differs from the standard 1D-HR (here referred to **C4'**) as outlined in previous section, since in **C4'** no coupling terms between the different internal rotations are considered. The reduced moments of inertia, entering in the expression (2.9) are exactly the diagonal elements of the kinetic energy matrix A_0. Inclusion of these coupling terms leads to a lower value of the total moments involved (at least for n-alkanes): $\det A_0 < I_x I_y I_z \prod_i I_i^{red}$.

A schematic overview of the different approximative schemes is given in Table 2.1 for the specific case of two internal rotations with rotational angles ϕ_2, ϕ_3.

To validate all these methods we apply them to the same test-set as before: n-alkanes, up to decane. The results are presented in Fig.2.3. Part (a) displays the deviations of the calculated entropy from the reference values found in the literature as a function of the alkane chain length. The divergent behavior of the C2 and C4 suggests that those implementations have no physical relevance. The three other schemes fulfill the convergence criterium and are valuable candidates. Obviously, the C4' model, or 1D-HR, is selected as the most cost-efficient method. Contrary to the entropy, the heat capacity turns out to be rather insensitive to the specific approach [Figs.2.3(b) and (c)].

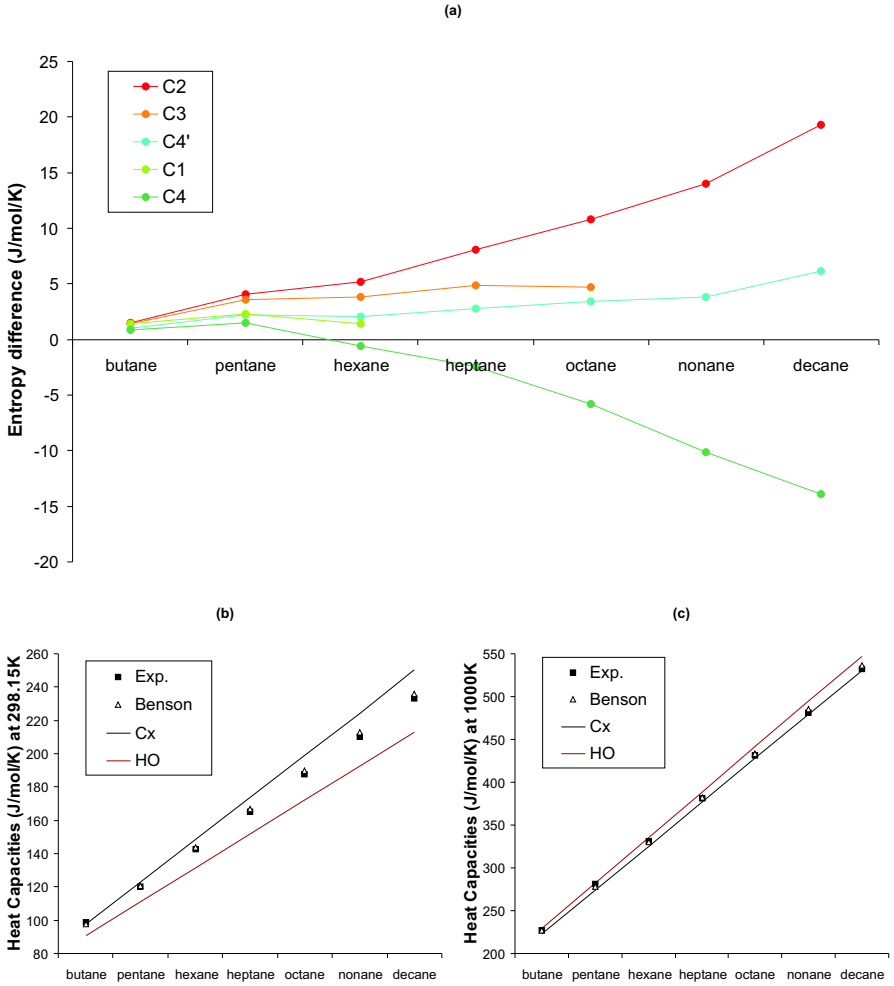

Figure 2.3: (a) Entropy difference between calculated and experimental values for *n*-alkanes. (b),(c) Heat Capacities at 298.15K and 1000 K in the various models together with experimental values.

	Approximate schemes		
level	$V(\phi_2,\phi_3)$	$A(\phi_2,\phi_3)$	$f(\phi_2,\phi_3)$
C1	2D-PES geometry optimization	$\Rightarrow$ full construction	$\Rightarrow$ full construction
C2	1D-PES geometry optimization $V(\phi_2)+V(\phi_3)$	$\Rightarrow A(\phi_2)$ $\Rightarrow A(\phi_3)$	$\Rightarrow f_2(\phi_2)$ $\Rightarrow f_3(\phi_3)$
C3	1D-PES geometry optimization $V(\phi_2)+V(\phi_3)$	full construction no geometry optimization	$\Rightarrow$ full construction no geometry optimization
C4	1D-PES geometry optimization $V(\phi_2)+V(\phi_3)$	A_0	1
C4'	1D-PES geometry optimization $V(\phi_2)+V(\phi_3)$	A_0' $(\Lambda_{23}'=0)$	$f=\frac{detA_0'(\Lambda_{23}=0)}{detA_0}$

Table 2.1: Schematic overview of the various HR schemes under consideration in case of two coupled internal rotations.

2.3.1 Branched alkanes

Before going into detail about the performance of the various schemes compared to C1 in n=pentane and n-hexane, we discuss the results of the 1D-schemes on some branched alkanes.

Next to linear molecules such a n-alkanes, one can question whether the above-mentioned observations are still valid for molecules with side branches. For this purpose we apply the various 1D-HR methods to three branched alkanes (2-methyl butane, 2-methyl pentane, en 3,3-di-methyl pentane). To a large extent the conclusions remain the same: the predictions for entropy are in fair agreement with the experiment. On the contrary the reproduction of heat capacities is less satisfactory (this item is discussed in detail in Chapter 4). This is very remarkable, since neither of the HR models succeed in doing better than the crude HO approximation. We are not able to get round this peculiar phenomenon. Especially at high temperatures this deviant behavior attracts attention. There is no obvious reason for this failure, except maybe the strong coupling between the branched chains. The vibrational (HO) analysis reveals the presence of some low-energetic vibrational modes corresponding with the relative movement of the different chains. Since (these) low frequency modes are a dominant factor in the determination of the molecular partition function, a more extended HR description should incorporate these modes, or at least treat in a correct way their dependence on the various (one-dimensional) internal rotation paths.

2.3.2 The 2D-HR description of n-pentane

In this paragraph an extensive comparative study between 1D-HR and 2D-HR models is performed. The two models have been applied to n-pentane. This linear molecule contains two consecutive rotations of an ethyl group and two ending methyl groups. Within 2D-HR the potential energy V^{2D} can exactly be constructed and correct partition functions for the internal modes be derived. In this context n-pentane is an ideal molecule to validate the various approximative models. The two-dimensional rotational potential energy surface $V^{2D}(\phi_2, \phi_3)$ (of the two ethyl rotations ϕ_2 and ϕ_3) is easily constructed and the various energy and minima are displayed in Table 2.2 while the values of the geometry factor f^{2D} [defined in Eq.(2.17)] at the stationary points are given in Table 2.3.
A comparative analysis of both 2D-HR and 1D-HR data learns that there are distinct differences in describing the two-dimensional potential surface. Some local minima are not present on the surface constructed in the 1D-approach. In addition the energy barriers between two minima are somewhat underestimated in 1D-HR, resulting to an overestimation of the Boltzman factor in the integrand of Eq.(2.9).

In Table 2.3 we also take up the average values $\langle f(\phi_2, \phi_3) \rangle$ for each level of model. With respect to the reference value of 1.36, corresponding with the exact coupled C1 model, we note that the rigid-rotation model C3 comes closest to C1, that the smallest value is given by C4, and the largest by C2.
The small $\langle f(\phi_2, \phi_3) \rangle$ values for C4 and C4' (1.00 and 1.19) may compensate the errors introduced by the 1D approximation of the potential energy. Indeed, the cumulating effect of the two opposite corrections leads to a global cancellation of errors for the C4' method: its results are almost coinciding with the C1 results (for entropy and heat capacity). This particular feature lies on the origin of the apparently systematic success of the relatively simple 1D-HR model.
It is striking that for each Cx method, the predicted entropy differences with experiment behave in a similar way as the relative values of $\langle f(\phi_2, \phi_3) \rangle$ (see Figure 2.3(a)).
Summarized:

Effect on Q	**C1**	**C2**	**C3**	**C4**	**C4'**
Kinetic energy contribution	reference	++	0	− −	−
Potential energy contribution	reference	+	+	+	+
Global effect	reference	+++	+	−	0

Energy Minima of $V^{2D}(\phi_2, \phi_3)$

Type	Symmetry	ϕ_2	ϕ_3	ΔE(kJ/mol)
tt	C_{2v}	0	0	0.0000
tg-	C_1	0	115	3.62
tg-	C_1	115	0	3.62
tg+	C_1	0	245	3.62
tg+	C_1	245	0	3.62
g-g-	C_2	115	115	6.74
g-g+	C_1	115	270	13.96
g-g+	C_1	85	245	13.96
g+g-	C_1	245	85	13.96
g+g-	C_1	270	115	13.96
g+g+	C_2	245	245	6.74

Energy Maxima of $V^{2D}(\phi_2, \phi_3)$

(0,60),(60,0),(300,0),(0,300)	12.84
(0,180)(180,0)	23.70
(60,60)(300,300)	28.94
(180,60)(180,300),(60,180),(300,180)	39.30
(300,60)(60,300)	29.04
(180,180)	69.81

Energy Minima of $V^{1D}(\phi_2) + V^{1D}(\phi_3)$

(0,0)	0
(0,115)(115,0),(0,245),(245,0)	3.62
(115,115)(115,245),(245,115),(245,245)	7.24

Energy Maxima of $V^{1D}(\phi_2) + V^{1D}(\phi_3)$

(0,60),(60,0),(300,0),(0,300)	12.84
(0,180)(180,0)	23.70
(60,60),(300,60),(60,300),(300,300)	23.70
(180,60)(180,300),(60,180),(300,180)	36.54
(180,180)	47.40

Table 2.2: The minima and maxima on the potential energy surfaces (1D en 2D) of the ethyl rotations in pentane.

	C1	C2	C3	C4	C4'
Minima					
(85,0)	1.51	1.51	1.54	1.00	1.19
(275,0)	1.51	1.51	1.54	1.00	1.19
(0,85)	1.51	1.51	1.54	1.00	1.19
(0,275)	1.51	1.51	1.54	1.00	1.19
(85,85)	1.88	2.29	1.83	1.00	1.19
(275,85)	2.00	2.29	1.96	1.00	1.19
(85,275)	2.00	2.29	1.96	1.00	1.19
(275,275)	1.88	2.29	1.83	1.00	1.19
Maxima					
(180,0)	0.86	0.86	0.83	1.00	1.19
(0,180)	0.86	0.86	0.83	1.00	1.19
(180,180)	0.61	0.73	0.58	1.00	1.19
$\langle f(\phi_2,\phi_3)\rangle$	1.36	1.46	1.34	1.00	1.19

Table 2.3: The geometry factor in the potential energy minima and maxima of pentane.

A similar study on n-hexane, using 3D-HR, confirms these results and conclusions.

2.3.3 The 2D- en 3D-HR description of n-hexane

In analogy with the previous subsection a detailed conformational analysis is made for n-hexane. For this molecule an exact 3D-HR calculation has been performed, which is just within the computational feasibility of the current workstations. This study enables us to investigate the possible impact of higher order coupling of multiple internal rotations on the results. To what extent the 3D-HR model performs better than consecutive 2D-HR treatments?
This issue is extensively studied in Chapter 5 [17]. It has been shown that an expansion according to:

$$V^{mD}(\phi_1,...,\phi_m) \approx \sum_{i=1}^{m-1} V^{2D}_{i(i+1)}(\phi_i,\phi_{i+1}) - \sum_{i=2}^{m-1} V^{1D}_i(\phi_i) \qquad (2.20)$$

is able to accurately construct the true three-dimensional potential surface in n-hexane: it generates all conformations, it includes all major coupling effects, situated near the g_-g_+ conformations of consecutive internal rotations. The expansion suggested in Eq.(2.20) is valid for any number m (> 2) representing

the number of 'real' internal rotations, except for the methyl tops which are treated one-dimensionally: $V^{nD} = V^{mD} + \sum_j V^{1D}_{Me,j}$, and $f^{1D}_{Me,j} \equiv 1$.
Similarly to Eq.(2.20) a factorization of the multi-dimensional geometry factor f^{nD} is proposed:

$$f_A^{mD}(\phi_1, \ldots, \phi_m) \approx \frac{\prod_{i=1}^{m-1} f^{2D}_{A,i(i+1)}(\phi_i, \phi_{i+1})}{\prod_{i=2}^{m-1} f^{1D}_{A,i}(\phi_i)} \tag{2.21}$$

These two approximations for constructing the multi-dimensional potential and geometry factor incorporate the coupling between adjacent internal rotations only.

Results are displayed in Figure 2.4 and reveal that both the 1D- and 2D-HR approximations closely approach the 3D-HR reference on the level of partition function and heat capacity. Still, the 2D-HR method with incorporation of consecutive coupling effects is nearly identical to the 3D-HR approach. It represents a valuable alternative for a complete mD-HR description whenever a high quality reference level is needed. It will be used in our study on alcohols, ethers, thiols and sulfides of chapter 7, where 1-hexanol and 1-hexane thiol ($m = 5$) are treated within this scheme.

At this stage the simple 1D-HR model remains standing as the best compromise between accuracy and computation time.

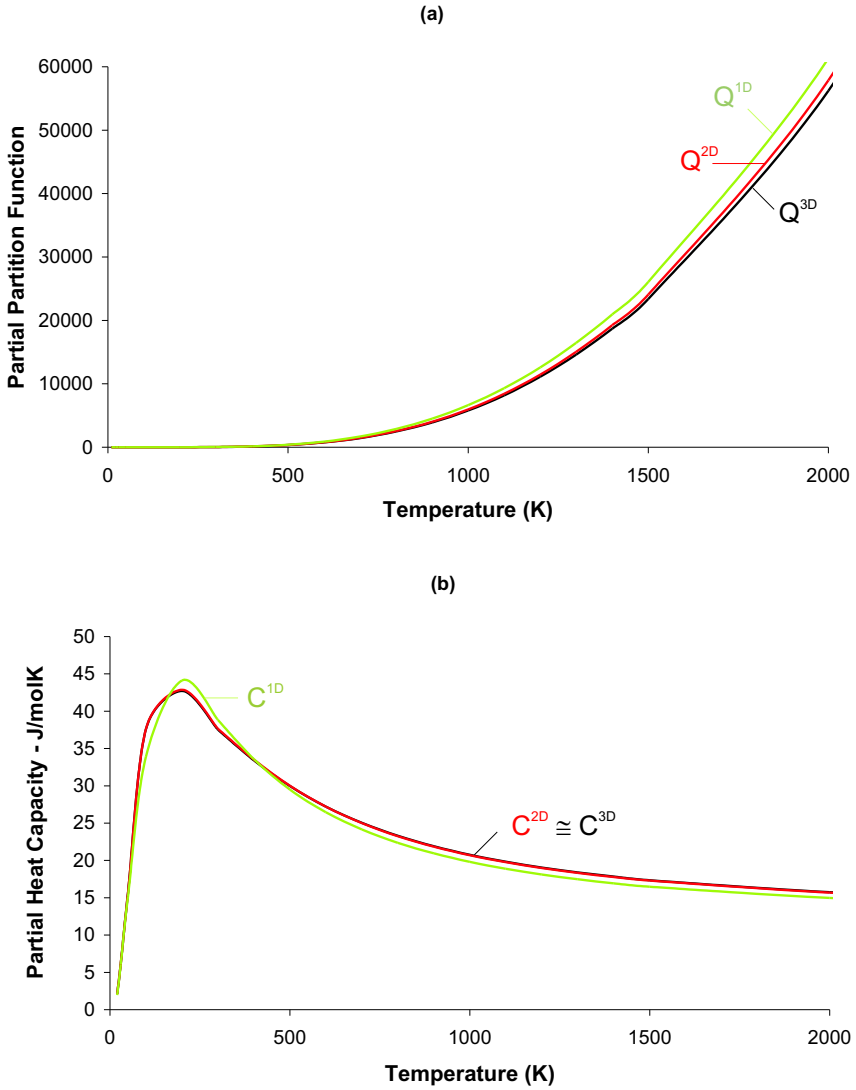

Figure 2.4: (a) Partition function and (b) heat capacity of the three internal rotations of *n*-hexane calculated with the exact model (Q^{3D}, C^{3D}), with the 2D-approximation (Q^{2D}, C^{2D}), and with the 1D-scheme (Q^{1D}, C^{1D}).

2.4 Ethers, alcohols, sulfides and thiols

In addition to the studied hydrocarbons, we investigate in how far previous findings are still valid for n-alkanes with an hetero element O or S: ethers, alcohols, sulfides and thiols. These molecules are also linear but the presence of an hetero element can disturb the conclusions made in previous subsections. Since we are now working with compounds containing the hetero elements O and S, a new level of theory analysis has to be performed. As mentioned before, the B3LYP/6-311g** level was found to produce accurate energy differences and barriers between conformers in hydrocarbons. For ethers and alcohols however, the preferred level of theory was shown to be B3LYP/6-31+g(d) (see Chapter 6 [18]), while for sulfides and thiols both levels turn out to be appropriate.

As the evaluation of partition functions strongly depends on the shape of the potential energy surface, it is instructive to investigate all possible conformers for this extended set of molecules. This conformational study will reveal substantial differences with the well-known n-alkanes, for which a set of rules has been developed to generate all possible conformers [19].
We were able to devise a similar set of rules to predict the conformers of each series of ethers, alcohols, sulfides and thiols. The results for ethers and sulfides are summarized in Table 2.4. Alcohols and thiols show a slightly different pattern and their behavior is discussed in detail in chapter 6.

These rules constitute a very interesting tool, but an accurate reproduction of partition functions requires more than knowledge about the existence of conformers. Also the energy barriers between these conformers have their impact on the partition function. The most appropriate method to gain this information is the construction of a multi-dimensional potential energy surface, but in view of a cost efficient tool we investigate whether the energy barriers are well reproduced within a one-dimensional approximation according to Eq.(2.6). The results discussed in Chapter 6 undoubtedly illustrate that this is not the case. Only a 2D-approximation following Eq.(2.20) is found to be sufficiently adequate to reproduce the energy minima within acceptable accuracy. Hence, one could expect that the 2D-HR model would represent a viable alternative, while 1D-HR would fail.
The success of the simple 1D-HR approach in n-alkanes is based on a coincidental cancellation of errors generated by an incorrect description of potential

Double gauche conformers:	$\phi_{s1}\phi_{l1}$	$\phi_{l1}\phi_{l2}$	$\phi_{l2}\phi_{l3}$	$\phi_{l3}\phi_{l4}$
Tasi	**Ethers:**			
$g\_g\_$	$x\_Ox\_$	$Og\_g\_$	$Otg\_g\_$	$Ottg\_g\_$
g_x_+	(x_Ox_+)		$Otg\_x'_+$	$Ottg\_x_+$
x_g_+				$Ottx\_g_+$
Tasi	**Sulfides:**			
$g\_g\_$	$g\_Sg\_$	$Sg\_g\_$	$Stg\_g\_$	$Sttg\_g\_$
g_x_+	g_Sx_+		$Stx'\_x'_+$	$Sttg\_x_+$
x_g_+	x_Sg_+	Sx_g_+		$Sttx\_g_+$

Triple gauche conformers:	$\phi_{s1}\phi_{l1}\phi_{l2}$	$\phi_{l1}\phi_{l2}\phi_{l3}$	$\phi_{l2}\phi_{l3}\phi_{l4}$
Tasi	**Ethers:**		
$g\_g\_g\_$	$x\_Ox\_g\_$	$Og\_g\_g\_$	$Otg\_g\_g\_$
$g_+x\_g\_$			
$x_+g\_g\_$			$Otx'_+g\_g\_$
$x\_g_+x\_$			$Otx'\_g_+x\_$
$g\_g\_x_+$		$Og\_g\_x'_+$	$Otg\_g\_x_+$
$g\_x\_g_+$			$Otg\_x\_g_+$
Tasi	**Sulfides:**		
$g\_g\_g\_$	$g\_Sg\_g\_$	$Sg\_g\_g\_$	$Stg\_g\_g\_$
$g_+x\_g\_$	$g_+Sx\_g\_$		$Stx'_+x'\_g\_$
$x_+g\_g\_$	$(x_+Sg\_g\_)$	$Sx_+g\_g\_$	
$x\_g_+x\_$		$Sx\_g_+g\_$	$Stx\_g_+x\_$
$g\_g\_x_+$		$Sg\_g\_x_+$	$Stg\_g\_x_+$
$g\_x\_g_+$	$g\_Sx\_g_+$	$Sg\_x\_g_+$	$Stg\_x\_g_+$
			$Stg\_x'\_x'_+$

The conformers given between brackets occur for the smallest molecules only, and are of no importance for the general behavior of (longer) ethers/sulfides.

Table 2.4: Overview of alterations of Tasi's rule for alkane conformers in ethers and sulfides.

energy surface and moments of inertia. Due to the completely different behavior of the conformers in this new training set, this balance may be disturbed. The various results are discussed in Chapter 7 [20], and validated with respect to the experimental values of the entropy and heat capacity and with respect to the other non-HR based ab initio calculations available in the literature.

It may be concluded that the accuracy of both entropy and heat capacity predictions for ethers and alcohols is very good, and of the same order as in n-alkanes. And this success is accomplished in both 1D-HR and 2D-HR models. In particular the good performance of the 1D-HR approximation is rather surprising in view of the above-made concerns.
For the sulfur compounds on the contrary, the assessment is less satisfying: the entropy reproduction is still within acceptable accuracy, but the ab initio calculated heat capacities show substantial deviancies from the reference values obtained from the literature. As for branched alkanes, these compounds exhibit

several low vibrational modes which are no internal rotations. These modes are large amplitude vibrations of the entire backbone of the linear molecules. They are also observed in the other investigated linear molecules (n-alkanes, ethers, alcohols), but their vibrational frequencies are much higher. The large mass of the sulfur atom –compared to C or even O– lies on the origin of a lower frequency for these modes ($\sim \sqrt{m^{-1}}$).
These findings suggest the development of a more extended hindered rotor model (EHR) taking into account the coupling with **all** other vibrational internal modes different from internal rotations.

2.5 Extension of the HR-formalism to four-membered rings

In this subsection the HR method is applied to compounds with one single large amplitude vibration. It has been stressed that the HR degree of freedom should not necessarily represent a torsional angle corresponding with a specific internal rotation. It can stand for any internal mode. Typical in cyclic molecules are the so called ring-puckering modes. They cause a significant deformation of the ring. Four-membered rings show only one such mode, and are ideal candidates to extend the practical implementation of the (E)HR methods to these non-IR motions.

In a first study of four-membered rings (chapter 8 [21]), we investigate cyclobutane, and eight derived molecules by substitution of a CH_2 fragment: oxetane, thietane, azetidine and phosphetane constitute the first class in which CH_2 is replaced by respectively O, S, NH en PH, all endo-substitutions. The class of exo-substituted four rings contains cyclobutanone, cyclobutanethione, cyclobutylideneamine and cyclobutylidenephosphine, where CH_2 is replaced by $C{=}O$, $C{=}S$, $C{=}NH$ and $C{=}PH$ respectively. A vibrational analysis confirms

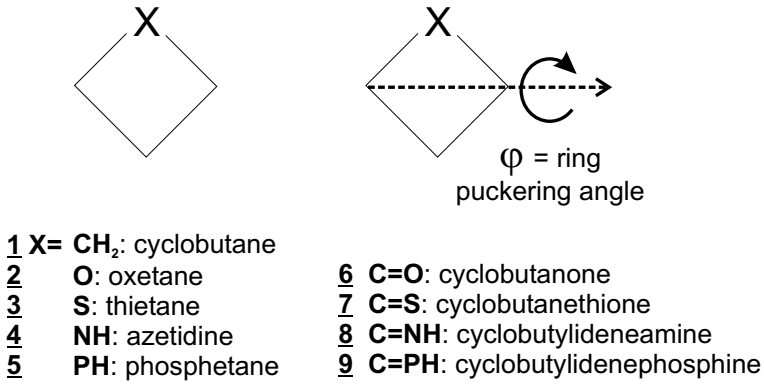

Figure 2.5: Definition of the ring-puckering dihedral in four-membered carbon rings with a single substitution.

that the lowest mode corresponds with the ring-puckering mode for all these molecules.

To our knowledge no theoretical study with application of the HR-formalism

has been performed earlier. In order to validate all possible models that can be applied to this puckering mode, we also perform the classical as well the quantum-mechanical version of 1D-HR. The conclusions are not altered with respect to those drawn when studying internal rotations: for temperatures above room temperature the differences between the classical and quantum-mechanical implementation of 1D-HR are minor.

The corrections on the thermodynamic properties (HR versus HO approach)

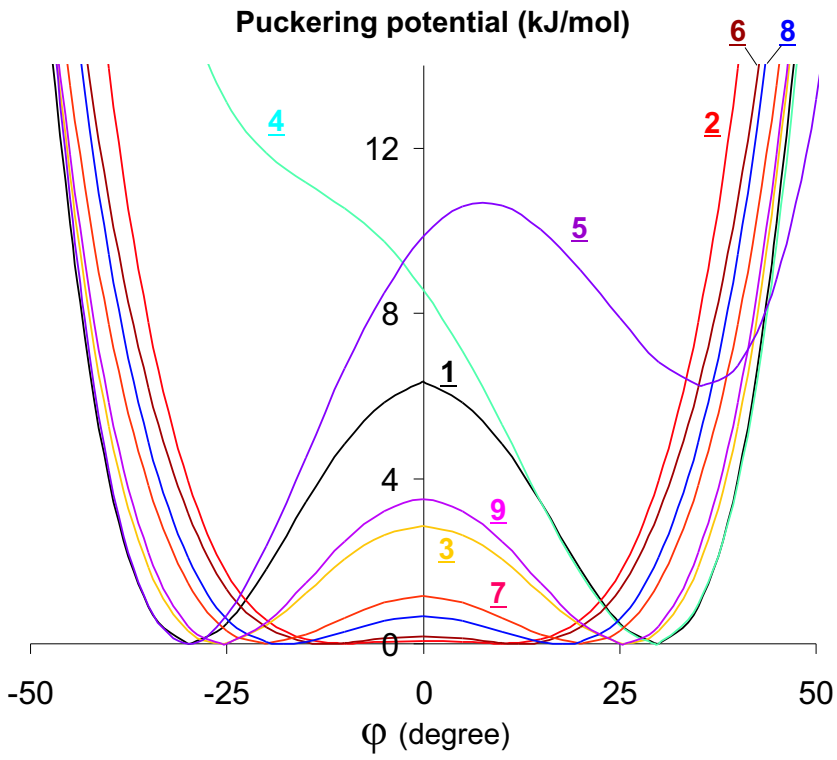

Figure 2.6: Potential energy profiles of cyclobutane **1**, oxetane **2**, thietane **3**, azetidine **4**, phosphetane **5**, cyclobutanone **6**, cyclobutanethione **7**, cyclobutylideneamine **8**, and cyclobutylidenephosphine **9**.

are almost completely determined by a correct use of the symmetry number of the puckering mode. Contrary to internal rotations, the potential energy variation of the ring-puckering (Fig.2.6) tends to infinity for $\varphi \rightarrow \pm\pi$. This means that the HO-formalism is not completely inappropriate, since it models the 'walls' rather well.

2.6 The EHR-model

In previous subsections, it has been shown that the Hindered Rotor model fails in some specific applications and that this failure can probably be attributed to the presence of other low vibrational modes. This would imply that the HR models are incomplete, and that they should be extended. The 'missing' low vibrational modes in HR models are treated uncoupled and described within the HO description. Moreover the characteristics of these modes are deduced without taking into account the dynamics of the system: they are fixed at the equilibrium geometry of the molecule [Eq.(2.16)], ignoring the dynamical effect under influence of the internal rotation(s) occurring in the molecule (structural changes). To some extent the description of these low vibrational modes should involve coupling terms taking into account the dynamical change of the molecular structure in a proper way.

In chapter 9 [22] we introduce the Extended Hindered Rotor (EHR) model. It addresses all concerns formulated above.
The proposed EHR model is based on entirely consistent grounds: **all** variables (internal and global degrees of freedom) are treated on an equal footing. Hence, it incorporates several coupling terms: coupling of the global rotation with the internal modes, and coupling of the large amplitude modes with the other vibrations.

- The global rotation coupling originates from the Coriolis terms in the kinetic energy. These terms are difficult to include in a quantum mechanical description, and are usually ignored in existing models in literature for calculating energy levels of (coupled) vibrations which are useful in spectroscopical applications. However, reproduction of energy levels is not the scope of this work, and we can rely on a classical desciption of the global rotation. This allows us to introduce a set of frames in which the Coriolis terms vanish at all times.
  A major drawback of this approach of varying frames is that the dynamics of the 'zero Coriolis' frame is essentially unknown. For the classical evaluation of the partition function however, these dynamics are not needed. The rotational partition function is determined by the values of the principal moments of inertia. Along the large amplitude path, the geometry of the molecule will change, and hence also the principal moments are submitted to fluctuations.
- The internal coordinates are split into two sets. The first set contains

the large amplitude variables φ, *e.g.* dihedral angles to generate internal rotations, for which the potential energy variation $V(\varphi)$ is calculated on a grid as for the nD-HR approaches. For each of the data points on the grid, the other set of (vibrational) variables Θ are optimized in order to ensure a 'constrained' minimum of potential energy. At the same time the corresponding Hessian matrix H is calculated. This Hessian is now dependent of the constraints φ, and involves the potential energy coupling of the large amplitude motions with the vibrations.
For each of these optimized geometries a kinetic energy matrix $A(\varphi)$ can be constructed, describing the kinetic coupling between the internal variables.

The HO based (partial) partition function of the vibrational coordinates Θ as a function of φ can now be evaluated based on the total Hamiltonian consisting of the total potential energy $V(\varphi) + \frac{1}{2}\Theta^T H(\varphi)\Theta$ and the kinetic energy $A(\varphi)$. The so-obtained function is now inserted in the classical partition function expression, leading to the final EHR molecular partition function. For the case of a one-dimensional φ, the total partition function in the EHR approach can be written as:

$$\begin{aligned} Q_{tot}^{EHR} &= Q_{trans}(T)\; K(T) \\ &\int_0^{2\pi} \mathrm{d}\varphi \sqrt{A_\varphi(\varphi)}\; e^{-\beta V^{HR}(\varphi)} \prod_{i=2}^{n} Q_i^{HO}(\varphi,T)\; Q_{rot}(\varphi,T) \end{aligned} \tag{2.22}$$

with $K(T) = \sqrt{\frac{2\pi k_B T}{h^2}}$, and A_φ the moment of inertia along the large amplitude path. It incorporates all kinetic coupling effects with the other (global and internal) motions.
In analogy with the HR methods, we still need to multiply this with the Pitzer-Gwinn correction factor $\frac{Q_\varphi^{HO,QM}}{Q_\varphi^{HO,Cl}}$.
For details we refer to chapter 9.

In order to be able to rewrite the formula of the total EHR partition function into a more transparent form we introduce a geometry factor

$$f_A(\varphi) = \sqrt{\frac{A_\varphi(\varphi)}{A_\varphi(0)} \frac{I_x(\varphi) I_y(\varphi) I_z(\varphi)}{I_x(0) I_y(0) I_z(0)}} \tag{2.23}$$

which is formally the same as the factor used in the nD-HR method, but with the reduced moment of inertia replaced by A_φ. This moment is different since it is calculated with inclusion of all degrees of freedom, whereas the reduced

moment is constructed in a model of reduced dimensionality.
This factor will be largely different from unity for deformed structures. This is discussed in chapter 4 for the 2D-HR geometry factor of n-pentane. The EHR geometry factor shows a similar behavior, but since a different IR moment of inertia is used some important changes are noted.
We also introduce the vibrational correction factor

$$f_{vib}(\varphi,T) = \frac{\prod_{i=2}^{n} Q_i^{HO}(\varphi,T)}{\prod_{i=2}^{n} Q_i^{HO}(0,T)} \tag{2.24}$$

which is dependent of φ **and** of the temperature.
This factor is very sensitive to the variation of the non-IR low frequency HO partition functions. Small variations of these frequencies will result in large variations of the ratio of the partition functions involved.

The two partition functions figuring in the Pitzer-Gwinn factor, now correspond exactly with a mode of the normal HO description, due to the correct A_φ moment. This allows us to rewrite the molecular EHR partition function as a product of the HO partition function with a scaling factor $\kappa_{EHR}(T)$:

$$\begin{aligned} Q_{tot}^{EHR}(T) &= Q_{tot}^{HO}(T)\sqrt{\frac{\beta}{2\pi}}\sqrt{\left.\frac{\partial^2 V}{\partial\varphi^2}\right|_0}\int_0^{2\pi} f_A(\varphi)\, f_{vib}(\varphi,T)\, e^{-\beta V^{HR}(\varphi)}\,\mathrm{d}\varphi \\ &= \kappa_{EHR}(T)\, Q_{rot,int}^{HO}(T) \end{aligned} \tag{2.25}$$

Note that, due to the presence of the classical partition function in the denominator of the PG factor, the scaling factor becomes independent of the absolute values of the moments of inertia. Only the relative variation of the moments plays an important role through the intrinsic structure of the geometry factor $f_A(\varphi)$ [Eq.(2.17)]. Corrections due to the vibrational coupling are taken into account by the presence of the $f_{vib}(\varphi,T)$ factor.

The 1D-HR partition function –discussed in subsection 2.2– can be written in a similar form:

$$\begin{aligned} Q_{tot}^{1D-HR}(T) &= Q_{tot}^{HO}(T)\sqrt{\frac{\beta}{2\pi}}\sqrt{\left.\frac{\partial^2 V}{\partial\varphi^2}\right|_0}\int_0^{2\pi} e^{-\beta V^{HR}(\varphi)}\,\mathrm{d}\varphi \\ &= \kappa_{HR}(T)\, Q_{rot,int}^{HO}(T) \end{aligned} \tag{2.26}$$

The resemblance with the EHR expression (2.25) is surprising since the two models are based on different grounds. The EHR description is complete in

the sense that it describes the whole molecule in a single model, while the 1D-HR method is a combination of the (complete) HO description with a model in reduced dimensions.

This striking similarity between the HR and the more advanced EHR expressions offers an explanation for the successful results obtained within the (1D-)HR description. Inspection of both expressions (2.25) and (2.26) learns that they only differ in a factor $f_A f_{vib}$ in the integrand. In the close vicinity of the equilibrium geometry, this factor is by definition equal to unity, giving rise to the same total partition function in both approaches. However, the factor $f_A(\varphi) f_{vib}(\varphi, T)$ is dependent on the torsional angle φ and may have a large impact on the evaluation of the integral. On the contrary the Boltzman factor $e^{-\beta V^{HR}(\varphi)}$ reduces the importance of the contributions to the integral for torsional angles differing from the reference geometry. Only very large values for the $f_A f_{vib}$ factor are able to compensate the exponentially decreasing function of the Boltzman factor. The occurrence of low-energy local minima on the HR potential can also be on the origin of noticeable discrepancies between the calculated partition functions of the two models, since the Boltzman factor will be relatively large, and the $f_A f_{vib}$ factor is no longer unity by definition.

For a 'normal' energy variation with a single dominant minimum, as in n-alkanes, we expect almost identical results in both 1D-HR and EHR treatments. For a potential energy with multiple minima the results may differ, depending on the $f_A f_{vib}$ values corresponding with the different local minima. This probably lies on the origin of the less reasonable agreement of the 1D-HR predictions of thermodynamic properties in sulfides with experiment.

In sulfides and branched alkanes large fluctuations of the geometry factor f_A may take place due to the repositioning of heavy parts of the molecule (containing heavy atoms such as S, or branched chains). This effect is reenforced by a similar behavior of the vibrational factor f_{vib} due to the presence of several low vibrational modes in sulfides and branched alkanes.

Concluding, we succeeded to explain on a microscopic ground the partial failure of the traditional HR methods in reproducing thermodynamical properties in sulfides and branched alkanes.

2.7 Examples of the EHR model

In order to assess the EHR model, we applied this formalism on three simple examples: thermodynamic properties have been evaluated in 1,3-butadiene and 1-butene, and as an accurate reproduction of partition functions has also its implication on the kinetics of a reaction we investigate the addition reaction of a vinyl radical to ethene. The 1-butene application requires a two-dimensional treatment, while in the two other examples only one large amplitude degree of freedom is present.

Figure 2.7 shows the scaling factors $\kappa(T)$ of the HO ($\kappa_{HO}(T) \equiv 1$), HR and EHR treatments. For 1,3-butadiene and the transition state of the addition reaction under study, the EHR scaling factor is larger than the HR factor, while for 1-butene it is smaller.
Experimental data suitable for validating the EHR model are the thermochemical quantities as entropy and heat capacity, and the reaction rate. The numerical results reveal rather small changes in the reproduction of the thermodynamic properties (see chapter 9). The variations are slightly more pronounced in the heat capacities which is not surprising since second order derivatives of the partition function are determinative in the evaluation of this quantity. The reaction rate on the other hand is clearly more sensitive to the model describing the internal rotation about the forming bond in the transition state as shown in Figure 2.8. This can best be visualized by comparing the kinetic parameters E_a (activation energy) and A (pre-exponential factor) as obtained in the various models. The Arrhenius plot in Fig.2.8 was fitted on the reaction rate in the temperature interval of 300-600K. There is a slight enhancement of the reaction rate within EHR with respect to 1D-HR. This trend is also reflected in the pre-exponential factor where an 17% increase is noticed between both EHR and HR predictions.

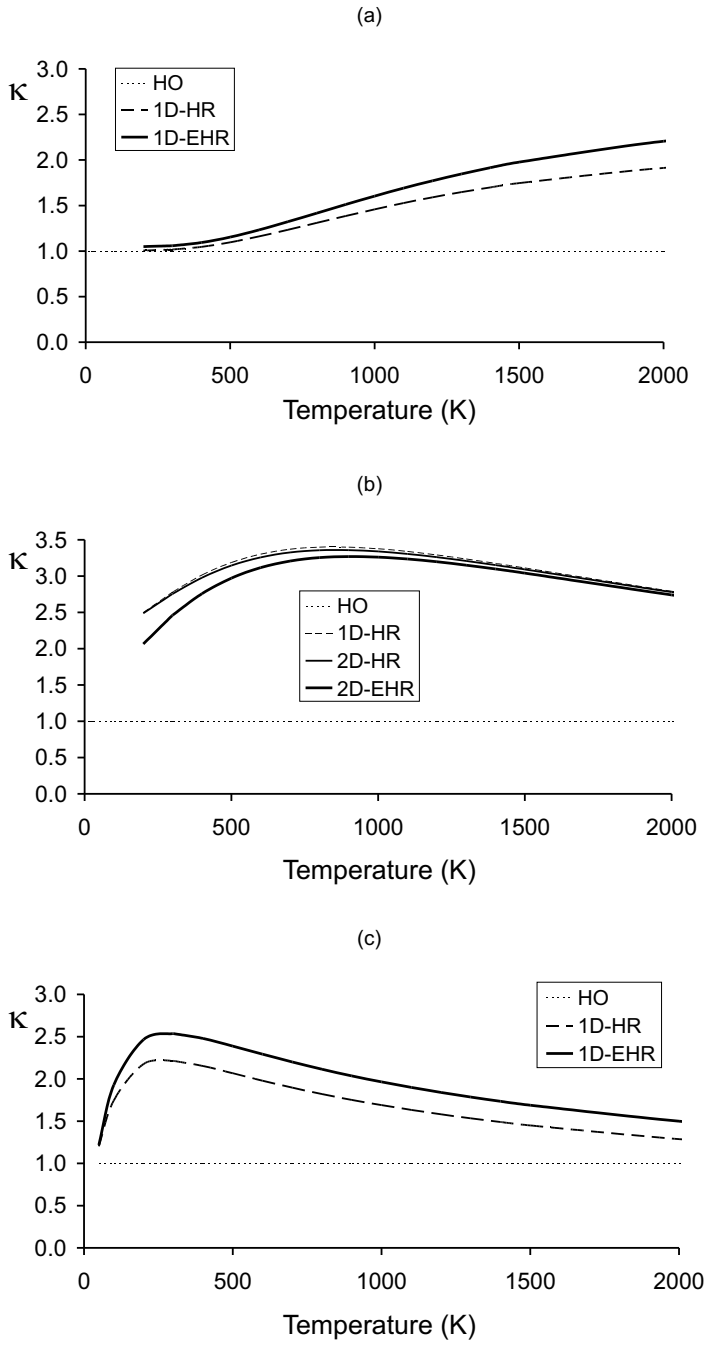

Figure 2.7: Scaling factors $\kappa(T)$ for the global partition function in (a) 1,3-butadiene, (b) 1-butene and (c) the transition state for the addition reaction of a vinyl radical to ethene.

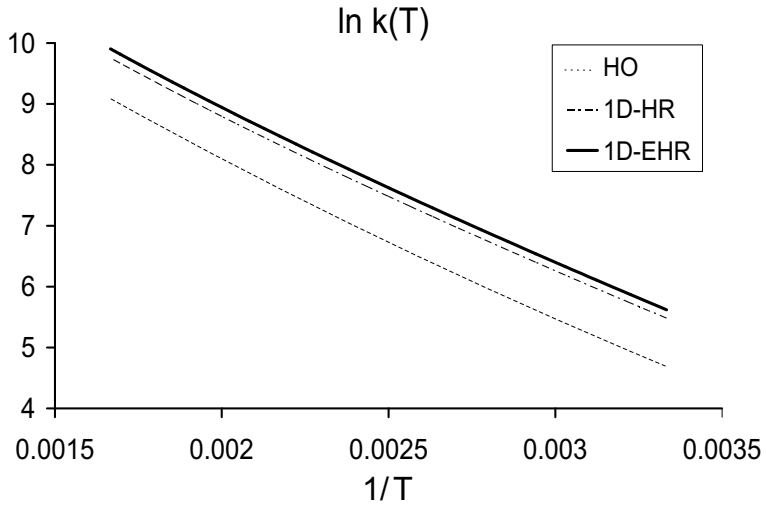

	HO	1D-HR	1D-EHR
E_a (kJ/mol)	21.98	21.40	21.46
A (m^3/mol/s)	6.48 E5	1.16 E6	1.36 E6

Figure 2.8: Arrhenius plot of ln k(T) for the addition of the ethyl radical to ethene.

In the next chapters 3–9, the above topics are discussed in detail.
The general conclusions and future prospects are given in the last chapter.

Chapter 3

Ab initio calculation of entropy and heat capacity of gas-phase n-alkanes using internal rotations

This chapter is based on Ref.[14]:

Vansteenkiste, P.; Van Speybroeck, V.; Marin, G.B.
and Waroquier, M.
J. Phys. Chem. A, **2003**, *107*, 3139–3145

Abstract

This chapter aims to improve the theoretical reproduction of thermodynamic properties, such like entropies and heat capacities of gas-phase n-alkanes, by a more precise quantum-mechanical treatment of the internal rotations. Present ab-initio methods all handle the internal modes in the harmonic oscillator approach. It has already been noticed [2, 33, 34, 35] that this approach underestimates the microscopic partition functions. In this chapter, an uncoupled scheme for internal rotations is applied to a large number of n-alkanes within the DFT-formalism at the B3LYP/6-311g** level. The method being examined in this chapter drastically improves the agreement between theoretical and experimental thermodynamic properties. Moreover, the method has shown to be efficient and to be easily implemented in each ab initio software package.

3.1 Introduction

Ab initio calculations provide a highly appropriate way to calculate various thermodynamic properties, such as the entropy and heat capacity, by statistical mechanics. Basic quantities are the microscopic partition functions related to all degrees of freedom present in the molecule, as the overall translation and rotation of the molecule and the remaining internal vibrational modes. In standard ab initio codes all internal vibrational modes are treated within the harmonic oscillator approach. However, in previous work of the authors [2, 33, 34] the importance of treating low vibrational modes in a more appropriate way was shown. As the molecule gets larger, the number of vibrational degrees of freedom increases and the contribution of internal rotations to the total entropy and other thermodynamic properties becomes larger. The larger the molecule, the higher the sensitivity of the approximations applied to calculate the partition function.

In this chapter, we show that even the most straightforward method of describing internal rotational modes which is based upon one-dimensional rotational potentials, obtained from ab initio calculations, drastically improves the accuracy of reproducing thermodynamic properties. The goal of this chapter is to apply the uncoupled model, outlined in previous work of the authors, on n-alkanes up to decane, and to study its influence on the reproduction of the entropy and heat capacity, for which good experimental values are available.

A more elaborate treatment of subsequent internal rotations in a coupled scheme is feasible [34, 16], but requires a high numerical cost in the construction of multi-dimensional torsional potential surfaces. This general scheme is not of practical use to implement in present ab initio codes, but gives an indication on the reliability of the various approximations which may be applied to the general scheme. Such generalization is outside the scope of the present study. This chapter primarily aims at emphasizing the importance of considering more elaborate treatments of low vibrational modes. They mostly correspond with quasi-free or hindered rotations of part of the molecule about a single bond.

n-alkanes constitute an ideal series of molecules to test the influence of internal rotations on thermodynamic properties. They contain methylene sequences with a chain of subsequent internal rotations. In addition accurate experimental estimates for the entropy and heat capacity are available at various temperatures, and in the range from ethane to decane [24, 36, 37, 38].

East and Radom [5] carried out an extensive study of small molecules at different levels of ab initio molecular orbital theory and different methods for

calculating entropies and showed that entropies could be calculated to within 1 (J/K)/mol. Therefore they used high levels of theory [ranging from MP2/6-31G(d) to MP2/6-311+G(2df,p)] and treated individual internal rotations explicitly with a cosine potential based on barrier heights of the torsional potential. Their method differs with the presented one in the number of contributions in the Fourier fit in reproducing the torsional potential.

Another recent paper regarding the ab initio calculation of the entropy of gas phase organic molecules concerns the work of J.P. Guthrie [39]. Entropy values are calculated at the B3LYP/6-31G** level of theory with an overall standard deviation of 5,35 (J/K)/mol in entropy at 298,15K. The training set consisted of 128 molecules with particular focus on relatively large molecules with up to 10 carbon atoms. In the work of Guthrie et al. the calculated entropy values have been adjusted by an empirical correction term which accounts for various low lying conformations. This study reports values of entropies which are quite satisfactory, emphasizing the adequacy of DFT-like models in reproducing thermodynamic properties with an acceptable accuracy.

3.2 Methodology and computational details

All ab initio calculations were performed using the Gaussian98 software package [12]. All optimizations, frequency calculations, and potential scans were done using density functional theory (DFT) [9], with Becke's three-parameter B3LYP functional [7]. The molecular orbitals were expanded in a triple-ζ 6-311G basis augmented with single first d and p polarization functions [8]. This functional is known to give a reliable and quantitatively acceptable description of geometries, frequencies, and potentials [40, 41, 42] for a reasonable computation time. In particular, a profound quantum chemical study of conformational energies and rotational energy barriers has been performed by G.D. Smith and R.L. Jaffe in n-alkanes using high-level ab initio methods [43]. As will be discussed later, a comparative study between their results and ours learns that the agreement is remarkable even on the quantitative level.
The frequency calculation gives all normal modes of the molecule and enables us to select those vibrational modes that correspond with internal rotations. In the uncoupled scheme adopted in this chapter the one-dimensional rotational potential is calculated for the selected modes by performing a scan in terms of the relevant torsional angle, and relaxing all other degrees of freedom. This procedure is slightly different with that applied by the authors in previous work [2, 33], where the potential is determined by some stationary points, corresponding with a full geometry optimization. The latter scheme is expected to yield more realistic values of the rotational barriers [35, 44], and the barrier heights resulting from the scan procedure are in good agreement with the high-level ab initio predictions, as will be shown later in the discussion.
The final potential is then obtained by fitting a cosine series through the calculated data points:

$$V_i(\phi_i) = \sum_{j=1}^{18} a_{ij} \left(1 - \cos(j\phi_i)\right) \tag{3.1}$$

with index i standing for the identification of the particular internal rotation under consideration.
The partition function can now be obtained quantum mechanically or classically dependent on the temperature range of interest. For low temperatures (below 400K) a quantum mechanical treatment is needed and one has to solve the one-dimensional Schrödinger equation

$$\left[-\frac{\hbar^2}{2I_i^{red}}\frac{\partial^2}{\partial\phi_i^2} + V_i(\phi_i)\right]\psi_{ki}(\phi_i) = \epsilon_{ki}\psi_{ki}(\phi_i) \tag{3.2}$$

This is done by the numerical procedure as outlined in [2], yielding all rotational energy eigenvalues ϵ_{ki} required for the evaluation of the partition function of internal rotation i defined by

$$q_i = \frac{1}{\sigma_i} \sum_k g_k e^{-\frac{\epsilon_{ki}}{kT}} \tag{3.3}$$

with σ_i the symmetry number of the rotational top, and g_k the degeneracy of the energy level k.
The quantity I_i^{red} in the one-dimensional Schrödinger equation represents the generalized reduced moment of inertia of an asymmetric top as defined in [3]. For symmetric tops it reduces to

$$I_i^{red} = I_i \left(1 - \sum_{k=x,y,z} \gamma_k^2 \frac{I_i}{I_{gl,k}} \right) \tag{3.4}$$

with γ_k the direction cosines between the rotational axis and the axes of inertia of the global molecule, I_i the moment of the top, and $I_{gl,k}$ the moments of inertia of the global molecule [3].
For temperatures above 500K the quantum mechanical and classical partition functions are expected to converge. The classical partition function is obtained as an integral [1]:

$$q_i = \frac{1}{\sigma_i} \frac{\sqrt{2\pi kT I_i^{red}}}{h} \int e^{-\frac{V_i(\phi_i)}{kT}} \mathrm{d}\phi_i \tag{3.5}$$

Finally the partition functions as determined in the harmonic oscillator approach are replaced by the new values.
Knowledge of the total molecular partition function Q allows us to evaluate macroscopic thermodynamic quantities, such as the entropy

$$S = R \left(\ln Q + T \left(\frac{\partial \ln Q}{\partial T} \right) \right) \tag{3.6}$$

and the heat capacity

$$C = RT \left(2 \frac{\partial \ln Q}{\partial T} + T \frac{\partial^2 \ln Q}{\partial T^2} \right) \tag{3.7}$$

3.3 Results and discussion

3.3.1 Torsional potentials

In n-alkanes two classes of rotational potentials are present: one corresponding with rotations of ending methyl groups (Fig.3.1), and another associated with CCCC carbon torsional variations (Fig.3.2).

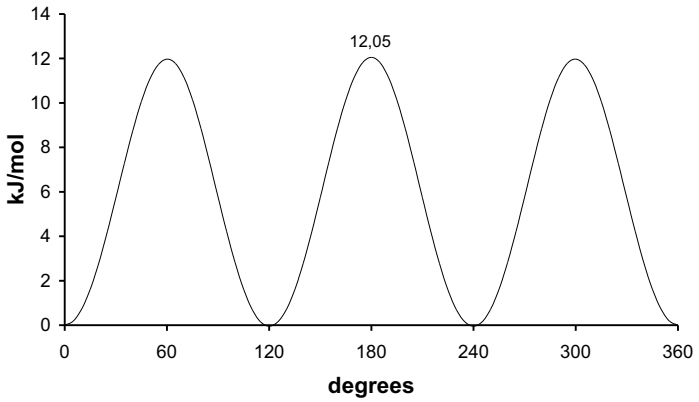

Figure 3.1: Potential energy of methyl rotation in pentane. Reference is the energetically most favored conformation: trans.

The potential of the methyl rotation has a three-fold symmetry and is determined by only one parameter: the relative potential barrier height; the reference conformation is defined as the all trans conformation. This parameter is plotted for the different alkanes in Fig.3.3. The relative potential barrier height seems to converge to a value of about 12 kJ/mol for the larger chains. This convergence can be expected since, as the chain length increases, the tops don't feel the effect of the other methyl end, but only of the closest CH_2 groups.
The inner rotational potentials all show a general behavior as schematically presented in Fig.3.2. The reference trans equilibrium (t) conformation at $\phi = 0°$ is separated from the higher energy gauche conformation (g) ($\phi \approx 115°$) by the t-g barriers ($\phi \approx 60°$), while direct transition between the gauche states requires traversing the cis barrier ($\phi = 180°$). The energy difference between the trans and gauche conformation has been the subject of much debate in the past, both from experimental and theoretical point of view [43]. It is also an

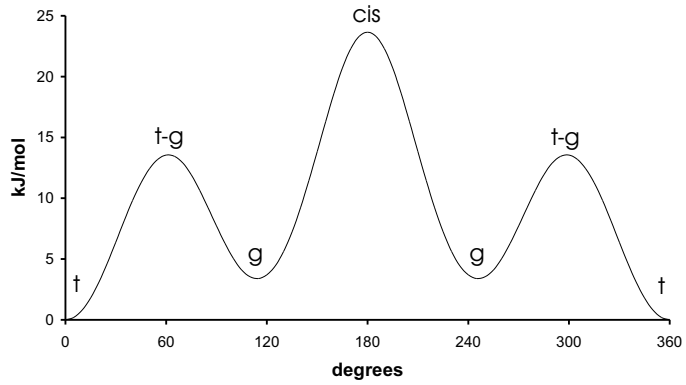

Figure 3.2: Potential energy of ethyl rotation in butane. Reference is the energetically most favored conformation: trans.

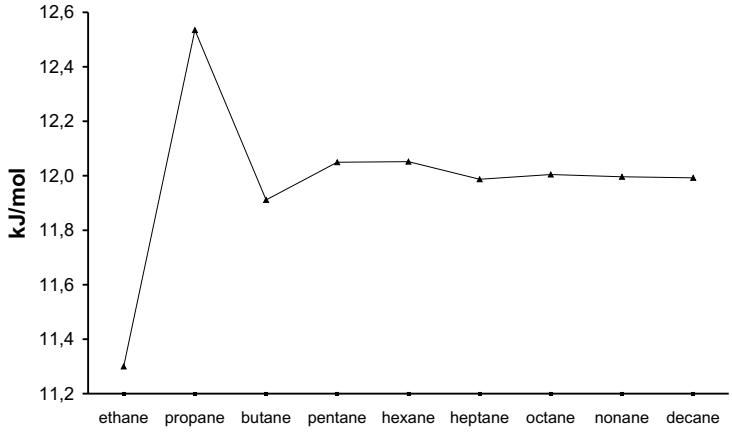

Figure 3.3: Potential barrier height of the methyl rotation in n-alkanes as a function of the chain length.

interesting issue to find out if convergence is achieved of the gauche energy and barrier heights in larger n-alkanes.

Although this is not the topic of the present study, some preliminary conclusions may still be drawn. Many ab initio calculations of the gauche energy in

	n-butane			
	MP2/6-311G** [a] kJ/mol	MP2/6-311G(2gf,p) //CCSD(T) [a] kJ/mol	Herrebout et al. [b] kJ/mol	B3LYP/6-311G** [c] kJ/mol
t	0,00	0,00		0,00
t-g	14,22	13,85		13,58
g	2,13	2,26	2,80	3,45
cis	24,77	22,93		23,67
	***n*-hexane**			
	MP2/6-311G** [a] kJ/mol		Herrebout et al. [b] kJ/mol	B3LYP/6-311G** [c] kJ/mol
t	0,00			0,00
t-g	12,09			12,95
g	1,84		2,18	3,52
cis	23,55			23,69

[a] Ref [43]
[b] Ref [50]
[c] This work

Table 3.1: Gauche energy and $t-g$ and *cis* rotational energy barriers in n-butane and n-hexane.

n-alkanes have been performed [45, 46, 47, 48, 49, 50]. An overview of the different results is given in [43]. We report in Table 3.1 the most advanced results of the gauche energy and the t-g and cis rotational energy barriers in n-butane and n-hexane. The B3LYP/6-311G** predictions of the barriers agree quite well with those obtained with very high-level computational calculations such as MP2/6-311G(2gf,p)//CCSD(T). The differences between the cis and the t-g barriers are very well reproduced, and this agreement strengthens the reliability of our predictions of the entropy corrections due to the internal rotations on the quantitative level. On the other hand, the gauche energies are somewhat overestimated, but it is expected that those energies have little influence on the rotational energy levels as obtained from the eigenvalue equation [Eq.(3.2)].
To check this assumption, we used the gauche energy value from Ref.[50] to calculate the energy levels of the inner rotation of hexane. This slight change lowers the ground rotational energy level by 1.2%, while the decrease of the higher energy levels is even smaller ($\approx$1%). These small changes give rise to an increase of the entropy by about 0.2 (J/K)/mol at 300K, while at higher temperatures the results are unaffected. The values of the heat capacity are somewhat more influenced: a decrease of about 0.9 (J/K)/mol at 300K, while at 1500K there is an increase of 0.05 (J/K)/mol, bringing the calculated values closer to experiment. The variations however are still very small. These results ensure that the potential values obtained by the B3LYP functional have enough accuracy for the goal of this chapter.
The different parameters characterizing the gauche and cis conformation (g and

cis) are plotted in Fig.3.4 and Fig.3.5 for the various internal rotations of the C-C-C-C torsional angle in terms of the length of the alkyl chain.

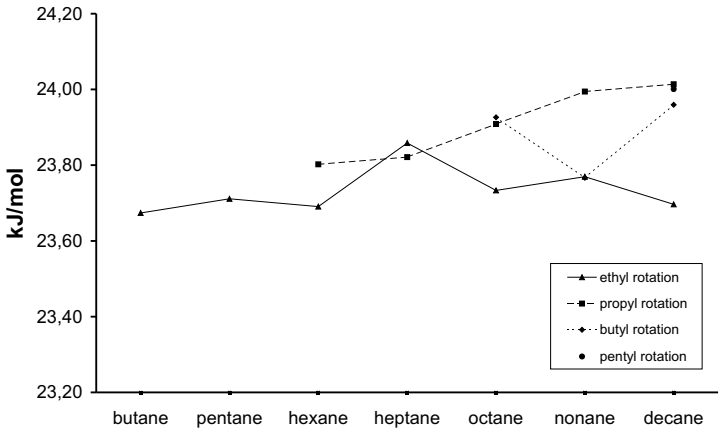

Figure 3.4: Potential barrier height of the *cis* conformation in n-alkanes as a function of the chain length.

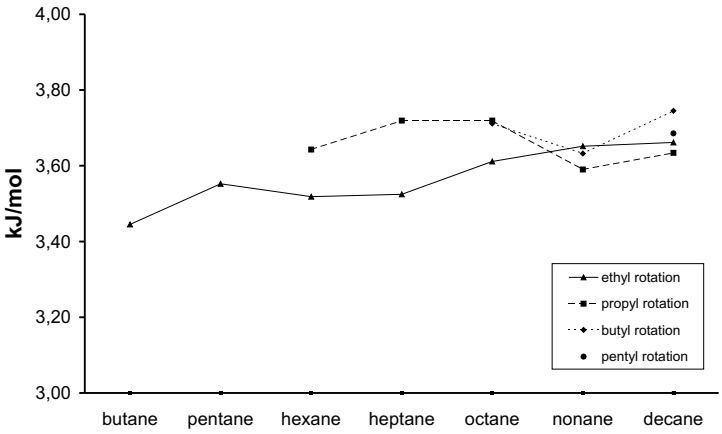

Figure 3.5: Gauche-trans energy difference in n-alkanes as a function of the chain length.

The cis conformation is always located at a torsional angle of 180° due to the symmetry of the rotational potential. This means that the energies resulting from our scan equal those obtained from full geometry optimizations towards a transition state. Convergence of the cis barrier height is obtained within 0.05–0.07 kJ/mol, which is within the numerical accuracy.
Not only convergence within each class of internal rotations is present, also the values of the cis barriers of the propyl, butyl and pentyl rotations are converged in decane. This was expected, since the larger the alkyl chain, the smaller the effect of the boundaries on the specific internal rotation.
The gauche conformation is not always located at the same position of the torsional angle for the different internal rotations and for the various alkanes. In our scan, a local minimum was found at 115°. In order to find the real gauche state, we performed optimizations starting from this 115° geometry. The resulting relative energy values of these stationary points are shown in Fig.3.5. Again convergence up to 0.05 kJ/mol is achieved in terms of the length of the alkyl chain. Moreover in decane, the relative gauche energies associated with the various torsional motions are also converged within the numerical accuracy.
In this chapter we adopt the uncoupled scheme. In other words, all torsional potentials are one-dimensional and for large deviations from the equilibrium values of the torsional angles in the chain we can expect that the uncoupled representations of subsequent internal rotations may seriously differ from the multidimensional scheme. Conformers with several gauche configurations (such as gtg, gg, $ggg\ldots$) are probably not very well described in this approximation. We give reference to Ref.[51] for a thorough discussion about the stability of those conformers. Nevertheless, we want to emphasize that our calculations give evidence for slight changes in the geometry in the applied constrained optimization procedure. If the constraint concerns one torsional angle, the relaxation affects the original conformation to a very small extent, and in addition the relaxation has only effect on the closest neighbors.
Anyway, an explicit application of the coupled scheme is recommended in order to draw general conclusions about the adequacy of the uncoupled scheme to predict entropy corrections due to internal rotations on a high quantitative level. Those calculations are very time consuming [16] and are the subject of some of the next chapters.

3.3.2 Entropy and heat capacity

We report the calculated values of the entropy and heat capacity for the n-alkanes in Tables 3.3–3.11, together with the experimental values over a large temperature range. We distinguish between the predictions made in a quantum mechanical approach –by solving Eq.(3.2)– and those obtained by evaluating the classical integral of Eq.(3.5). These results are respectively indicated by 1D-HR$^{Q.M.}$ and 1D-HR$^{Cl.}$. For low temperatures the quantum mechanical approach is recommended, but for high temperatures both values are converging to each other.

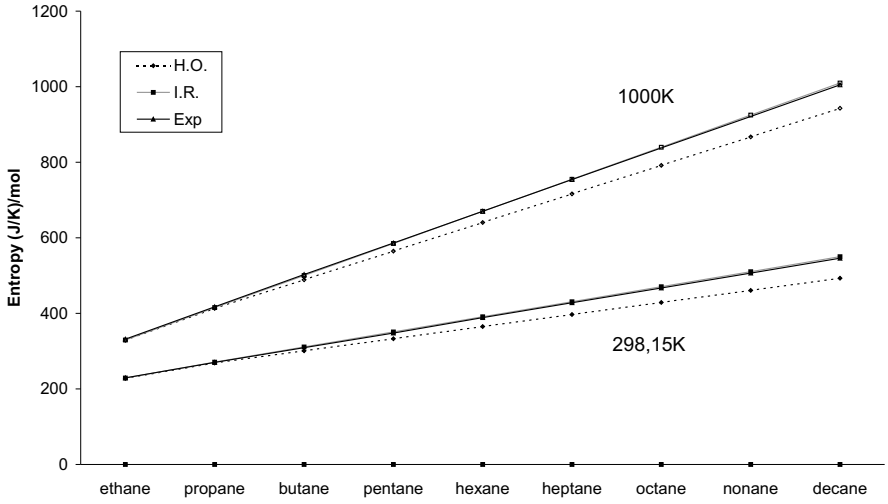

Figure 3.6: Entropy of n-alkanes at 298,15K and at 1000K as a function of the chain length.

When treating internal rotations, we notice a systematic increase of the two thermodynamic quantities at low temperature with regard to the theoretical predictions within the harmonic oscillator (HO) model, while at higher temperatures the heat capacity is lower than the one predicted by the HO model. In Fig.3.6 the entropy at room temperature and at 1000K is plotted throughout the whole range of the n-alkanes under study. The overall agreement with experiment is remarkable. The HO predictions for the entropy systematically underestimate the experimental values. The discrepancies increase with the

length of the alkyl-chain. The corrections predicted by the 1D-HR model bring the theoretical predictions very close to the experimental values. The corrections are larger for the longer n-alkanes, in this way compensating the larger discrepancies noticed in the HO results. The observation that the corrections due to the inclusion of internal rotations are systematically increasing with the length of the chain is not surprising, but the fact that the magnitude of these correction terms almost coincides with the deviation of the HO results from the experiment, is spectacular and gives a clear indication of the inadequacy of the HO model to predict reliable microscopic properties in molecules that contain a large number of internal rotations.

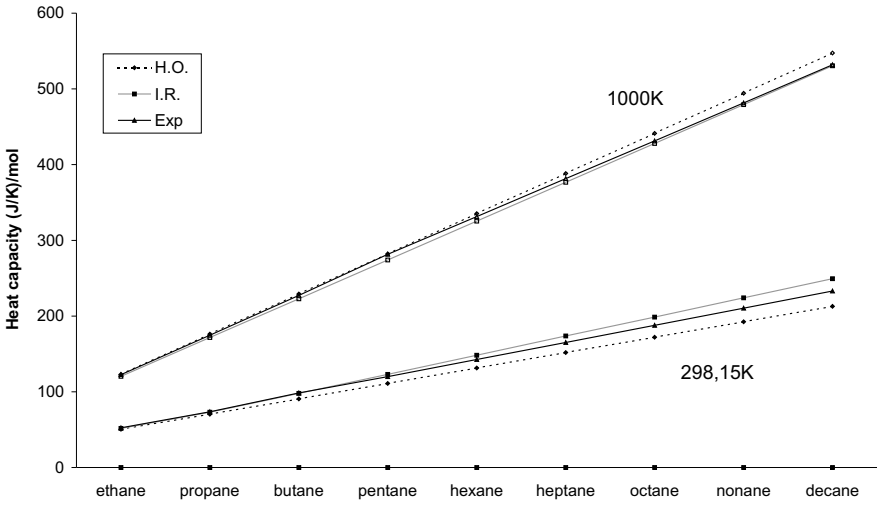

Figure 3.7: Heat capacity of n-alkanes at 298,15K and at 1000K as a function of the chain length.

The HO approximation also fails in reproducing a correct temperature dependence of the heat capacity. At low temperatures the HO predictions underestimate the experimental values, while at high temperatures we notice an overestimation of the heat capacity which is systematically increasing with the chain length. The behavior of the heat capacity as a function of the length of the chain also strongly depends on the temperature (Fig.3.7). Large discrepancies are noticed at low temperature. The corrections due to 1D-HR overshoot the experimental values. This is probably due to the use of the uncoupled

scheme [34].
In order to get an overall impression about the quantitative level of agreement regarding the reproduction of the entropy at various temperatures for the n-alkanes, we report in Table 3.2 the relative standard deviation defined by

$$\sigma = \left[\frac{1}{N} \sum \left(\frac{S^{th} - S^{exp}}{S^{exp}} \right)^2 \right]^{\frac{1}{2}} \tag{3.8}$$

with N the number of data points. In the HO model the standard deviation amounts to almost 10% for the higher alkanes, while in the 1D-HR approach it remains constant, and is less than 1%.

Standard deviations on S			
	HO	1D-HR$^{Q.M.}$	1D-HR$^{Cl.}$
ethane	0,80%	0,57%	0,60%
propane	0,90%	0,42%	0,42%
butane	3,08%	0,33%	0,27%
pentane	4,46%	0,36%	0,21%
hexane	5,63%	0,50%	0,36%
heptane	6,60%	0,53%	0,41%
octane	8,17%	0,69%	0,47%
nonane	9,01%	0,78%	0,57%
decane	8,48%	0,89%	0,80%

Table 3.2: Standard deviations on the entropy of n-alkanes.

3.4 Conclusion

In this chapter a model is presented to treat internal rotations in a very appropriate way. Although described in an uncoupled scheme, it has proved to be very efficient in evaluating corrections to the HO predictions on entropy and heat capacity in n-alkanes. The reproduction of the entropies is even that satisfactory that one would hardly expect better agreement when enhancing the level of the model. Subsequent internal rotations about a very long chain of single bonds require a more profound investigation of the coupling effects. This work will be presented in the following chapters.

	ethane				
	Temp	HO	1D-HR$^{Q.M.}$	1D-HR$^{Cl.}$	experimental
S (J/mol/K)	**298,15**	227,770	229,011	228,349	**229,161** [a]
	300	228,083	229,331	228,677	**229,487** [a]
	400	244,385	245,912	245,547	**246,378** [a]
	500	259,940	261,526	261,304	**262,344** [a]
	600	274,913	276,411	276,267	**277,568** [a]
	700	289,288	290,610	290,513	**292,080** [a]
	800	303,053	304,154	304,085	**305,904** [a]
	900	316,218	317,073	317,022	**319,075** [a]
	1000	328,800	329,401	329,363	**331,628** [a]
	1100	340,824	341,170	341,141	**343,597** [a]
	1200	352,316	352,410	352,387	**355,012** [a]
	1300	363,301	363,151	363,133	**365,908** [a]
	1400	373,808	373,421	373,406	**376,314** [a]
	1500	383,864	383,249	383,237	**386,260** [a]
C_p (J/mol/K)	**298,15**	50,52	51,73	53,00	**52,49** [b]
	300	50,74	51,94	53,20	**52,71** [b]
	400	63,44	64,08	64,86	**65,46** [b]
	500	76,32	76,19	76,70	**77,94** [b]
	600	88,07	87,23	87,58	**89,19** [b]
	700	98,49	97,06	97,31	**99,14** [b]
	800	107,70	105,81	105,99	**107,94** [b]
	900	115,83	113,57	113,70	**115,71** [b]
	1000	122,99	120,44	120,54	**122,55** [b]
	1100	129,29	126,50	126,58	**128,55** [b]
	1200	134,81	131,83	131,89	**133,80** [b]
	1300	139,64	136,51	136,56	**138,39** [b]
	1400	143,88	140,62	140,66	**142,40** [b]
	1500	147,59	144,23	144,27	**145,90** [b]

[a] Ref. [36]
[b] Ref. [24]

Table 3.3: Entropy and heat capacity of ethane.

	propane				
	Temp	HO	1D-HR$^{Q.M.}$	1D-HR$^{Cl.}$	experimental
S (J/mol/K)	**298,15**	268,645	271,013	270,120	**270,313** [a]
	300	269,081	271,466	270,583	**270,769** [a]
	400	292,079	295,164	294,666	**294,739** [a]
	500	314,335	317,728	317,421	**317,768** [a]
	600	335,862	339,252	339,051	**339,753** [a]
	700	356,546	359,727	359,590	**360,668** [a]
	800	376,338	379,186	379,088	**380,528** [a]
	900	395,237	397,682	397,610	**399,381** [a]
	1000	413,271	415,276	415,222	**417,293** [a]
	1100	430,476	432,025	431,983	**434,321** [a]
	1200	446,892	447,983	447,950	**450,526** [a]
	1300	462,564	463,201	463,175	**465,961** [a]
	1400	477,535	477,727	477,706	**480,675** [a]
	1500	491,847	491,606	491,589	**494,721** [a]
C_p (J/mol/K)	**298,15**	70,33	73,00	74,70	**73,60** [b]
	300	70,68	73,34	75,03	**73,93** [b]
	400	90,35	92,34	93,38	**94,01** [b]
	500	109,57	110,24	110,93	**112,59** [b]
	600	126,72	125,98	126,47	**128,70** [b]
	700	141,69	139,71	140,06	**142,67** [b]
	800	154,74	151,74	151,99	**154,77** [b]
	900	166,15	162,32	162,51	**165,35** [b]
	1000	176,12	171,62	171,77	**174,60** [b]
	1100	184,84	179,79	179,91	**182,67** [b]
	1200	192,45	186,96	187,05	**189,74** [b]
	1300	199,09	193,24	193,31	**195,85** [b]
	1400	204,89	198,74	198,80	**201,21** [b]
	1500	209,96	203,56	203,61	**205,89** [b]

[a] Ref. [36]
[b] Ref. [24]

Table 3.4: Entropy and heat capacity of propane.

	butane				
	Temp	HO	1D-HR$^{Q.M.}$	1D-HR$^{Cl.}$	experimental
S (J/mol/K)	**298,15**	300,760	311,082	310,138	**309,910** [a]
	300	301,323	311,689	310,756	**310,746** [b]
	400	331,110	343,208	342,686	
	500	360,083	372,934	372,614	**372,794** [b]
	600	388,156	401,150	400,941	
	700	415,137	427,910	427,767	**428,986** [b]
	800	440,942	453,281	453,180	
	900	465,566	477,352	477,278	
	1000	489,042	500,212	500,155	**502,749** [b]
	1100	511,420	521,942	521,899	
	1200	532,757	542,622	542,587	
	1300	553,111	562,321	562,294	
	1400	572,542	581,108	581,086	
	1500	591,107	599,045	599,026	
C_p (J/mol/K)	**298,15**	90,69	97,87	99,69	**98,49** [c]
	300	91,15	98,29	100,09	**98,95** [c]
	400	117,41	122,09	123,19	**124,77** [c]
	500	142,81	144,80	145,53	**148,66** [c]
	600	165,30	164,87	165,38	**169,28** [c]
	700	184,79	182,36	182,72	**187,02** [c]
	800	201,69	197,65	197,91	**202,38** [c]
	900	216,39	211,06	211,25	**215,73** [c]
	1000	229,18	222,82	222,97	**227,36** [c]
	1100	240,32	233,12	233,24	**237,48** [c]
	1200	250,02	242,14	242,23	**246,27** [c]
	1300	258,48	250,02	250,10	**253,93** [c]
	1400	265,84	256,92	256,99	**260,58** [c]
	1500	272,28	262,97	263,02	**266,40** [c]

[a] Ref. [37]
[b] Ref. [38]
[c] Ref. [24]

Table 3.5: Entropy and heat capacity of butane.

	pentane				
	Temp	HO	1D-HR$^{Q.M.}$	1D-HR$^{Cl.}$	experimental
S (J/mol/K)	**298,15**	332,899	350,830	349,840	**349,450** [a]
	300	333,587	351,592	350,613	**349,699** [b]
	400	370,142	390,978	390,429	
	500	405,810	427,881	427,544	**426,266** [b]
	600	440,411	462,800	462,579	
	700	473,676	495,851	495,701	**495,469** [b]
	800	505,485	527,144	527,036	
	900	535,826	556,797	556,718	
	1000	564,738	584,928	584,868	**586,137** [b]
	1100	592,285	611,647	611,600	
	1200	618,538	637,054	637,017	
	1300	643,571	661,240	661,210	
	1400	667,460	684,293	684,268	
	1500	690,277	706,290	706,270	
C_p (J/mol/K)	**298,15**	110,99	122,96	124,87	**120,00** [c]
	300	111,57	123,46	125,35	**120,62** [c]
	400	144,37	151,93	153,08	**152,55** [c]
	500	175,96	179,42	180,18	**182,59** [c]
	600	203,79	203,81	204,34	**208,78** [c]
	700	227,82	225,07	225,45	**231,38** [c]
	800	248,57	243,62	243,90	**250,62** [c]
	900	266,56	259,86	260,07	**266,94** [c]
	1000	282,19	274,08	274,24	**281,58** [c]
	1100	295,76	286,51	286,64	**293,72** [c]
	1200	307,57	297,38	297,48	**304,60** [c]
	1300	317,83	306,88	306,96	**313,80** [c]
	1400	326,77	315,17	315,24	**322,17** [c]
	1500	334,58	322,43	322,49	**330,54** [c]

[a] Ref. [37]
[b] Ref. [38]
[c] Ref. [24]

Table 3.6: Entropy and heat capacity of pentane.

	hexane				
	Temp	HO	1D-HR$^{Q.M.}$	1D-HR$^{Cl.}$	experimental
S (J/mol/K)	**298,15**	365,034	390,995	389,986	**388,820** [a]
	300	365,849	391,915	390,918	**389,321** [b]
	400	409,206	439,244	438,685	
	500	451,601	483,376	483,033	**480,407** [b]
	600	492,756	525,030	524,806	
	700	532,322	564,396	564,242	**562,664** [b]
	800	570,146	601,624	601,514	
	900	606,212	636,868	636,786	
	1000	640,567	670,276	670,214	**670,235** [b]
	1100	673,287	701,986	701,938	
	1200	704,458	732,121	732,083	
	1300	734,172	760,795	760,764	
	1400	762,519	788,113	788,088	
	1500	789,587	814,172	814,150	
C_p (J/mol/K)	**298,15**	131,40	148,34	150,29	**142,60** [a]
	300	132,10	148,92	150,85	**143,26** [a]
	400	171,48	182,02	183,19	**181,54** [a]
	500	209,25	214,25	215,02	**217,28** [a]
	600	242,41	242,92	243,45	**248,11** [a]
	700	270,94	267,90	268,28	**274,05** [a]
	800	295,53	289,68	289,96	**296,23** [a]
	900	316,80	308,72	308,93	**315,06** [a]
	1000	335,23	325,38	325,54	**331,37** [a]
	1100	351,23	339,93	340,06	**345,18** [a]
	1200	365,13	352,64	352,74	**357,31** [a]
	1300	377,20	363,73	363,81	**368,19** [a]
	1400	387,71	373,42	373,48	**376,56** [a]
	1500	396,87	381,89	381,95	**389,11** [a]

[a] Ref. [24]
[b] Ref. [38]

Table 3.7: Entropy and heat capacity of hexane.

	heptane				
	Temp	HO	1D-HR$^{Q.M.}$	1D-HR$^{Cl.}$	experimental
S (J/mol/K)	**298,15**	397,030	430,597	429,578	**427,980** [a]
	300	397,971	431,673	430,667	**428,944** [b]
	400	448,107	486,936	486,372	
	500	497,206	538,287	537,941	**534,590** [b]
	600	544,896	586,669	586,442	
	700	590,750	632,341	632,186	**629,901** [b]
	800	634,581	675,498	675,387	
	900	676,366	716,329	716,246	
	1000	716,159	755,013	754,950	**754,333** [b]
	1100	754,048	791,712	791,662	
	1200	790,136	826,574	826,535	
	1300	824,528	859,735	859,703	
	1400	857,333	891,319	891,292	
	1500	888,653	921,438	921,415	
C_p (J/mol/K)	**298,15**	151,74	173,68	175,65	**165,20** [c]
	300	152,56	174,34	176,29	**165,98** [c]
	400	198,49	212,07	213,26	**210,66** [c]
	500	242,43	249,03	249,81	**252,09** [c]
	600	280,93	281,97	282,51	**287,44** [c]
	700	313,99	310,68	311,07	**317,15** [c]
	800	342,43	335,70	335,98	**342,25** [c]
	900	366,98	357,56	357,77	**363,59** [c]
	1000	388,25	376,66	376,82	**381,58** [c]
	1100	406,68	393,33	393,46	**397,06** [c]
	1200	422,67	407,88	407,98	**410,45** [c]
	1300	436,56	420,58	420,66	**422,58** [c]
	1400	448,64	431,66	431,73	**435,14** [c]
	1500	459,17	441,35	441,40	**443,50** [c]

[a] Ref. [37]
[b] Ref. [38]
[c] Ref. [24]

Table 3.8: Entropy and heat capacity of heptane.

	octane				
	Temp	HO	1D-HR$^{Q.M.}$	1D-HR$^{Cl.}$	experimental
S (J/mol/K)	**298,15**	429,071	470,444	469,427	**467,060** [a]
	300	430,139	471,675	470,670	
	400	487,060	534,771	534,209	
	500	542,871	593,284	592,938	
	600	597,104	648,358	648,132	
	700	649,252	700,317	700,162	
	800	699,094	749,391	749,279	
	900	746,602	795,801	795,718	
	1000	791,835	839,755	839,691	
	1100	834,896	881,440	881,390	
	1200	875,902	921,028	920,988	
	1300	914,975	958,675	958,641	
	1400	952,239	994,522	994,494	
	1500	987,811	1028,702	1028,677	
C_p (J/mol/K)	**298,15**	172,10	198,66	200,62	**187,80** [b]
	300	173,03	199,40	201,34	**188,70** [b]
	400	225,52	241,82	243,00	**239,74** [b]
	500	275,65	283,58	284,37	**286,81** [b]
	600	319,50	320,87	321,40	**326,77** [b]
	700	357,08	353,35	353,74	**360,24** [b]
	800	389,36	381,65	381,93	**388,28** [b]
	900	417,20	406,34	406,55	**411,71** [b]
	1000	441,28	427,90	428,06	**431,37** [b]
	1100	462,14	446,71	446,83	**448,52** [b]
	1200	480,23	463,11	463,21	**463,17** [b]
	1300	495,93	477,42	477,49	**476,98** [b]
	1400	509,58	489,90	489,96	**489,53** [b]
	1500	521,47	500,80	500,85	**497,90** [b]

[a] Ref. [37]
[b] Ref. [24]

Table 3.9: Entropy and heat capacity of octane.

	nonane				
	Temp	HO	1D-HR$^{Q.M.}$	1D-HR$^{Cl.}$	experimental
S (J/mol/K)	**298,15**	460,872	510,426	509,409	**506,500** [a]
	300	462,065	511,815	510,810	
	400	525,767	582,871	582,308	
	500	588,282	648,621	648,274	
	600	649,052	710,435	710,208	
	700	707,488	768,712	768,556	
	800	763,337	823,725	823,612	
	900	816,563	875,729	875,645	
	1000	867,234	924,964	924,899	
	1100	915,465	971,645	971,593	
	1200	961,387	1015,966	1015,923	
	1300	1005,140	1058,104	1058,068	
	1400	1046,861	1098,220	1098,190	
	1500	1086,685	1136,464	1136,437	
C_p (J/mol/K)	**298,15**	192,44	224,10	226,07	**210,40** [a]
	300	193,50	224,92	226,86	**211,42** [a]
	400	252,53	271,95	273,14	**268,82** [a]
	500	308,84	318,44	319,22	**321,54** [a]
	600	358,02	359,99	360,53	**366,10** [a]
	700	400,13	396,21	396,59	**403,34** [a]
	800	436,26	427,74	428,02	**433,88** [a]
	900	467,39	455,24	455,45	**459,82** [a]
	1000	494,30	479,24	479,40	**481,58** [a]
	1100	517,59	500,17	500,29	**499,99** [a]
	1200	537,77	518,41	518,51	**516,31** [a]
	1300	555,29	534,32	534,39	**531,37** [a]
	1400	570,51	548,19	548,25	**543,92** [a]
	1500	583,77	560,31	560,36	**556,47** [a]

[a] Ref. [24]

Table 3.10: Entropy and heat capacity of nonane.

	decane				
	Temp	HO	1D-HR$^{Q.M.}$	1D-HR$^{Cl.}$	experimental
S (J/mol/K)	**298,15**	492,902	550,087	549,077	**545,800** [a]
	300	494,222	551,633	550,634	**546,096** [b]
	400	564,710	630,615	630,055	
	500	633,938	703,574	703,229	**695,381** [b]
	600	701,250	772,107	771,881	
	700	765,980	836,686	836,529	**829,771** [b]
	800	827,841	897,623	897,509	
	900	886,790	955,210	955,124	
	1000	942,902	1009,717	1009,650	**1004,871** [b]
	1100	996,304	1061,384	1061,330	
	1200	1047,145	1110,430	1110,385	
	1300	1095,578	1157,052	1157,014	
	1400	1141,758	1201,432	1201,398	
	1500	1185,834	1243,735	1243,705	
C_p (J/mol/K)	**298,15**	212,80	249,44	251,40	**233,10** [a]
	300	213,97	250,34	252,27	**234,18** [a]
	400	279,58	301,97	303,14	**297,98** [a]
	500	342,07	353,17	353,95	**356,43** [a]
	600	396,59	399,00	399,53	**405,85** [a]
	700	443,22	438,95	439,33	**446,43** [a]
	800	483,19	473,72	474,00	**479,90** [a]
	900	517,61	504,04	504,25	**508,36** [a]
	1000	547,34	530,49	530,64	**531,79** [a]
	1100	573,06	553,54	553,66	**551,87** [a]
	1200	595,33	573,63	573,73	**569,44** [a]
	1300	614,66	591,14	591,21	**585,76** [a]
	1400	631,45	606,41	606,47	**598,31** [a]
	1500	646,07	619,74	619,79	**610,86** [a]

[a] Ref. [24]
[b] Ref. [38]

Table 3.11: Entropy and heat capacity of decane.

Chapter 4

Origins of the success of the 1D-HR method for the thermodynamics in n-alkanes

This chapter is an extended version of Ref.[16]:

Van Speybroeck, V.; Vansteenkiste, P.; Van Neck, D.
and Waroquier, M.
Chem. Phys. Lett. **2005**, *402*, 479–484

Abstract

In this chapter a range of fully ab initio computational schemes are presented to treat internal rotations in an accurate way. The methods are based upon the exact classical scheme developed in the 1940's by Pitzer and co-workers (KP theory). The scheme is exact in the sense that it can couple mutual internal rotations of asymmetric tops which are also coupled to the global rotation of the molecule. It also allows an easy extension to other internal modes. Beside the exact coupling treatment various approximative schemes in an ascending order of assumptions are presented allowing for a practical implementation of the methodology in applications with a medium number of internal rotors present. We focus on (i) the computation of thermodynamic quantities (total partition function, entropy, and heat capacity) for alkanes with a specific ab initio application of exact KP theory, and (ii) the unravelling of the mechanism of internal rotations and a comparative study of simpler ab initio schemes versus the exact one. An accurate reproduction of microscopic partition functions from first principles opens a lot of perspectives for an universal description of thermochemistry and reaction kinetics. In this chapter the validation of the various schemes is restricted to the reproduction of thermodynamical properties in linear and branched alkanes for which a huge number of experimental data and theoretical calculations are available. The efficiency of the exact and different approximative schemes is tested. The exact coupled scheme has been numerically applied to the n-alkanes up to hexane. For all alkane hydrocarbons it turns out that the simplest approach, which obviously is the most cost-efficient model, is closest to the exact scheme giving the best experimental agreement. Attempts have been made to find out the underlying reasons for the success of the simplest approach. The presented computational tools are all based on first principles and may be applied in arbitrary molecules. This work is a first step in the development of a suitable algorithm for hindered rotors that go beyond the semi-empirical approaches and that can be incorporated in quantum chemistry packages.

4.1 Introduction

Recently there is a lot of interest in calculating various thermodynamical and kinetic properties, such as entropies, heat capacities, rate constants,... from first principles. Many of these properties cannot be assessed easily from the experiment. Moreover, theoretical calculations can reveal microscopic insight into macroscopic phenomena. The molecular partition function Q forms the bridge between the macroscopic and microscopic description of the molecular system. For a general polyatomic molecule the most difficult part to evaluate is the contribution arising from the global rotation and internal motions of the molecule, since the latter can generally not be decoupled. A general and exact theoretical framework has been developed by Kilpatrick and Pitzer (KP) [28] in the 1940's. Numerical computation of this exact model was by far out of computational feasibility, and even for simple systems some crucial simplifications have been incorporated in the model to make it applicable. In addition empirically adjusted parameters are used in order to allow some numerical applications and their practical scheme was mainly based on analytical elaborations in classical mechanics. But this way of handling was principally inspired by computational limitations of that time. Anyway their theoretical framework was exact and forms the starting model of most subsequent work in the last decades in this field. Multiple articles have been published in this area and most of the proposed models have been applied on alkanes as they offer a lot of reliable experimental data on thermodynamic quantities. They constitute an ideal set of molecules to validate the various derived methods.
It is not the intention of the authors to give a complete overview of all relevant work in the literature. We restrict ourselves to sketch some milestones in the further development of the exact KP model. One way is the construction of an empirical expression for thermodynamic functions with group-additivity contributions. This has been successfully done by Scott [52] who succeeded in deriving a general expression to compute the chemical thermodynamic properties for all alkane hydrocarbons including a lot of correlations with a total of 37 parameters which are all empirically adjusted by least squares fitting. The applied formulas implement elements of the KP theory. Despite the great success of their empirical model for computing alkane thermochemistry, it is not the proper way for further developing general utilities for a widespread application. But Scott's work remains very valuable as a reliable database for all alkane thermochemical properties has been constructed.

Meanwhile, the computer capacities were systematically increasing and first attempts to evaluate the thermochemical properties in an ab initio way have been done by a lot of authors. Current quantum chemical computational packages give ab initio predictions for entropies, etc., but the nuclear motion is described within the Harmonic Oscillator approximation. This may be adequate for some molecules at low temperatures and as long as the system remains in the part of the potential energy surface where the harmonic oscillator approximation to the potential energy surface holds. Many molecules contain "large amplitude" or "low frequency motions" that are characterized by strongly anharmonic potentials. Examples are internal rotations, inversions, quartic oscillations,... [53, 54, 55]. Hindered rotations are the most known and have been widely studied in one dimension, when the potential can be expressed as a sum of single Fourier terms. Slanina [56], Pan [57], and Truhlar [58] have presented analyses of internal rotation (IR) for the case of a symmetric top attached to a rigid body with rotational potential barriers of the form $V = \frac{V_0}{2}(1 - \cos(m\phi))$, or the sum of such potentials if more than one internal rotor is present. More recently this method has been extended to multiple Fourier terms of the rotational potential in deriving a new numerical algorithm in solving the (1D) Schrödinger differential equation for the evaluation of the partition function [2, 33, 35, 44]. It has been shown that even a simplified model with asymmetric internal rotors can improve the partition functions substantially.

In the development of ab initio methods for an accurate evaluation of thermochemical properties, we particularly report the work of East and Radom [5], DeTar [59] and Guthrie [39]. The papers of DeTar and Guthrie use the rigid rotor harmonic oscillator approximation and make an approximate correction for the entropy of mixing when there is more than one conformation. Their results are very promising but are limited in their general applicability. Their model is restricted for reproducing entropies and heat capacities and not suitable for the evaluation of accurate partition functions for the internal modes of the molecule. The work of East and Radom [5] does represent a milestone in the ab initio computation of molecular entropies for gases. Three general utility procedures were presented differing in the choice for calculating the internal rotor partition function. The rotational potential was found on an ab initio basis and was fitted to a general Fourier series potential, which limits the use for more asymmetric molecules. The KP model is applied in the sense that the tables of Pitzer et al. are used to provide the corrections to the entropy, but the work of East and Radom does not pretend to further elaborate on the KP model and to develop an algorithm for hindered rotors (coupled and/or

uncoupled) that could be incorporated in the quantum chemistry packages. Finally we report the work of Robertson and co-workers [60, 61, 62, 63]. Their work approaches closely the goal of the present study. Theoretical schemes are proposed to predict accurate densities of states (inverse Laplace transforms of the statistical partition functions) that take into account the interaction of the global rotation with the internal motions of the molecule (Coriolis interaction). However, a full ab initio approach is missing, relaxation of the atomic nuclei in the evaluation of the torsional potentials is not taken into account and the potentials are assumed to be separable.

The aim of this chapter is not to do better in predicting thermochemical properties for alkane hydrocarbons than do previous works. The ultimate aim is to develop accurate but feasible computational procedures, *i.e.* tools, for generating the partition function Q for hindered rotors and other internal modes based on first principles that can be incorporated in the quantum chemistry packages and that can be applied to any molecule. Starting model is the exact classical KP scheme. The scheme is exact in the sense that it can couple mutual internal rotations of asymmetric tops which are also coupled to the global rotation of the molecule. The scheme also allows extension to other internal modes. Beside the exact coupling treatment various approximative schemes in ascending order of assumptions are presented allowing for a practical implementation of the methodology in applications with a medium number of internal rotors present. We focus on a validation of the various approximative –still ab initio– schemes with respect to the exact coupled model. An accurate reproduction of microscopic partition functions from first principles opens a lot of perspectives for an accurate description of thermochemistry and reaction kinetics.

All basic elements for the construction of the kinetic energy matrix are given in the pioneering works of Pitzer [26, 15, 27, 28, 29, 30]. The description is based on classical mechanics and the kinetic energy can be written as a quadratic form in which a generalized inertial tensor is figuring [64]. It contains the overall moments of inertia (global rotation), the moments of the internal motions (e.g. of internal rotation), the kinetic coupling between internal motions, and the kinetic coupling between the internal modes and the overall rotation (Coriolis coupling). All of its elements depend on the geometry of the molecule, which can be determined on a microscopic ab initio basis. In an exact scheme of coupled internal rotors, one has to combine the kinetic energy with a multi-dimensional potential energy surface.

The practical usage of such scheme for a general polyatomic molecule with several attached asymmetric tops has been rather limited up to now. Some work in this field has been done by Smeyers and co-workers [65, 66, 67, 68] with the aim to determine far infrared spectra from ab initio calculations. Most of the studied molecules (acetone, propanal, ethanol, dimethylamine) have two branched side groups that are rotating.

The implementation of the exact coupled scheme in this chapter is more general compared with already published work in the literature in the sense that we construct the multidimensional potential energy surface associated with mutually coupled asymmetric rotors on a fully ab initio basis, where all geometrical parameters were allowed to relax on the constrained energy surface. Such an approach was already followed by the authors in [34] to determine the effect of the coupling between two rotors on the kinetics of the addition of ethene to the ethylbenzene radical. Here the kinetic energy matrix is constructed on the basis of the relaxed geometries as obtained from the previous calculation. The applications are focussed on alkanes, both linear (up to decane) and branched. For these systems a huge number of experimental data on entropies and heat capacities is available and thus the proposed set of molecules is ideally suited to validate the suggested theoretical procedures.

Starting from the exact coupled scheme, we also present some approximative methods in order to make the computations feasible for further practical applications. They cover a variety of methods that were already suggested in literature. The hindered rotor (HR) model is the most commonly known. It uncouples both the kinetic and potential energy contribution and keeps the moments of inertia fixed along the one-dimensional potential. It has been widely used in recent literature and has proven to substantially improve the thermodynamic and kinetic properties [2, 33, 35, 44, 69, 70]. The IR model was also used in a previous paper of the authors, in order to reproduce the entropies and heat capacities of n-alkanes [14]. It was found that the uncoupled approach surprisingly gives very good predictions of the partition functions and derived quantities. The question remains what lies on the origin of this "well behavior". Since the present chapter covers both the exact and derivative methods that were already used in literature, this work is ideally suited to unravel the origin of the quality of some literature results. A detailed comparison of our results will be made not only with experimental values but also with other literature values on similar systems.

4.2 Theory

The computational tools presented later on in this section are based upon the theoretical framework offered by the basic paper of Kilpatrick and Pitzer (KP) [28] and related pioneering papers of Pitzer and coworkers [26, 15, 27, 28, 29, 30]. Their work offers an exact classical scheme for constructing the kinetic energy of general use to any molecule with internal rotations of attached tops either symmetric or asymmetric.
Our applications of KP theory incorporate numerical algorithms and recipes for computing the partition function Q in completely ab initio ways.

4.2.1 Internal rotations of asymmetric groups in heavy rigid bodies

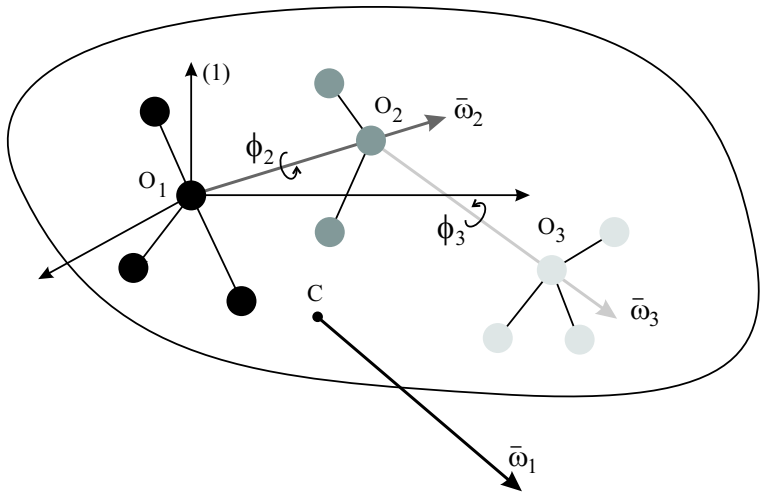

Figure 4.1: Schematic representation of the different coordinate systems in a molecule with several rotating tops.

Unlike in the original KP paper we systematically express all atom coordinates with respect to the body fixed frame (1) (Fig.4.1) instead of introducing additional frames corresponding with the individual rotating subclusters. This convention helps us to generalize the computer code for describing all possible internal modes.

The center of mass of the entire molecule is determined by

$$\left(x_C^{(1)}\right) = \frac{1}{M}\sum_A m_A \left(x_A^{(1)}\right) \tag{4.1}$$

with the total mass $M = \sum_A m_A$ and varies with the torsional angles.
To illustrate the further notation we consider two consecutive subclusters (subgroup (2) and subgroup (3) as displayed in Fig.4.1). The center of mass of the cluster rotating about the first internal rotation axis O_1O_2 (which is a single bond) with respect to frame (1) is given by

$$\left(x_{C_2}^{(1)}\right) = \frac{1}{M'}\sum_A{}' m_A \left(x_A^{(1)}\right) \tag{4.2}$$

where we use the abbreviation $\sum'_A$ to restrict the summation over all atoms of subgroups (2) and (3). M' represents the total mass of the two subgroups. It might be clear that the position of C_2 depends on the torsional angles ϕ_2 and ϕ_3 of the two rotors. In a similar way the summation restricted to atoms of subgroup (3) is abbreviated by $\sum''_A$.
A straightforward analytical calculation along the lines of the Pitzer work [28] and taking into account a proper handling of center of mass fluctuations of the different subclusters, the dynamics of the various atomic positions with regard to an arbitrary space fixed frame (0) can be deduced.

4.2.2 Classical kinetic energy

The total kinetic energy with respect to a space fixed frame (0) is given by

$$T = \frac{1}{2}\sum_A m_A \left(\dot{x}_A^{(0)}\right)^T \left(\dot{x}_A^{(0)}\right) \tag{4.3}$$

By a proper treatment of the center of mass of the various rigid bodies coming into play, as outlined in previous subsection, the overall translation separates out in a natural way. The remaining kinetic energy has now the following structure :

$$T = \frac{1}{2}\left(\left(\omega_1^{(1)}\right)^T, \omega_2, \omega_3\right) A \begin{pmatrix} \left(\omega_1^{(1)}\right) \\ \omega_2 \\ \omega_3 \end{pmatrix} \tag{4.4}$$

In this general framework it is recommendable to not switch to other local frames and to refer the rotation axes with respect to the body-fixed frame (1):

$$\left(\omega_2^{(1)}\right) = \begin{pmatrix} \lambda_{2x}^{(1)} \\ \lambda_{2y}^{(1)} \\ \lambda_{2z}^{(1)} \end{pmatrix} \omega_2 \quad , etc... \tag{4.5}$$

with the introduction of the direction cosines.
The quadratic form in the kinetic energy expression (4.4) has the following general structure :

$$A = \begin{pmatrix} I & \Lambda_{12} & \Lambda_{13} \\ \Lambda_{12}^T & I_2 & \Lambda_{23} \\ \Lambda_{13}^T & \Lambda_{23}^T & I_3 \end{pmatrix} \tag{4.6}$$

(i) I stands for the inertial tensor

$$I = \sum_A m_A \chi_1^{(1)} (A - C)^T \chi_1^{(1)} (A - C) = \begin{pmatrix} I_{xx} & -I_{xy} & -I_{xz} \\ -I_{xy} & I_{yy} & -I_{yz} \\ -I_{xz} & -I_{yz} & I_{zz} \end{pmatrix} \tag{4.7}$$

with

$$I_{xy} = \sum_A m_A \left(x_A^{(1)} - x_C^{(1)} \right) \left(y_A^{(1)} - y_C^{(1)} \right), \text{ etc..} \tag{4.8}$$

and the 3x3 matrix $\chi^{(1)}(A)$ is given by

$$\chi^{(1)}(A) = \begin{pmatrix} 0 & -z_A^{(1)} & y_A^{(1)} \\ z_A^{(1)} & 0 & -x_A^{(1)} \\ -y_A^{(1)} & x_A^{(1)} & 0 \end{pmatrix} \tag{4.9}$$

In view of the type of $\chi^{(1)}(A)$, the linear superposition property is also valid :

$$\chi^{(1)}(c_1 A + c_2 B) = c_1 \chi^{(1)}(A) + c_2 \chi^{(1)}(B) \tag{4.10}$$

The matrix elements in Eq.(4.7) represent the moments of inertia of the entire molecule about the axes of frame (1) but referred to the center of mass C. It should be stressed that in this general picture of rotating asymmetric tops, the position of the global center of mass is floating and not fixed in the body-fixed frame (1). The axes of frame (1) are coinciding with the principal axes of inertia corresponding with a conformation of the global molecule. For convenience, the energetically most favorable conformation is chosen. By varying the torsional angles the inertial tensor loses its diagonal structure.

(ii) Λ_{12} and Λ_{13} describe the coupling of the global rotation with the internal rotation of the subgroups (2) and (3) respectively. They are represented by three-dimensional column matrices:

$$\Lambda_{12} = \sum_A{}' m_A \chi^{(1)} (A - C)^T \chi^{(1)} (A - O_2) \left(\lambda_2^{(1)} \right) \tag{4.11}$$

and

$$\Lambda_{13} = \sum_A{}'' m_A \chi^{(1)}(A-C)^T \chi^{(1)}(A-O_3)\left(\lambda_3^{(1)}\right) \tag{4.12}$$

(iii) I_2 represents the instantaneous moment of inertia of the two attached subgroups about the ω_2-axis, with a correction term resulting from the asymmetric nature of the rotating tops :

$$\begin{aligned} I_2 &= \sum_A{}' m_A \left(\lambda_2^{(1)}\right)^T \chi^{(1)}(A-O_2)^T \chi^{(1)}(A-O_2)\left(\lambda_2^{(1)}\right) \\ &\quad -\frac{M'^2}{M}\left(\lambda_2^{(1)}\right)^T \chi^{(1)}(C_2-O_2)^T \chi^{(1)}(C_2-O_2)\left(\lambda_2^{(1)}\right) \end{aligned} \tag{4.13}$$

(iv) Similarly, I_3 stands for the instantaneous moment of inertia of the last attached subgroup about the ω_3-axis, again with a correction term:

$$\begin{aligned} I_3 &= \sum_A{}'' m_A \left(\lambda_3^{(1)}\right)^T \chi^{(1)}(A-O_3)^T \chi^{(1)}(A-O_3)\left(\lambda_3^{(1)}\right) \\ &\quad -\frac{M''^2}{M}\left(\lambda_3^{(1)}\right)^T \chi^{(1)}(C_3-O_3)^T \chi^{(1)}(C_3-O_3)\left(\lambda_3^{(1)}\right) \end{aligned} \tag{4.14}$$

(v) The coupling term between the two subsequent rotations is given by

$$\begin{aligned} \Lambda_{23} &= \sum_A{}'' m_A \left(\lambda_2^{(1)}\right)^T \chi^{(1)}(A-O_2)^T \chi^{(1)}(A-O_3)\left(\lambda_3^{(1)}\right) \\ &\quad -\frac{M'M''}{M}\left(\lambda_2^{(1)}\right)^T \chi^{(1)}(C_2-O_2)^T \chi^{(1)}(C_3-O_3)\left(\lambda_3^{(1)}\right) \end{aligned} \tag{4.15}$$

Almost all quantities of the quadratic kinetic energy matrix depend on the two torsional angles ϕ_2 and ϕ_3.

4.2.3 Canonical form of the kinetic energy

The global rotation of the molecule is completely determined by the cartesian components of $\left(\omega_1^{(1)}\right)$ with respect to the body-fixed frame, but these are not generalized velocities. The evaluation of the partition function in the classical approach needs the kinetic energy expressed in terms of canonical conjugate variables.

We therefore introduce the Euler angles θ, φ, ψ (we follow the definition as

given in Ref.[64]).

$$\begin{pmatrix} \omega_{1x}^{(1)} \\ \omega_{1y}^{(1)} \\ \omega_{1z}^{(1)} \\ \omega_2 \\ \omega_3 \end{pmatrix} = \begin{pmatrix} \cos\psi & \sin\theta\sin\psi & 0 & 0 & 0 \\ -\sin\psi & \sin\theta\cos\psi & 0 & 0 & 0 \\ 0 & \cos\theta & 1 & 0 & 0 \\ 0 & 0 & 0 & 1 & 0 \\ 0 & 0 & 0 & 0 & 1 \end{pmatrix} \begin{pmatrix} \dot{\theta} \\ \dot{\varphi} \\ \dot{\psi} \\ \dot{\phi}_2 \\ \dot{\phi}_3 \end{pmatrix} \tag{4.16}$$

or in shorthand notation $\Omega = F\dot{\Phi}$
For the internal rotations we keep the torsional angles ϕ_2 and ϕ_3 as generalized coordinates.
The kinetic energy is then written in terms of the generalized velocities $\dot{\Phi}$:

$$T_{rot} = \frac{1}{2}\,\dot{\Phi}^T B \dot{\Phi} \tag{4.17}$$

with $B = F^T A F$.
Since the conjugate moments are defined according to

$$L_\Phi = \frac{\partial T}{\partial \dot{\Phi}} = B\dot{\Phi} \tag{4.18}$$

we get the final canonical form of the kinetic energy:

$$T = \frac{1}{2} L_\Phi^T B^{-1} L_\Phi \tag{4.19}$$

We emphasize that the B^{-1} matrix is a function of the Euler and torsional angles.

4.2.4 Partition function

The total energy of the molecule submitted to an overall rotation and two subsequent rotations of attached tops is given by the general expression:

$$H = \frac{1}{2} L_\Phi^T B^{-1}(\theta, \varphi, \psi, \phi_2, \phi_3) L_\Phi + V(\phi_2, \phi_3) \tag{4.20}$$

Applying the Aston and Eidinoff integral [71] the corresponding classical partition function simply transforms to an integration over the two-dimensional grid of torsional angles:

$$q_{rot} = \frac{1}{\sigma}\frac{1}{h^5}\left(\frac{2\pi}{\beta}\right)^{\frac{5}{2}} 8\pi^2 \int_0^{\frac{2\pi}{\sigma_2}} \mathrm{d}\phi_2 \int_0^{\frac{2\pi}{\sigma_3}} \mathrm{d}\phi_3 \sqrt{\det A(\phi_2, \phi_3)}\, e^{-\beta V(\phi_2, \phi_3)} \tag{4.21}$$

with $\beta = \frac{1}{k_B T}$.
This can be performed in a numerical way. In Eq.(4.21), σ stands for the symmetry number of the whole molecule, while σ_2 and σ_3 are the symmetry numbers associated to the two internal rotations about ϕ_2 and ϕ_3.
Expression (4.21) can easily be generalized to any number of attached rotating tops, including branched tops.

Finally quantum effects are also taken into consideration by use of the Pitzer and Gwinn [15] approximation. For further comment and validation, reference is given to Ref.[72].

4.2.5 Approximative schemes

We propose four general utility procedures for calculating the partition functions of coupled internal rotors, designated as C1,C2,C3(C3'),C4(C4') in order of descending order of model accuracy. They are schematically visualized in Table 4.1 and they can be applied in principle for any number of internal rotations. In the following we disentangle the different approaches in case of **two** coupled internal rotations. It facilitates the discussion and makes it more transparent.

		Approximate schemes	
level	$V(\phi_2, \phi_3)$	$A(\phi_2, \phi_3)$	$f(\phi_2, \phi_3)$
C1	2D-PES geometry optimization	$\Rightarrow$ full construction	$\Rightarrow$ full construction
C2	1D-PES geometry optimization $V(\phi_2) + V(\phi_3)$	$\Rightarrow A(\phi_2)$ $\Rightarrow A(\phi_3)$	$\Rightarrow f_2(\phi_2)$ $\Rightarrow f_3(\phi_3)$
C3	1D-PES geometry optimization $V(\phi_2) + V(\phi_3)$	full construction no geometry optimization	$\Rightarrow$ full construction no geometry optimization
C4	1D-PES geometry optimization $V(\phi_2) + V(\phi_3)$	A_0	1
C4'	1D-PES geometry optimization $V(\phi_2) + V(\phi_3)$	A'_0 $(\Lambda'_{23} = 0)$	$f = \frac{det\, A'_0(\Lambda_{23}=0)}{det\, A_0}$

Table 4.1: Schematic overview of the various HR schemes under consideration in case of two coupled internal rotations.

C1 This is the exact scheme, referred to as 'exact-coupled'. It consists of an exact construction of the two-dimensional energy surface determined on a two-dimensional grid ranging from 0° to 360° in both torsional angles. For each grid point the potential is calculated by optimizing all variables with

constrained ϕ_2 and ϕ_3 angles. The kinetic energy matrix $A(\phi_2, \phi_3)$ of Eq.(4.6) is constructed on the basis of the relaxed geometries obtained from the potential energy calculation. Thus no geometric variable is assumed to be fixed at the equilibrium position but instead they are allowed to fully relax.
It is convenient to separate out the reference kinetic energy matrix A_0 ($\equiv A(\phi_2^{ref}, \phi_3^{ref})$) belonging to the energetically most favored conformation:

$$\det A(\phi_2, \phi_3) = \det A_0 \cdot f(\phi_2, \phi_3) \tag{4.22}$$

$f(\phi_2, \phi_3)$ is defined as the correlation function for the kinetic energy matrix.

C2 The most time consuming step in the exact procedure is the construction of the two-dimensional potential energy surface (2D-PES). This can be drastically reduced by constructing the uncoupled two-dimensional potential by means of the one-dimensional rotational potentials: $V(\phi_2, \phi_3) \approx V(\phi_2) + V(\phi_3)$. These rotational potentials are obtained by pointwise geometry optimizations at a discrete set of torsional angles corresponding with one of the two internal rotations under consideration. All further approximation schemes make use of this uncoupled potential energy surface (1D-PES).
It is no longer possible to construct the kinetic energy matrix from the optimized geometries at each point of the two-dimensional grid. Instead one can construct two different sets of matrices $A(\phi_2, \phi_3)|_{\phi_3 = rel}$ and $A(\phi_2, \phi_3)|_{\phi_2 = rel}$. In a one-dimensional constrained geometry optimization the other torsional angle is no longer a free parameter but completely determined by the relaxation. (More technical details about the construction of the one-dimensional potential energy surfaces and associated kinetic energy matrices will be given in the next section). Both sets of matrices yield separate correlation functions $f_2(\phi_2)$ and $f_3(\phi_3)$ according to equation (4.22). In scheme C2 we assume a factorization of the two-dimensional correlation function:

$$f(\phi_2, \phi_3) = f_2(\phi_2) \cdot f_3(\phi_3) \tag{4.23}$$

This approximate scheme is inspired by the situation in which the kinetic energy matrix exhibits a diagonal structure. In that case the determinant is simply a product of the various inertial moments of rotation, which all behave independently.
The adequacy of this factorized scheme C2 should be tested numerically. It offers a lot of perspectives in simplifying the procedure in calculating the partition function associated with a long chain of rotating tops. It is easily seen

that the rotational partition function (Eq.4.21) factorizes according to:

$$\begin{aligned} q_{rot} &= \frac{1}{\sigma}\frac{1}{h^3}\left(\frac{2\pi}{\beta}\right)^{\frac{3}{2}} 8\pi^2\sqrt{\det A_0} \\ &\cdot\left(\frac{1}{h}\sqrt{\frac{2\pi}{\beta}}\int_0^{\frac{2\pi}{\sigma_2}} \mathrm{d}\phi_2\ \sqrt{f_2(\phi_2)}e^{-\beta V_2(\phi_2)}\right) \\ &\cdot\left(\frac{1}{h}\sqrt{\frac{2\pi}{\beta}}\int_0^{\frac{2\pi}{\sigma_3}} \mathrm{d}\phi_3\ \sqrt{f_3(\phi_3)}e^{-\beta V_3(\phi_3)}\right) \end{aligned} \tag{4.24}$$

All integrations are one-dimensional and numerical integration poses no problem at all even with increasing number of IR's.

C3 (C3') In the approximation scheme C3 the factorization of the correlation function $f(\phi_2, \phi_3)$ is no longer maintained. The kinetic energy matrix is constructed from geometries as obtained by performing the two-dimensional torsional motions starting from the reference geometry (of the most stable conformer) and without any further geometry optimization. This has the numerical inconvenience that the integrations are no longer one-dimensional but two-dimensional. This aspect can pose severe constraints on the total number of "coupled" IR's, as each rise of the dimensionality, will increase the computational cost with almost two orders. Current workstations are able to numerically evaluate multi-dimensional integrations over cyclic coordinates up to a dimension of 5 or 6. This numerical limitation restricts the applicability of the C3 approach to large molecules with more than 6 IR's. The additional IR's should be considered as uncoupled and this scheme is called C3'.

C4 (C4') Finally, at the C4 level the kinetic energy matrix A is kept fixed at the position of the reference conformer $A_0 = A(\phi_2^{ref}, \phi_3^{ref})$. In this simple case, the correlation function becomes unity. The inertial tensor I in A_0 is diagonal, as the axes of the body-fixed frame (1) are chosen parallel with the principal axes of inertia of the reference conformer.
If the torsional motions are expected to slightly change the principal axes, this C4 approximation can be physically supported. This can be the case in molecules where massive groups are associated to the main rigid group in our model. For long chain alkanes this physical argument is no longer valid, but the validity of the C4 level must be tested numerically versus the higher level approaches C1, C2 and C3.
The diagonal structure of I [in Eq.(4.7)] for the reference geometry suggests the

application of a congruent transformation P making the kinetic energy matrix A_0 block diagonal:

$$A_0' = P^T A_0 P = \begin{pmatrix} I_0 & 0 \\ 0 & I_{23}^{red} \end{pmatrix} \tag{4.25}$$

with $I_{23}^{red} = \begin{pmatrix} I_2^{red} & \Lambda_{23}' \\ \Lambda_{23}'^T & I_3^{red} \end{pmatrix}$.

I_2^{red} $[I_3^{red}]$ represents the reduced moment of inertia of the torsional motion about the z_2-axis (*i.e.* rotation axis O_1O_2) [z_3 axis (*i.e.* rotation axis O_2O_3)]:

$$I_2^{red} = I_2 - \frac{\Lambda_{x2}^2}{I_x} - \frac{\Lambda_{y2}^2}{I_y} - \frac{\Lambda_{z2}^2}{I_z} \tag{4.26}$$

with

$$\Lambda_{x2} = (\Lambda_{12})_1 \ , \quad \Lambda_{y2} = (\Lambda_{12})_2 \ , \quad \cdots \tag{4.27}$$

For symmetric tops the interaction reduces to $\Lambda_{x2} = \lambda_{x_1}(z_2) I_2$, etc. with $\lambda_{x_1}(z_2)$ the direction cosine between the z_2-axis, and the x_1-axis. This gives rise to standard expressions for the reduced moments of inertia [2, 34].
The interaction between the two torsional motions is given by

$$\Lambda_{23}' = \Lambda_{23} - \frac{\Lambda_{x2}\Lambda_{x3}}{I_x} - \frac{\Lambda_{y2}\Lambda_{y3}}{I_y} - \frac{\Lambda_{z2}\Lambda_{z3}}{I_z} \tag{4.28}$$

The congruent transformation also affects the variables of the bilinear form [Eq.(4.16)]:

$$\Omega' = P^{-1}\Omega = P^{-1} F \dot{\Phi} \tag{4.29}$$

In this approach the kinetic energy in terms of the conjugate momenta L_Φ becomes:

$$T = \frac{1}{2} L_\Phi^T \left(F^{-1} P (A_0')^{-1} P^T (F^{-1})^T \right) L_\Phi \tag{4.30}$$

If we neglect –in addition– the interaction between the two internal rotations ($\Lambda_{23}' = 0$), the kinetic energy matrix A_0' (Eq.4.25) is completely diagonal and the kinetic energy separates out clearly the contribution from the global rotation and those from the two internal torsional motions:

$$T = \frac{1}{2} L_E^T \left(E^T I_0 E \right)^{-1} L_E + \frac{1}{2} L_{\Phi_2}^T I_2^{red\,-1} L_{\Phi_2} + \frac{1}{2} L_{\Phi_3}^T I_3^{red\,-1} L_{\Phi_3} \tag{4.31}$$

E stands for the first 3x3 block in the transformation matrix F [Eq.(4.16)].

In this approach, which we refer to as **C4'**, the rotational partition function simplifies into

$$\begin{aligned} q_{rot} &= \frac{1}{\sigma}\frac{1}{h^3}\left(\frac{2\pi}{\beta}\right)^{\frac{3}{2}} 8\pi^2\sqrt{I_x I_y I_z} \\ &\cdot\left(\frac{1}{h}\sqrt{\frac{2\pi}{\beta}}\int_0^{\frac{2\pi}{\sigma_2}} \mathrm{d}\phi_2\ \sqrt{I_2^{red}}e^{-\beta V_2(\phi_2)}\right) \\ &\cdot\left(\frac{1}{h}\sqrt{\frac{2\pi}{\beta}}\int_0^{\frac{2\pi}{\sigma_3}} \mathrm{d}\phi_3\ \sqrt{I_3^{red}}e^{-\beta V_3(\phi_3)}\right) \end{aligned} \tag{4.32}$$

This C4' scheme coincides with the standard procedure applied by the authors in earlier works on the influence of internal rotors on the kinetics of chemical reactions [2, 34] and thermodynamic quantities [14] (1D-HR).

4.3 Numerical implementation

All ab initio calculations were performed using the Gaussian98 and Gaussian03 (for the construction of the 3D-PES in hexane) software package [12, 13]. The molecular orbitals were expanded in a triple-ζ 6-311G basis augmented with single first d and p polarization functions [8]. All electronic structure calculations were done within the Density Functional Theory framework with use of the B3LYP functional [7].

Due to its nature the C1 method is limited in its applicability. It needs the construction of a multi-dimensional rotational potential and corresponding kinetic energy matrix and it is obvious that their exists a limit to the dimension of the coupled potential surface. Each rise of the dimension with one unit causes an increase of the total computing cost with a factor corresponding with the number of grid points chosen to define the rotational potential in one torsional angle. We systematically take grid increments of 5° yielding 72^n grid points with n representing the dimension of the surface. In this work the C1 method is applied to pentane (C1=2D-HR) and hexane (C1=3D-HR). In pentane the coupled potential energy surface was determined for the ethyl-ethyl torsions. For 72×72 grid points the potential is calculated at the B3LYP/6-311g** level according to :

$$V(\phi_i, \phi_j) = \underset{\forall \eta_k \neq \phi_i, \eta_k \neq \phi_j}{\mathbf{min}} V(\eta_1, \ldots, \eta_{3N-6}) \tag{4.33}$$

In this formula η_k stand for the geometrical parameters defining uniquely the molecular configuration and thus all geometrical parameters are allowed to relax, except ϕ_i and ϕ_j. To investigate the influence of the level of theory on the potential energy, the coupled surface was also calculated at the UHF/6-31g(d) level. The Hartree-Fock based method is computationally less intensive and in view of application to other molecules it is interesting to perform a sensitivity analysis in terms of variations in the potential caused by various levels of theory. Due to symmetry consideration of the molecule the number of grid points in which the potential must be calculated can be reduced by a factor four. The optimized geometries on the constrained potential energy surface serve as an input for the construction of the two-dimensional kinetic energy matrix A.

We also applied the exact C1 scheme to hexane with coupled ethyl-propyl-ethyl rotations. We did the calculations using Gaussian03 within the B3LYP/6-311g** level. Extension to higher dimensions of coupled torsions is for the moment almost unfeasible, and is probably not really necessary to validate the

different schemes proposed in this work.

For the recipes C2, C3 and C4, the coupled potential energy surface is replaced by a sum of one-dimensional potentials. These were calculated at the B3LYP/6-311g** level by evaluating :

$$V(\phi_i) = \min_{\forall \eta_k \neq \phi_i} V(\eta_1, \ldots, \eta_{3N-6}) \tag{4.34}$$

on a one-dimensional grid in the specific torsional angle with grid increments of 5°. The obtained geometrical parameters are used to evaluate the kinetic energy matrices as used in the method C2 and their correlation function.

In order to evaluate the final corrected molecular partition function one has to replace the various relevant harmonic oscillator contributions to the partition function and the global rotational partition function of the reference conformer as obtained from the standard quantum chemical packages (*e.g.* from G98 or G03 output) by the new constructed partition functions following the lines outlined in the present chapter. The harmonic oscillator contributions can be obtained from a frequency calculation on the reference structure. When the molecule under consideration becomes longer or heavily branched various internal motions can be mixed up and it is no longer possible to extract from a frequency calculation the harmonic oscillator contributions of the pure internal rotations. In these cases only part of the harmonic oscillator partition function should be replaced and more precisely that part corresponding with the vibrational mode responsible for the internal rotation under consideration. This can be accomplished by determining the harmonic oscillator frequency numerically from the second derivative of the rotational potential at $\phi_i = 0°$.

Once the molecular partition function Q is known, the entropy and heat capacity can be evaluated as follows :

$$S = R\left(\ln Q + T\left(\frac{\partial \ln Q}{\partial T}\right)\right) \tag{4.35}$$

$$C = RT\left(2\frac{\partial \ln Q}{\partial T} + T\frac{\partial^2 \ln Q}{\partial T^2}\right) \tag{4.36}$$

4.4 Results and discussion

4.4.1 The schemes C1, C2, C3, C4 and C4' applied to pentane

Pentane has four internal rotations: two are the torsional motions of the terminal methyl groups and the other two are asymmetric rotations of the ethyl groups about the two interior C-C bonds. The exact coupled scheme C1 is applied to the coupling of the two ethyl rotors. The angular coordinates describing the motion of the asymmetric rotors will be denoted by the angles ϕ_2 and ϕ_3.

Coupled potential energy surface

The coupled potential energy surface for the two ethyl rotations was calculated at both the B3LYP/6-311g** and UHF/6-31g(d) level. The 2D-PES of the two ethyl rotations in pentane at the B3LYP/6-311g(d,p) level of theory and the contour plot together with the identification of the stable conformers are displayed in Fig.4.2. If we consider all combinations for each dihedral angle of 180° (trans,t), 60° (gauche, g+) and −60° (gauche, g-), nine stable conformers would result on the potential energy surface. Some of them are equivalent or are enantiomers due to symmetry considerations. The conformers characterized by two adjacent gauche bonds with opposite sign (g+g- or g-g+), are characterized by severe steric interactions between the end-standing methyl groups. Without further relaxation these points are first order saddle points, but when relaxing these strains through a strongly asymmetric torsion of the carbon backbone, each of these first-order saddle points give rise to one racemic pair of enantiomeric structures. In conclusion, we obtain 11 stable conformers on the potential energy surface. The strain energies and the dihedral angles are given in Table 4.2 for the minima and maxima on the coupled surface. Our results are in agreement with other literature data [73, 74, 75].

As the construction of a 2D-PES needs large computer time, it is instructive to investigate whether the coupled 2D surface can be decomposed into two separate 1D potentials: $V(\phi_2, \phi_3) \approx V_2(\phi_2) + V_3(\phi_3)$. This decomposition forms the core of the approaches C2,C3,C4 and C4' (see Table 4.1). The difference between the two models can be best evaluated by comparing the characteristics of the stable minima and maxima on the coupled and uncoupled surface (cfr. Table 4.2). Whereas on the coupled surface four energetically different minima could be found, only three energetically different minima are found on

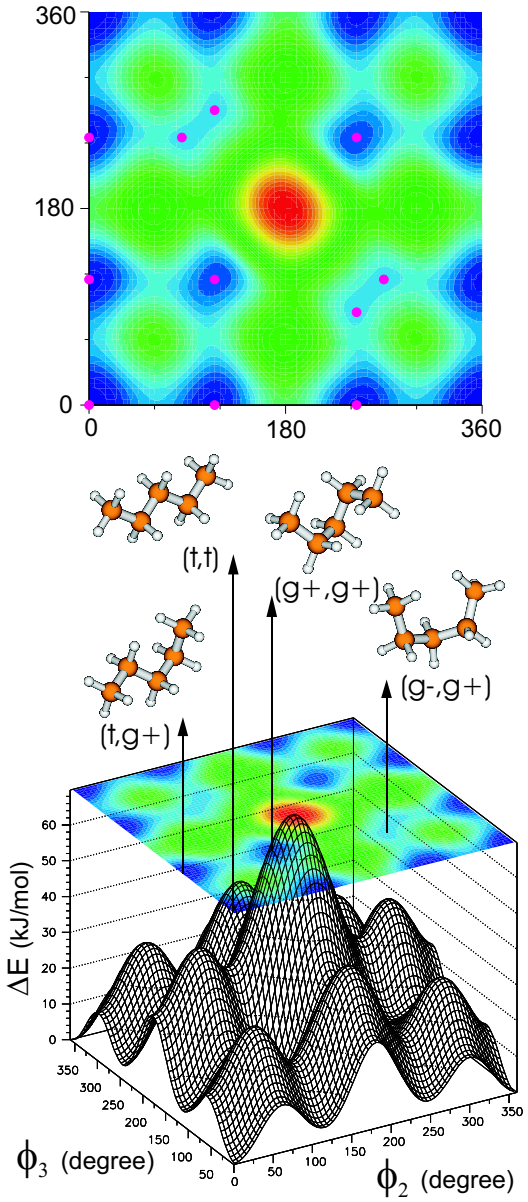

Level of theory: B3LYP/6-311g(d,p)
The *trans* reference conformer corresponds with $\phi_2 = 0°$ and $\phi_3 = 0°$.

Figure 4.2: The 2D-PES of the two ethyl rotations in pentane, with identification of the stable minima.

Energy Minima on coupled surface								
		B3LYP/6-311G**			UHF/6-31G*			
Type	Symmetry	ϕ_1^{relax}	ϕ_2^{geopt}	ΔE(kJ/mol)	ϕ_1^{relax}	ϕ_2^{geopt}	ΔE (kJ/mol)	
tt	C_{2v}	0	0	0.0000	0	0	0.0000	
tg-	C_1	0	115	3.62	0	115	4.32	
tg-	C_1	115	0	3.62	115	0	4.32	
tg+	C_1	0	245	3.62	0	245	4.32	
tg+	C_1	245	0	3.62	245	0	4.32	
g-g-	C_2	115	115	6.74	115	115	7.93	
g-g+	C_1	115	270	13.96	115	275	16.24	
g-g+	C_1	85	245	13.96	85	245	16.24	
g+g-	C_1	245	85	13.96	245	85	16.24	
g+g-	C_1	270	115	13.96	275	115	16.24	
g+g+	C_2	245	245	6.74	245	245	7.93	
Energy Maxima on coupled surface								
(0,60),(60,0),(300,0),(0,300)				12.84			14.60	
(0,180)(180,0)				23.70			26.14	
(60,60)(300,300)				28.94			33.18	
(180,60)(180,300),(60,180),(300,180)				39.30			44.85	
(300,60)(60,300)				29.04			33.24	
(180,180)				69.81			78.81	
Energy Minima on uncoupled surface								
(0,0)				0			0	
(0,115)(115,0),(0,245),(245,0)				3.62			4.32	
(115,115)(115,245),(245,115),(245,245)				7.24			8.64	
Energy Maxima on uncoupled surface								
(0,60),(60,0),(300,0),(0,300)				12.84			14.60	
(0,180)(180,0)				23.70			26.14	
(60,60),(300,60),(60,300),(300,300)				23.70			26.14	
(180,60)(180,300),(60,180),(300,180)				36.54			40.74	
(180,180)				47.40			52.28	

The energy minima and maxima are the points on the calculated grid that resemble closely the real extrema. To find the exact locations and energy values, calculations should be performed in which all variables including the torsional angles of the ethyl rotations are allowed to relax.

Table 4.2: Characteristics of minima and maxima on the potential energy surface of the two ethyl rotations in pentane.

the uncoupled surface. The conformers that are reached by applying two subsequent internal rotations (g+g-,g-g+,g-g-,g+g+) are not correctly described in the uncoupled model. No distinction can be made between conformers with two adjacent gauche bonds with the same sign and opposite sign and thus the stability of the g-g+ type conformers is underestimated while the strain energies of the g-g- type conformers is seriously underestimated. Moreover the double degeneracy of the g+g- and g-g+ conformers is not taken into account, bringing the total number of minima on nine on the uncoupled surface and eleven on the coupled surface.

Similar conclusions can be made for the energy maxima. In both the coupled and uncoupled surface the total number of maxima is fifteen, but in the coupled approach six of them are energetically different while uncoupling reduces this number to five. All "coupled" maxima, which are situated in the

middle of the surface, are seriously underestimated in the uncoupled approach. This is most visible for the broad central bump, which is located in the middle of the potential energy surface and that corresponds to a cis-position of both subsequent ethyl rotations. By calculating the potential by full geometry optimizations like in 2D-PES an extra barrier of about 22.5 kJ/mol is taken into account of which the origin can be traced back to the large steric hindrance present at the energy maxima. Those effects are not taken into account correctly by assuming superposition of the one-dimensional rotational energy barriers. These extra barriers may largely affect the density of states in the low-energy spectrum. When the central peaks are much higher in energy, the whole energy spectrum is shifted toward higher energy values. This causes a lowering of the partition function. We conclude that all approximations which are based on uncoupled 1D-PES but which takes into account the fluctuations of the inertial momenta and principal axes –these correspond with the C2 and C3 approaches– have the tendency to overestimate the partition function and related thermodynamic quantities like entropy. This behavior may not be extrapolated to C4 and C4'. In molecules where the main group is associated to a heavy massive cluster of atoms, the inertial momenta and the principal axes are not fluctuating too much with the torsional motions. In this case the argumentation about a decrease of the partition function in the coupled C1 framework due to the increasing central bump remains valid. This is confirmed by the results in Ref.[34] where the 2D-PES has been constructed in butylbenzene radical. But in long n-alkanes this scenario does not happen. Large fluctuations of the center-of-mass generate kinetic energy contributions to the partition function which compensate the effect arising from the increasing central potential bump in the 2D-PES. Concluding, in long n-alkanes the C4 (C4') partition functions may be smaller than the correct coupled C1 predictions.

Geometries: two-dimensional correlation function

Based on the optimized geometries of the coupled potential energy surface, one can construct the exact two-dimensional kinetic energy matrix for the two ethyl rotations. As it concerns asymmetric rotating tops, large fluctuations in the inertial tensor describing the external rotation, can be expected. The principal moments of inertia and the center of mass become functions of the internal rotation coordinates. In order to separate this dependence, we factorize the kinetic energy matrix according to Eq.(4.22) by introducing the multidimensional correlation function f. In this specific application of the two ethyl rotations in pentane, the dimension is restricted to 2, and $f(\phi_2, \phi_3)$ is displayed in Fig.4.3.

It is not a smooth surface and the correlation function varies between 0.8 and 2.0. The two-dimensional average

$$\left(\frac{1}{2\pi}\right)^2 \int_0^{2\pi} \mathrm{d}\phi_2 \int_0^{2\pi} \mathrm{d}\phi_3 \; f(\phi_2, \phi_3) \tag{4.37}$$

amounts to 1.36.

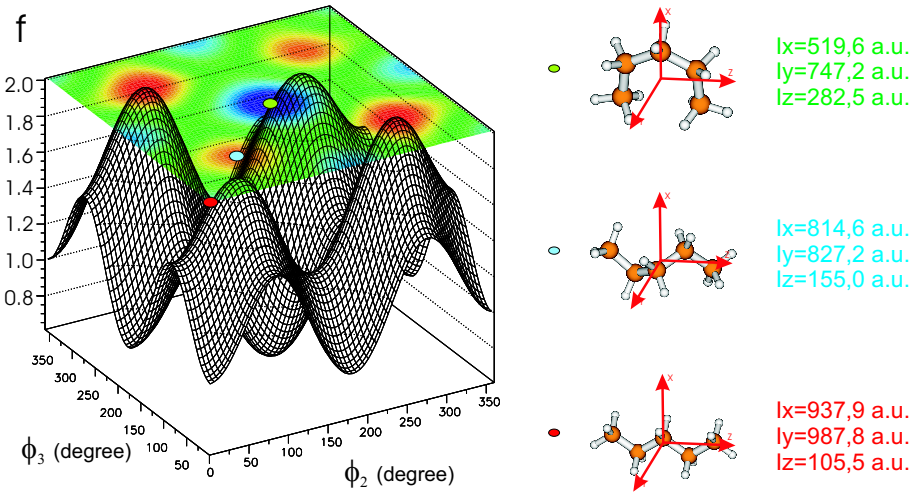

Level of theory: B3LYP/6-311g(d,p)

Figure 4.3: Two dimensional surface of the 2D correlation function $f(\phi_2, \phi_3)$ in pentane. For some critical points on the correlation surface, the inertial axes are shown.

The minima and maxima of the correlation function and potential energy do not necessarily coincide. The potential energy is determined by the electrostatic interactions in the molecule while the correlation function is determined by the geometries. We illustrate this by visualizing the inertial axes for some stable minima and maxima of the correlation function (Fig.4.3). All minima of the correlation function correspond to planar configurations of the molecule. In that case two of the inertial axes lie in the plane of the molecule and thus the distance of the atoms with respect to these axes is minimized, resulting in a minimum for the moments of inertia. The maxima on the other hand are characterized by maximized distances of all of the atoms with respect to the axes of inertia and thus produce maxima in the moments of inertia.

At this point it is interesting to validate the accuracy of the other approximation schemes for constructing the kinetic energy matrix. The values for the correlation function in the various schemes at the position of the minima and the maxima is given in Table 4.3. The exact fully coupled scheme C1 is very time-consuming as it constructs the 2D-PES and the kinetic energy matrix at the two-dimensional grid of torsional angles after complete geometry optimization. The release of the two-dimensional constraint drastically reduces the computing time: the 2D-PES is decomposed into the sum of two 1D-PES: $V(\phi_2, \phi_3) \approx V_2(\phi_2) + V_3(\phi_3)$. This approach also implies that the kinetic energy matrix $A(\phi_2, \phi_3)$ is also no longer fully constructed.

	C1	C2	C3	C4	C4'
Minima					
(85,0)	1.51	1.51	1.54	1.00	1.19
(275,0)	1.51	1.51	1.54	1.00	1.19
(0,85)	1.51	1.51	1.54	1.00	1.19
(0,275)	1.51	1.51	1.54	1.00	1.19
(85,85)	1.88	2.29	1.83	1.00	1.19
(275,85)	2.00	2.29	1.96	1.00	1.19
(85,275)	2.00	2.29	1.96	1.00	1.19
(275,275)	1.88	2.29	1.83	1.00	1.19
Maxima					
(180,0)	0.86	0.86	0.83	1.00	1.19
(0,180)	0.86	0.86	0.83	1.00	1.19
(180,180)	0.61	0.73	0.58	1.00	1.19
$< f(\phi_2, \phi_3) >$	1.36	1.46	1.34	1.00	1.19

Table 4.3: Characteristics of minima and maxima on the correlation function surface of the two ethyl rotations in pentane.

In approach C2, A is factorized according to Eqs.(4.22) and (4.23) and both uncoupled correlation functions $f_2(\phi_2)$ and $f_3(\phi_3)$ are obtained from the separate, aforementioned 1D-rotational geometry optimizations. The two-dimensional product correlation function $f_2(\phi_2) \cdot f_3(\phi_3)$ systematically overestimates the real correlation function $f(\phi_2, \phi_3)$, and hence the corresponding partition function acts as an upper limit. The average integral amounts to 1.46, *i.e.* an average deviation of 7.4%. As for the uncoupled potential energy surface the asymmetry of the two dimensional surface is not taken into account correctly in the C2 scheme, *e.g.* no difference is made between the maxima

characterized by the following couples of torsional angles (85,85) and (85,275).

In the approach C3, the kinetic energy matrix is constructed without any geometry optimization. Starting from the reference conformer (the tt conformer), the torsional angles are varied while keeping all other variables in their equilibrium geometry. In this case the inertial matrix does not differ largely from the real optimized case (C1). The average integral amounts to 1.34, and deviates within 1.5% of the true case. The symmetry of the correlation surface is also taken into account correctly.

The most crude approximations are C4 and C4', where the inertial moments are kept constant during the torsional motion. In the C4' method, the coupling terms between the various rotating tops is additionally neglected and one can come to the standard expression for the reduced moment of inertia of Eq.(4.26). In the C4' method, where kinetic coupling between tops is neglected, these constant moments of inertia are somewhat larger than the C4 moments and the resulting correlation function is larger than one for pentane and remains constant during the rotation of the tops. In the case of pentane the correction is small, but for molecules with more internal rotations the difference between C4 and C4' may rise in importance. The absence of any correlation factor larger than unity in C4' suggests a systematic underestimation of the moments of inertia over phase space.

Influence on the partition function

Fig. 4.4(a) displays the rotational partition function of the two ethyl rotations in pentane according to the various approximative schemes. The effect of the kinetic and potential energy contribution on the partition function is schematically illustrated in the following scheme for the various methods. The reference is C1, the exact coupled scheme.

Effect on q_{rot}	**C1**	**C2**	**C3**	**C4**	**C4'**
Kinetic energy contribution	reference	++	0	− −	−
Potential energy contribution	reference	+	+	+	+
Global effect	reference	+++	+	−	0

The effect of the kinetic energy on q_{rot} can be estimated by comparing the average value of the correlation function with respect to the value obtained in C1 (see Table 4.3). The methods C2, C3, C4 and C4' use uncoupled rotational

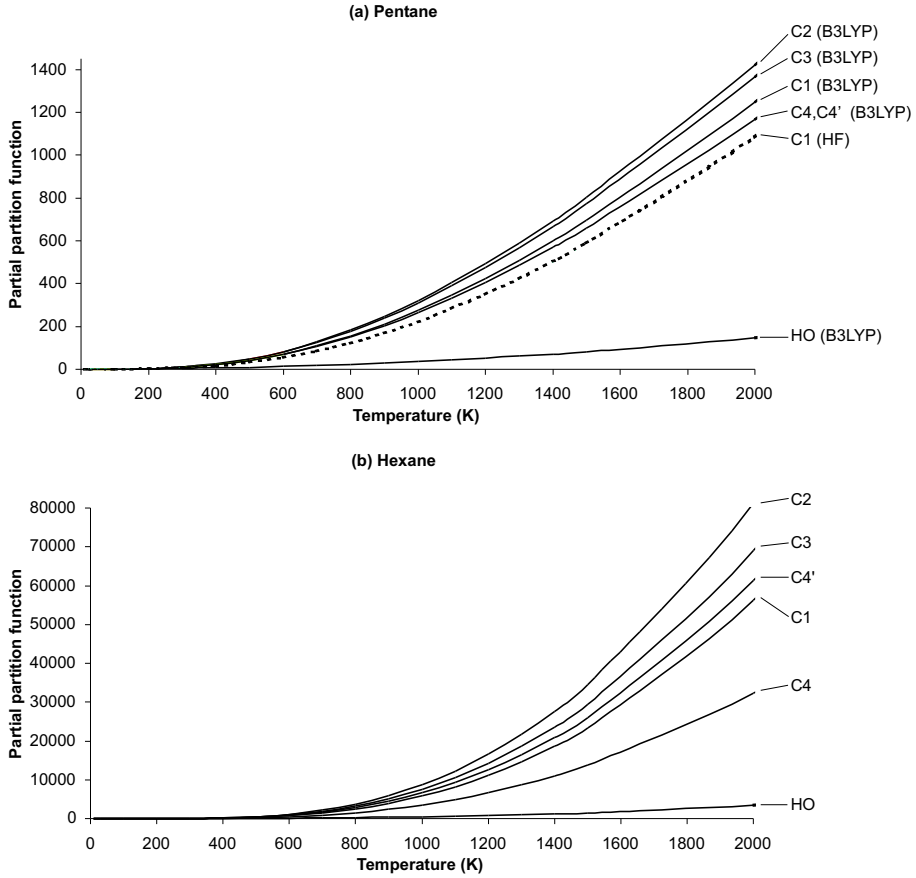

Figure 4.4: (a) Partition function of the two ethyl rotations in pentane calculated according to the various approximative schemes at the B3LYP/6-311g(d,p) level of theory. In addition the C1 scheme at the HF/6-31g(d) level of theory is given. (b) Partition function of the three subsequent rotors in hexane (ethyl, propyl, ethyl) according to the various approximative schemes.

potential energy surfaces. The 1D potentials underestimate the central peak of the potential energy surface. This results to a shift of the rotational energy levels to lower energies, enhancing the level density of the low-energy spectrum and leading finally to an increase of the partition function. The C2 method predicts the highest value of the partition function as already expected on basis of the factorization of the 2D correlation function, and yields an upper boundary for the partition function.
The C3 approach which is regarded as the best approximation beyond the exact coupled C1 scheme also overestimates the C1 prediction.
The crude C4 and C4' approaches may not be disentangled from each other, and the contributions to the partition function accounting for the two ethyl rotations, are very close to the exact coupled values, but are slightly underestimated. It turns out that the effects of the approximative schemes on the potential and kinetic energy compensate each other in both C4 and C4' schemes, predicting a final global effect on the partition function which does not largely deviate from the exact coupled C1 scheme.
This simplified approach (C4 and C4') for treating internal rotations has already shown its adequacy in reproducing thermodynamic quantities in long-chain alkanes with an excellent agreement with experiment [14].

Influence on the entropy

The various approximative schemes are validated in a comparative analysis of the theoretically predicted thermodynamic quantities and experimental data. For the entropy and heat capacity experimental data are available for most alkanes and both quantities are essentially determined by the molecular partition function. When examining the experimental values at higher temperatures, some caution is needed, since some of these values are obtained by using extrapolation schemes on the experimental data that were obtained in the lower temperature regime [52]. The entropy and heat capacity are shown in Fig.4.5(a) and 4.5(b) for pentane in terms of temperature and the difference between the calculated entropy and experimental values is displayed in Fig.4.5(c). As generally known the HO approximation seriously underestimates the entropy values [14]. In the other limiting case, the rotating top can be treated as a free rotor about the rotation axes. The free rotor (FR) model overestimates the experiment but tends to converge to the correct values at higher temperatures. In some extreme cases of very low vibrational frequencies or nearly unhindered rotating tops the relative position of the FR and HO curve can switch but the picture as shown here is the most common one. All internal rotor models ap-

proximate the experimental values within 5 J/mol.K whereas the HO and FR model introduce errors of the order of 30J/mol.K. The closest agreement with experimental values is found within the C4' model (2 J/mol.K). Once again one is stunned with the striking resemblance of the most crude approximation C4' with the exact scheme C1. As explained for the partition functions this can be attributed to the cancellation of errors on kinetic and potential energy contributions in the uncoupled scheme without varying moments of inertia. One must however be careful in extrapolating this conclusion, based on cancellation effects, to other systems with hetero atoms (O,N,P,...) or to other more branched systems.

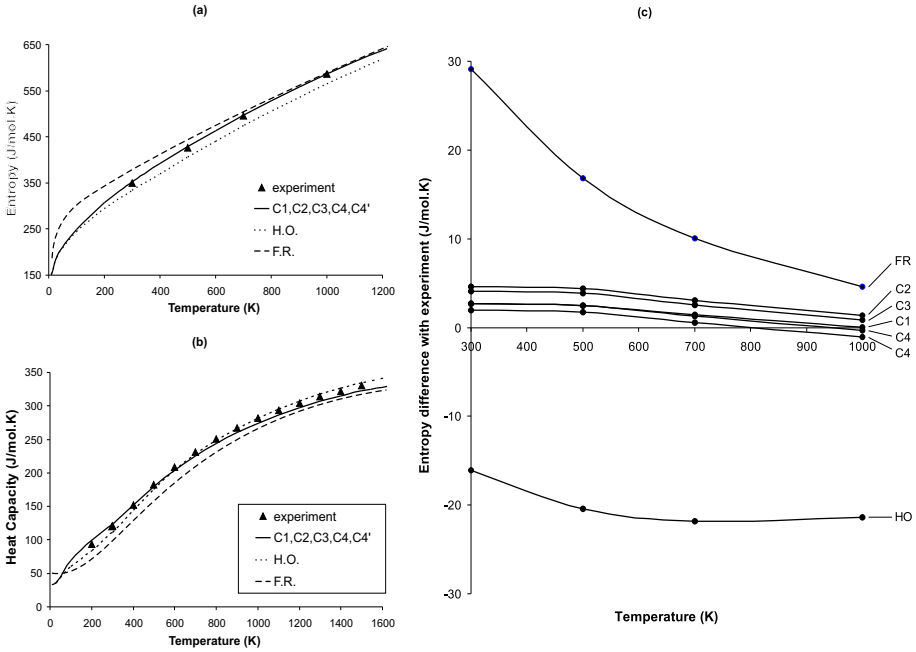

Figure 4.5: (a),(b) Entropy and Heat Capacity of pentane in various approximate schemes in terms of the temperature. (c) Entropy difference between calculated values and experiment for pentane in terms of the temperature.

It is instructive to compare our results with the entropies reported by Robertson en al. in Ref.[61]. They reported an entropy of 356.0 J/molK for pentane at 298.15 K. This is a discrepancy of 7 J/molK with respect to the experiment. Their method closely resembles the C3 approximation of our model. Our C3 value for the entropy on pentane is 353.05 J/molK and is also slightly

higher than the C4 prediction of 350.92 J/molK (see Table 4.4).

Other calculated values were reported in the literature for the entropy on pentane with good experimental agreement (these data are also taken up in Table 4.4). In particular we report the value of 350.24 J/molK of DeTar [59] and 349.74 J/molK of Guthrie [39], agreeing well with the experimental value of 349.45 J/molK. This apparent quantitative agreement requires special attention. One of the key ingredients in Ref.[59] is the introduction of a scaling factor of 0.90 applied to the frequencies. It enhances the HO prediction to 334.48 J/molK (HF/6-31G**), compared to 332.90 J/molK in this work (DFT/B3LYP/6-311G**) where no scaling is taken into account. The scaling factor for frequencies in DFT calculations is closer to one (0.98). Applying this scaling correction enlarges our HO prediction to 334.49 J/molK, which is completely equivalent with the DeTar prediction. Second crucial ingredient in the DeTar calculation [59] is the correction arising from the presence of multiple conformers (at higher energies than the reference conformer). The correction is derived on statistical grounds (Bolzmann distribution) and amounts to 14.67 $J.K^{-1}.mol^{-1}$ in this particular case. This method works perfectly well but the aim of the work of DeTar is the ab initio prediction of accurate thermochemical properties for a large series of alkanes. The focus of this work is fundamentally different as stressed in the introduction. The work of Guthrie [39] is based on the same concept in the sense that the rigid rotor harmonic oscillator approximation is used with the B3LYP/6-311G** level and that an approximative correction for the entropy of mixing is introduced when there is more than one conformation. The correction due to the existence of nine low-energy conformations in pentane amounts to 18.31 J/molK and is of the same magnitude than the IR value predicted by the C1,C4 and C4' [see Fig.4.5(c)].

For completeness we also report the values given predicted by using Benson's group additivity method. These values are not based on ab initio calculations but on a fitting procedure with experimental values.

Influence of level of theory

The discussion held in the preceding paragraphs deals with results obtained within the ab initio DFT model and use of the B3LYP functional and 6-311g** basis set. It is instructive to verify whether the use of another level of theory will affect the conclusions as such. We therefore redo all calculations in pentane within the HF framework, and 6-31g(d) basis set. We are not going into details about geometry differences with the DFT level of theory, as this is not the focus.

We only report the main features. The geometry correlation function $f(\phi_2, \phi_3)$ has a similar behavior as in Fig.4.3. The most significant deviation is noticed in the bond lengths, which are shorter in HF than in B3LYP. This manifestly leads to smaller values of the moments of inertia and thus the value of $\det A_0$ lowers from DFT to HF with 5%. The higher potential barriers and the lower moments of inertia (and hence $\det A_0$) give rise to a depletion of the partition function of about 15% [Fig.4.4(a)].

4.4.2 The schemes C1, C2, C3, C4 and C4' applied to hexane

For completeness we also performed the C1 scheme to hexane, which has demanded an huge computing time for the construction of the three-dimensional potential surface in terms of the three torsional angles characterizing the asymmetric rotation of an ethyl, a propyl and an ethyl cluster. In contrast to the investigation on pentane we did not perform a conformational analysis, nor do we present a detailed discussion on the correlation function. We limit ourselves in comparing the results from the different schemes and drawing some conclusions in accordance with the previous case. Fig.4.4(b) displays the rotational partition function of the three subsequent rotors in hexane according to the various approximative schemes. The general trend as in Fig.4.4(a) in case of pentane is maintained although some specific features emerge which were not observed in pentane. The upper limit scheme C2 appears to separate out from the other schemes in a more pronounced way, while C4 is now totally distinct from C4' and predicts partition functions differing by a factor 2 from the "exact" C1 values. Surprisingly, the most crude approximation C4' again succeeds in reproducing the partition functions close to C1. The same observation is noticed for the C3 scheme, which is less surprising since the method is more founded.

Some interesting features emerge from the three dimensional potential surface (3D-PES) which cannot be extracted from the 2D-PES. In particular the influence of the coupling between not adjacent rotors (the two ethyl rotations in hexane) can now be studied thoroughly. Without going into details we plot in Fig.4.6(a) the difference between the 2D-PES, obtained by cutting the 3D-PES at the trans position of the propyl rotation, and the sum of the two one-dimensional rotational potentials of the two ethyl rotations separately. We learn that the influence of the coupling on the potential surface is small. On the contrary the influence of the coupling is substantial in the kinetic energy ma-

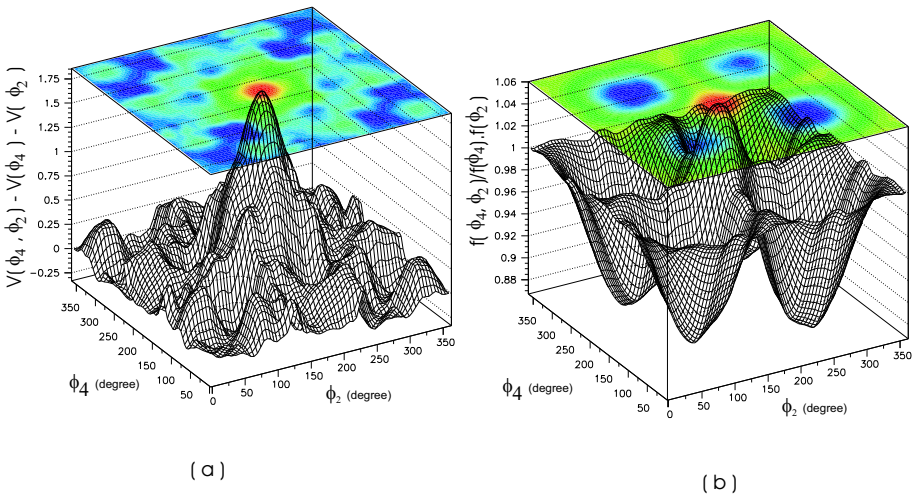

(a) (b)

Level of theory: B3LYP/6-311g(d,p)
The 2D-PES is obtained by cutting the 3D-PES at the *trans* position of the propyl rotation.

Figure 4.6: (a) Difference between the 2D-PES and the sum of the two one-dimensional rotational potentials of the two ethyl rotations. (b) Two dimensional surface of the 2D correlation function relative to 1D correlation function.

trix, which is reflected by the ratio $f(\phi_2, \phi_4)/f(\phi_2).f(\phi_3)$ (see Fig.4.6b). The correlation surface shows large fluctuations from unity and lies on the origin of the increasing deficiency of the C2 scheme the longer the chain of the alkane. The strongly varying shape of the correlation surface suggests the necessity to incorporate to some extent the variations of the kinetic energy matrix with the torsional motions. This favors the C3-scheme where these effects are involved but without a systematic geometry optimization at each torsional angle. In Fig.4.7 the deviancies of the heat capacity from experiment in hexane are displayed for the various schemes. All schemes predict a similar qualitative behavior in function of the temperature. The exact coupled scheme yields the smallest experimental discrepancies.

In the next chapter we present a more detailed discussion about the coupling of nearest versus next-nearest internal rotations in hexane.

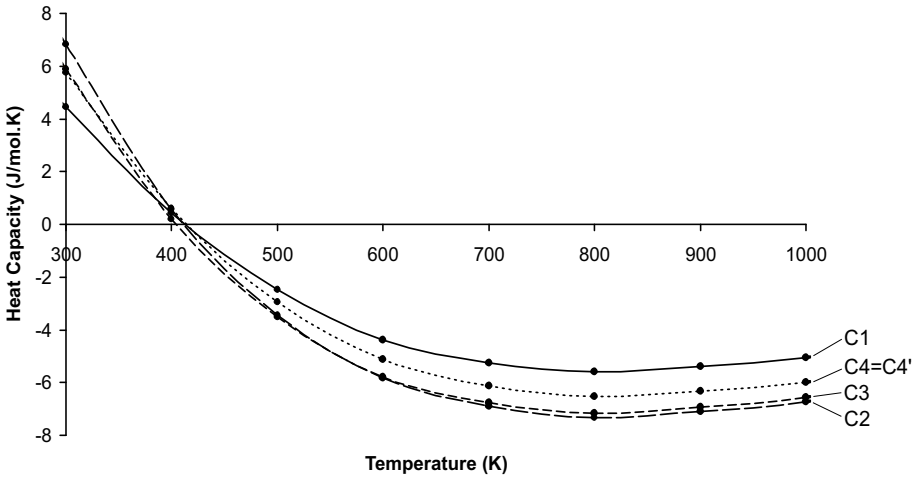

Figure 4.7: Heat capacity difference between calculated values and experiment for hexane in terms of temperature for the different schemes.

4.4.3 The schemes C2, C3, C4 and C4' applied to n-alkanes

The exact coupled scheme C1 is limited in its dimension taken into account in the coupling of IR's. In the previous subsections we performed the C1 scheme to pentane and hexane, but it is not our intention to promote C1 as the most ideal scheme, as it is unfeasible for long chain molecules that may occur, *e.g.* in polymer chemistry. The goal is rather to promote approximative schemes which are able to yield adequate ab initio predictions for IR partition functions within acceptable computational efforts and which may be implemented into quantum chemical packages. These approximative schemes have been validated with respect to the exact C1 scheme and experiment in pentane and hexane. Conclusions have been made which may be extended to longer linear alkanes. In this perspective the heat capacity and entropy were calculated for linear alkanes up to decane,in the C2, C3 (C3'), C4 and C4' scheme. The results are tabulated in Table 4.4.

In Fig.4.8 the contributions to the entropies and heat capacities of various internal modes in decane are plotted in terms of temperature to get an idea about the nature, origin and magnitude of anharmonic contributions in alkanes. The dashed curves correspond with the HO predictions, while the solid curves

	S_0(298.15K)	Cp(298K)	Cp(400K)	Cp(600K)	Cp(800K)	Cp(1000K)	Cp(1500K)
butane							
exp.	309.60 [76]	98.49	124.77	169.28	202.38	227.36	266.40
HO	300.76	90.69	117.41	165.30	201.69	229.18	272.28
C1	311.35	98.07	122.21	164.83	197.54	222.69	262.86
C2	311.40	98.10	122.24	164.85	197.55	222.69	262.87
C3	311.33	98.05	122.19	164.82	197.53	222.68	262.86
C4	310.76	97.93	122.19	164.93	197.66	222.80	262.94
C4'	310.94	97.93	122.19	164.93	197.66	222.80	262.94
Benson [81]	309.41	97.86	123.82	168.62	201.68	226.96	266.48
DeTar [59]	310.03						
pentane							
exp.	349.49 [76]	120.00	152.55	208.78	250.62	281.58	330.54
HO	332.90	110.99	144.37	203.79	248.57	282.19	334.58
C1	351.71	122.53	152.16	204.35	244.12	274.54	322.82
C2	353.50	123.59	152.09	203.56	243.26	273.72	322.17
C3	353.05	123.26	151.91	203.53	243.28	273.75	322.20
C4	350.92	123.05	152.05	203.88	243.63	274.07	322.41
C4'	351.64	123.05	152.05	203.88	243.63	274.07	322.41
Benson	348.84	120.88	152.91	207.76	248.02	278.61	326.13
Guthrie [39]	349.74						
DeTar	350.24	116.94				288.82	
hexane							
exp.	388.82 [77]	142.60	181.54	248.11	296.23	331.37	389.11
HO	365.03	131.40	171.48	242.41	295.53	335.23	396.87
C1	389.83	147.11	181.99	243.73	290.63	326.32	382.74
C2	393.99	149.53	182.12	242.27	288.91	324.65	381.39
C3	392.65	148.60	181.74	242.33	289.07	324.82	381.51
C4	388.24	148.44	182.14	242.98	289.69	325.37	381.87
C4'	390.90	148.44	182.14	242.98	289.69	325.37	381.87
Benson	388.27	143.90	182.00	246.90	294.36	330.26	385.78
Guthrie	390.20						
DeTar	389.70	140.54				343.67	
heptane							
exp.	427.90 [78]	165.20	210.66	287.44	342.25	381.58	443.50
HO	397.03	151.74	198.48	280.93	342.43	388.25	459.17
C2	436.04	175.54	212.02	280.79	334.39	375.45	440.54
C3'	432.84	173.73	211.44	281.04	334.79	375.85	440.81
C4	425.58	173.77	212.19	282.03	335.71	376.64	441.33
C4'	430.79	173.77	212.19	282.03	335.71	376.64	441.33
Benson	427.70	166.92	211.09	286.04	340.70	381.91	445.43
DeTar	427.90	163.51				398.78	
octane							
exp.	467.06 [77]	187.80	239.74	326.77	388.28	431.37	497.90
HO	429.07	172.10	225.52	319.50	389.36	441.28	521.47
C2	478.02	201.10	241.47	319.01	379.67	426.13	499.62
C3'	471.90	198.36	240.79	319.59	380.44	426.85	500.11
C4	461.41	198.74	241.94	320.92	381.66	427.88	500.77
C4'	470.69	198.74	241.94	320.92	381.66	427.88	500.77
Benson	467.13	189.94	240.18	325.18	387.04	433.56	505.08
DeTar	466.98	186.86				453.75	
nonane							
exp.	506.52 [77]	210.40	268.82	366.10	433.88	481.58	556.47
HO	460.87	192.44	252.53	358.02	436.26	494.30	583.77
C2	520.54	227.19	271.24	357.35	425.01	476.81	558.70
C4	496.37	224.18	272.07	360.05	427.74	479.22	560.28
C4'	510.30	224.18	272.07	360.05	427.74	479.22	560.28
Benson	506.56	212.96	269.27	364.32	433.38	485.21	564.73
decane							
exp.	545.84 [77]	233.10	297.98	405.85	479.90	531.79	610.86
HO	492.90	212.80	279.58	396.59	483.19	547.34	646.07
C2	565.07	253.90	300.95	395.39	470.07	527.28	617.65
C4	531.88	250.19	302.42	399.11	473.72	530.45	619.70
C4'	551.93	250.19	302.42	399.11	473.72	530.45	619.70
Benson	545.99	235.98	298.36	403.46	479.72	536.86	624.38

Experimental values for the entropies are taken from [76, 77, 78].
The values for the heat capacities at different temperatures indicated in the "experimental" row are Scott's empirical values [52], which were least-square fitted to experimental data.

Table 4.4: Entropies and Heat Capacities (J/molK) for n-alkanes as predicted by various models.

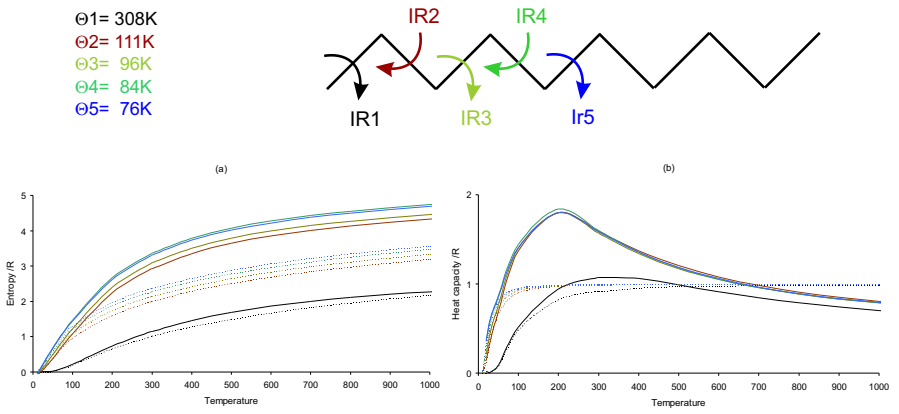

Figure 4.8: Contributions to the entropy and heat capacity of the various internal rotations in decane. The solid curves correspond with C4', whereas the dashed curves are the HO predictions.

represent the results obtained in C4'.

Entropies In Fig.4.9(a) the entropy differences between the calculated values in the various schemes and the experimental data are shown in terms of varying chain length at 298.15 K. The tendencies predicted for pentane and hexane can be further extrapolated for the larger systems. Accordingly, C2 gives an upper limit for the entropy. The method has the tendency to diverge for larger alkanes and can not be suggested as a viable method for larger hydrocarbons. A divergent behavior is also observed in C4, but in the opposite side. Only two schemes C3 and C4' succeed in predicting the entropy quite accurately also for larger carbon sequences since the exact C1 scheme is no longer feasible. These methods suggest a persistent mechanism of cancelling errors. Some of the geometries that are taken into account for constructing the kinetic energy matrix in the C3 scheme are not realistic, since they correspond with folded positions of the chain where atoms can even overlap. These last conformations in larger systems have the tendency to underestimate the true moments of inertia and thus the effect of the kinetic energy contribution on q_{rot} is slightly negative, resulting in a global compensation of errors in the partition function.

Heat Capacities The heat capacities in the HO model converge to a value of R for higher temperatures whereas in the HR model the high temperature limits tends to R/2. In the lower temperature regime - the extent of this region

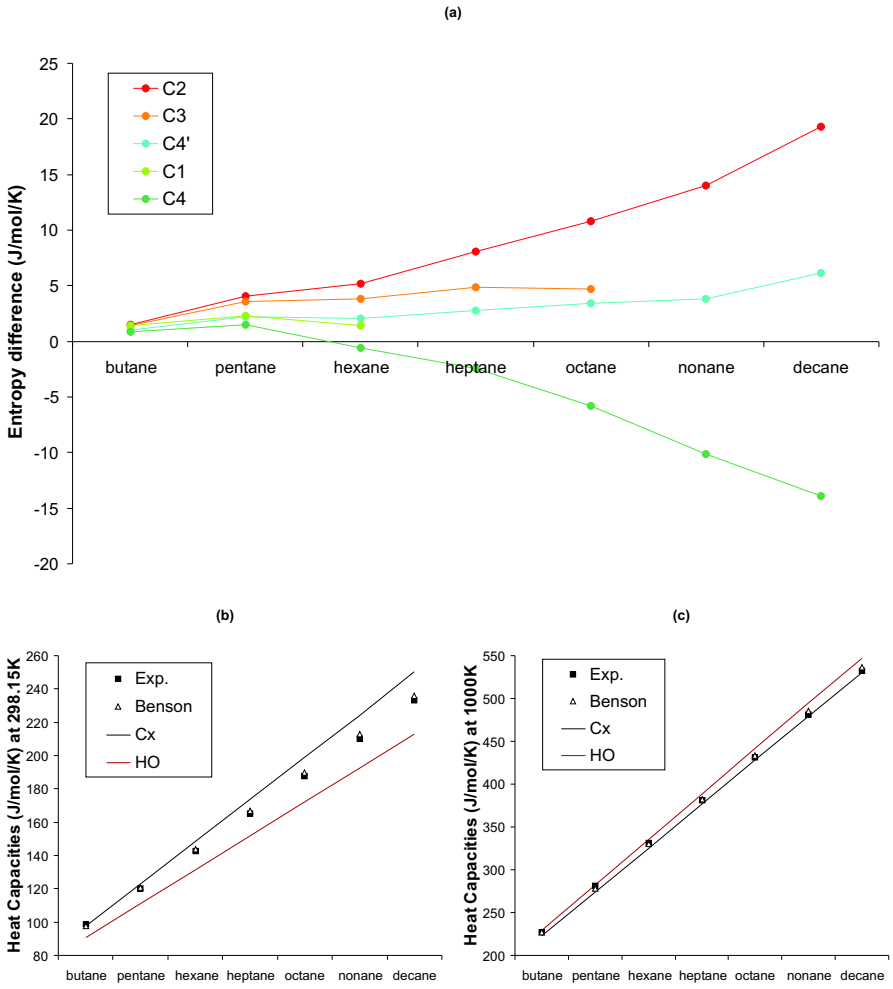

Figure 4.9: (a) Entropy difference between calculated and experimental values for *n*-alkanes. (b),(c) Heat Capacities at 298.15K and 1000 K in the various models together with experimental values.

is determined by the specific temperature - the HR predictions lie above the HO values for most internal rotations. Only for very low activated torsions which nearly behave as a free rotor, the heat capacity is almost constant at R/2 in the entire temperature range. These results are completely in agreement with the results of Katzer and Sax who studied the impact of anharmonic molecular vibrations in the thermochemistry of silicon hydrides [53].

In Fig.4.9(b) and (c) the heat capacities are plotted in terms of the length of the alkane chain at T=298.15K and T=1000K, respectively. At 298.15 K the HO model systematically underestimates the heat capacities, whereas the IR models slightly overshoot the experimental values. The deviation from the experiment seems to increase for larger chains.

At 1000K the correspondence between the experimental and HR models are in very good agreement. At these temperatures the HO values overestimate the experiment, since the high temperature limit in this model overestimates the real value.

4.4.4 Application to branched alkanes

In view of application to general hydrocarbons, it is interesting to validate the accuracy of the various schemes on branched alkanes. The molecules 2-methylbutane, 2-methylpentane and 3,3-dimethylpentane were chosen for our model study. To get insight into the effects of anharmonicities induced by internal rotations, the contributions of the various torsional modes to the entropy and the heat capacity in 3,3-dimethylpentane are plotted in Fig.4.10 in terms of temperature.

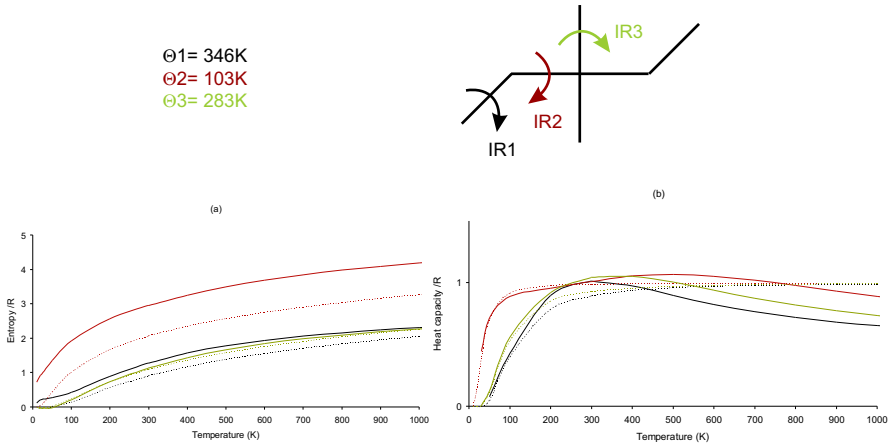

Figure 4.10: Contributions to the entropy and heat capacity of the various internal rotations in 3,3-dimethylpentane. The solid curves correspond with C3, whereas the dashed curves are the HO predictions.

	S_0(298.15K)	Cp(298K)	Cp(400K)	Cp(600K)	Cp(800K)	Cp(1000K)	Cp(1500K)
2-methylbutane							
exp.	343.55 [79]	120.41	153.54	208.31	251.47	285.11	338.30
HO	334.34	113.54	146.89	205.48	249.58	282.78	334.74
C2	345.44	119.60	151.28	204.52	244.25	274.47	322.48
C3	345.29	119.49	151.18	204.45	244.21	274.44	322.47
C4	345.26	119.48	151.21	204.54	244.30	274.52	322.52
C4'	345.51	119.48	151.21	204.54	244.30	274.52	322.52
Benson	343.38	119.75	152.67	208.35	248.81	279.21	327.18
DeTar	345.56	116.15				287.94	
2-methylpentane							
exp.	380.83 [80]	144.12	184.47	249.88	299.91	337.75	396.35
HO	364.76	133.71	173.77	243.92	296.43	335.75	397.01
C2	384.82	145.89	183.11	245.07	291.30	326.47	382.33
C3	384.64	145.66	182.89	244.93	291.22	326.42	382.30
C4	383.50	145.04	182.62	245.10	291.52	326.73	382.54
C4'	384.11	145.04	182.62	245.10	291.52	326.73	382.54
Benson	382.81	142.77	181.76	247.49	295.15	330.86	386.83
Guthrie	382.12						
3,3-dimethylpentane							
exp.	398.02 [78]	167.27	216.35	294.77	354.75	401.18	474.70
HO	381.29	158.23	204.90	285.01	344.69	389.44	459.34
C2	402.50	162.48	208.09	282.79	337.04	377.65	441.56
C3'	402.18	162.38	208.00	282.74	337.02	377.63	441.56
C4	401.84	162.38	208.01	282.75	337.03	377.65	441.57
C4'	402.76	162.38	208.01	282.75	337.03	377.65	441.57
Benson	398.80	167.97	215.12	292.95	347.39	387.29	447.65

Experimental values for the entropies are taken from [78, 79, 80].
The values for the heat capacities at different temperatures indicated in the "experimental" row are Scott's empirical values [52], which were least-square fitted to experimental data.

Table 4.5: Entropies and heat capacities (J/molK) for some branched alkanes as predicted by various models.

For the entropy contributions, two effects play a major role: the effect of the true anharmonic potential and the symmetry numbers for the internal rotors. For the two methyl rotations, the potential induces an enlargement of the entropy while the symmetry number of three gives rise to a decrease of $R\ln 3$=9.1 J/molK. These two effects nearly cancel each other. For the ethyl rotation only the effect of the true internal rotor potential contributes and therefore the enlargement in the entropy is quite substantial for this rotation. This is reflected in the total values of the entropy in the HO and HR models. The HO substantially underestimates the experimental value whereas all HR models bring the theoretical estimate quite close to the experiment.

The heat capacity contributions are almost entirely determined by the specific form of the rotational potential. All three internal rotations in 3,3-dimethylpentane, produce three nearly undistinguishable isomers. Therefore the heat capacity contributions in the low temperature regime do not reach far above the HO limit value of R. The asymmetric potential characterized by different heights of the minima and maxima along the internal rotation path, are necessary to obtain heat capacities per internal rotation in the low temperature

regime that are larger than R. As a result the heat capacities predicted in the HO model and HR model do not differ substantially for 3,3-dimethylpentane. For other branched alkanes where more asymetric potentials come into play the corrections may be larger. Generally for branched alkanes the agreement with the experiment in the various HR models is not sufficient and other effects can be expected to come into play. It is known that in the HO approximation, internal vibrations start to contribute to the heat capacity at about 20% of the vibrational temperature and are almost at full strength (R) at about 80% of the vibrational temperature. This means that not only low lying frequencies are important for the heat capacities but also a range of intermediate modes. For these branched systems a lot of skeletal motions are mixed up in the low and intermediate normal mode spectrum and there is a need to describe them also beyond the HO model.

4.5 Conclusions

This chapter can be regarded as a revisiting of the original and exact Kilpatrick and Pitzer (KP) model and the implementation of ab initio computed data in the model instead of empirical ones with the final goal to present an uniform ab initio procedure for all molecules. Beside the correct scheme to describe multiple rotating tops various approximative models are presented which are deduced from realistic assumptions and still based on first principles. The various approaches are tested on their validity, applicability and feasibility for the prediction of accurate partition functions for the internal molecular rotations. The final aim is the development of ab initio procedures that might be used in general utility programs for generating molecular partition functions for any molecule with reasonable accuracy at minimal cost and adequate for a widespread application (thermochemistry, kinetics). The exact coupled C1 scheme is the reference for the validation of the various derived approaches as direct comparison with experimental partition functions is not achievable. In addition validation of the models versus experiment is also required. As experimental data on thermochemical properties as entropies and heat capacities are available in alkanes, these long chain molecules are highly suitable for this kind of validation, although prudence is called for a strongly extended generalization.

In an earlier work of the authors it has been pointed out that the harmonic oscillator approach is inadequate for a satisfactory reproduction of the thermodynamic quantities. A very crude approach (C4' in the notation of this chapter, 1D-HR as general name) for treating IR's turned out to considerably improve the experimental agreement.
The presented work provides an ideal framework to unravel the origin of this "well behavior". It seems that the C4' method which is commonly used in literature gives results that lie surprisingly close to the values given by the exact coupled scheme, due to a subtle cancellation of errors on both the potential and kinetic energy contribution. This is at least true for the systems that were investigated in this work, but to generalize a thorough investigation is needed on molecules that contain other hetero atoms such as Cl,O,N,... This work is in progress.

The results of the exact coupled scheme for pentane and hexane are calculated. For the latter a three-dimensional rotational potential has been constructed with geometry optimization at each of the almost 12000 grid points

op the 3D-PES. Extension to higher dimensions is almost unfeasible and will probably not reveal new features. The 3D-PES yields sufficient information to be able to make viable conclusions about the various approximative schemes. In view of applications on larger systems we also investigated the accuracy of the various approximative schemes in terms of the length of the studied chain. Some methods such as C2 and C4 are not suited for long hydrocarbons since the entropies diverge in terms of the length of the alkyl chain. Only C3 (C3') and C4' are viable alternatives for these systems. For branched alkanes, we found a substantial improvement of the entropy by applying the internal rotor models. It is however more difficult to get the heat capacity very accurate for these systems. The origin of this must be probably traced to other vibrational modes that contribute to the heat capacity. It is well known that the entropy is primarily determined by the low frequency spectrum, whereas the heat capacity may be substantially altered by medium lying frequencies. Further model development is needed to describe the anharmonicities of these modes correctly.

We repeat that we do not pretend to do better in predicting thermochemical properties for alkane hydrocarbons than do previous works in the literature such like the work of DeTar [59] and Guthrie [39], which is based on the statistical concept of the entropy of mixing. One of the focuses of this work lies in unravelling the mechanism of internal rotations and their impact on the partition functions, and in presenting an accurate but feasible model for reproducing correct partition functions in a microscopic way without incorporation of any adjustable parameter. It opens a wide range of interesting perspectives, which go beyond the reproduction of thermochemical properties. For example, knowledge of accurate partition functions for reactants, products and transition states will offer highly reliable information on the kinetics of a chemical reaction.

Chapter 5

How to calculate multi-dimensional potential energy surfaces for an accurate reproduction of partition functions?

This chapter is based on Ref.[17]:

Vansteenkiste, P.; Van Speybroeck, V.; Pauwels, E.
and Waroquier, M.
Chem. Phys. **2005**, *314*, 109–117

Abstract

The potential energy of n-hexane is studied since it constitutes a typical example of a single chain molecule in which various internal rotations are present and a large number of conformations are existing, which cannot be reached by using one-dimensional rotational energy profiles. For an accurate reproduction of the global partition function and all derived thermodynamic properties an adequate description of all possible conformers is necessary. The full three-dimensional potential energy surface of the internal rotations in n-hexane (3D-PES) is calculated at an ab initio level and compared with one-dimensional schemes to reproduce the energy. Due to the higher dimensionality of the relevant potential energy surface, the computational cost is very high. A new approximate scheme based on two dimensional cuts is proposed that gives good accuracy for the relative conformational energies and kinetic energies at a reasonable computational cost. This scheme is of general use for any long chain molecule.

5.1 Introduction

n-Alkanes constitute a class of very simple molecules where the all-trans conformation is the energetically most stable form. The one-dimensional internal rotation about a single CC bond (apart from methyl tops) gives rise to a typical potential energy curve which is shown in Fig.5.1. Besides the trans conformation, corresponding to the absolute minimum, the CCCC torsional angle can reside in two possible gauche orientations corresponding to local minima, and usually referred to as g_+ and g_-. For a series of m subsequent rotations about single CC bonds, one expects to find 3^m minima. However, 3^m appears to be only a lower limit as pointed out by Tsuzuki et al. [47] and Tasi et al. [19].

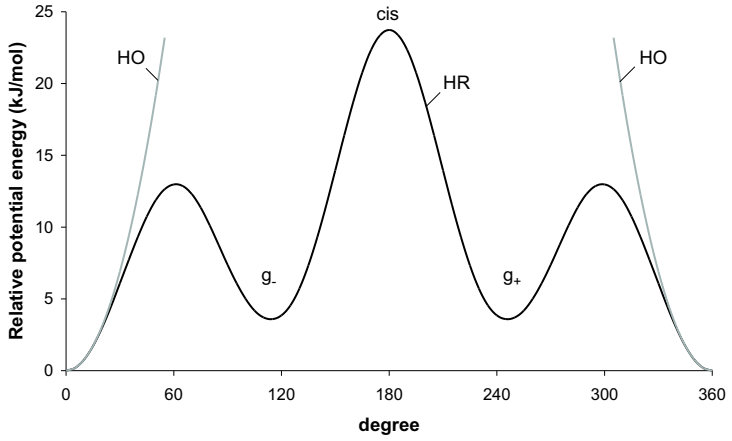

Figure 5.1: Potential energy variation of the one-dimensional ethyl rotation in n-hexane according to the HR and HO description. Reference at 0° is the all-*trans* conformer. The two gauche states are labelled.

The occurrence of a multitude of possible conformers - all but a few kJ/mol higher in energy than the all-trans conformation - will have a serious impact on the partition function, from which all thermodynamic properties can be derived. An accurate identification and description of these local minima in the potential energy surface (PES) is therefore decisive for the accuracy of the calculated partition function.
In this respect, the harmonic oscillator approximation (HO) is completely inadequate as it accounts for only one minimum as illustrated in Fig.5.1. To

include all rotational minima into the calculations, one must treat the internal rotations with an appropriate hindered rotor scheme (HR) that is capable of treating molecules with a number of asymmetric tops [16]. This scheme depends on the availability of the PES as a function of the various torsional angles. Unfortunately, due to the substantial computational cost, most literature works are restricted to a one-dimensional approximation of this PES: for each internal rotation a one-dimensional potential energy curve (1D-PES) is calculated, and the total multi-dimensional potential energy surface (mD-PES) is assumed to be the sum of these one-dimensional contributions:

$$V^{mD}(\phi_1, \ldots, \phi_m) \approx \sum_{i=1}^{m} V_i^{1D}(\phi_i) \tag{5.1}$$

In this approximation, the interaction between the different internal rotations is completely ignored: the rotations are not coupled to each other, and hence the potential energy curve of one rotation is not influenced by any other rotation.
General improvements of this description can be suggested. The most accurate scheme is to determine the fully coupled mD-PES, but this is computationally not feasible for most systems at an ab initio level. We present an alternative scheme that goes beyond the one-dimensional approximation, but still is feasible and practical.

In this chapter, we will concentrate on the three internal rotations in n-hexane: two ethyl rotations and one propyl rotation ($m = 3$). For this molecule, the validity of the one-dimensional approximation [Eq.(5.1)] will be evaluated by a comparative study with the completely determined 3D-PES , and by the accuracy of the relative energies of the different conformers resulting from the uncoupled scheme. Based on this analysis we suggest an approximative scheme that relies on two-dimensional surfaces, and which gives far more accurate results than the one-dimensional approach. Simultaneously, a similar study is performed for the construction of the kinetic energy. When the 3D-PES is not fully calculated, the kinetic energy matrix cannot be constructed exactly since the optimized geometries at each point of the 3D-PES are not known. The approximation scheme introduced for the potential energy enables us to construct also the kinetic energy matrix quite accurate and without additional computational cost.

5.2 Methodology and computational details

All ab initio calculations were performed using the Gaussian03 software package [13] in a density functional theory (DFT) [9] framework, with Becke's three-parameter B3LYP functional [7]. The molecular orbitals were expanded in a triple-ζ 6-311G basis augmented with single first d and p polarization functions [8]. This functional is known to give a reliable and quantitatively acceptable description of geometries, frequencies, and potentials [40][41][42] for a reasonable computation time. In particular, a profound quantum chemical study of conformational energies and rotational energy barriers in n-alkanes has been performed by G.D. Smith and R.L. Jaffe using high-level ab initio methods [43]. As already discussed in Ref.[14] the relative energies of the gauche conformers on this level of theory correspond very well with the results found with high level post-HF methods.

The 3D-PES was constructed using constrained geometry optimizations: all variables were allowed to relax to the minimal energy geometry, except for the three dihedral angles of the internal rotations under investigation. These three variables were fixed on values of the grid ($k \cdot 10°$,$l \cdot 10°$,$m \cdot 10°$), with k, l and m integer numbers going from 0 to 35. The potential energy profile is constructed using periodic cubic spline interpolation on the energy values of the 36^3 (46656) grid points.

The conformers that were identified on this 3D-PES were then optimized without constraints in separate optimization runs.

The 1D potential energy contributions $V^{1D}(\phi_i)$ are also calculated using constrained geometry optimizations, with all variables allowed to relax, except for the considered ϕ_i dihedral angle. The 1D grid constitutes of 72 evenly distributed points: $k \cdot 5°$.

The 2D-PES $V_{12}^{2D}(\phi_1, \phi_2)$ is obtained by varying the (ϕ_1, ϕ_2) angles on the grid ($k \cdot 10°$,$l \cdot 10°$) with ϕ_3 fixed in trans (see Fig.5.2 for the numbering of the angles). All other variables are allowed to relax. Due to symmetry considerations the 2D-PES $V_{23}^{2D}(\phi_2, \phi_3)$ coincides with $V_{12}^{2D}(\phi_1, \phi_2)$.

5.3 Analysis of the multidimensional potential energy surface

In an attempt to visualize the features of the 3D-PES, two-dimensional cuts of this hypersurface are given in Figures 5.2 and 5.3. The obvious choices for such cuts, giving information on the ethyl-propyl and the ethyl-ethyl interaction, are those in which the third torsion is kept either at the trans position or at the gauche standing[1]. Hence two plots are presented for the ethyl-propyl interaction: Fig.5.2(a) represents the 2D-PES where the second ethyl torsion is kept in trans, while Fig.5.2(c) gives the ethyl-propyl 2D-PES with the second ethyl rotation at approximately the gauche standing (115° from trans). For the ethyl-ethyl interaction a similar procedure was followed, resulting in two energy cuts where the propyl rotation was either fixed at its trans [Fig.5.3(a)] or gauche position [Fig.5.3(c)].

The first potential energy surface of Fig.5.2(a) is very similar to the ethyl-ethyl surface of pentane, reported earlier in Ref.[16]. In principle, if we consider all possible combinations 0° (trans, t), 115° (gauche, g_-), and 245° (gauche, g_+), nine local minima should be present on the two-dimensional surface. The conformers of two adjacent gauche bonds with opposite sign (g_-g_+ or g_+g_-) are however characterized by severe steric interactions [47]. Without further relaxation these points are first order saddle points, but when these strains relax through a strongly asymmetric torsion of the carbon backbone, each of these saddle points give rise to two distorted gauche positions, located at about 90° from trans. These distorted gauche positions will be referred to as x_- (90°) and x_+ (270°), conform previous literature on this subject [19].
The ethyl-propyl interaction is further visualized in Fig.5.2(c) with the second ethyl in the g_- position. This surface clearly shows different features than Fig.5.2(a), where the second ethyl was at the trans position. The local minimum at $g_-g_+g_-$, which we would expect from combining one-dimensional potentials, disappears due to the presence of an extra barrier in this region of the surface. Again distorted gauche positions come into play leading to a $x_-g_+x_-$ conformer.
The 1D-approximation fails to reproduce the correct features of the ethyl-propyl interaction in the sense that it does not reproduce the exact number of conformers, and also the central peaks are not correctly described. This can be

[1] This is only approximate: the specific dihedral is kept at 115° relative to the trans dihedral ($\approx g_-$).

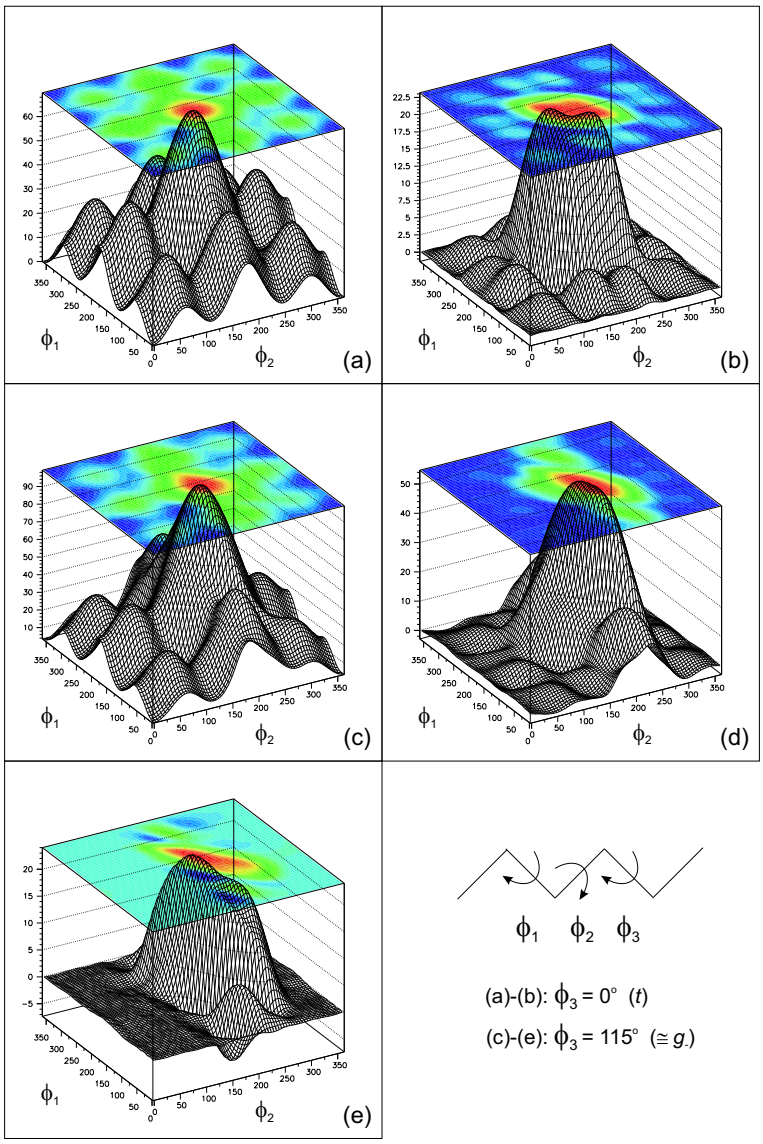

Level of theory: B3LYP/6-311G(d,p).
Reference at 0° is the *trans* conformation.

Figure 5.2: Potential energy of the ethyl-propyl interaction in n-hexane: (a) second ethyl torsion in *trans*: $\phi_3 = 0°$; (b) difference of the 1D-approximation with (a); (c) second ethyl torsion at approximately g_-: $\phi_3 = 115° \approx g_-$); (d) difference of the 1D-approximation with (c); (e) difference of the 2D-approximation with (c).

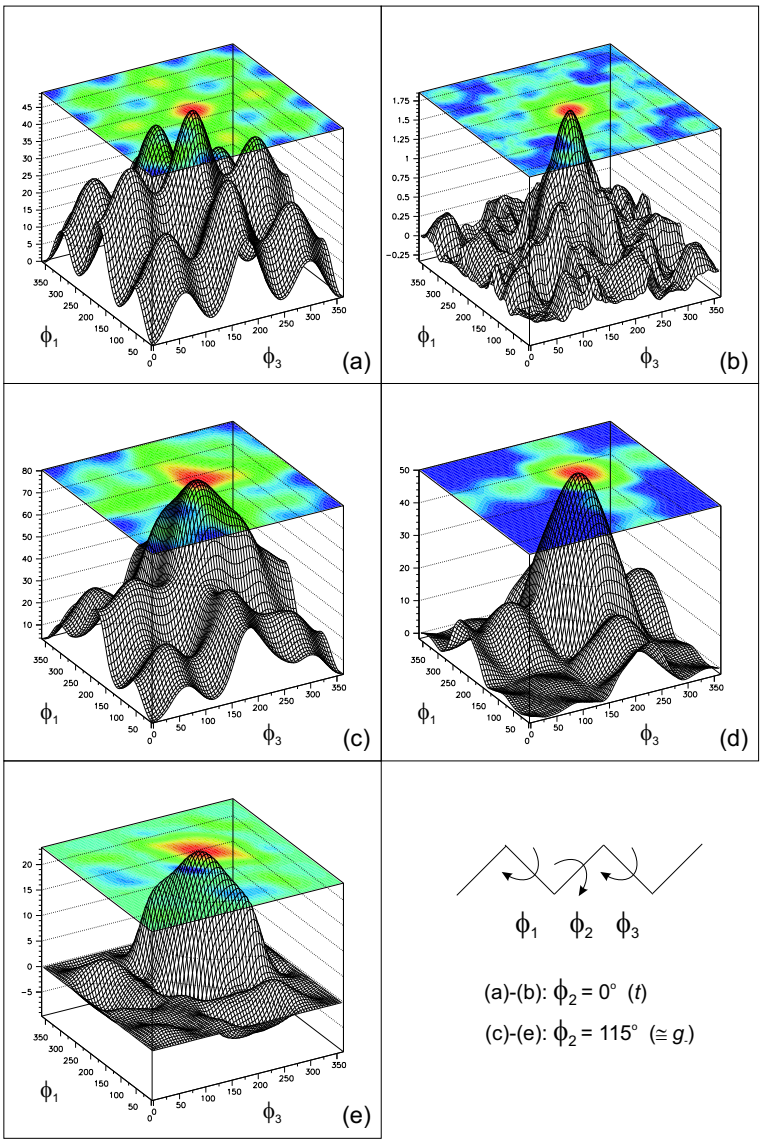

Level of theory: B3LYP/6-311G(d,p).
Reference at 0° is the *trans* conformation.

Figure 5.3: Potential energy of the ethyl-ethyl interaction in *n*-hexane: (a) propyl torsion in trans: $\phi_2 = 0°$; (b) difference of the 1D-approximation with (a); (c) propyl torsion at approximately g_-: $\phi_2 = 115° \approx g_-$); (d) difference of the 1D-approximation with (c); (e) difference of the 2D-approximation with (c).

deduced from Figures 5.2(b) and 5.2(d) which visualize the difference between the 3D-PES and the sum of one-dimensional potentials. The differences can amount to 50 kJ/mol for the energy maxima.

A similar analysis of the ethyl-ethyl coupling is presented in Fig.5.3. For the propyl rotation in the trans geometry, the resulting 2D energy cut [Fig.5.3(a)] is merely a summation of the 1D potentials. The difference of the exact with the 1D approximated values is plotted in Fig.5.3(b), and reveals only small fluctuations. Maximal deviation is noticed at the cis-cis position and is still limited to only 1.75kJ/mol. This fair correspondence was to be expected since both ethyl tops are far apart when the propyl torsion is in trans, and their mutual interaction is therefore almost non-existent.
For a gauche orientation of the propyl top on the other hand, the two ethyl tops are closer to each other, and both rotations are expected to largely affect each other. This should result in large coupling effects. The g_-g_+-effect gives rise to the conformers $x_+g_-g_-$, $x_+g_-x_+$ and $g_-g_-x_+$ in which distorted gauche positions occur due to the relaxation of the carbon backbone to release steric hindrance. The 1D-approximation fails again in reproducing the correct number of conformers and in predicting the correct barriers. Differences up to 50 kJ/mol are noticed in Fig.5.3(d).

Analysis of conformers

In this paragraph, we will focus on the different conformers found in n-hexane, and assess the accuracy of the 1D-approximation for the reproduction of these stationary points.
In principle, if we consider all possible combinations of t, g_- and g_+ for the three internal rotations in hexane, this would result in a total of $3^3 = 27$ conformers. The coupling between two adjacent gauche states of the type g_+g_- gives rise to additional distorted gauche positions designated as x_- or x_+. The same exercise learns that all combinations of t, g_-, g_+, x_- and x_+ may construct a maximum of $5^3 = 125$ conformers. In reality 35 conformers are found on the 3D-PES, in accordance with the study of Tasi et al. [19] where some selection rules to eliminate possible conformers were presented. In n-hexane –and all other normal alkanes– two symmetry operations are applicable in the reference all-trans geometry: a two-fold rotation axis (C_2), and a mirroring surface (σ_h) containing all carbon atoms. Due to these symmetry operations some of the conformers are energetically equivalent, for example, ttg_- is equivalent with ttg_+ due to the σ_h symmetry, and because of the C_2 axis they are also equivalent

to g_tt and g_+tt.

conformer	ΔE	ΔE^{1D}	ΔE^{2D}	f_A	f_A^{1D}	f_A^{2D}
ttt	0.00	**0.00**	**0.00**	1.00	**1.00**	**1.00**
g_+tt, g_tt, ttg_+, $ttg\_$	3.54	**3.54**	**3.54**	1.71	**1.71**	**1.71**
tg_+t, tg_t	3.63	**3.63**	**3.63**	2.13	**2.13**	**2.13**
gtg (4x)		7.08	7.08		2.92	2.92
→ g_+tg_+, $g\_tg\_$	7.02			2.64		
→ g_tg_+, $g_+tg\_$	7.36			2.60		
ggt (8x)		7.17			3.64	
→ g_+g_+t, g_g_t, tg_+g_+, $tg\_g\_$	6.96		**6.96**	2.52		**2.52**
→ $g\_^xg_+^t$, $g_+^xg\_^t$, $t^xg_+g\_$, $t^xg\_g_+$	13.76		**13.76**	2.95		**2.95**
→ $^xg\_g_+^t$, $^xg_+g\_^t$, $tg_+^xg\_$, $tg\_^xg_+$	13.94		**13.94**	2.89		**2.89**
ggg (8x)		10.71			6.22	
→ $g_+g_+g_+$, $g\_g\_g\_$	10.18		10.29	2.89		2.98
→ $g\_^xg_+$, $g_+^xg\_$, $g_+^xg\_$, $g\_^xg_+$	17.41		17.09	3.72		3.49
→ $^xg_+g_+$, $^xg\_g\_$, $g_+g_+^x\_$, $g\_g\_^xg_+$	17.54		17.27	3.49		3.42
→ $^xg\_g_+^x$, $^xg_+g\_^x$	25.26		24.25	4.00		3.91

ΔE is the relative potential energy difference between the fully optimized conformer and the all-trans conformer which is taken as reference conformer. The column labelled f_A is the correlation function of the fully optimized conformer. Columns (ΔE^{1D},f_A^{1D}) and (ΔE^{2D},f_A^{2D}) give estimated values based on the 1D respectively 2D method.
All energy values are in kJ/mol.

Table 5.1: List of stable conformers found in n-hexane, and their energy difference with the all-*trans* conformer.

In Table 5.1 all conformers are listed together with the electronic energy of the fully optimized geometries relative to the energy of the all-trans conformer (ΔE column). Also the energies of the conformers constructed in this uncoupled scheme are also given (reported as ΔE^{1D}).
Within the one-dimensional scheme only 27 conformers are found due to the ignorance of coupling between adjacent gauche standings of opposite sign. In this approach, three energy values turn out to coincide with the 3D predictions. This is not surprising since these *ttt*, *gtt* and *tgt* classes of conformers can be reached by a single internal rotation in the reference conformer. The energy values that are exactly reproduced are given in bold. For the other conformers, no distinction can be made between gauche states of different orientation, or between distorted and normal gauche geometries. These limitations lead to three additional different energy values for *gtg*, *ggt* and *ggg* geometries, independent of the orientations of the gauche geometries. Table 5.1 reveals that these values are very close to the 3D conformer energy differences where subsequent gauche standings have the same orientation (g_+g_+t, $g_+g_+g_+$). On the other hand, in the cases where the orientations are different, the correspondence 1D-3D is no longer valid, and discrepancies of the order of 6.5 kJ/mol are noticed.

5.4 Approximation schemes for the kinetic and potential energy

One of the main goals of this paper is to present a method for reproducing accurate partition functions belonging to the multiple internal rotations figuring in long chain molecules, and which is computationally feasible. As outlined in previous section, the 1D approximation is inadequate to describe the correct features of the multi-dimensional PES. In the following, we will investigate how large the discrepancies of the partition function are in this 1D approach, compared with the coupled 3D result.
In its simplest form the classical partition function Q_{cl} of the internal rotations and the global rotation is defined as [71]:

$$Q_{cl} \sim \int \sqrt{\det A}\ e^{-\frac{V(\phi_1,\ldots,\phi_m)}{k_B T}} \mathrm{d}^{\mathrm{m}}\Phi \tag{5.2}$$

where k_B is the Boltzmann factor, T is the temperature, and V is the potential energy in function of the torsional angles. A represents the kinetic energy matrix, and incorporates the moments of inertia of the internal rotations. In Fig.5.4(a) the rotational partition function is shown in terms of temperature for hexane. The 1D result overestimates the coupled partition function generated from the 3D-PES. The 1D approximation scheme affects both the potential and kinetic energy. The underestimation of the central peaks and nonexistence of some conformers on the approximate three dimensional PES constructed with 1D contributions, as defined in Eq.(5.1), do shift the rotational energy states to lower energies and will enhance the partition function.

Most one-dimensional hindered rotor approaches found in literature combine a potential energy constructed along the lines of Eq.(5.1) with constant moments of inertia. These reduced moments are evaluated in the reference conformer geometry and hence are independent of the torsional angles. This 1D-HR approach does not include kinetic coupling between the various rotations and underestimates the kinetic energy contribution to the partition function [16]. We refer to this method as Q^{1D} shown in Fig.5.4(a).
Summarizing, the 1D-HR scheme overestimates the true partition function. As both potential and kinetic energy contributions tend to cancel each other, the final result is subject of large cancellation errors. By coincidence this 1D approach turned out to give excellent agreement with experiment in reproducing thermodynamic properties in n-alkanes [14, 16] which are evaluated from the

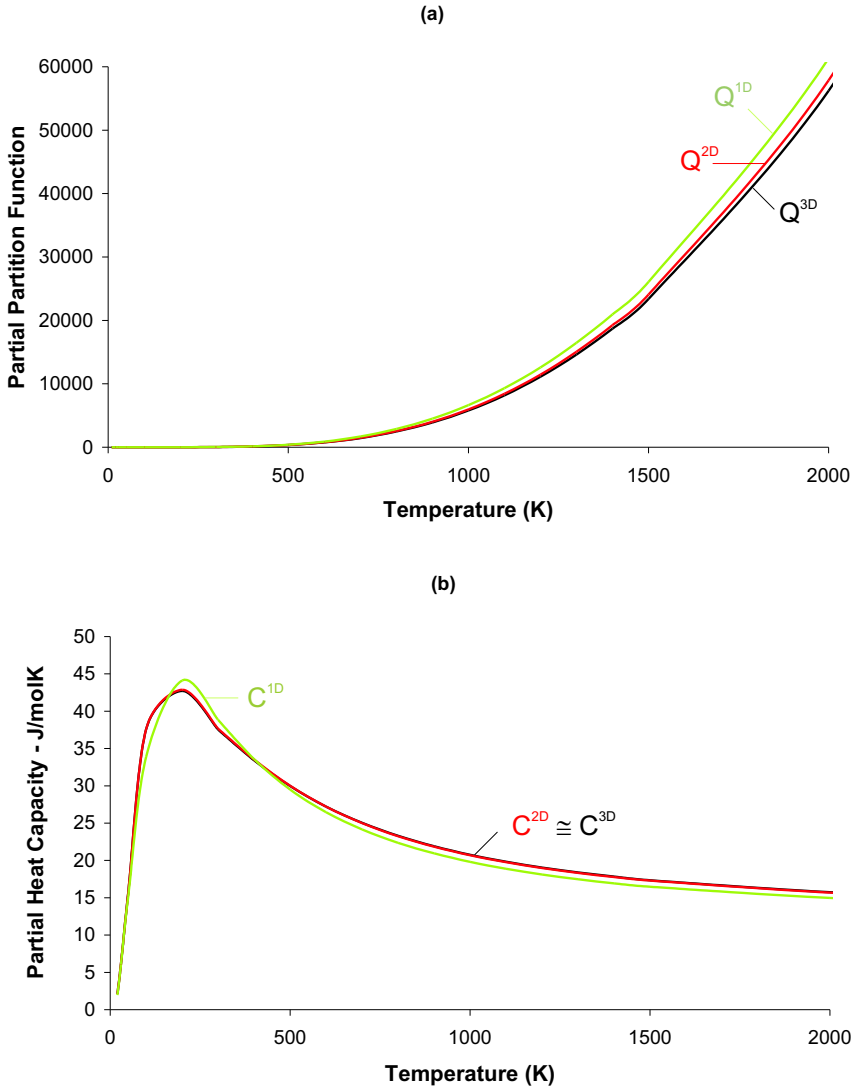

Figure 5.4: (a) Partition function and (b) heat capacity of the three internal rotations of n-hexane calculated with the exact model (Q^{3D}, C^{3D}), with the 2D-approximation (Q^{2D}, C^{2D}), and with the 1D-scheme (Q^{1D}, C^{1D}).

global partition functions.

It is instructive to find a procedure which is computational feasible and which is able to reproduce partition functions close to those predicted by the 'exact', computationally intensive, 3D model. This is offered by an adapted 2D approximation. The multidimensional PES is approximated as follows :

$$V^{mD}(\phi_1,...,\phi_m) \approx \sum_{i=1}^{m-1} V^{2D}_{i(i+1)}(\phi_i,\phi_{i+1}) - \sum_{i=2}^{m-1} V^{1D}_i(\phi_i) \qquad (5.3)$$

For the present case of n-hexane, the two 2D-PES (V^{2D}_{12} and V^{2D}_{23}) are identical due to symmetry, and correspond to the surface shown in Figure 5.2(a).
In this expression the coupling between consecutive internal rotations is taken into account whereas coupling between non-adjacent internal rotations is ignored. To prevent double counting the one-dimensional potentials are subtracted.

It turns out that the 2D approximated PES, as constructed along Eq.(5.3), is able to reproduce the correct number of minima. The relative energies of the various conformers are given in Table 5.1 under ΔE^{2D}, referred to the all trans conformation energy. All conformers where coupling between adjacent rotors comes into play are exactly reproduced. Thus the minima of the *ggt* class are exactly described, including the distorted gauche standings. The stationary points belonging to the *gtg* and *ggg* subclasses still suffer from some deviations from the exact energies but these are limited to less than 1kJ/mol. Some peaks on the PES are still underestimated, e.g. the peak in Fig.5.2(c), but the discrepancies are reduced from 50 kJ/mol in the one-dimensional scheme to 20 kJ/mol. The plots given in Figs.5.2(e) and 5.3(e) visualize the differences of the 2D-approximation with the fully calculated 3D-PES for the ethyl-propyl surface (with the second ethyl torsion near g_-), respectively for the ethyl-ethyl coupling (where the propyl rotation resides in g_-). Another striking aspect is that the fluctuations of the surface of Figs.5.2(d) and 5.3(d), apart from the central bump, disappear in the proposed 2D scheme, in contrast to the 1D approximation.
Summarizing, the approximate 3D-PES, constructed with two 2D potential energy surfaces along the lines of Eq.(5.3), closely resembles the true 3D surface: the number of conformers is exactly reproduced, the conformational energies are predicted within a maximum error of 1 kJ/mol, the central bumps are substantially better described, and the energy increase of the g_-g_+ effect is also

taken into account.

The accuracy in which the PES is determined has its implications on the method for constructing the kinetic energy matrix. A fully constructed multi-dimensional PES requires a geometry optimization at each point of the grid in terms of the various torsional angles, and thus it obviously offers all necessary ingredients for constructing the exact kinetic energy matrix and its variation in function of the torsional angles. As already proposed in Ref.[16], it is convenient to factorize the determinant of the kinetic energy matrix into:

$$\det A\left(\phi_1,\ldots,\phi_m\right) = \det A_0 \cdot f_A^{mD}\left(\phi_1,\ldots,\phi_m\right) \tag{5.4}$$

with f_A^{mD} the multidimensional correlation function and A_0 the kinetic energy matrix corresponding with the reference conformer which does not depend on the torsional angles. The correlation function thus gives an indication of the fluctuation of the moments of inertia in terms of the rotational angles. In the 1D scheme this function can be approximated as:

$$f_A^{mD}\left(\phi_1,\ldots,\phi_m\right) \approx \prod_{i=1}^{m} f_{A,i}^{1D}\left(\phi_i\right) \tag{5.5}$$

In literature, the 1D scheme often uses a variant to this description. The determinant is then approximated as a product of all (constant) reduced moments of inertia (I^{red}) of the different internal rotations and the (constant) principal moments of inertia ($I_x I_y I_z$) of the molecule:

$$\det A\left(\phi_1,\ldots,\phi_m\right) \approx I_x I_y I_z \prod_{i=1}^{m} I_i^{red} \tag{5.6}$$

These principle and reduced moments are calculated using the geometry of the reference conformer.
In a 2D-scheme, where coupling between adjacent rotors is taken into account, the correlation function may be approximated according to:

$$f_A^{mD}\left(\phi_1,\ldots,\phi_m\right) \approx \frac{\prod_{i=1}^{m-1} f_{A,i(i+1)}^{2D}\left(\phi_i,\phi_{i+1}\right)}{\prod_{i=2}^{m-1} f_{A,i}^{1D}\left(\phi_i\right)} \tag{5.7}$$

The construction of the correlation function according to Eq.(5.7) is based on similar grounds as what has been proposed in Eq.(5.3). The nominator in Eq.(5.7) is required to prevent double counting.
In Table 5.1 the correlation functions are given for the conformers in the exact

3D scheme and approximate 1D and 2D schemes. The 2D approximation performs quite well, while the 1D scheme causes a serious overestimation of the correlation function.

The accuracy of the various schemes can further be tested by evaluating the partition function. Fig.5.4(a) shows the rotational partition function in the 2D scheme. The partition function Q^{1D} (with constant reduced moments of inertia) lies rather close to the partition function Q^{3D} generated by the 3D-PES. At low temperature ($\approx$ 300K) Q^{1D} overestimates Q^{3D} by 18%, whereas at higher temperatures ($\approx$ 2000K) the overrating reduces to about 9%. The 2D based partition function Q^{2D} almost coincides with Q^{3D}, and its overestimation of the reference Q^{3D} remains lower than 3% over the full temperature range. As a consequence, also the derivatives of the 2D partition function with respect to temperature –needed for the calculation of derived thermodynamic quantities– will be very close to the 3D derivatives. On the other hand, the derivatives of Q^{1D} will show larger deviations.
As a result, the thermodynamic properties derived from Q^{2D} will be extremely close to the 3D based properties. In Fig.5.4(b) we show the (partial) heat capacity of the three investigated internal rotations. The values of the 2D-scheme coincide with those of the exact 3D-scheme (C^{3D}). This is remarkable because calculation of the heat capacity involves second derivatives of the partition function, making the results relatively sensitive to subtle differences between these functions.
The 1D results C^{1D}, although very close to the reference values, show a distinct behavior compared with C^{3D}.

5.5 Conclusions

In this chapter we studied n-hexane as a typical example in which various consecutive internal rotations about single bonds are present and where effects of coupling on the potential energy and kinetic energy surfaces are important. The exact potential energy surface in these dimensions was determined from ab initio calculations at the B3LYP/6-311g** level. The 1D approximation fails in reproducing the correct features of this surface. An adopted 2D approach has been presented which succeeds in reproducing the most important characteristics of the exact potential energy surface, such as the correct number of conformers, incorporation of the g_-g_+ effect, and good estimates for the various energy peaks of the surface. Also the kinetic energy part of this 2D scheme reproduces the variation of the kinetic correlation function in a very satisfying way. The partition function calculated within this 2D scheme almost coincides with the exact 3D based partition function. All thermodynamic features which are expressed in terms of the global partition function have the same kind of accuracy.

Chapter 6

Rules for generating conformers and their relative energies in ethers, alcohols, sulfides and thiols

This chapter is based on Ref.[18]:

Vansteenkiste, P.; Pauwels, E.; Van Speybroeck, V.
and Waroquier, M.
J. Phys. Chem. A **2005**, *109*, 9617–9626

Abstract

With the aid of density functional theory calculations, all conformers of several single chain alcohols, thiols, ethers and sulfides are investigated. Starting from earlier computational works on n-alkanes, an extended set of general rules is constructed to predict the number and occurrence of conformers in these oxygen or sulfur containing compounds. In alcohols and thiols, it is found that only the conformers generated by internal rotations in the $HXCH_2CH_2CH_2$-top ($X = O, S$) are distinctive from those in n-alkanes. In ethers and sulfides, the primary influence of the hetero element also extends up to three internal rotations, but much more conformers are possible. However, a number of double gauche sequences are forbidden and therefore several conformers can be eliminated. These exclusions in particular make up a set of rules to eventually deduce all possible conformers. Furthermore, based only on an exact calculation of these gg-conformations in addition to single gauche conformers it is possible to make an accurate estimate of the relative energy. This two dimensional approximation scheme constitutes an effective tool to adequately describe the relative energies of all possible conformers at a minimal computational cost.

6.1 Introduction

In this chapter we focus on the conformers of four types of single chain molecules. We choose the hetero-elements O or S to substitute a CH_2 fragment in n-alkanes. The resulting compounds (ethers/alcohols or sulfides/thiols) are, like n-alkanes, also single chain molecules but their energetically most stable structure is not a priori an all-trans conformation. Furthermore, it is unclear what the geometries and relative energies are of the different conformers.

The considered molecules are omnipresent in (fine) chemistry and biochemistry [82, 83, 84, 85, 86, 87, 88, 89, 90, 91], and have a tremendous economic importance. For a thorough understanding of the (bio)chemical processes in which these molecules are involved, one needs an accurate description of the conformational flexibility. A microscopic evaluation of molecular properties mainly depends on the knowledge of the various conformers which can be formed, and in particular on their relative energies. This is essential, since it is far from certain that the active conformer always corresponds to the global minimum of the potential energy surface.

It is well known that internal rotation about a single CC bond generates a potential energy curve with three local minima: one trans (t) and two gauche (g_- and g_+) conformations [14, 16, 17, 19]. Rotation about a single CO or CS bond produces a similar potential energy profile. An easy conclusion would be that there are 3^n conformers for any molecule having n such (CC, CO or CS) single bonds. This was shown not to be true for n-alkanes [17, 19] and, in fact, 3^n presents only a lower bound for the actual number of possible conformers. However, for longer molecules with many internal rotations this number of conformers grows exponentially, and it becomes almost impossible to locate and describe them all. For this reason, Tasi et al. [19] introduced a general set of rules to predict the number and occurrence of conformers in n-alkanes. However, it has not been established whether these rules also apply for similar compounds, such as those of the present study.
We therefore deduce an additional set of general rules for the occurrence of conformers in alcohols, thiols, ethers and sulfides. Despite their apparent similarities (O and S are situated in the same column of Mendelev's table), the properties of oxygen or sulfur containing molecules may vary substantially and the most important differences and analogies are highlighted. In addition, the relative energies of all conformers are rigorously determined and an approxima-

tion scheme is suggested to make reasonable estimates for the relative energies without the need for explicit ab initio calculations on all conformers.

The introduction of general rules to determine the number and occurrence of conformers, and the availability of a fast method to produce reliable energy estimates for these structures presents an important step forward in tackling long chain alcohols/thiols and ethers/sulfides. The methodology presented in this paper can readily be extrapolated to examine other types of single-chain compounds.

6.2 Labelling convention for conformers

In order to unambiguously describe the different conformers, a convenient and consistent labelling system must be introduced. A first step is to specify the conformation of an individual internal rotation. In Fig.6.1 a typical potential energy variation is shown as a function of the dihedral angle controlling the internal rotation about a CC-bond[1]. There are three minima corresponding to three conformations, labelled by the indices t, g_- and g_+, corresponding to a trans or a gauche $-/+$ orientation. Rotations about a CO or CS single bond generate similar potential energy profiles, and the minima are labelled in a similar way.

When multiple internal rotations within a molecule are considered, the individual conformation of each rotation has to be assigned. The appropriate labelling convention for a sequence of internal rotations in the molecules considered, is illustrated in Fig.6.2. For alcohols and thiols [Fig.6.2(a)], the first internal rotation (with dihedral angle ϕ_{l1}) is about the CX bond ($X = O$ or S). The other rotations are labelled as ϕ_{lx} where x indicates the position of the CC rotation axis with regard to the CX bond. Also the position of the hydroxyl top is written explicitly. For example, the HOg_+tg_-t conformer

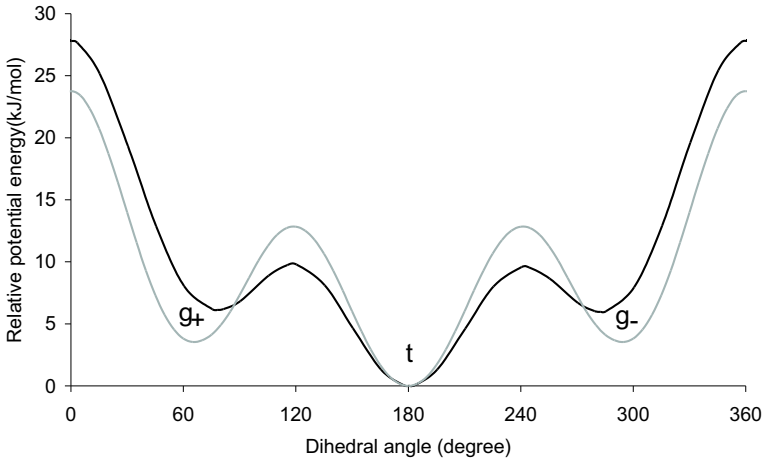

Figure 6.1: Typical potential energy profiles of internal rotation about a $(C)CC(C)$-bond (grey line) and $(C)CO(C)$-bond (black line). The reference of the (absolute) dihedral angle corresponds with the *cis* geometry.

[1]This figure does not apply for internal rotation of ending methyl tops.

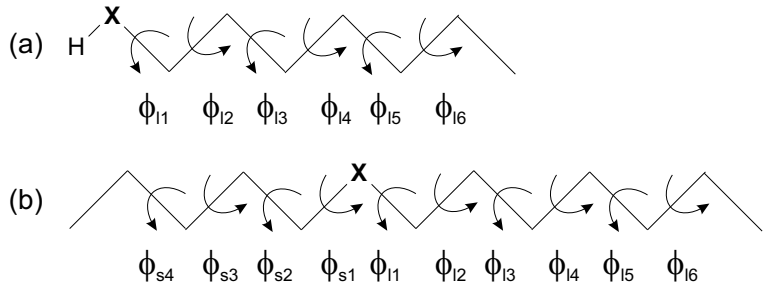

Figure 6.2: Illustration of labels used to identify specific internal rotations (with their dihedral angles) in (a) primary alcohols ($X = O$) and thiols ($X = S$), and (b) in ethers ($X = O$) and sulfides ($X = S$).

of 1-pentanol (or HSg_+tg_-t for 1-pentane thiol) is a shorthand notation for $\phi_{l1} = g_+$, $\phi_{l2} = t$, $\phi_{l3} = g_-$, and $\phi_{l4} = t$ where $l4$ indicates the ethyl torsion, $l3$ the propyl torsion, and so on.

For ethers and sulfides, the same convention applies, but one has to distinguish between the two alkyl fragments [Fig.6.2(b)]. The 'l' subscript indicates that the rotation is situated in the longest alkyl top on the hetero-element, and the 's' refers to the shortest alkyl branch. The numbers refer to the position of the involved bond with respect to X: '1' specifies the rotation about the CX-bond, '2' specifies the consecutive rotation, and so on. In general, we refer to a conformer by specifying the individual conformations in the order $\phi_{smax} \ldots \phi_{s1} X \phi_{l1} \ldots \phi_{lmax}$[2], with $X = O$ or S. For example, in ethyl propyl ether tOg_-g_+ is the shorthand notation for $\phi_{s1} = t$, $\phi_{l1} = g_-$, and $\phi_{l2} = g_+$, while the same configuration in ethyl propyl sulfide is referred to as tSg_-g_+.

We remark that all molecules in this work are subject to the symmetry operation σ_h which converts all gauche +/- orientations into its gauche -/+ mirror image. The trans conformations are not affected. For example, the above mentioned HOg_+tg_-t conformer of 1-pentanol is converted to HOg_-tg_+t. Similarly, the tSg_-g_+ conformer in ethyl-propyl sulfide is converted into tSg_+g_-. As a result, all tabulated conformers except the all trans conformers, correspond to two mirror geometries with the same electronic energy.

[2]For alcohols and thiols there are no 's' internal rotations, making the above defined nomenclature a special case of this more general definition.

6.3 Computational details

Within the class of density functionals it is well known that the hybrid B3LYP and B3PW91 functionals [7, 92] have proven to be a successful approach for obtaining accurate molecular structures, vibrational frequencies, heats of formation and bond energies [93][94][95][96]. In particular, we have shown in Ref.[14] that the triple zeta 6-311g** basis set in combination with the B3LYP functional produces reliable potential energy profiles for n-alkanes, and for this reason we select this functional for the calculations in this work. Although the current set of molecules is very similar to n-alkanes (only one CH_2 fragment is replaced by an O or S atom), this level of theory (more particular the basis set) can not be used without further analysis. As oxygen and sulfur both have electron lone-pairs and are hence likely to require a more extended basis set and diffuse functions, we have to select an appropriate basis set to be used in the B3LYP calculations. Moreover, S is a third period element in Mendelev's table for which more polarization functions may be required, although the 6-311g** (combined with MP2) was found to be more than adequate for dimethyl sulfoxide [97]. In this light, the 6-311+G(3df,2p) and 6-311++G(3df,3pd) basis sets will be employed. As these two larger basis sets are computationally very demanding, we also add the smaller 6-31+g* basis set to our basis set investigation. This basis has the advantage over 6-311g** that it includes a diffuse function, and that it considerably reduces the computational time. The inclusion of a diffuse function is expected to improve the results considerably [98], even more than the addition of polarization functions or improvement of the valence description.
For the transparency of the notation, we introduce the shorthand acronyms B1 for the 6-31+g* basis, B2 for 6-311g**, B3 for 6-311+G(3df,2p) and B4 for the 6-311++G(3df,3pd) basis set.
All calculations are performed with the Gaussian98 [12] and Gaussian03 [13] software packages.

We investigate the combination of the mentioned basis sets B1, B2, B3 and B4 with B3LYP, and also B3PW91 combined with the B1 and B4 basis sets, in order to select the appropriate DFT-level of theory. These 6 approaches are used to evaluate the basis set dependence for 1-propanol, 1-propanethiol, methyl propyl ether and methyl propyl sulfide which are model compounds for alcohols, thiols, ethers and sulfides respectively. For each of these molecules, all conformers are identified and the electronic energies obtained from full ge-

ometry optimizations on these conformers are compared with each other. In addition to these molecules, also the conformers of methyl ethyl ether (MEE), methyl ethyl sulfide (MES), di-ethyl ether (DEE) and di-ethyl sulfide (DES) are calculated at different levels of theory. For these molecules experimental data are available.

Each of the mentioned conformers is found by performing full, unrestrained geometry optimizations. No potential energy scans or surfaces are employed. An initial set of conformer geometries was created, based on the possible conformations of a single internal rotation (gauche, trans, *etc.*). The set was then extended by additional sampling of the conformations of consecutive internal rotations. Finally, the initial geometries were optimized without any constraints.

6.3.1 Basis set dependence

As primary task, the basis set dependence of the B3LYP (B3PW91) functional for alcohols, thiols, ethers and sulfides is studied. One of the principal aims of this study is the selection of a cost-effective level of theory that still produces accurate results. For this reason we only apply the B3LYP and B3PW91 functionals in the DFT calculations. We use two 'small' basis sets (B1 and B2), and two more extended basis sets (B3 and B4). The latter basis sets are used to calculate the reference energy differences. The values predicted by the smaller B1 and B2 sets can then be compared with these reference values.

Four reference molecules are chosen to represent the different classes of molecules that are studied: 1-propanol (alcohols), methyl propyl ether (ethers), 1-propane thiol (thiols) and methyl propyl sulfide (sulfides). Each of these molecules shows two single bonds about which an internal rotation can generate different conformations, and forms the smallest compound of each class to have more than two energetically different conformers. In accordance with the labelling convention, these rotations are identified as ϕ_{l1} and ϕ_{l2}, each rotation covering three conformations t, g_- and g_+. Combination of these geometries leads to a total of nine conformers. Due to the σ_h symmetry this number reduces to five sets of energetically different conformers: Xtt, Xg_-t/Xg_+t, Xtg_-/Xtg_+, Xg_-g_-/Xg_+g_+, and finally Xg_-g_+/Xg_+g_- ($X = (H)O$ or $(H)S$). The latter set of conformers is a result of the combination of gauche standings with different orientation. Only for methyl propyl ether no

such Og_-g_+/Og_+g_- conformer could be found.

	B3LYP				B3PW91	
	B1	**B2**	**B3**	**B4**	**B1**	**B4**
1-propanol						
HOg_-g_-/HOg_+g_+	0.85	**0.00**	0.68	0.65	0.91	0.67
HOg_-g_+/HOg_+g_-	1.05	1.23	0.83	0.89	1.07	0.84
$HOtg_-/HOtg_+$	0.39	1.48	0.35	0.21	0.77	0.58
HOg_-t/HOg_+t	**0.00**	1.19	**0.00**	0.04	**0.00**	**0.00**
$HOtt$	0.19	2.44	0.11	**0.00**	0.43	0.22
methyl propyl ether						
Og_-g_-/Og_+g_+	6.70	6.07	6.35	6.45	6.46	6.34
Otg_-/Otg_+	0.19	**0.00**	0.02	0.03	0.29	0.15
Og_-t/Og_+t	6.33	7.50	6.22	6.30	6.10	6.16
Ott	**0.00**	1.38	**0.00**	**0.00**	**0.00**	**0.00**
1-propane thiol						
HSg_-g_-/HSg_+g_+	2.31	1.63	1.91	1.88	1.96	1.56
HSg_-g_+/HSg_+g_-	2.66	2.20	2.01	1.98	2.52	1.84
$HStg_-/HStg_+$	5.71	5.37	5.23	4.97	5.69	4.83
HSg_-t/HSg_+t	**0.00**	**0.00**	**0.00**	**0.00**	**0.00**	**0.00**
$HStt$	2.92	3.01	2.66	2.43	3.13	2.49
methyl propyl sulfide						
Sg_-g_-/Sg_+g_+	1.98	1.22	1.60	1.66	1.49	1.33
Sg_-g_+/Sg_+g_-	5.94	5.54	5.88	5.96	6.01	6.06
Stg_-/Stg_+	2.83	2.84	2.56	2.51	2.60	2.27
Sg_-t/Sg_+t	0.08	**0.00**	0.17	0.32	0.05	0.39
Stt	**0.00**	0.40	**0.00**	**0.00**	**0.00**	**0.00**

B1=6-31+g*, B2=6-311g**, B3=6-311+G(3df,2p), B4=6-311++G(3df,3pd).
The conformer with lowest electronic energy is taken as reference.
Relative energies in kJ/mol without ZPE contributions.

Table 6.1: Relative energies of the various conformers of the model compounds 1-propanol, methyl propyl ether, 1-propane thiol and methyl propyl sulfide.

Table 6.1 shows the relative energies of the different conformers of 1-propanol. The most stable conformer at each level of theory is the reference for the potential energy differences. Except for B3LYP/6-311g**(B2), all other levels of theory attribute the global minimum to either the $HOtt$ or $HOgt$ conformers.

B3LYP	B1	B2	B3	B4
Og_-g_-	1,00	**0,00**	0,91	0,94
Og_-g_+	1,30	0,95	1,16	1,28
Ogt	0,35	0,88	0,38	0,35
Otg	0,14	0,95	0,22	0,29
Ott	**0,00**	1,70	**0,00**	**0,00**

B1=6-31+g*, B2=6-311g**, B3=6-311+G(3df,2p), B4=6-311++G(3df,3pd).
The conformer with lowest electronic energy is taken as reference.
Relative energies in kJ/mol with inclusion of the ZPE.

Table 6.2: Relative energies of the five conformers of 1-propanol when the zero point energy is taken into account.

The energy difference between these two types of conformers is quite small: 0.4 kJ/mol at most. These differences are smaller than the expected accuracy of the B3LYP or B3PW91 functionals, and therefore it is not possible to conclude from these data which geometry is the real global minimum. Moreover, with the inclusion of zero point energies (Table 6.2), the $HOtt$ conformer becomes the lowest energy conformer for all methods (except B3LYP/B2). The energies of the other conformers follow the sequence $HOtg < HOg_-g_- < HOg_-g_+$ in all methods (except B3LYP/B2), with a maximal energy difference of about 1 kJ/mol.

The B3LYP/6-311g**(B2) results show a slightly different pattern, but we should be careful in drawing conclusions as the energy discrepancies are of the order of 2 kJ/mol. Anyway, there are indications that B2 is not the most adequate basis set to describe these molecules. This is confirmed by the results predicted for methyl propyl ether (see Table 6.1). Within the same level of theory, the basis sets B1, B3 and B4 give almost identical results, while the results obtained with the B3LYP/B2 method are deviating for the conformers with ϕ_{l2} in trans (Og_-t/Og_+t and Ott).

For both molecules, the results with the B1 basis set show a very good quantitative agreement with the larger B3 and B4 basis sets. Additionally, the geometries of the conformers optimized with B1 are almost identical to the B3 and B4 geometries, while the B2 geometries are somewhat divergent.

We now discuss the relative energy values for the conformers of the sulfur compounds 1-propane thiol and methyl propyl sulfide (Table 6.1). In contrast with oxygen compounds, the influence of the selected basis set is rather limited, and the B2 set produces results that are comparable with the B1 values. As B1 is

somewhat faster than B2, and because we wish to use the same level of theory for both oxygen and sulfur compounds, the B1 basis still has a preferential status.

The above discussion supports the preference of basis set 6-31+g*(B1) to basis set 6-311g**(B2) for DFT/B3LYP calculations on the selected set of molecules, but a validation with experimental data is needed to draw final conclusions on the most suitable basis set.
The smallest alcohol of our set of molecules for which experimental data are available is ethanol. Several experimental papers have reported that the trans conformer in this molecule is slightly more stable than its gauche conformer. Depending on the experimental methods, the measured energy differences vary from 0.49 kJ/mol for microwave spectroscopy [99], over 1.31 kJ/mol for gas phase Raman spectroscopy [100], to 2.9 kJ/mol for overtone spectroscopy [101]. Also on the theoretical level a lot of work has been done, *e.g.* [102]. A recent study of Weibel et al. [103] gives an interesting overview of several theoretical results on this trans-gauche energy difference. A correct theoretical prediction of the trans as the most stable conformer is not uniformly obtained, and is very sensitive to the level of theory used. The assignation of the lowest energy conformer can even change by inclusion of zero point energy (ZPE). In this work the B3LYP/6-31+g*(B1) results favor the trans conformer by 0.27 kJ/mol (no ZPE included). The predicted energy difference is rather low, but acceptable. More recently, Takahashi et al. [104] performed a DFT calculation on the B3LYP /6-311++ G(3df,3pd) (B4) level of theory, resulting in an energy difference of 0.41 kJ/mol in favor of the trans conformer in ethanol, with inclusion of ZPE. They also reported energy differences (including ZPE contributions) on the same level of theory between the conformers of 1-propanol. They predict that the all-trans conformer is the most stable conformer, followed by the $HOtg$ and $HOgt$ conformers with a mere 0.25 kJ/mol maximal energy difference. The HOg_-g_- and HOg_-g_+ geometries are 0.8 kJ/mol respectively 1.2 kJ/mol higher in energy than the $HOtt$ reference. These results almost coincide with the values reported in this work (Table 6.2), except for the B3LYP/B2 level of theory.
Other available experimental and/or ab initio data are very scarce, and are collected in Table 6.3. The agreement between experiment and the theoretical calculations is very satisfactory.

Finalizing, this basis set investigation allows us to conclude that B3LYP/6-31+g*(B1) is the best cost-effective level of theory for use in all further calculations.

	B3LYP				Experiment	
	B1	B2	B3	B4		
methyl ethyl ether						
Og	6.48	6.14	6.35	6.48	4.6 → 6.3	[105][106]
methyl ethyl sulfide						
Og	0.57	0.07	0.46	0.67	-0.8 → 1.5	[105][107]
di-ethyl ether						
g_-Og_-/g_+Og_+	12.70	11.33	12.47	12.71		
g_-Og_+/g_+Og_-	16.21	15.49	16.04	16.27		
$tOg_-/tOg_+/g_-Ot/g_+Ot$	6.60	6.13	6.42	6.59	4.81	[108]
tOt	0.00	0.00	0.00	0.00	0.00	[108]
di-ethyl sulfide						
g_-Sg_-/g_+Sg_+	1.14	0.15	0.82	1.15	≈ 0	[109]
g_-Sg_+/g_+Sg_-	4.47	3.73	4.38	4.78	$high$	[109]
$tSg_-/tSg_+/g_-St/g_+St$	0.69	0.24	0.52	0.73	≈ 0	[109]
tSt	0.00	0.00	0.00	0.00	$small$	[109]

The basis sets are defined as: B1=6-31+g*, B2=6-311g**, B3=6-311+G(3df,2p), B4=6-311++G(3df,3pd).
The conformer with lowest electronic energy is taken as reference.
Relative energies in kJ/mol without ZPE contributions.

Table 6.3: Relative energies of the various conformers of the compounds methyl ethyl ether, methyl ethyl sulfide, di-ethyl ether and di-ethyl sulfide compared with experiment.

6.4 Conformational analysis

The different conformers of n-alkanes are reached by performing internal rotations about the CC bonds apart from the methyl tops. Each rotational profile is characterized by three distinct potential energy minima (as shown in Fig.6.1: t, g_+, and g_-). Obviously, one could expect that a molecule with n such internal rotations would lead to 3^n conformers.
In several papers, the occurrence of conformers in n-alkanes was studied [19, 47, 17]. The most extensive study was performed by Tasi et al. [19]. They reported the existence of distorted gauche standings x, for which the typical dihedral angle has a value of about $\pm 85°$, or $95°$ from trans, while normal gauche standings in n-alkanes have a dihedral of $\pm 65°$, or $115°$ from the trans conformation [Fig.6.3(a)]. The combination of these five possible conformations leads to 5^n conformers. The actual number of conformers lies in between 3^n and 5^n, since the distorted gauche conformations only exist with special circumstances. In particular, the x-gauche conformations are found in n-alkanes when two consecutive internal rotations reside in gauche standings of opposite orientation. This g_-g_+ combination brings two carbon atoms in close vicinity, forcing the carbon backbone to relax. This relaxation was also observed by the authors for n-pentane and n-hexane [16, 17] in their study of coupled internal rotations. On the two-dimensional potential energy profiles of consecutive internal rotations, two local minima were identified around the g_-g_+ geometry, corresponding to x_-g_+ and g_-x_+ conformers. The relative energy associated with these conformers was found to be considerably higher than the conformers with consecutive gauche standings of the same orientation (g_-g_-/g_+g_+).

In this study we will evaluate the geometries of the conformers of respectively alcohols, thiols, ethers and sulfides. The possible interactions between consecutive internal rotations will be investigated and the occurrence of distorted gauche conformations x will be examined. Based on these findings, we will introduce a complementary set of rules which allows the determination and structural identification of the total number of conformers in these compounds at a minimal computational expense. In addition, we also calculate the relative energies of the different conformers and compare these to the corresponding values in n-alkanes.

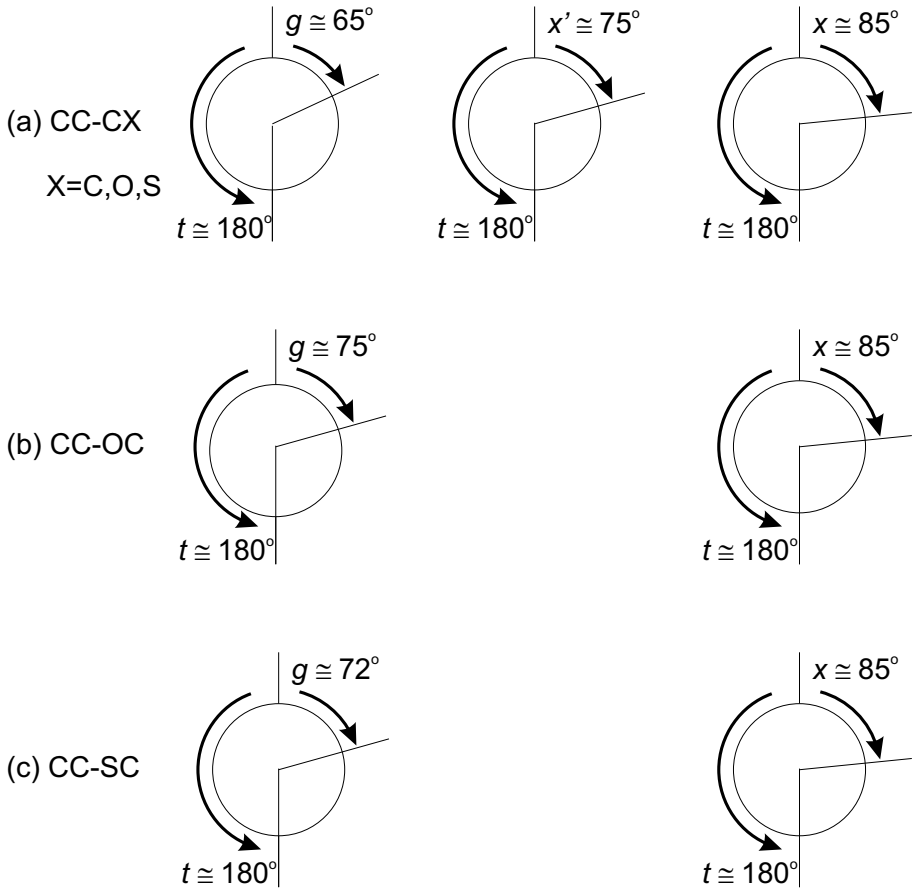

Figure 6.3: Newman projections of the typical dihedral angle values for gauche g, slightly distorted gauche x', and distorted gauche x conformation about a (a)CC, (b)CO and (c)CS single bond.

$\phi_{l1}\phi_{l2}\phi_{l3}\phi_{l4}\phi_{l5}$	ethanol	1-propanol	1-butanol	1-pentanol	1-hexanol
The $HOCH_2CH_2CH_2$- functional group conformers:					
$HOt(tttt)$	0.00	0.19	0.10	0.10	0.10
$HOg_-(tttt)$	0.27	0.00	0.00	0.00	0.00
$HOtg_-(ttt)$		0.39	0.00	0.13	0.08
$HOg_-g_-(ttt)$		0.85	0.61	0.76	0.76
$HOg_+g_-(ttt)$		1.05	0.80	0.75	0.71
$HOttg_-(tt)$			4.22	4.30	4.26
$HOg_-tg_-(tt)$			4.26	4.25	4.24
$HOg_+tg_-(tt)$			3.82	3.83	3.80
$HOtg_-g_-(tt)$			3.42	3.69	3.57
$HOg_-g_-g_-(tt)$			3.68	3.91	3.78
$HOg_+g_-g_-(tt)$			4.83	5.10	4.96
$HOtg_-x'_+(tt)$			7.00	6.95	7.08
$HOg_-g_-x'_+(tt)$			7.14	7.09	7.11
$HOg_+x_-g_+(tt)$			9.20	8.97	8.75
Alkane-like conformers:					
$HOtttg_-(t)$				4.01	3.92
$HOttg_-g_-(t)$				7.98	8.06
$HOttx_-g_+(t)$				13.66	13.43
$HOttg_-x_+(t)$				14.16	13.88
$HOttttg_-$					4.15
$HOttg_-tg_-$					8.16
$HOttg_-tg_+$					8.61
$HOtttg_-g_-$					7.52
$HOtttx_-g_+$					14.67
$HOtttg_-x_+$					14.69

Level of theory: B3LYP/6-31+g*.
The conformer with lowest electronic energy is taken as reference.
Relative energies in kJ/mol without ZPE contributions.

Table 6.4: Relative energies of selected conformers of primary alcohols.

6.4.1 Alcohols

Since primary alcohols are n-alkanes in which a methyl top has been replaced by an OH group, similar conformations can be expected to occur, especially for rotations about bonds that are far from the hydroxy group. Table 6.4 displays the relative electronic energy of a selection of conformers in ethanol to hexanol, determined at the B3LYP/6-31+g* level of theory. The conformers are arranged according to the labelling convention for the five rotations ϕ_{l1} to ϕ_{l5}, even when the involved primary alcohol has less than 5 internal rotations. For instance, the notation $HOg_+g_-(ttt)$ refers to the HOg_+g_-ttt conformer in 1-hexanol, HOg_+g_-tt in 1-pentanol, HOg_+g_-t in 1-butanol, and the HOg_+g_- conformer in 1-propanol. No energy value for ethanol is given, since only the ϕ_{l1} rotation is available in this molecule.
Table 6.4 is divided into two parts. The first part treats conformers with one or more gauche standings in the $\phi_{l1}\phi_{l2}\phi_{l3}$ internal rotations, while the $\phi_{l4}\phi_{l5}$ dihedral angles remain in trans. The second part shows the conformers with one or more gauche conformations in the latter three $\phi_{l3}\phi_{l4}\phi_{l5}$ rotations, now with ϕ_{l1} and ϕ_{l2} in trans. It is clear that these latter conformers have geometries and relative energy differences that are in accordance with alkane fragments (see Ref.[19]). The relative energies of the $HOtttg(t)$ and $HOttttg$ conformers in 1-pentanol and 1-hexanol amount to almost 4 kJ/mol, which is about the typical 3.9 kJ/mol found in n-alkane conformers with one gauche standing (at the B3LYP/6-31+g* level of theory). Alcohol conformers with consecutive gauche standings of the same orientation in the $\phi_{l3}\phi_{l4}\phi_{l5}$ part of the molecule ($HOttg_-g_-(t)$ and $HOtttg_-g_-$) have an energy of about 8 kJ/mol, which is merely twice the energy value for the single gauche conformers. The energy of the $HOttg_-tg_-$ and $HOttg_-tg_+$ conformers is also in accordance with this summing rule. For a g_-g_+ sequence steric hindrance comes into play. As in n-alkanes, this g_-g_+ geometry actually corresponds to a transition state between two energy minima, each with one distorted gauche conformation: $g_-g_+ \rightarrow g_-x_+$ and x_-g_+. The energy of these conformers cannot be deduced by simply adding the energies of the conformers with only one gauche. The steric hindrance causes an energy rise, varying between 5.5 kJ/mol and 6.5 kJ/mol in excess of the earlier 8 kJ/mol. These additional energy values are close to the ab initio values in n-hexane [17].

The conformers with one or more gauche standings in the $\phi_{l1}\phi_{l2}\phi_{l3}$ part of the alcohol sequence seem to have a particular behavior, in contrast with the

alkane-like behavior of the $\phi_{l3}\phi_{l4}\phi_{l5}$ interactions. The all-trans conformer and the conformers with only one gauche for either ϕ_{l1} or ϕ_{l2} have approximately the same energy. For all alcohols the reference conformer is $HOg(tttt)$, except for ethanol, where the all-trans conformer has the lowest energy. A g_-g_- or g_+g_- sequence for the ϕ_{l1} and ϕ_{l2} rotations results in a slightly higher energy value, but this still remains below 1 kJ/mol. Apparently, the ϕ_{l3} rotation, and its interaction with the other internal rotations in the $HOCH_2CH_2CH_2-$ top, mainly determines the electronic energy. The $HOttg(tt)$ conformers have relative energies of 4.25 kJ/mol on average. These energies are not significantly altered by an additional gauche (g_+ or g_-) standing in ϕ_{l1}. Hence, the interaction of the ϕ_{l3} and ϕ_{l1} internal rotations can be considered negligible. A small stabilization is observed for the $HOtg_-g_-(tt)$ and $HOg_-g_-g_-(tt)$ conformers. This interaction between ϕ_{l2} and ϕ_{l3} becomes more apparent when these internal rotations assume gauche conformations of opposite orientation (g_-g_+). The relative energies become significantly higher than the $\phi_{l2}\phi_{l3} = g_-g_-$ conformers, due to the occurrence of a slightly distorted (x') or fully distorted (x) gauche conformation [Fig.6.3(a)]. However, in this part of the alcohols only one conformer is present around the g_-g_+ geometry, in contrast to the double minima typical for n-alkanes. Depending on the value of the ϕ_{l1} dihedral angle, their structures become: $HOtg_-x'_+(tt)$, $HOg_-g_-x'_+(tt)$, or $HOg_+x_-g_+(tt)$. The latter conformer has the most distorted geometry ($\phi_{l2} = x$) and also has the highest relative energy (about 9 kJ/mol). Still, this is significantly lower than the corresponding energy difference in n-alkanes.

The net result of these interactions is that the $HOCH_2CH_2CH_2$-top of primary alcohols does not obey the typical behavior of n-alkanes, as summarized by Tasi et al. [19]. At the B3LYP/6-31+g* level of theory, the first *fourteen* conformers in Table 6.4 are identified as specific for the $\phi_{l1} \rightarrow \phi_{l3}$ internal rotations. Hence, they must be considered as an extension of Tasi's rules for primary alcohols and an exact description of these alcohol conformers is required. However, the relative energies in Table 6.4 do not vary largely when increasing the chain length, as are the geometries of the different conformers practically not affected (Table 6.5). We may therefore conclude that the *fourteen* functional group conformers as given in Table 6.4 may serve as a suitable, valuable data set for the determination of all conformers in long primary alcohols.

		ϕ_{l1}	ϕ_{l2}	ϕ_{l3}
$HOg\_(tt)$:	*ethanol*	61.8		
	1-propanol	62.0	177.2	
	1-butanol	61.4	176.9	179.7
	1-pentanol	61.3	176.8	179.8
	1-hexanol	61.0	176.9	179.9
$HOtg\_(t)$:	*1-propanol*	-178.8	63.6	
	1-butanol	-179.2	64.0	180.0
	1-pentanol	-179.2	64.2	180.0
	1-hexanol	-179.2	64.5	-179.9
$HOg\_g\_(t)$:	*1-propanol*	65.0	61.3	
	1-butanol	65.1	61.8	-178.8
	1-pentanol	64.8	62.1	-178.7
	1-hexanol	65.1	62.2	-178.6
$HOg\_g_+(t)$:	*1-propanol*	67.3	-64.9	
	1-butanol	67.4	-65.8	-177.4
	1-pentanol	66.9	-65.8	-177.5
	1-hexanol	66.6	-65.9	-177.4
$HOttg\_$:	*1-butanol*	178.0	175.8	65.7
	1-pentanol	178.1	175.3	66.1
	1-hexanol	177.9	175.2	65.3
$HOg\_tg\_$:	*1-butanol*	62.2	174.3	66.9
	1-pentanol	62.4	173.8	67.4
	1-hexanol	62.3	173.9	66.8
HOg_tg_+ :	*1-butanol*	59.7	-179.8	-66.3
	1-pentanol	59.6	-179.4	-67.1
	1-hexanol	59.4	-179.4	-66.5
$HOtg\_g\_$:	*1-butanol*	-179.9	61.1	64.6
	1-pentanol	179.7	61.0	66.0
	1-hexanol	179.4	60.4	64.4
$HOtg\_x'_+$:	*1-butanol*	177.8	68.8	-75.5
	1-pentanol	177.8	68.7	-76.2
	1-hexanol	177.7	69.1	-76.2
$HOg\_g\_g\_$:	*1-butanol*	62.9	59.1	65.6
	1-pentanol	62.9	58.9	66.6
	1-hexanol	62.7	58.6	65.5
$HOg\_g\_x'_+$:	*1-butanol*	62.7	67.0	-72.7
	1-pentanol	62.6	67.1	-72.9
	1-hexanol	62.4	66.8	-73.6
$HOg\_x_+g\_$:	*1-butanol*	64.2	-81.3	63.2
	1-pentanol	64.1	-80.8	63.8
	1-hexanol	63.3	-81.6	62.8
$HOg_+g\_g\_$:	*1-butanol*	-66.2	64.3	64.2
	1-pentanol	-65.8	64.4	65.4
	1-hexanol	-65.9	63.8	64.1

Level of theory: B3LYP/6-31+g*.
ϕ_{l3} refers to the ethoxy group dihedral, ϕ_{l2} denotes the methoxy torsion, and ϕ_{l1} refers to the dihedral of the OH top geometry.

Table 6.5: Absolute dihedral angles in the different conformers of primary alcohols.

6.4.2 Thiols

A similar analysis has been done for ethane thiol to 1-hexane thiol. As in alcohols, the influence of the SH- end group only has a limited range. The conformers found by the three rotations in the $HSCH_2CH_2CH_2$-top ($\phi_{l_1}, \phi_{l_2}, \phi_{l_3}$) determine the specific functional group behavior of the thiol and are presented in Table 6.6 (with ϕ_{l_4} and ϕ_{l_5} both in trans). The conformers resulting from internal rotations further away from the hetero-element exhibit typical alkane-like behavior. The results for these rotations are supplied in Table 6.7 and are not further discussed.

$\phi_{l1}\phi_{l2}\phi_{l3}\phi_{l4}\phi_{l5}$	**ethane thiol**	**1-propane thiol**	**1-butane thiol**	**1-pentane thiol**	**1-hexane thiol**
$HSt(tttt)$	2.37	2.92	2.75	2.72	2.72
$HSg_-(tttt)$	0.00	0.00	0.00	0.00	0.00
$HStg_-(ttt)$		5.71	5.44	5.51	5.46
$HSg_-g_-(ttt)$		2.31	2.44	2.53	2.53
$HSg_+g_-(ttt)$		2.66	2.65	2.66	2.62
$HSttg_-(tt)$			6.60	6.78	6.77
$HSg_-tg_-(tt)$			4.07	4.22	4.22
$HSg_+tg_-(tt)$			3.66	3.87	3.84
$HStg_-g_-(tt)$			8.35	8.57	8.50
$HSg_-g_-g_-(tt)$			5.51	5.76	5.64
$HSg_+g_-g_-(tt)$			6.14	6.43	6.28
$HStx'_-x'_+(tt)$			15.17	15.28	15.25
$HSg_-x'_-x'_+(tt)$			14.22	X	X
$HSg_-g_-x_+(tt)$			14.16	13.96	13.96
$HSg_+g_-x_+(tt)$			15.48	14.97	15.11
$HSg_+x_-g_+(tt)$			15.33	15.14	15.10

Level of theory: B3LYP/6-31+g*.
Relative energies in kJ/mol without ZPE contributions.

Table 6.6: Relative energies of some conformers in primary thiols.

The most striking difference with alcohols is that the various thiol conformers are energetically more distinct from each other. The $HSg_-(tttt)$ conformer systematically has the lowest energy, and all other thiol conformers are at least

$\phi_{l1}\phi_{l2}\phi_{l3}\phi_{l4}\phi_{l5}$	**1-pentane thiol**	**1-hexane thiol**	**1-pentane thiol**	**1-hexane thiol**
	Reference: $HSg\_ttt(t)$		**Reference:** $HStttt(t)$	
$HStttg\_(t)$	6.58	6.56	**3.85**	**3.84**
$HSg\_ttg\_(t)$	**3.83**	**3.88**	1.11	1.16
$HSg_+ttg\_(t)$	**3.96**	**3.98**	1.24	1.25
$HSttg\_g\_(t)$	10.19	10.40	**7.47**	**7.68**
$HSg\_tg\_g\_(t)$	**7.97**	**8.11**	5.25	5.39
$HSg_+tg\_g\_(t)$	**7.42**	**7.55**	4.69	4.82
$HSttx\_g_+(t)$	16.67	16.53	**13.95**	**13.81**
$HSg\_tx\_g_+(t)$	**13.91**	**13.82**	11.18	11.10
$HSg_+tx\_g_+(t)$	**13.86**	**13.70**	11.14	10.98
$HSttg\_x_+(t)$	17.25	16.91	**14.52**	**14.19**
$HSg\_tg\_x_+(t)$	**14.74**	**14.44**	12.01	11.72
$HSg_+tg\_x_+(t)$	**14.47**	**14.11**	11.75	11.39
$HStttg\_$		6.67		**3.95**
$HSg\_ttg\_$		**3.96**		1.24
$HSg_+ttg\_$		**3.96**		1.24
$HStttg\_g\_$		10.23		**7.51**
$HSg\_ttg\_g\_$		**7.54**		4.81
$HSg_+ttg\_g\_$		**7.68**		4.96
$HStttx\_g_+$		17.18		**14.46**
$HSg\_ttx\_g_+$		**14.52**		11.80
$HSg_+ttx\_g_+$		**14.57**		11.85
$HStttg\_x_+$		17.47		**14.75**
$HSg\_ttg\_x_+$		**14.68**		11.95
$HSg_+ttg\_x_+$		**14.88**		12.16

Level of theory: B3LYP/6-31+g*.
The conformers $HSg\_ttt(t)$ (left) or $HStttt(t)$ (right) are taken as reference.
Relative energies in kJ/mol without ZPE contributions.

Table 6.7: Relative energies of selected alkane-like conformers of primary thiols.

Reference	<ΔE> Conformational class			Alkane	Reference
	HSg±**g**-ttt	HSg±t**g**-tt	HSg±tt**g**-t	gtt**g**-t	
HSg-tttt	2.55	3.98	3.85	3.94	gtttt
HStttt	2.75	3.99	3.84	3.96	ttttt
	HSt**g**-ttt	HStt**g**-tt	HSttt**g**-t	ttt**g**-t	
	HSg±**g**-**g**-tt	HSg±t**g**-**g**-t	HSg±tt**g**-**g**-	gtt**g**-**g**-	
HSg-tttt	5.96	7.83	7.61	7.80	gtttt
HStttt	5.74	7.68	7.51	7.82	ttttt
	HSt**g**-**g**-tt	HStt**g**-**g**-t	HSttt**g**-**g**-	ttt**g**-**g**-	
	HSg±**g**-**g**+tt	HSg±t**g**-**g**+t	HSg±tt**g**-**g**+	gtt**g**-**g**+	
HSg-tttt	14.74	14.02	14.66	14.66	gtttt
HStttt	12.50	14.00	14.61	14.65	ttttt
	HSt**g**-**g**+tt	HStt**g**-**g**+t	HSttt**g**-**g**+	ttt**g**-**g**+	

Level of theory: B3LYP/6-31+g*.
The energy differences $\langle \Delta E \rangle$ with respect to the displayed reference conformer, are average values over several thiols and over various gauche orientations in the same class.
Corresponding energy differences are also given for alkanes.

Table 6.8: Schematic of the different classes of conformers in thiols.

2 kJ/mol higher in energy. We have condensed all calculated data in Table 6.8, where relative energies are presented with reference to the HSg_tttt as well as the $HStttt$ conformer. Each $\langle \Delta E \rangle$ value represents an averaged energy difference over all thiol conformers corresponding to a specific conformational class. The shorthand notation **g** can refer to either a g, an x or an x' conformation. For example, the 14.74 kJ/mol energy difference of the $HSg_{\pm}\mathbf{g}\_\mathbf{g}_{+}tt$ conformational class with respect to the HSg_tttt reference is an average over the relative energies of the $HSg\_x'\_x'_{+}(tt)$, $HSg\_g\_x_{+}(tt)$, $HSg_{+}g\_x_{+}(tt)$ and $HSg_{+}x\_g_{+}(tt)$ conformers of 1-butane thiol, 1-pentane thiol and 1-hexane thiol. Several main characteristics and rules applicable to thiol conformers can be extracted from this table in a transparent way:

(i) The energy rise due to a single gauche standing in one of the torsions ϕ_{l_i} with $i > 1$ is almost independent of the conformation for ϕ_{l_1}. Only a small discrepancy of about 0.2 kJ/mol is noticed between the $HSt\mathbf{g}\_ttt$ (with respect to the $HStttt$ reference) and $HSg_{\pm}\mathbf{g}\_ttt$ conformational classes (with respect to the HSg_tttt reference). One easily concludes that the conformational interaction of ϕ_{l_1} with the other torsional motions is rather small.

(ii) In general, the above rule is also valid when multiple gauche standings are present in the conformer. The average relative energies for the $HSg_{\pm}\mathbf{g}_{-}\mathbf{g}_{-}tt$ and $HSt\mathbf{g}_{-}\mathbf{g}_{-}tt$ conformational classes, for example, differ by only some 0.2 kJ/mol. Moreover, the energy of the $HSg_{-}g_{-}g_{-}(tt)$ and $HSg_{+}g_{-}g_{-}(tt)$ conformers in Table 6.6 is virtually independent of a g_{-} or g_{+} conformation for ϕ_{l_1}. The only exception to this rule occurs for the $HSg_{\pm}\mathbf{g}_{-}\mathbf{g}_{+}tt$ conformational class, where notably higher average energy values are obtained in comparison with the $HSt\mathbf{g}_{-}\mathbf{g}_{+}tt$ class. Here, ϕ_{l_1} does interact with ϕ_{l_2} and influences the relative energy.

(iii) Sequences with two consecutive gauche standings of opposite orientation in positions ϕ_{l_i} and $\phi_{l_{i+1}}$ with $i > 1$, cause large interactions (up to 15 kJ/mol) and give rise to double minima around the $g_{-}g_{+}$ maximum. So, starting from ϕ_{l_2} and ϕ_{l_3}, consecutive internal rotations interact. However, only for 1-butane thiol this specific interaction results in four different conformations: $HSg_{-}x'_{-}x'_{+}(tt)$, $HSg_{-}g_{-}x_{+}(tt)$, $HSg_{+}g_{-}x_{+}(tt)$ and $HSg_{+}x_{-}g_{+}(tt)$ (Table 6.6). In 1-pentane thiol and 1-hexane thiol, the $HSg_{-}x'_{-}x'_{+}(tt)$ conformer does not occur.

(iv) The influence of the thiol functional group is virtually negligible from the ϕ_{l_4} torsion on. This is suggested in the table as the average energies seem to converge to those found in n-alkanes.

The $HSCH_2CH_2CH_2$-top in thiols also does not meet the typical behavior of n-alkanes. This is a similar result as in alcohols but here interaction effects between the internal rotations are more apparent, which gives rise to energetically distinct conformers. In all compounds, $fifteen$ conformers are identified that uniquely characterize the $\phi_{l1} \rightarrow \phi_{l3}$ internal rotations in the thiol functional group. In 1-butane thiol, one additional conformer is found ($HSg_{-}x'_{-}x'_{+}$).

6.4.3 Ethers

In this section the different conformers in a series of eight ethers are discussed: methyl ethyl ether (MEE), methyl propyl ether (MPE), methyl butyl ether (MBE), methyl pentyl ether (MPeE), di-ethyl ether (DEE), ethyl propyl ether (EPE), ethyl butyl ether (EBE) and di-propyl ether (DPE).
Whereas in alcohols or thiols it was possible to list all conformers and their calculated energies, this would present an inefficient approach to examine ethers (or sulfides). Their functional group is not an end-group and the influence of

the hetero element can extend to both sides of the molecule. As a result, a considerably larger number of conformers has to be studied. Ethyl butyl ether, for example, is characterized by four internal rotations and gives rise to at least $3^4 = 81$ conformers. A more functional approach is to subsequently examine conformers with one single, two consecutive and three consecutive gauche conformations, and to deduce some general rules which apply to all possible ether conformers.
Additionally, we will evaluate two approximation schemes on their ability to produce reasonable estimates of the relative energy of a conformer, based on minimal conformational data.

Conformers with a single gauche

A summary of the results for the conformers with a single gauche conformation in ethers is given in Table 6.9. The table lists the energy differences relative to the all-trans conformer of the molecules along with absolute dihedral angles. A gauche conformation for a dihedral angle alongside the oxygen (ϕ_{l1} or ϕ_{s1}) results in an energy increase of about 6.5 kJ/mol for ethyl tops, and about 6.3 kJ/mol for longer alkyl chains. This is quite in contrast to n-alkanes where a single gauche conformation causes an energy rise of about 3.9 kJ/mol at the B3LYP/6-31+g*(B1) level of theory[3]. Furthermore, the corresponding dihedral angles of normal gauche conformations about the $CC - OC$ dihedrals in ethers assume values in the range 75-77° [Figure 6.3(b)]. This is much larger than the typical 65° dihedral angle in n-alkanes and rather resembles the x'-gauche angle of a $CC - CC$ dihedral [Figure 6.3(a)]. A gauche standing in the next neighboring internal rotation alongside the oxygen (ϕ_{l2} or ϕ_{s2}), causes an almost as stable conformer as the all-trans conformer, with dihedral angles of 64°. Note that this applies for ethers as well as alcohols, where the ϕ_{l2} single gauche conformer has the same energy as the all-trans. Further away from the oxygen, the values seem to 'relax' to the n-alkane situation: angles of about 65° and relative energies of 4 kJ/mol for ϕ_{l3} and 3.8 kJ/mol for ϕ_{l4}.

In conclusion, the nearest (ϕ_{l1} and ϕ_{s1}) and next-nearest (ϕ_{l2} and ϕ_{s2}) internal rotations show a behavior which is distinctly different from n-alkanes. For rotations which are further distanced from the oxygen atom, the alkane-like behavior seems to be restored.

[3]At the B3LYP/6-311g**(B2) level of theory this is 3.6 kJ/mol [14].

Conformer	MEE	MPE	MBE	MPeE	DEE	EPE	EBE	DPE	
gtOtttt								0.22 *63.7*	V_{s2}^{1D} ϕ_{s2}
tgOtttt					6.60 *75.3*	6.42 *75.2*	6.53 *75.2*	6.24 *76.7*	V_{s1}^{1D} ϕ_{s1}
ttOgttt	6.48 *74.8*	6.33 *76.4*	6.28 *76.7*	6.25 *75.9*	6.60 *75.3*	6.30 *77.2*	6.39 *77.1*	6.24 *76.7*	V_{l1}^{1D} ϕ_{l1}
ttOtgtt		0.19 *63.6*	-0.07 *64.1*	0.01 *64.4*		0.24 *63.8*	0.02 *64.3*	0.22 *63.7*	V_{l2}^{1D} ϕ_{l2}
ttOttgt			3.99 *66.0*	4.02 *65.8*			4.03 *66.1*		V_{l3}^{1D} ϕ_{l3}
ttOtttg				3.83 *65.2*					V_{l4}^{1D} ϕ_{l4}
Conformer	**MES**	**MPS**	**MBS**	**MPeS**	**DES**	**EPS**	**EBS**	**DPS**	
gtStttt								2.75 *66.2*	V_{s2}^{1D} ϕ_{s2}
tgStttt					0.69 *72.3*	0.62 *72.6*	0.63 *72.8*	0.02 *73.1*	V_{s1}^{1D} ϕ_{s1}
ttSgttt	0.57 *70.0*	0.08 *72.5*	0.20 *71.4*	0.16 *71.7*	0.69 *72.3*	0.17 *74.1*	0.27 *73.2*	0.02 *73.1*	V_{l1}^{1D} ϕ_{l1}
ttStgtt		2.83 *65.9*	2.70 *66.5*	2.66 *66.1*		2.80 *65.7*	2.64 *65.8*	2.75 *66.2*	V_{l2}^{1D} ϕ_{l2}
ttSttgt			3.80 *65.4*	3.91 *65.9*			3.79 *65.3*		V_{l3}^{1D} ϕ_{l3}
ttStttg				3.80 *65.5*					V_{l4}^{1D} ϕ_{l4}

Level of theory: B3LYP/6-31+g*.
Relative energies in kJ/mol, and absolute dihedral angle values in degree.
Reference is the all-*trans* conformer.

Table 6.9: Conformers of various ethers and sulfides with a single gauche.

Two consecutive gauche standings

All possible ether conformers with two consecutive gauche orientations are listed in Table 6.10. For each conformer, the energy (V_{AB}^{2D}) is given relative to the all-trans conformer. In addition the two corresponding dihedral angles (ϕ_A and ϕ_B) are given. In the supposition of non-interacting internal rotations, it would be possible to make a rough guess of these relative energies and dihedral angles using the data of single gauche conformers (Table 6.9). This energy estimate corresponding to two consecutive gauche standings would then be:

$$\Delta E_{AB}^{1D-est} = V_A^{1D}(\phi_A = g_A^{1D}) + V_B^{1D}(\phi_B = g_B^{1D}) \tag{6.1}$$

with V_A^{1D} the relative energy obtained in a one-dimensional approach corresponding to a gauche orientation in torsional angle ϕ_A. g_A^{1D} refers to the gauche angle in the single gauche conformer and this dihedral generally differs

from the corresponding angle in the conformer with two consecutive gauche orientations. In Table 6.10 the difference between both angles ($\Delta\phi_A$) is presented along with the one-dimensional energy guess (ΔE_{AB}^{1D-est}). However, it is clear from the previous discussions, that the interaction between consecutive internal rotations is not negligible. This was thoroughly confirmed on n-alkanes in Refs.[19, 17]. Still, it is valuable to discuss double gauche conformers in terms of their differences with a one-dimensional approach.

(ϕ_A, ϕ_B)	conformer	molecule	V_{AB}^{2D}	ϕ_A	ϕ_B	ΔE_{AB}^{1D-est}	$\Delta\phi_A$	$\Delta\phi_B$
(ϕ_{s1}, ϕ_{l1})	$x\_Ox\_$	DEE	12,70	86,0	86,0	13,20	10,7	10,7
		EPE	12,20	86,6	88,3	12,72	11,4	11,1
		EBE	12,24	86,6	87,4	12,92	11,4	10,3
		DPE	11,69	88,3	88,2	12,48	11,6	11,5
	x_Ox_+	DEE	16,21	91,8	-91,8	13,20	16,5	16,5
		EPE	15,67	91,9	-92,3	12,72	16,7	15,1
		EBE	N/A	N/A	N/A	12,92	N/A	N/A
		DPE	N/A	N/A	N/A	12,48	N/A	N/A
(ϕ_{l1}, ϕ_{l2})	$Og\_g\_$	MPE	6,70	75,3	59,1	6,52	-1,1	-4,5
		MBE	6,57	75,7	60,1	6,21	-1,0	-4,0
		MPeE	6,52	75,8	60,2	6,25	-0,1	-4,2
		EPE	6,90	75,2	59,3	6,54	-2,0	-4,5
		EBE	6,58	76,3	60,5	6,41	-0,8	-3,8
		DPE	6,75	74,9	58,7	6,46	-1,8	-5,0
(ϕ_{l2}, ϕ_{l3})	$Otg\_g\_$	MBE	3,37	61,5	65,2	3,92	-2,6	-0,8
		MPeE	3,56	61,5	65,6	4,02	-2,9	-0,2
		EBE	3,37	61,5	64,6	4,04	-2,8	-1,5
	$Otg\_x'_+$	MBE	6,93	69,8	-74,8	3,92	5,7	8,8
		MPeE	6,82	69,6	-75,3	4,02	5,2	9,5
		EBE	7,19	69,9	-75,8	4,04	5,6	9,7
(ϕ_{l3}, ϕ_{l4})	$Ottg\_g\_$	MPeE	7,74	64,0	61,8	7,85	-1,8	-3,4
	$Ottg\_x_+$	MPeE	13,81	65,7	-87,3	7,85	0,1	22,1
	$Ottx\_g_+$	MPeE	13,52	97,4	-63,7	7,85	31,6	-1,5
(ϕ_{s1}, ϕ_{l1})	g_Sg_tt	EBS	0,96	72,4	73,0	0,91	-0,4	-0,2
	g_Sx_+tt		3,94	73,3	-97,3	0,91	0,5	24,1
	x_Sg_+tt		4,03	96,1	-74,4	0,91	23,3	1,2
(ϕ_{l1}, ϕ_{l2})	tSg_g_t	EBS	2,21	76,3	67,1	2,91	3,1	1,3
	tSx_g_+t		5,37	97,1	-66,2	2,91	23,9	0,4
(ϕ_{l2}, ϕ_{l3})	$tStg\_g\_$	EBS	5,58	62,5	60,7	6,42	-3,3	-4,6
	$tStx'\_x'_+$		12,02	75,7	-76,4	6,42	9,9	11,1

Level of theory: B3LYP/6-31+g*.
Relative energies are given in kJ/mol, and absolute dihedral angles in degrees.
Reference is the all-*trans* conformer.
N/A means that the conformer is not present.
ΔE_{AB}^{1D-est} is defined according to Eq.(6.1).

Table 6.10: Conformers of various ethers and of EBS with two consecutive gauche standings.

When the gauche standings take place at either side of the oxygen (gOg), $\Delta\phi$ angles can amount to 10° or even more. This is mainly due to the strong

interaction existing between the ϕ_{s1} and ϕ_{l1} torsions, manifesting in strongly distorted gauche positions ($\phi \approx 90°$). Those gauche positions with opposite orientation (x_-Ox_+) show very shallow minima and give no evidence for a double minimum. They are only detected in the smaller ethers DEE and EPE at the B3LYP/B1 level of theory. At the B3LYP/B2 level, this minimum is even only observed in DEE. In addition, their relative energies are underestimated by some 3 kJ/mol in the one-dimensional approximation. The minima corresponding with equal orientation (x_-Ox_-) are more pronounced and occur in all investigated ethers. The relative energies are well described within the 1D-approach, but evidently the gauche dihedral angles deviate substantially.

Conformers with two consecutive gauche standings alongside the oxygen (Ogg) occur only when both ϕ_{l1} and ϕ_{l2} assume equivalent gauche orientations. Their properties are rather well predicted in the 1D-approximation: ΔE_{AB}^{1D-est} closely resembles V_{AB}^{2D} and $\Delta\phi_{A,B}$ values are small.

When moving the two consecutive gauche standings one torsion further ($Otgg$), the typical n-alkane like pattern already begins to manifest. The Otg_-g_- conformers reveal dihedral angles that are very close to the typical undisturbed 65°. But, as in the preceding case, two consecutive gauche standings with opposite orientation do not yet give rise to the double conformational minimum. Instead, only one $Otg_-x'_+$ conformer is found with a slightly distorted ϕ_{l3} gauche angle. A similar effect was observed in alcohols (*e.g.* the $HOtg_-x'_+(tt)$ type conformer in Table 6.4).

Finally, when the consecutive gauche conformations are further away from the oxygen (*e.g.* $\phi_{l3}\phi_{l4}$ in MPeE), the same behavior is revealed as in n-alkanes with the double $Ottg_-x_+$ and $Ottx_-g_+$ minima around the $Ottg_-g_+$ maximum.

Three consecutive gauche standings

The number of ether conformers with three consecutive gauche conformations is rather limited (Table 6.11) as the restrictions on two consecutive gauches also seem to apply for three successive gauche standings. The g_-g_+ conformation never appears for the $\phi_{s1}\phi_{l1}$ and $\phi_{l1}\phi_{l2}$ dihedral angles. This implies that only the $x_-Ox_-g_-$ conformer is formed in the class $\phi_{s1}\phi_{l1}\phi_{l_2}$ and $Og_-g_-g_-$ and $Og_-g_-x'_+$ in the class $\phi_{l1}\phi_{l2}\phi_{l3}$.

(ϕ_A, ϕ_B, ϕ_C)	conformer	molecule	V^{3D}_{ABC}	ϕ_A	ϕ_B	ϕ_C	ΔE^{1D-est}_{ABC}	ΔE^{2D-est}_{ABC}
$(\phi_{s1}, \phi_{l1}, \phi_{l2})$	$x\_Ox\_g\_$	EPE	12,83	86,4	87,7	61,7	12,96	12,80
		EBE	12,53	86,4	87,6	62,3	12,94	12,44
		DPE	12,32	88,0	87,4	61,5	12,70	12,20
$(\phi_{l1}, \phi_{l2}, \phi_{l3})$	$Og\_g\_g\_$	MBE	9,82	73,8	56,2	64,3	10,20	10,01
		MPeE	9,84	73,2	56,1	65,2	10,27	10,07
		EBE	9,87	74,9	56,6	63,9	10,43	9,94
	$Og\_g\_x'_+$	MBE	13,18	76,9	66,9	-74,0	10,20	13,57
		MPeE	12,90	76,2	66,1	-75,3	10,27	13,33
		EBE	13,37	77,8	68,1	-72,5	10,43	13,76
$(\phi_{l2}, \phi_{l3}, \phi_{l4})$	$Otg\_g\_g\_$	MPeE	7,31	60,7	63,3	63,1	7,85	7,28
	$Otx'_+g\_g\_$		10,14	73,5	-68,9	-62,9	7,85	10,54
	$Otx'_-g_+x\_$		17,53	78,8	-67,4	88,8	7,85	16,61
	$Otg\_x\_g_+$		14,17	65,3	93,6	-65,1	7,85	13,06
	$Otg\_g\_x_+$		14,49	59,7	62,9	-92,5	7,85	13,35
$(\phi_{s1}, \phi_{l1}, \phi_{l2})$	$g\_Sg\_g\_t$	EBS	2,89	73,3	75,2	66,3	3,58	2,77
	$g_+Sx\_g\_t$		5,40	-70,2	101,5	66,6	3,58	5,88
	$g\_Sx\_g_+t$		6,03	75,6	100,1	-67,1	3,58	6,06
$(\phi_{l1}, \phi_{l2}, \phi_{l3})$	$tSg\_g\_g\_$	EBS	5,57	72,9	62,4	63,9	6,70	5,15
	$tSx_+g\_g\_$		9,91	-98,7	66,8	66,3	6,70	8,31
	$tSx\_g_+x\_$		17,94	95,9	-68,4	90,5	6,70	14,75
	$tSg\_x\_g_+$		13,42	79,4	86,6	-67,4	6,70	11,59
	$tSg\_g\_x_+$		13,66	70,7	66,7	-88,8	6,70	11,59

Level of theory: B3LYP/6-31+g*.
Relative energies are given in kJ/mol, and absolute dihedral angles in degrees.
Reference is the all-*trans* conformer.

Table 6.11: Conformers of various ethers and of EBS with three consecutive gauche standings.

The influence of the oxygen on the conformers with three consecutive gauche standings decreases when they occur at large distances from the oxygen (*e.g.* in the dihedral angles $\phi_{l2}\phi_{l3}\phi_{l4}$). An n-alkane like behavior makes its appearance in a more pronounced way. According to the Tasi rules [19] one could expect six conformers: $g\_g\_g\_$, $x_+g\_g\_$, $g_+x\_g\_$, $x\_g_+x\_$, $g\_x\_g_+$ and $g\_g\_x_+$. However, this pattern is not entirely found according to the constraints reported in previous paragraph restricting the first two rotations ($\phi_{l2}\phi_{l3}$) to reside in $g\_g\_/g_+g_+$ or $x'_+g\_/x'\_g_+$ double gauche conformations. This additional constraint reduces the total number of conformations of this class to five, as given in Table 6.11.

These findings enable us to propose an adjusted version of Tasi's rules which can be applied on ethers. Starting from the original rules suitable for n-alkanes, one can impose some additional constraints in the sense that *when a particular double gauche sequence is not allowed in a conformer, it remains excluded in the structure of all other conformers with multiple gauche conformations.* To illustrate with an example: from Table 6.10 it follows that some g_g_+ se-

quences are not occurring. In the formation of conformers with three or more gauche standings we can a priori eliminate all combinations having this particular g_g_+ sequence.

Since the occurrence of a triple gauche conformer is mainly determined by the rules governing two consecutive gauche conformations, it is reasonable to assume that its energy could be better approximated by including energy effects of all gg conformations. In this two-dimensional approach, the relative energy is estimated as:

$$\begin{aligned} \Delta E_{ABC}^{2D-est} &= V_{AB}^{2D}(\phi_A = g_A^{2D}, \phi_B = g_B^{2D}) + V_{BC}^{2D}(\phi_B = g_B^{2D}, \phi_C = g_C^{2D}) \\ &\quad -V_B^{1D}(\phi_B = g_B^{1D}) \end{aligned} \tag{6.2}$$

which is merely an extrapolation of Eq.(6.1). This estimate is also given in Table 6.11 compared to the one-dimensional guess ΔE_{ABC}^{1D-est}. The calculated energy V_{ABC}^{3D} is given relative to the all-trans conformer.
The energies of the triple gauche conformers show large variations, and they are not reproduced correctly by the one-dimensional scheme. Whenever a g_+ or x_+ conformation occurs, discrepancies are even enormous. The two-dimensional approach, on the other hand, is quite accurate. The difference between the exact and the 2D prediction only exceeds 1 kJ/mol for the $Otg\_x\_g_+$ and $Otg\_g\_x_+$ conformers of MPeE. For all other conformers, the discrepancy is limited to 0.5 kJ/mol. The adequacy of the 2D approximation to describe fully coupled 3D features in n-alkanes has already been reported in Ref.[17]. Energy estimates based on a one-dimensional scheme (ΔE^{1D-est}) are manifestly inadequate.

Summarizing, we have found a set of rules to deduce all conformers in ethers. These are based on the possible occurrence of double gauche sequences in these compounds. Starting from the general n-alkane rules of Tasi et al. [19], several conformers can be eliminated on the basis of these gg-combinations. In addition, a two-dimensional scheme has been proposed which is adequate to describe all possible conformers and their relative energies solely based on information of conformers with single and double gauche standings.

6.4.4 Sulfides

In view of the evident similarity between the two types of molecules, all sulfides are discussed in comparison with the ether properties. More specifically,

methyl ethyl sulfide (MES), methyl propyl sulfide (MPS), methyl butyl sulfide (MBS), methyl pentyl sulfide (MPeS), di-ethyl sulfide (DES), ethyl propyl sulfide (EPS), ethyl butyl sulfide (EBS) and di-propyl sulfide (DPS) are considered.

The analogy between the conformers with a single gauche of both systems can be examined in Table 6.9. The energies of sulfide conformers with one gauche in either ϕ_{l1} or ϕ_{s1} is very close to the all-trans reference energy. In this aspect sulfides clearly differ from ethers, in which the ϕ_{l2} or ϕ_{s2} single gauche conformers closely match the all-trans energy. The ϕ_{l2} rotations in sulfides show the opposite behavior: the energy differences amount to 2.7 kJ/mol, with dihedral angles of 66°. A complete accordance between ethers and sulfides is only found for the ϕ_{l3} and ϕ_{l4} gauche conformers, for which the energies and dihedral angles are actually converged to typical alkane values.

The discussion of conformers with two gauche dihedrals is limited to EBS (Table 6.10), since the other sulfides yield similar results. Some striking differences with ethers are observed. It appears that several sequences of gauche standings with opposite orientation are not forbidden. For the (ϕ_{s1}, ϕ_{l1}) interaction, there is even a doubling of conformers (x_-Sg_+tt and g_-Sx_+tt). This is analogous with the alkane situation, but here the dihedrals are substantially more distorted with angles up to 97°. These conformers have an additional energy of 3 kJ/mol as compared to the g_-Sg_-tt conformer.
There is only one conformer with opposite gauche orientations for the (ϕ_{l1},ϕ_{l2}) and (ϕ_{l2},ϕ_{l3}) interactions: tSx_-g_+t and $tStx'_-x'_+$ respectively. As from the (ϕ_{l3},ϕ_{l4}) interaction, the conformers have full alkane-like features.
The one-dimensional energy estimates ΔE_{AB}^{1D-est} are only adequate for conformers with two consecutive gauche standings of equal orientation. In contrast, the ΔE_{AB}^{1D-est} values considerably underestimate the energy of the conformers with opposite gauche orientations, up to 6 kJ/mol for $tStx'_-x'_+$. This partial success and partial failure is also observed for ethers, alcohols and thiols, and for n-alkanes [17].
An overview of the relative energies of the double gauche sulfide conformers is given in Table 6.12.

For the study of three consecutive gauche standings (Table 6.11, and Table 6.13) we also restrict the discussion to EBS. The number of conformers is definitely higher than in ethers, but still less than predicted by Tasi's alkane

conformer	MPS	MBS	MPeS	DES	EPS	EBS	DPS
g_-g_-Stt							1.98
g_-x_+Stt							5.49
$(t)g_-Sg_-(tt)$				1.14	0.88	0.96	0.28
$(t)g_-Sx_+(tt)$				4.47	3.95	3.94	3.17
$(t)x_-Sg_+(tt)$				4.47	4.08	4.03	3.17
$(tt)Sg_-g_-(tt)$	1.98	2.18	2.15		2.06	2.21	1.98
$(tt)Sx_-g_+(tt)$	5.94	6.00	5.98		5.56	5.37	5.49
$(t)Stg_-g_-(t)$		5.60	5.74			5.58	
$(t)Stx'_-x'_+(t)$		11.99	11.90			12.02	
$Sttg_-g_-$			7.35				
$Sttg_-x_+$			14.40				
$Sttx_-g_+$			14.00				

Level of theory: B3LYP/6-31+g*.
Relative energies in kJ/mol, with the all-*trans* conformer as reference.

Table 6.12: Relative energies of the double gauche conformers of sulfides.

rules. Furthermore, it is not possible to predict the occurrence of triple gauche conformers based on the double gauche conformers. This also applies for the (ϕ_{l2},ϕ_{l3},ϕ_{l4}) conformers of MPeS (Table 6.13).
Confronting the relative energies for these conformers with the predictions obtained in the 1D and 2D approaches, it is confirmed that the ΔE_{AB}^{1D-est} energies do not describe the correct features. The ΔE_{ABC}^{2D-est} values on the other hand are very satisfactory, describing both stabilization effects ($g_-g_-g_-$) and additional energies for conformers with g_-g_+ sequences.

conformer	**MBS**	**MPeS**	**EPS**	**EBS**	**DPS**
$g_-g_-Sg_-t$					2.20
$g_+x_-Sg_-t$					5.39
$g_-g_-Sx_+t$					5.30
$g_-x_-Sg_+t$					4.68
$(t)g_-Sg_-g_-(t)$			2.86	2.89	2.20
$(t)g_+Sx_-g_-(t)$			5.57	5.40	4.68
$tx_+Sg_-g_-$			X	X	5.30
$(t)g_-Sx_-g_+(t)$			6.13	6.03	5.39
$(t)Sg_-g_-g_-(t)$	5.52	5.69		5.57	
$(t)Sx_+g_-g_-(t)$	10.39	10.61		9.91	
$(t)Sx_-g_+g_-(t)$	18.27	18.01		17.94	
$(t)Sg_-g_-x_+(t)$	13.41	12.95		13.66	
$(t)Sg_-x_-g_+(t)$	13.48	13.19		13.42	
$Stg_-g_-g_-$		9.60			
$Stx'_+x'_-g_-$		15.75			
$Stx_-g_+x_-$		24.10			
$Stg_-g_-x_+$		17.66			
$Stg_-x_-g_+$		17.01			
$Stg_-x'_-x'_+$		17.85			

Level of theory: B3LYP/6-31+g*.
Relative energies in kJ/mol, with the all-*trans* conformer as reference.

Table 6.13: Relative energies of the triple gauche conformers of sulfides.

6.5 Overview of conformational rules

The revised Tasi rules (up to triple gauche) for ethers and sulfides are presented in Table 6.14. It is obvious that the region exposed to the specific influence of the hetero element is $\phi_{s2} \rightarrow \phi_{l2}$. In other words, all double or triple consecutive gauche conformers involving one of these internal rotations do not obey Tasi's alkane rule.

Double gauche conformers:				
	$\phi_{s1}\phi_{l1}$	$\phi_{l1}\phi_{l2}$	$\phi_{l2}\phi_{l3}$	$\phi_{l3}\phi_{l4}$
Tasi	**Ethers:**			
$g\_g\_$	$x\_Ox\_$	$Og\_g\_$	$Otg\_g\_$	$Ottg\_g\_$
g_x_+	(x_Ox_+)		$Otg\_x'_+$	$Ottg\_x_+$
x_g_+				$Ottx\_g_+$
Tasi	**Sulfides:**			
$g\_g\_$	$g\_Sg\_$	$Sg\_g\_$	$Stg\_g\_$	$Sttg\_g\_$
g_x_+	g_Sx_+		$Stx'\_x'_+$	$Sttg\_x_+$
x_g_+	x_Sg_+	Sx_g_+		$Sttx\_g_+$
Triple gauche conformers:				
	$\phi_{s1}\phi_{l1}\phi_{l2}$	$\phi_{l1}\phi_{l2}\phi_{l3}$	$\phi_{l2}\phi_{l3}\phi_{l4}$	
Tasi	**Ethers:**			
$g\_g\_g\_$	$x\_Ox\_g\_$	$Og\_g\_g\_$	$Otg\_g\_g\_$	
$g_+x\_g\_$				
$x_+g\_g\_$			$Otx'_+g\_g\_$	
$x\_g_+x\_$			$Otx'\_g_+x\_$	
$g\_g\_x_+$		$Og\_g\_x'_+$	$Otg\_g\_x_+$	
$g\_x\_g_+$			$Otg\_x\_g_+$	
Tasi	**Sulfides:**			
$g\_g\_g\_$	$g\_Sg\_g\_$	$Sg\_g\_g\_$	$Stg\_g\_g\_$	
$g_+x\_g\_$	$g_+Sx\_g\_$		$Stx'_+x'\_g\_$	
$x_+g\_g\_$	$(x_+Sg\_g\_)$	$Sx_+g\_g\_$		
$x\_g_+x\_$		$Sx\_g_+g\_$	$Stx\_g_+x\_$	
$g\_g\_x_+$		$Sg\_g\_x_+$	$Stg\_g\_x_+$	
$g\_x\_g_+$	$g\_Sx\_g_+$	$Sg\_x\_g_+$	$Stg\_x\_g_+$	
			$Stg\_x'\_x'_+$	

The conformers given between brackets occur for the smallest molecules only, and are of no importance for the general behavior of (longer) ethers/sulfides.

Table 6.14: Overview of alterations of Tasi's rule for alkane conformers in ethers and sulfides.

The specific conformers of primary alcohols and thiols not obeying Tasi's law are already presented in Tables 6.4 and 6.6.

6.6 Summary

In this work we performed a conformational analysis of alcohols, thiols, ethers and sulfides. Our main goal was to modify the general rules for the occurrence of conformers in n-alkanes deduced by Tasi et al. [19] for these systems. Essentially, this was accomplished by identifying that part of the molecule not obeying Tasi's law, and by analyzing all possible conformers in this part of the molecule.

For alcohols and thiols, it was found that the $HXCH_2CH_2CH_2$-top ($X = O, S$) is the distinct part from n-alkanes, while for ethers and sulfides, third order rotations from the hetero element ($\phi_{s3} \rightarrow \phi_{l3}$) have to be taken into consideration to sufficiently account for the effects of the oxygen or sulfur. The conformational structure and pattern of the hetero region differ in the four types of molecules.
The identification of this region of hetero influence ($\phi_{s3} \rightarrow \phi_{l3}$) enables us to make some assumptions for carbon chains with multiple hetero elements. It is clear that when these hetero atoms are separated by less than six bonds, both regions of influence are likely to interact and change the relative energy and geometry of the conformations in this area. When the hetero elements are separated by at least six bonds, a reduced mutual influence can be expected, although other intramolecular effects (*e.g.* hydrogen bonding, anomeric resonance) cannot be excluded. This will no doubt affect the predicted conformations.
Only thiols exhibit a distinct global minimum ($HSg(tttt)$). All other conformers are at least 2 kJ/mol less bound. For the three other types of molecules, no strict rules can be proposed for the ground-state configuration. Many conformers are competing within an energy interval of 1 kJ/mol. An accurate description of molecular properties –even at low temperature– requires a complete knowledge of all existing conformers. It is thus important to use a model that generates all low energy conformers.

While for primary alcohols and thiols it is possible to reproduce all conformers specific to the functional group (fourteen and fifteen respectively), this becomes more cumbersome for ethers and sulfides, because the hetero element now affects two alkyl side chains. For this reason we have focussed on conformers with up to three consecutive gauche standings, and we have introduced rules that allow the successful determination of all conformers in the func-

tional group region. Moreover, an exact calculation of conformers with two consecutive gauches, in addition to single gauche conformers permit a reliable prediction of their relative energies. This reduces the calculation time considerably as only a fraction of the total number of conformers has to be determined explicitly. Furthermore, conformers with more than two gauche standings are considerably higher in electronic energy than single or double gauche structures. As a result, they are of lesser importance.

Generally, the contribution of each conformer to thermodynamic properties (*e.g.* enthalpies of formation) is proportional to the Boltzman factor $e^{-\beta\Delta E}$, with ΔE the energy difference with the reference conformer [110][111]. Using the energy scheme introduced in this work, one is able to determine the importance of every conformer (at a given temperature) without the need of explicit calculations.

The presented rules may thus serve as a fast method to select those conformers with associated energies below a given energy threshold, and therefore with a significant contribution to the desired property.

Chapter 7

Ab initio calculation of entropy and heat capacity of ethers, alcohols, sulfides and thiols

This chapter is an extended version of Ref.[20]:

Vansteenkiste, P.; Verstraelen, T.; Van Speybroeck, V. and Waroquier, M.
Chem. Phys. **2006**, submitted

Abstract

In this chapter the performance of two ab initio hindered rotor approaches, based on either one-dimensional (1D-HR) or two-dimensional (2D-HR) potential energy profiles, is evaluated for n-alkanes with hetero elements O and S. The internal rotations in these molecules have a behavior distinct from those in n-alkanes, for which such a study was already presented in two recent papers by the authors [16, 17]. The partition functions corrected for internal rotors are validated to their accuracy by computation of thermodynamic quantities like entropy and heat capacity. For all these hetero alkanes it turns out that the simplest approach, which is also the most cost effective method, gives the best experimental agreement. This work is a confirmation of the results for n-alkanes, suggesting that this easily implemented 1D-HR approach is the appropriate model to describe the thermodynamic features of all single chain molecules.

7.1 Introduction

The microscopic evaluation of thermodynamic properties of stable species and kinetic data for chemical reactions has now found widespread use in physical chemistry. For molecules containing various single bonds, the one-dimensional hindered rotor (1D-HR) treatment has become an essential tool for the ab-initio evaluation of chemical properties. Various works in literature have shown that the standard Harmonic Oscillator approach (HO) is largely inadequate for the treatment of large amplitude vibrations and a correct description of microscopic partition functions and deduced thermochemical and kinetic quantities. There are different ways to implement the HR concept:

(i) the simplest corrections can be obtained from the tabulated values proposed by Pitzer in the early days [26, 15, 27, 28, 29, 30],

(ii) later interpolating formulae between harmonic oscillator (HO) and free rotor (FR) treatments were proposed by Truhlar and co-workers [58] and more recently,

(iii) 'full' ab-initio treatments are proposed by various groups [5, 112, 60, 113, 114, 61, 62, 115, 116, 117, 63, 2, 14] in which one-dimensional ab-initio calculated potentials are used and moments of inertia are calculated from the optimized geometries.

Even within these full treatments there are many approaches on how to construct the one-dimensional potential, and the (reduced) moments of inertia. In a previous paper of the authors [14] it was found that a simple one-dimensional model (1D-HR) was able to reproduce the thermodynamic features –more specifically, third law entropy and heat capacity– of n-alkanes quite well (within the level of theory B3LYP/6-311g**).
Although the reproduction of thermodynamic features within these 1D-HR treatments is found very satisfying, more extended theoretical approximations need to be investigated, especially in molecules where internal motions are strongly coupled with each other. Various groups made efforts to extend the HR model with construction of two-dimensional potential energy surfaces, and with the associated kinetic energy also given in a two-dimensional form [112, 60, 113, 114, 61, 62, 115, 116, 117]. However, a full ab initio approach is missing, and relaxation of the atomic nuclei in the evaluation of the torsional potentials is not taken into account. The practical usage of such scheme for a general polyatomic molecule with several attached asymmetric tops has been

rather limited up to now. Some work in this field has been done by Smeyers and co-workers [65, 66, 67, 119, 120, 121, 118, 68, 122, 102, 123] with the aim to determine far infrared spectra from ab initio calculations. Most of the studied molecules (acetone, propanal, ethanol, dimethylamine) have two branched side groups that are rotating. The potential energy surface was determined by calculating some specific points on the multidimensional potential. The other points of the 2D-surface are constricted by means of a double Fourier expansion in terms of the torsional angles.

Recently, a two-dimensional scheme (in both potential and kinetic energy: 2D-HR) based on the work of Pitzer [26, 15, 27, 28, 29, 30] has been developed and numerically elaborated by the authors [16]. In that work both 1D-HR and 2D-HR schemes turned out to reproduce in an adequate way thermodynamic quantities in n-alkanes. In the exact scheme subsequent internal rotations are described without any restriction on the symmetry and with full kinetic coupling of the global and internal rotations of the molecule (Coriolis coupling). Theoretical grounds that lie on the basis of success of the simplest approximation (1D-HR) as proposed in [14] have been traced back for the case of n-alkanes: the errors introduced by using one-dimensional rotational potentials are compensated by the use of constant reduced moments of inertia [16]. The conclusions made on n-alkanes may not a priori be extended to other single chain molecules. The principal aim of this study is to extend the previous calculations on n-alkanes to compounds as ethers/alcohols and sulfides/thiols where a CH_2 fragment is substituted by the hetero-elements O and S. Sufficient experimental data are available to validate the various approximative schemes to handle internal rotors. As already suggested by East and Radom [5] it is not excluded that the standard procedure coinciding with 1D-HR does no longer achieve the desired accuracy for some of these molecules.

The resulting compounds (ethers/alcohols and sulfides/thiols) are, like n-alkanes, also linear chain molecules but their energetically most stable structure (reference conformer) is not a priori an all-trans conformation. This makes them from conceptual point of view ideal candidates for a validation of the method.

In the literature, a large spectrum of theoretical studies on some small molecules of the hetero alkanes is found: ab initio studies concerning a variety of properties and reactions, and concerning CH –or in alcohols OH– overtone

spectra; for example Ref.[124]. The investigations of the vibrational levels in ethanol, dimethyl ether (DME) and dimethyl sulfide (DMS) Senent and Smeyers [119, 120, 121, 102, 123] are very relevant for the work in this chapter as they reported potential energy surfaces of internal rotations, and because they also used variable moments of inertia similar to our more elaborated models of hindered rotation.
Most articles covering ab initio calculated thermodynamic properties focus on the enthalpy of formation [110, 111], but to our knowledge only few studies are available reporting results on entropies and/or heat capacities in ethers/alcohols [125, 106, 126].

An accurate reproduction of the global partition function from which all thermodynamic properties may be derived, requires an adequate description of all possible conformations. A thorough conformational analysis of the selected compounds was recently made by the authors [18] and this chapter will rely on the results made in that study.

The structure of the article is as follows: in the first section we summarize the construction of the partition function (and derived thermodynamic quantities) in the 1D-HR and 2D-HR schemes. In the next sections the role of internal rotations is investigated, emphasizing the similarities and differences between ethers/alcohols and sulfides/thiols and also focussing on relaxation effects. We compare these data with the previously investigated n-alkanes [14, 16, 17] The final section reports on the calculated entropies and heat capacities.

7.2 Methodology and computational details

In a previous paper [18] extended rules were reported to predict the number and occurrence of conformers in oxygen or sulfur containing compounds: alcohols, thiols, ethers and sulfides. It was established that B3LYP/6-31+g* (B1) is the most appropriate and most cost-effective level of theory for this kind of calculations on these series of molecules. The small basis 6-31+g* has the advantage over 6-311g** that it includes a diffuse function while the latter basis contains polarization functions. The two levels of theory B1 and B2 do not generate the same conformational behavior: slight changes in energy barriers and energy minima occur, but they are sufficient to assign different global minima. As we will apply the hindered rotor model in this study the potential energy profiles - in particular in 1D-HR - depend on the nature of the reference conformer, which may differ in both basissets. Therefore we found it instructive to consider both basissets in order to investigate the effect of a deviating conformational surface to the partition functions.

The 1D-HR requires one-dimensional energy profiles (1D-PES), while the 2D-HR scheme needs two-dimensional potential energy surfaces (2D-PES).
The 1D potential energy contributions $V^{1D}(\phi_i)$ are calculated using constrained geometry optimizations, with all variables allowed to relax, except for the considered ϕ_i dihedral angle. The 1D grid constitutes of 72 evenly distributed points: $k \cdot 5°$. The total potential energy is then approximated as:

$$V^{mD}(\phi_1, \ldots, \phi_m) \approx \sum_{i=1}^{m} V_i^{1D}(\phi_i) \tag{7.1}$$

where m is the number of internal rotations of the considered molecule.
This energy approximation can be improved by the use of 2D-PES [16, 17]. The potential energy variation of the methyl top rotations is considered uncoupled from other rotations, reducing the dimension of the potential energy to be described by one for alcohols and thiols, and by two for ethers and sulfides. The 2D approximation for the n remaining internal rotations is defined as:

$$V^{nD}(\phi_1, ..., \phi_n) \approx \sum_{i=1}^{n} V_{i(i+1)}^{2Dcut}(\phi_i, \phi_{i+1}) - \sum_{i=2}^{n-1} V_i^{1Dcut}(\phi_i) \tag{7.2}$$

The V_i^{1Dcut} and $V_{i(i+1)}^{2Dcut}$ contributions are 1D and 2D cuts of the n-dimensional energy-surface:

$$V_i^{1Dcut}(\phi_i) \equiv V^{nD}(\phi_1^{ref}, ..., \phi_i ..., \phi_n^{ref}) \tag{7.3}$$

$$V_{i(i+1)}^{2Dcut}(\phi_i, \phi_{i+1}) \equiv V^{nD}(\phi_1^{ref}, ..., \phi_i, \phi_{i+1} ..., \phi_n^{ref}) \tag{7.4}$$

where ϕ^{ref} is the value of the dihedral angle in the reference conformer. The ϕ_i and ϕ_{i+1} torsional angles are varied with increments of 10°.

The final goal is the evaluation of the total partition function for all of these methods from which thermodynamic quantities such like the entropy S and heat capacity C, of the selected molecules are straightforwardly deduced:

$$S = R\left(\ln q + T\left(\frac{\partial \ln q}{\partial T}\right)\right) \tag{7.5}$$

$$C = RT\left(2\frac{\partial \ln q}{\partial T} + T\frac{\partial^2 \ln q}{\partial T^2}\right) \tag{7.6}$$

The total partition function q is a product of partial partition functions of the translation, global rotation, and internal modes [1].
The hindered rotor procedures (1D-HR, 2D-HR) redefine the partition function Q_{cl} of the internal rotations and the global rotation as [71]:

$$Q_{cl} \sim \int \sqrt{\det A(\phi_1, \ldots, \phi_m)}\ e^{-\frac{V(\phi_1, \ldots, \phi_m)}{k_B T}} \mathrm{d}^{\mathrm{m}}\Phi \tag{7.7}$$

where k_B is the Boltzmann factor, T is the temperature, and V is the potential energy in function of the torsional angles. A represents the kinetic energy matrix, and incorporates the moments of inertia of the global and internal rotations.

For the 1D-HR, Eq.(7.1) is used to construct the potential energy $V(\phi_1, \ldots, \phi_m)$. For the kinetic energy contribution to Q_{cl}, the determinant of the kinetic energy matrix is approximated as a product of all (constant) reduced moments of inertia (I^{red}) of the different internal rotations and the (constant) principal moments of inertia ($I_x I_y I_z$) of the molecule:

$$\det A\,(\phi_1, \ldots, \phi_m) \approx I_x I_y I_z \prod_{i=1}^{m} I_i^{red} \tag{7.8}$$

In the 2D-HR method, the kinetic energy will not be considered constant at the values of the reference conformer. In accordance with Ref.[17] it is instructive to introduce a multi-dimensional kinetic correlation function

$$f_A^{nD}\,(\phi_1, \ldots, \phi_n) = \frac{\det A\,(\phi_1, \ldots, \phi_n)}{\det A_0} \tag{7.9}$$

This factor gives a measure to describe the fluctuations of the moments of inertia from the reference conformer (given by A_0). In the 2D-scheme we can

assume that the multi-dimensional correlation function may approximately be factorized as:

$$f_A^{nD}(\phi_1, \ldots, \phi_n) \approx \frac{\prod_{i=1}^{n-1} f_{A,i(i+1)}^{2Dcut}(\phi_i, \phi_{i+1})}{\prod_{i=2}^{n-1} f_{A,i}^{1Dcut}(\phi_i)} \tag{7.10}$$

in complete agreement with the approximative scheme for constructing the multidimensional potential energy surface [Eq.(7.2)].

7.3 Labelling convention for conformers

In order to unambiguously describe the different (reference) conformers, a consistent labelling system must be introduced. This was already done in a previous study on alcohols, thiols, ethers and sulfides [18], and a short overview is outlined in this paragraph.
Individual conformations about an internal rotation are defined in Figure 7.1: t, g_- and g_+, corresponding to a trans or a gauche $-/+$ orientation. Rotations about a CO or CS single bond generate similar potential energy profiles, and the minima are labelled the same way.

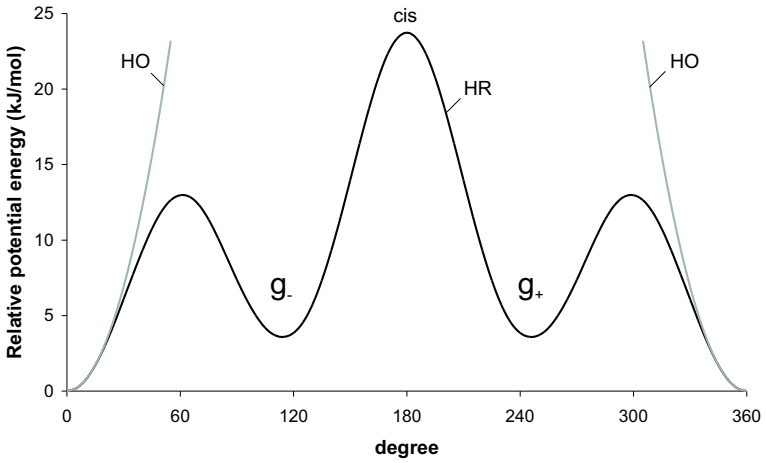

Figure 7.1: Example of a typical potential energy profile (HR) of internal rotation about a CC-bond: Potential energy relative to the all-trans conformer for the one-dimensional ethyl rotation in n-hexane. The two gauche states are labelled.

When multiple internal rotations within a molecule are considered, the individual conformation of each rotation has to be assigned. The appropriate labelling convention for a sequence of internal rotations is illustrated in Fig.7.2. For alcohols and thiols [Fig.7.2(a)], the first internal rotation (with dihedral angle ϕ_{l1}) is about the CX bond ($X = O$ or S). The other rotations are labelled as ϕ_{lx} where x indicates the position of the CC rotation axis in reference to the CX bond. Also the position of the hydroxyl top is written explicitly. For example, the HOg_+tg_-t conformer of 1-pentanol (or HSg_+tg_-t for 1-pentane thiol) stands for $\phi_{l1} = g_+$, $\phi_{l2} = t$, $\phi_{l3} = g_-$, and $\phi_{l4} = g_-$ where $l4$ indicates the ethyl torsion, $l3$ the propyl torsion, etc.

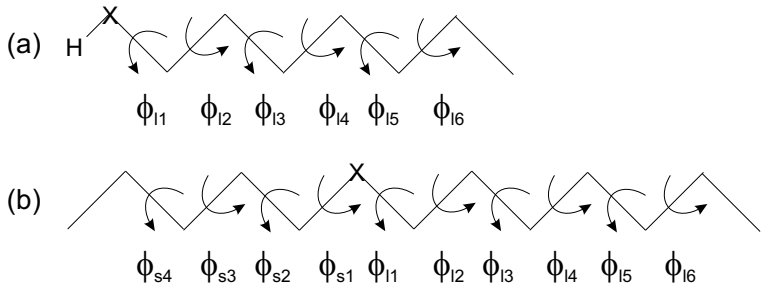

Figure 7.2: Labels used to identify specific internal rotations (with their dihedral angles) in (a) primary alcohols ($X = O$) and thiols ($X = S$), and (b) in ethers ($X = O$) and sulfides ($X = S$).

For ethers and sulfides, the same convention applies, but one has to distinguish between the two alkyl fragments [Fig.7.2(b)]. The 'l' subscript indicates that the rotation is situated in the longest alkyl top on the hetero-element, and the 's' refers to the shortest alkyl branch. We refer to a conformer by specifying the individual conformations in the order $\phi_{smax} \ldots \phi_{s1} X \phi_{l1} \ldots \phi_{lmax}$, with $X = O$ or S. For example, in ethyl propyl ether tOg_-g_+ stands for $\phi_{s1} = t$, $\phi_{l1} = g_-$, and $\phi_{l2} = g_+$, while the same configuration in ethyl propyl sulfide is referred to as tSg_-g_+.

Note that all molecules in this chapter are subject to the symmetry operation σ_h which converts all gauche +/- orientations into its gauche -/+ mirror image. The trans conformations are not affected. For example, the above mentioned HOg_+tg_-t conformer of 1-pentanol is converted to HOg_-tg_+t.

7.4 General discussion on rotational potential energy profiles

In this section we will focus on the general behavior of the internal rotation potentials observed in the n-alkanes with hetero elements. These energy profiles differ from those in n-alkanes and we will consider pentane as reference alkane. We stress that the one-dimensional torsional potential scan is obtained by fixing the dihedral angle of the selected rotation in the desired position, and by relaxing all other variables to their energetically most favored value. A pure rigid rotation is computationally less intensive but can lead to unrealistic barrier heights due to strong steric hindrance, as in this approach all coordinates are frozen at the equilibrium conformation except for the concerned torsional angle. The usefulness of this relaxation in the procedure of constructing rotational potential surfaces will be discussed.

7.4.1 One-dimensional potential energy profiles

In the test set of 28 studied alcohols/thiols and ethers/sulfides we distinguish three categories of potential energy profiles: (i) methyl top rotations, (ii) OH- and SH-top rotations, and (iii) the remaining 'deeper' rotations.

Methyl tops

Methyl top rotations have a threefold symmetry and the barrier height determines unambiguously the rotational potential. For n-alkanes this barrier converges about the value of 12.1 kJ/mol for long enough chains [B3LYP/6-311g**(B2)]. In n-alkanes with substitution of a CH_2 fragment by an hetero element O or S, the methyl barrier height depends on the position of the hetero element in the chain with respect to the ending methyl top. The largest variations take place in the smallest molecules: C_2H_6O may represent ethanol as well as dimethyl ether (DME) but the barrier varies from 11 kJ/mol in DME to 15,5 kJ/mol for ethanol (Fig.7.3) within the B3LYP/B2 level of theory. The variation of the barriers decreases for longer hetero substituted alkanes and converges to the pure n-alkane value of 12.1 kJ/mol. The lowest barrier is noticed in molecules where the methyl top is nearest to the hetero element and its magnitude largely depends on the nature of the hetero element: 6 kJ/mol for methyl tops close to S, which is the result of the (very) long bond length of $S-C$.

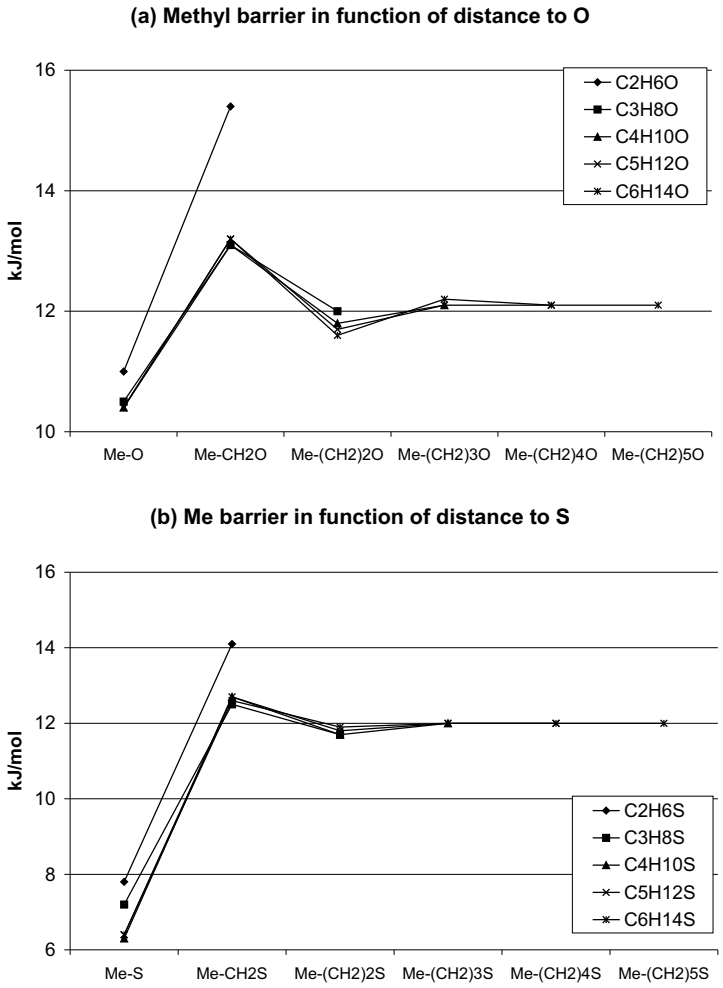

Figure 7.3: Methyl top barrier height in function of chain length and position of the hetero element in the chain, calculated at the B3LYP/B2 level of theory. Note that for n-alkanes the barrier amounts to about 12.1 kJ/mol.

The results on the B3LYP/6-31+g*(B1) level are qualitatively the same, with somewhat lower values (maximal 0.2 kJ/mol) for the barrier energies.

OH- and SH-tops

The rotational potential energy profiles of an OH- or SH-top can show a distinct behavior dependent on the reference geometry of the most stable conformation which can differ in alcohols and thiols and in different basissets. For primary alcohols the reference conformer is $HOgt(ttt)$ at the B3LYP/B1 while $HOg_-g_-(ttt)$ at the B3LYP/B2 level of theory. For thiols, both basissets generate the same lowest energy conformer ($Sgt(ttt)$). This slightly different behavior is best visualized in Figures 7.4 and 7.5.

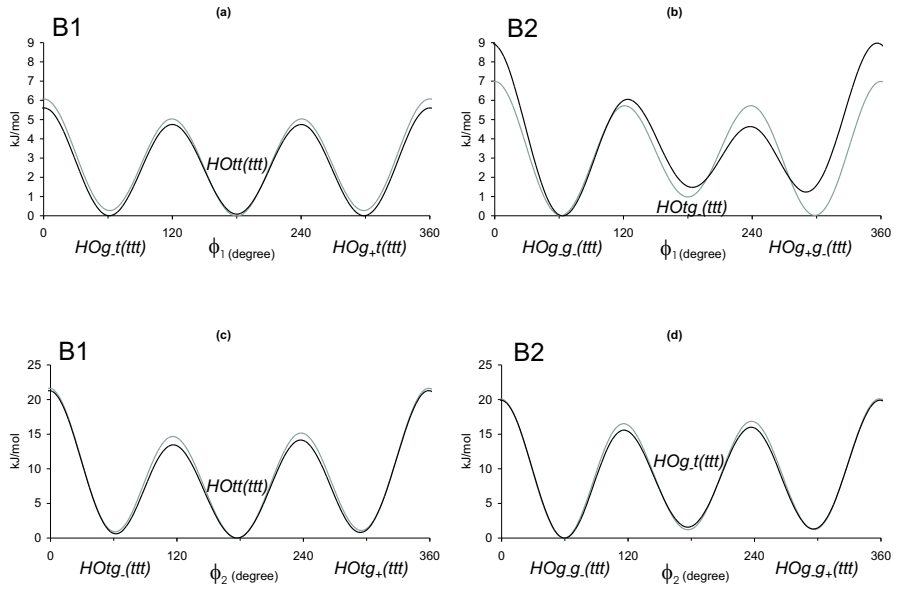

Figure 7.4: Potential energy profiles of (a,b) OH-top: the black line corresponds with ethanol, the grey line represents the other alcohols; (c,d) CH_2OH-top: the black line corresponds with 1-propanol, the grey line represents the other alcohols. The (a) and (c) plots show the B3LYP/B1 results, while the (b) and (d) plots are calculated with B3LYP/B2.

In the case of alcohols the two different basissets B1 and B2 predict different global minima for the OH-top (ϕ_{l1} rotation) although the differences are very small (about 1 kJ/mol or less). As a result the 1D energy profiles [Figs.7.4(a) and (b)] are different. For example the $HOg_+g_-(ttt)$ conformer is only reached by a ϕ_{l1} rotation starting from the $HOg_-g_-(ttt)$ lowest energy conformer at

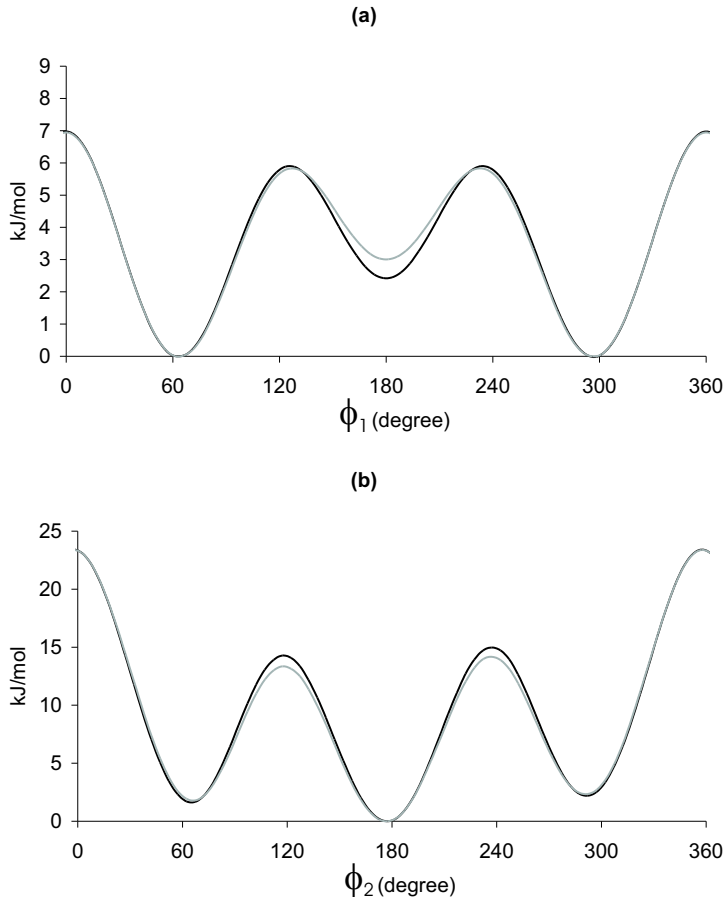

Figure 7.5: Potential energy profiles of (a) SH-top: the black line corresponds with ethanethiol, the grey line represents the other thiols; (b) CH_2SH-top: the black line corresponds with 1-propanethiol, the grey line represents the other thiols. Both plots are calculated with B3LYP/B2.

the B3LYP/6-311g**(B2) level; in addition it breaks the symmetry of the potential energy profile. We mention this example in particular as it generates the famous g_-g_+ effect which has been observed in pentane [16] and is discussed in detail in Ref.[18].
The CH_2OH (ϕ_{l2}) rotation shows a similar behavior but now the barriers are substantially higher [Figures 7.4(c) and (d)].

The specific nature of the hetero element can also give rise to an altered potential profile. The reference conformer in thiols is now $HSgt(ttt)$ but the trans minimum is found at about 3 kJ/mol while similar barriers as for the OH-tops are found (Fig.7.5). As the bond distance of $S-C$ is noticeably larger than the $O-C$ bond length, one could intuitively expect lower barriers for the SH group, in analogy with the methyl rotation on S. The reason for this counter-intuitive behavior may be found in the presence of the spatially wide-spread lone pair in sulfur, whereas the oxygen's lone pairs are much closer to the atom.

Note that again, for both ϕ_{l1} and ϕ_{l2} rotations, convergence of the energy profiles in function of the chain length of the molecule is reached very fast: only the smallest thiols (ethanethiol and 1-propanethiol respectively) have a slightly different behavior.

Rotations of large alkyl groups about the hetero element

Similarly as in the preceding subsection the most interesting features in 1D potential energy profiles for this category of internal rotations appear when starting from the $HOg\_g\_(ttt)$ conformer, as found with the B3LYP/B2 level of theory. For all molecules under study here one distinguishes subclasses with specific rotational profiles. The length of the alkyl chain on the hetero element has only little affect on the potential suggesting the introduction of a genuine potential for each subclass.

For the alcohols and ethers two subclasses come forward. In Fig.7.6(a) we display the torsional potential of the ethyl top to the hetero atom O in ethylalcohol, methyl ethyl ether (MEE), di-ethyl ether, ethyl propyl ether etc. (full lines) compared with the ethyl rotation in pentane (dotted line). The length of the hydrocarbon cluster at the other side of the hetero element seems not to be of any significance as all curves are almost coinciding. The relaxation effects during the rotation are negligible, and the genuine rotational profiles apply for all rotations. For this first subclass of torsional motions the rigid rotor model can be applied.
This situation is no longer valid if the rotating cluster becomes longer (propyl, butyl, pentyl top) [Fig.7.6(b)]. As already observed the energetically most favored conformation is the gauche position of the ϕ_{l2} torsion. A potential scan with relaxation of all geometrical parameters apart from the torsional angle results into a drastic geometrical distortion: one of the two gauche minima is completely removed and the cis barrier becomes substantially larger. This

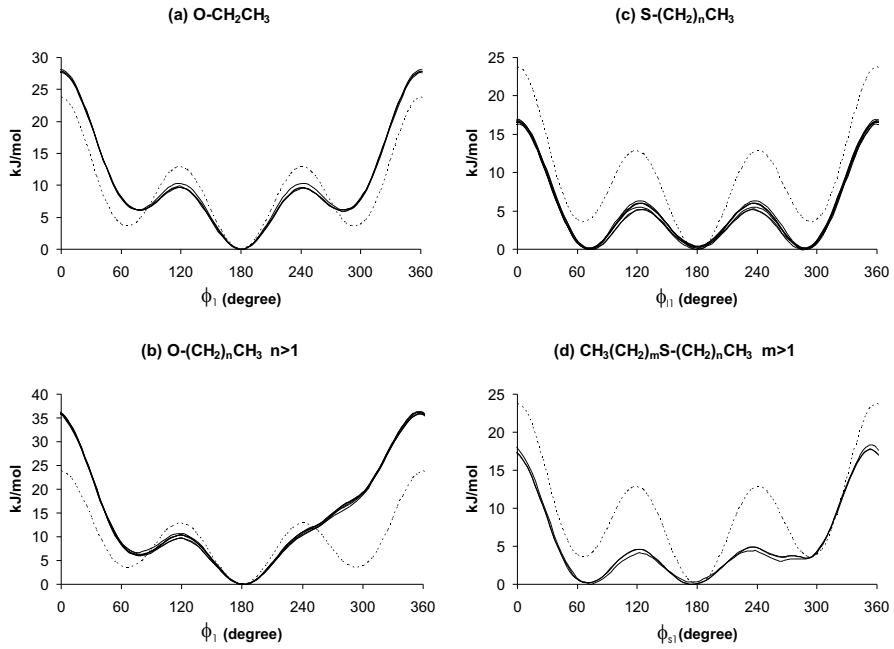

Figure 7.6: Potential energy profiles of ϕ_{l1} rotations: (a) ethyl top on O; (b) propyl (butyl, pentyl, ...) top on O; (c) all geometrically undistorted $S-C$ rotations; (d) geometrically distorted $S-C$ rotations: ethyl rotations of ethyl propyl sulfide and ethyl butyl sulfide, and propyl rotation in dipropyl sulfide; dotted lines in all plots represent the ethyl rotation in pentane. All plots are calculated at the B3LYP/B2 level of theory.

distortion of a gauche minimum is already known as the g_-g_+ effect and is thoroughly described in reference [18] for these kind of compounds. It forms the second subclass and it should be noted that a genuine potential may be introduced as convergence is obtained whatever the length of the rotating alkyl chain. We stress that the behavior of the potential is structurally different in n-alkanes.

For $X = S$ the genuine rotational profiles apply for most rotations [Fig.7.6(c)]. For these rotations there is a (near) degeneracy between the trans and the two gauche conformers. The skew (tg) barriers are also remarkably low. The rotations giving rise to substantial geometrical distortions are those where on the other side of S there is a propyl chain or longer [Fig.7.6(d)] for which the ϕ_{s1} rotation is in gauche. In this second subclass the second gauche minimum goes

over to a shallow plateau. The cis barrier is only slightly affected. Compared to ethers, the distortions are very small, probably because of the larger bond lengths involved in sulfides.
Concluding, study of the torsional energy profiles of the ethyl and longer clusters on the hetero elements learns that various conformers are present exhibiting an almost energy degeneracy. This feature suggests that the one-dimensional model is probably too limited to describe the multidimensional potential accurately, as the profiles of the other rotations must surely be different for each of these minima.
In the construction of the one-dimensional torsional potential one starts from only one of these various profiles. This poses no problem if there is only one dominant energy minimum. However, if more degenerate minima are present, all different profiles contribute strongly to the partition function, and hence to the calculated thermodynamic properties. This effect is even enforced by the low t-g barriers.

Finally we study the rotations at larger distance from the hetero element (ϕ_{ln} or ϕ_{sn} with $n > 1$). In Fig.7.7(a) we display the ethyl rotation in propyl segments on O, the propyl rotation in butyl segments, etc. [Fig.7.7(b)]. In all energy profiles the gauche conformers turn out to be in the absolute energy minimum, and the trans conformer appears to be slightly higher in energy. The skew tg barriers between them are relatively high. The profile is dependent on the chain length: in propyl segments [Fig.7.7(a)] the trans energy is about 1.27 kJ/mol above the gauche minimum, while for longer tops [Fig.7.7(b)] it is about 1.77 kJ/mol. Different basissets have little effect on the behavior of the potential: one notices only a slight lowering of the trans energy. The above observations are also applicable to the sulfides under study. There appears some geometrical distortion due to the neighboring gauche position, but it only lowers one gauche minimum and raises the other.

7.4.2 Relaxation effects

As mentioned in the computational details the rotational potential profiles have been constructed allowing full relaxation of all geometrical parameters apart from the torsional angle of interest. This procedure is fundamentally different from the rigid rotor approach, where the geometry is frozen at the equilibrium geometry except for the dihedral angle that describes the rotation. In this sub-

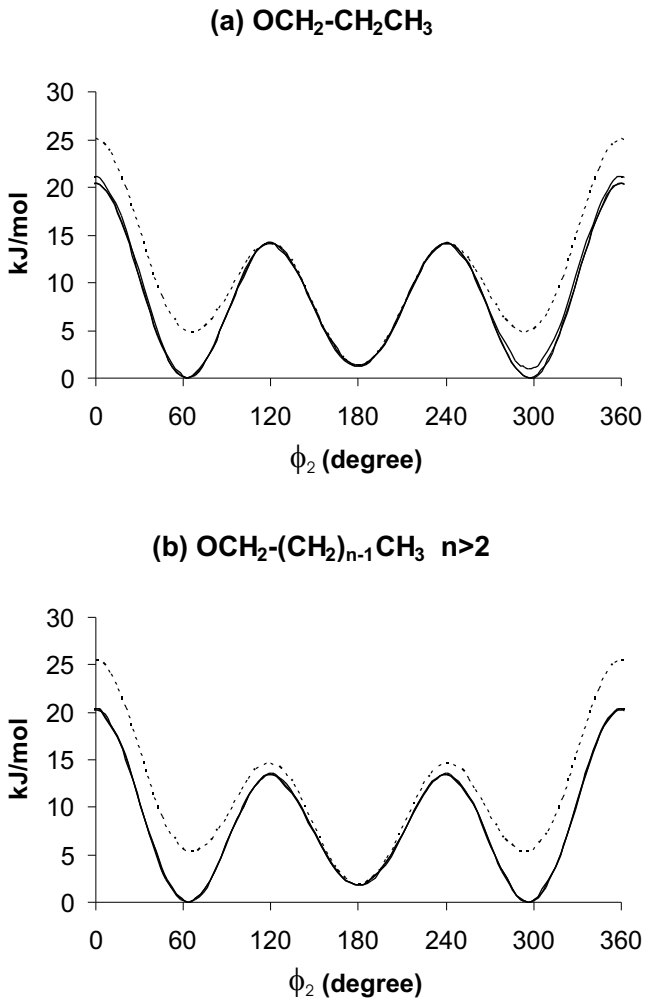

Figure 7.7: Potential energy profiles of ϕ_{l2}/ϕ_{s2} rotations in ethers: (a) ethyl rotation in propyl segments, and (b) propyl rotation in butyl and butyl rotation in pentyl segments. The dotted line in both plots represents the ethyl rotation in pentane. Trans-gauche energy difference amounts to 1.27 kJ/mol in (a) and 1.77 kJ/mol in (b). Results obtained at the B3LYP/B2 level of theory.

section we emphasize the importance of relaxation effects in the construction of the one-dimensional potential energy surface (1D-PES) as input in the 1D-HR scheme for evaluating the partition functions for the internal modes. In pure n-alkanes relaxation effects are rather small [14]: a torsional motion only affects dihedral angles of adjacent torsions within $\pm 5°$, with extremes around the gauche position. The distortion induced by the methyl rotation is even less important.

In alcohols and thiols the situation does not change drastically. The relaxations are of the same order of magnitude as for n-alkanes. However in ethers and sulfides where the hetero element is situated inside the n-alkane chain relaxation effects are no longer smooth and one can question the validity of the one-dimensional treatment of some rotations. We illustrate with the propyl rotation in MPE [Fig.7.8(a)]. The ethyl dihedral can vary by about 30° while the methyl top can rotate over 15° from its reference position. These large relaxations are probably due to the gauche standing in the reference conformers at the B3LYP/B2 level of theory. Relaxation effects due to the ethyl rotation in MPE cause deviations of dihedrals of less than 4° and are not of any importance.
The situation is reversed in MPS: propyl rotation limits the relaxation of the ethyl dihedral within 5°, but now it is the ethyl rotation which may vary the propyl dihedral with more than 25° [Fig.7.8(b)] reflecting the g_-g_+ effect as already mentioned.

Concluding, the relaxation effects observed in the geometrical parameters of the molecule may affect the moments of inertia to a large extent. In particular, when some conformers show gauche standings as energetically favored positions, the relaxation effects may induce large corrections. We show the one-dimensional correlation function for the moments of inertia of the ethyl and propyl rotations in MPE and MPS (Fig.7.9). This correlation function is defined as the value of the determinant of the kinetic energy matrix of the current geometry, divided by the determinant of the matrix of the reference structure. In other words, it is the relative variation of all considered moments of inertia treated in its full dimensionality. Contrary what could be expected from the large relaxation effects noticed at some 1D-rotations, we may conclude that the moments are rather well described in the one-dimensional approximation. This means that, as for n-alkanes, a cancellation of errors (in kinetic and potential energy contributions) is possible [16], and that the 1D-HR approach

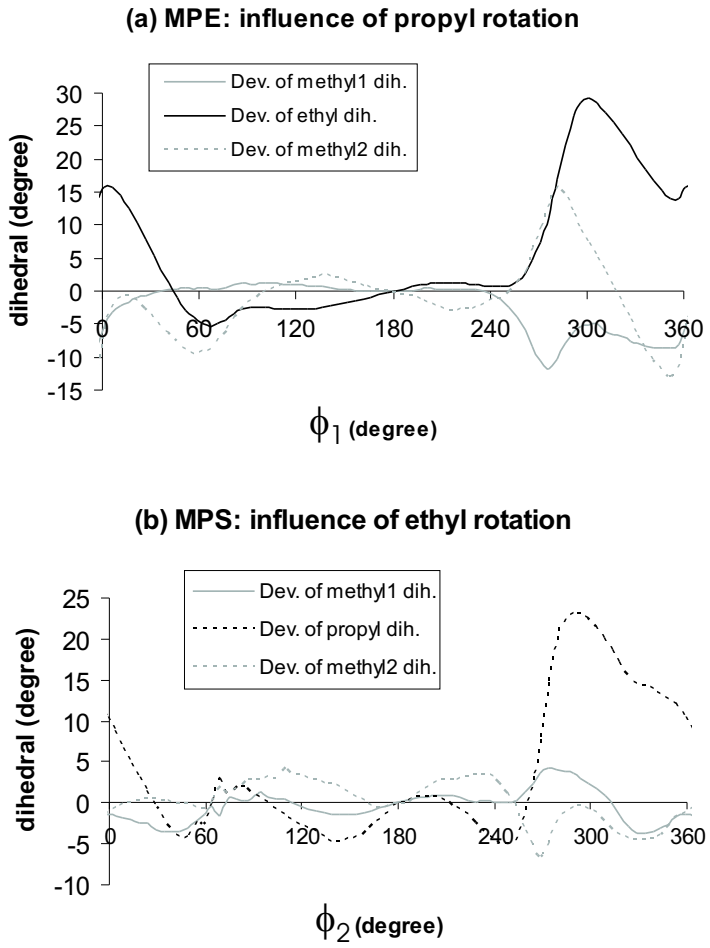

Figure 7.8: Deviation of the relaxed dihedral angles as a function of (a) ethyl and (b) propyl rotation in MPE, and c) ethyl and (d) propyl rotation in MPS.

may be adequate for the calculation of the partition function.

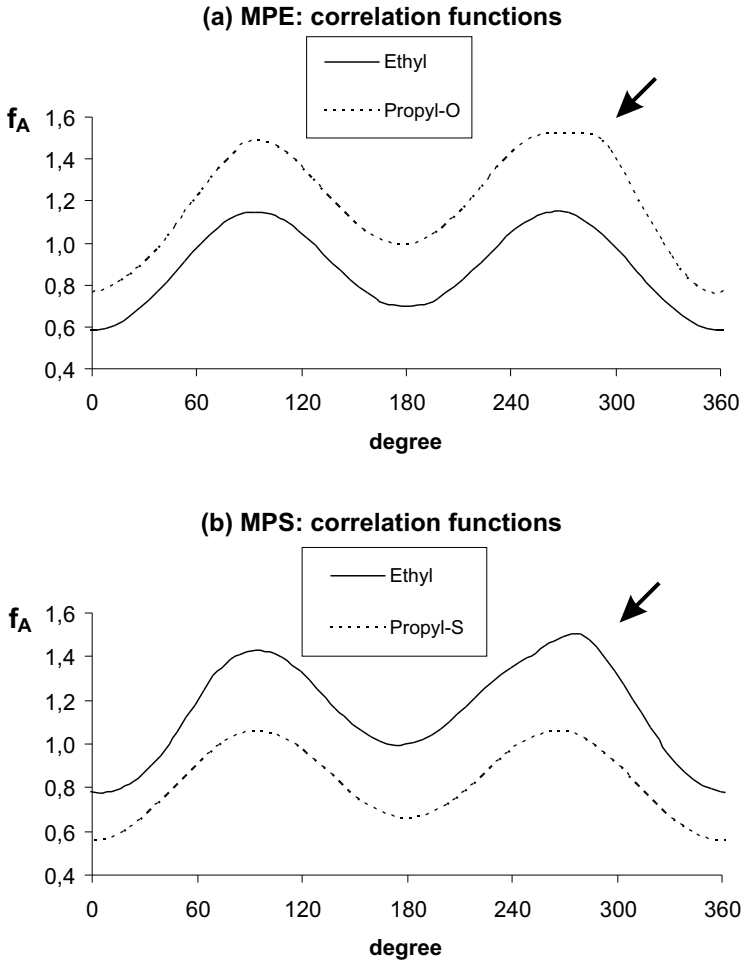

Figure 7.9: Variation of the determinant of the kinetic energy matrix relative to the reference conformer: one-dimensional correlation functions in (a) MPE and (b) MPS.

7.4.3 Two-dimensional potential energy profiles

Due to the presence of several (very) low energy conformers in the hetero compounds under study in this chapter (Ref.[18]), one could expect multi-dimensional potential surfaces differing from those obtained in pure n-alkanes. On the other hand, in the preceding subsection we emphasized the almost similar behavior of the kinetic energy variation in function of the internal rotations (Fig.7.9). It is thus very well possible that the balance between the errors generated by the potential and the kinetic energy contributions in the partition function is disturbed. This balance lies on the origin of the success of the uncoupled hindered rotor model (1D-HR) in n-alkanes [16]. A disturbed balance could question the validity of the 1D-HR for the hetero molecules investigated here.
For this reason we calculate some two-dimensional energy surfaces of molecules that can serve as examples for a whole series of compounds. For alcohols and thiols 1-hexanol and 1-hexanethiol are selected, where the $\phi_{l1}\phi_{l2}$, $\phi_{l2}\phi_{l3}$ and $\phi_{l3}\phi_{l4}$ 2D-surfaces have been investigated (Fig.7.10). For ethers and sulfides we studied the $\phi_{s1}\phi_{l1}$ (Fig.7.11) and $\phi_{l1}\phi_{l2}$ surfaces (Fig.7.12) in methyl propyl ether (MPE) and sulfide (MPS), di-ethyl ether (DEE) and sulfide (DES), and finally di-propyl ether (DPE) and sulfide (DPS).

We will not discuss all calculated 2D-surfaces, but limit ourselves to those which are relevant and transparent for the discussion. Main focus is the evaluation of the partition function and corresponding thermodynamic properties and the comparison between 1D-HR and 2D-HR predictions.
The conformational study [18] and the 1D potential energy plots of ϕ_{l1} (Fig.7.6) and ϕ_{l2} (Fig.7.7) suggest that coupling of consecutive internal rotations $\phi_{l1}\phi_{l2}$ could be important. We illustrate with the coupled $\phi_{l1}\phi_{l2}$ rotations in MPE, DPE, MPS and DPS (figure in SI). The ether and sulfide surfaces show deviating coupling effects: in ethers the typical **alkane** double minima around the g_-g_+ geometry is completely destroyed.
The $\phi_{s1}\phi_{l1}$ potential energy surfaces (Fig.7.11) are very instructive. As could be expected from the above discussion on basis of one-dimensional rotational profiles the energy surfaces for ethers and sulfides show very distinct features. First the minima on the sulfide surfaces are numerous and clearly more spread out and less localized than those on the ether surfaces. Also the energy barriers are substantially higher at the ethers (note the different scale of the contour plots in Fig.7.11). Secondly the influence of the level of theory on the 2D-

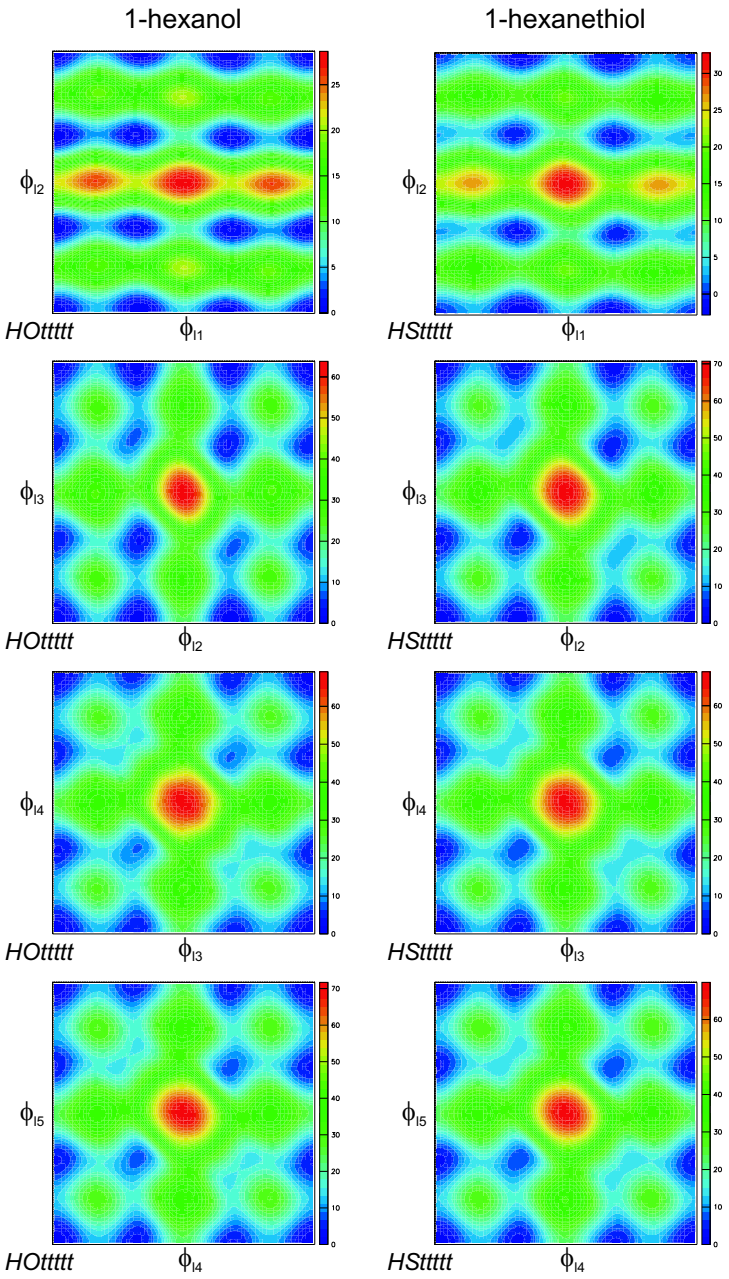

Figure 7.10: Two-dimensional potential energy profiles of 1-hexanol [B3LYP/6-31+g*(B1)] and 1-hexane thiol [B3LYP/6-311g**(B2)].

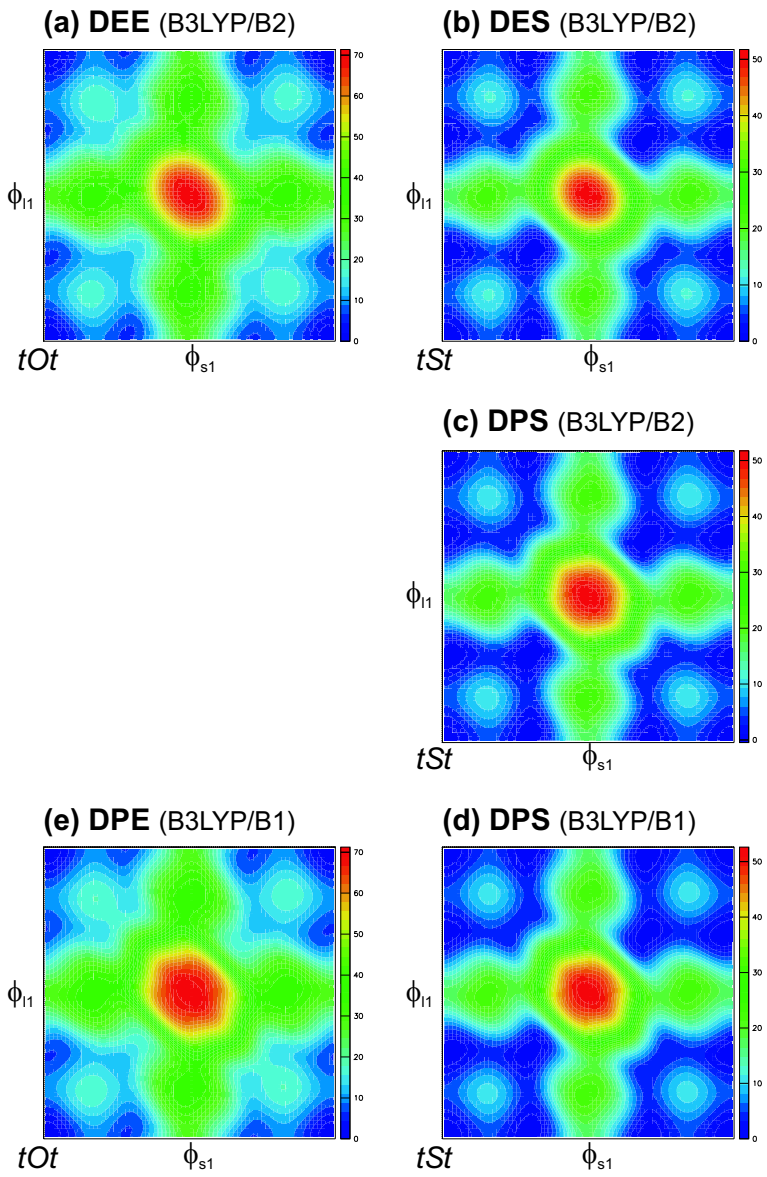

Figure 7.11: Two-dimensional potential energy profiles of the $\phi_{s1}\phi_{l1}$ energy surfaces in di-ethyl ether (DEE), di-propyl ether (DPE) and di-ethyl sulfide (DES), di-propyl sulfide (DPS): (a) DEE on the B3LYP/6-311g**(B2) level of theory, (b) DES on the B3LYP/B2 level of theory, (c) DPS on the B3LYP/B2 level of theory, (d) DPS on the B3LYP/B1 level of theory, (e) DPE on the B3LYP/6-31+g*(B1) level of theory.

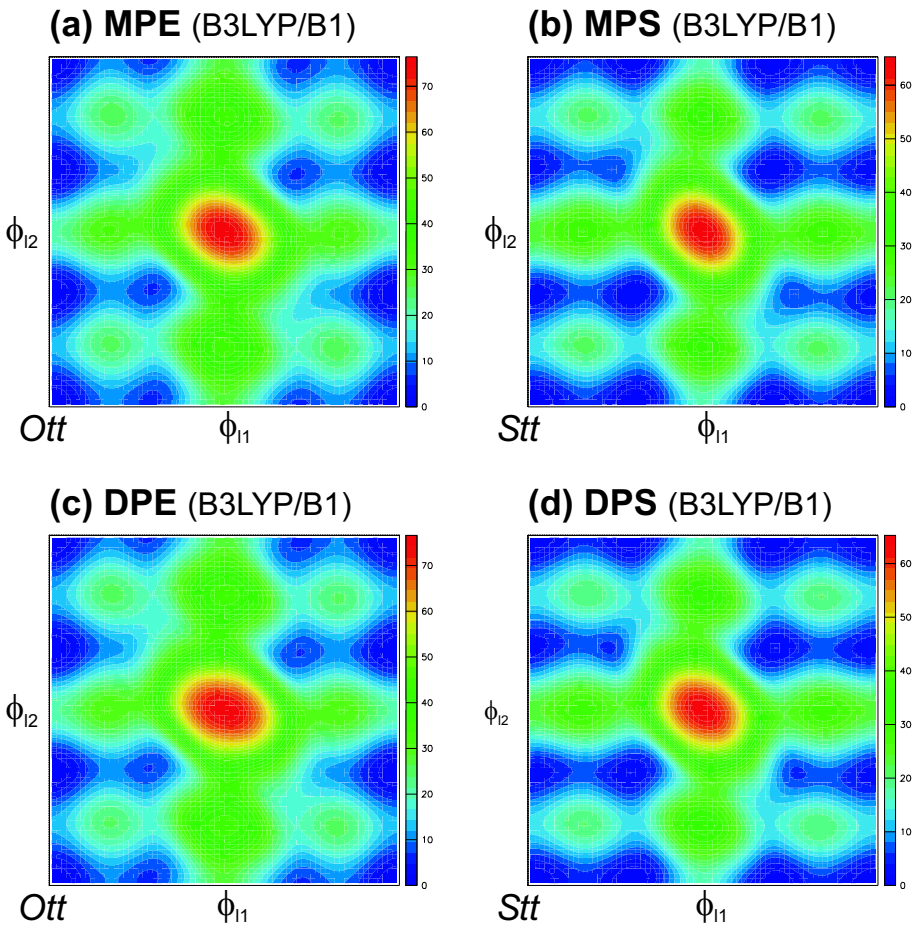

Figure 7.12: Two-dimensional potential energy profiles of the $\phi_{l1}\phi_{l2}$ energy surfaces in methyl propyl ether (MPE), di-propyl ether (DPE) and methyl propyl sulfide (MPS), di-propyl sulfide (DPS): (a) MPE on the B3LYP/6-31+g*(B1) level of theory, (b) MPS on the B3LYP/B1 level of theory, (c) DPE on the B3LYP/B1 level of theory, (d) DPS on the B3LYP/B1 level of theory.

profiles is less pronounced. We display the 2D-PES obtained with the two basissets B1 and B2 and opposite what has been observed at the 1D-profiles we scarcely notice any discrepancy. This is not surprising due to the specific nature of constructing 2D-PES. Another feature arising from the smooth minima present on the sulfide surfaces is the cumulation of inaccuracies in the two-dimensional integration for the evaluation of the partition function. The presence of localized minima on a surface ensures a larger numerical stability of the integration and less dependent on the used level of theory than in case of integration over a large smooth plateau of minima. This would give rise to larger uncertainties in the partition functions for sulfides.

The impact of these specific 2D-PES on the partition function, and hence thermodynamic properties, is difficult to predict as a mixture of coupling effects is present.

7.5 Thermodynamic properties

The final aim of present chapter is to assess the performance of the 2D-HR versus 1D-HR scheme in reproducing thermodynamic quantities in the selected oxygen and sulfur compounds. The experimental reference values are taken from Refs.[24] and [23].

7.5.1 Oxygen compounds

Table 7.1 gives a summary of the results obtained in the considered set of alcohols and ethers. It contains entropy and heat capacity values calculated at different levels of theory: B3LYP/6-31+g*(B1) and B3LYP/6-311g**(B2), and with different calculation schemes: the harmonic oscillator model (HO), and the two hindered rotor schemes 1D-HR and 2D-HR. The reference conformer from which the 1D or 2D energy profiles are calculated are also specified. When this reference is not the energetically most stable conformer on the selected level of theory, it is given in italic. For transparency we also report the results from refs.[39] and [106] when available.

The entropy values are given at 298.15 K. All HO values systematically underestimate the experimental data. The discrepancies are of the order of 10 % of the total magnitude.
The full ab initio corrections arising from taking into account 1D internal rotors bring the theoretical predictions to values which are very close to the experimental estimates (within a few J/mol.K) independent of the level of theory B1 or B2. In some ethers the agreement is even spectacular, especially on the B3LYP/6-311g**(B2) level of theory. For 1-propanol and 1-hexanol, also entropy values are provided that are calculated from potential energy profiles starting from a different reference geometry. The resulting corrections are remarkably small.
The 2D-HR values are obtained from 2D energy surfaces around the all-trans conformer, which is not the most stable conformer in 1-hexanol. This lowest energy conformer is however exactly described as it is present on the $\phi_{l1}\phi_{l2}$ energy surface.
The 2D-HR entropy values are somewhat higher than the 1D-HR results, and the discrepancy with the experimental values increases. This was also noted for n-alkanes [16], and it seems that the same conclusions apply: there is a cancellation of errors (potential versus kinetic energy) in the construction of 1D-HR partition function.

		basis	ref. conf.	S(298.15K)	C(100K)	C(200K)	C(298.15K)	C(400K)	C(600K)	C(800K)	C(1000K)	C(1500K)
ethanol	exp.			282,59	39,10	52,45	66,17	80,41	106,41	127,71	143,35	167,56
	HO	B1	HOt	269,68	39,31	51,64	64,65	80,34	108,22	129,22	145,13	170,53
		B2	HOg	268,78	38,46	51,14	64,63	80,58	108,62	129,60	145,44	170,70
	1D-HR	B1	HOt	278,11	41,05	53,03	64,88	79,31	104,94	124,37	139,27	163,44
		B2	HOg	282,33	41,25	53,15	65,38	80,19	106,14	125,48	140,19	163,96
dimethyl ether	exp			266,69	43,18	54,00	66,03	79,18	104,56	126,40	142,82	165,15
	HO	B1		264,47	41,25	51,89	62,43	76,79	104,88	127,13	144,10	170,71
		B2		264,48	41,24	51,94	62,68	77,27	105,58	127,87	144,80	171,25
	1D-HR	B1		267,28	42,09	54,34	65,04	77,98	102,84	122,97	138,66	163,79
		B2		269,15	42,03	54,22	65,26	78,61	103,78	123,91	139,53	164,41
1-propanol	exp			324,72	53,81	74,56	93,48	111,63	143,05	169,23	190,58	225,92
	HO	B1	HOgt	301,81	48,40	66,41	85,03	107,31	146,58	175,90	197,90	232,63
		B2	HOgg	298,93	46,38	64,91	84,47	107,40	147,13	176,49	198,43	232,96
		B2	*HOgt*	301,22	48,03	66,13	85,02	107,55	147,05	176,40	198,36	232,92
	1D-HR	B1	HOgt	324,25	53,08	69,36	86,60	107,19	143,08	169,86	190,14	222,61
		B2	HOgg	322,05	56,90	69,19	86,84	108,17	144,56	171,21	191,25	223,24
		B2	*HOgt*	324,52	55,51	70,39	87,42	108,09	144,08	170,76	190,88	223,04
methyl ethyl ether	exp			310,62	53,51	72,80	92,04	111,70	147,38	176,87	198,87	227,63
	HO	B1	Ot	302,05	49,65	66,18	82,99	104,31	143,85	174,27	197,21	232,97
		B2	Ot	302,26	49,73	66,28	83,32	104,91	144,68	175,12	198,01	233,56
	1D-HR	B1	Ot	309,88	51,26	74,65	92,94	111,01	143,86	170,26	190,81	223,68
		B2	Ot	311,89	51,51	74,86	92,77	111,06	144,48	171,10	191,68	224,38
	Ref.[106]:			312,63	52,13	74,85	92,47	110,33	143,01	168,91	188,91	220,83
1-butanol	exp			362,75		81,64	111,91	139,76	185,05	219,82	246,12	286,09
	HO	B1	HOgtt	333,82	58,31	81,10	105,22	134,14	184,90	222,61	250,75	294,81
		B2	HOggt	331,28	56,08	79,59	104,78	134,42	185,68	223,42	251,47	295,27
	1D-HR	B1	HOgtt	365,44	65,16	90,82	112,09	137,29	182,00	215,71	241,26	281,97
		B2	HOggt	362,36	72,73	90,20	111,56	137,82	183,34	216,98	242,32	282,56
	Ref.[39]			361,00								
methyl propyl ether	exp			349,13			112,38	138,66	183,40	218,82	244,63	
	HO	B1	Ott	334,60	59,92	81,16	103,34	131,23	182,18	220,97	250,03	295,13
		B2	Otg	332,56	58,23	80,22	103,29	131,82	183,24	222,06	251,04	295,84
	1D-HR	B1	Ott	351,13	62,11	90,92	114,22	138,22	181,43	215,37	241,47	282,81
		B2	Otg	349,71	62,14	88,22	112,75	139,05	184,12	218,24	244,12	284,75
	2D-HR	B1	Ott	352,71	62,04	90,23	114,12	138,74	182,10	215,90	241,90	283,17
	Ref.[39]			352,21								
diethyl ether	exp			341,00		92,06	118,26	143,95	188,79	225,01	252,40	292,77
	HO	B1	tOt	327,74	58,87	80,53	103,53	131,79	182,78	221,39	250,31	295,22
		B2	tOt	328,56	59,12	80,72	103,99	132,57	183,81	222,41	251,24	295,89
	1D-HR	B1	tOt	341,96	61,18	94,94	120,64	143,85	184,87	217,62	243,07	283,67
		B2	tOt	341,61	61,92	95,71	119,80	142,96	184,99	218,26	243,88	284,41
	2D-HR	B2	tOt	347,90	62,89	99,59	119,66	140,82	182,85	216,66	242,68	283,84
	Ref.[39]			345,97								

		basis	ref. conf.	S(298.15K)	C(100K)	C(200K)	C(298.15K)	C(400K)	C(600K)	C(800K)	C(1000K)	C(1500K)
1-pentanol	exp			402,50		96,60	133,70	168,19	224,45	266,71	297,07	341,91
	HO	B1	HOgttt	364,55	68,01	95,69	125,32	160,86	223,13	269,25	303,54	356,96
		B2	HOggtt	362,57	65,97	94,33	125,10	161,44	224,23	270,34	304,50	357,57
	1D-HR	B1	HOgttt	408,39	79,10	112,70	137,48	167,23	220,86	261,55	292,38	341,31
		B2	HOggtt	402,81	86,83	111,42	136,21	167,35	222,18	262,93	293,57	342,03
	Ref.[39]			401,45								
methyl butyl ether	exp			390,10								
	HO	B1	Ottt	366,80	70,02	95,90	123,57	158,09	220,55	267,71	302,91	357,33
		B2	Otgt	364,74	68,07	95,04	123,70	158,94	221,87	269,03	304,11	358,17
	1D-HR	B1	Ottt	389,05	75,23	112,73	139,87	168,43	220,44	261,30	292,64	342,20
		B2	Otgt	389,46	76,31	110,17	138,61	169,55	223,33	264,25	295,32	344,11
ethyl propyl ether	exp			388,10			134,49	168,18	223,89	266,70	298,34	345,65
	HO	B1	tOtt	366,56	69,51	95,63	123,94	158,76	221,17	268,13	303,16	357,40
		B2	tOtg	365,01	67,86	94,71	123,99	159,52	222,40	269,37	304,29	358,19
	1D-HR	B1	tOtt	384,83	72,41	111,32	141,82	170,95	222,40	262,72	293,72	342,81
		B2	tOtg	386,91	72,67	108,96	139,85	171,07	224,69	265,43	296,33	344,79
1-hexanol	exp			441,50		113,32	156,97	197,57	263,66	312,88	347,68	398,02
	HO	B1	HOgtttt	398,31	78,93	110,84	145,84	187,97	261,68	316,13	356,52	419,21
		B1	*HOttttt*	396,69	78,65	110,73	145,67	187,80	261,56	316,07	356,50	419,23
		B2	HOggttt	395,26	76,42	109,29	145,57	188,58	262,88	317,33	357,58	419,91
	1D-HR	B1	HOgtttt	442,06	93,16	134,76	163,17	197,47	259,93	307,53	343,60	400,72
		B1	*HOttttt*	441,32	90,09	134,07	162,97	197,24	259,62	307,29	343,44	400,68
		B2	HOggttt	445,57	102,11	132,68	161,02	197,07	261,12	308,91	344,83	401,48
	2D-HR	B1	*HOttttt*	446,32	95,89	133,51	161,97	197,52	260,93	308,77	344,91	401,95
	Ref.[39]			441,83								
methyl pentyl ether	HO	B1	Otttt	398,95	80,36	110,80	143,89	185,01	258,93	314,48	355,80	419,54
		B2	Otgtt	397,28	78,31	109,88	144,11	186,04	260,49	316,01	357,18	420,50
	1D-HR	B1	Otttt	421,17	89,36	134,62	165,18	198,30	259,27	307,14	343,77	401,56
		B2	Otgtt	417,12	90,42	131,79	163,74	199,47	262,42	310,35	346,69	403,63
ethyl butyl ether	exp			429,00			157,75	197,83	263,12	312,73	349,31	403,45
	HO	B1	tOttt	398,70	79,63	110,36	144,12	185,56	259,47	314,83	356,01	419,59
		B2	tOtgt	396,45	77,56	109,45	144,32	186,54	260,95	316,28	357,31	420,49
	1D-HR	B1	tOttt	424,12	85,76	133,19	167,46	201,08	261,29	308,56	344,84	402,17
		B2	tOtgt	427,72	86,59	130,81	165,93	201,82	264,06	311,55	347,61	404,18
dipropyl ether	exp			422,50			153,41	196,75	263,55	312,67	349,10	
	HO	B1	ttOtt	394,03	80,41	110,84	144,38	185,72	259,53	314,85	356,01	419,57
		B2	gtOtg	388,58	76,50	108,67	143,96	186,43	260,97	316,29	357,30	420,46
	1D-HR	B1	ttOtt	429,74	84,12	127,97	163,08	198,04	259,85	307,77	344,33	401,92
		B2	gtOtg	420,92	85,61	121,37	160,23	200,09	265,06	312,92	348,91	405,12
	2D-HR	B1	ttOtt	434,57	84,72	129,88	163,49	197,64	259,50	307,70	344,53	402,56
	Ref.[39]			428,53								

Table 7.1: Thermodynamic properties of alcohols and ethers

The reproduction of the heat capacity is of the same order of accuracy as observed in the n-alkanes, and almost independent of the specific HR scheme (1D or 2D). The calculated values are somewhat too high for lower temperatures as a result of the classical implementation of our hindered rotor treatments [14]. On the other hand for medium and higher temperatures we achieve a very satisfactory agreement. In Figure 7.13(a) the temperature behavior of the heat capacity in ethyl butyl ether is plotted. It confirms our conclusions.

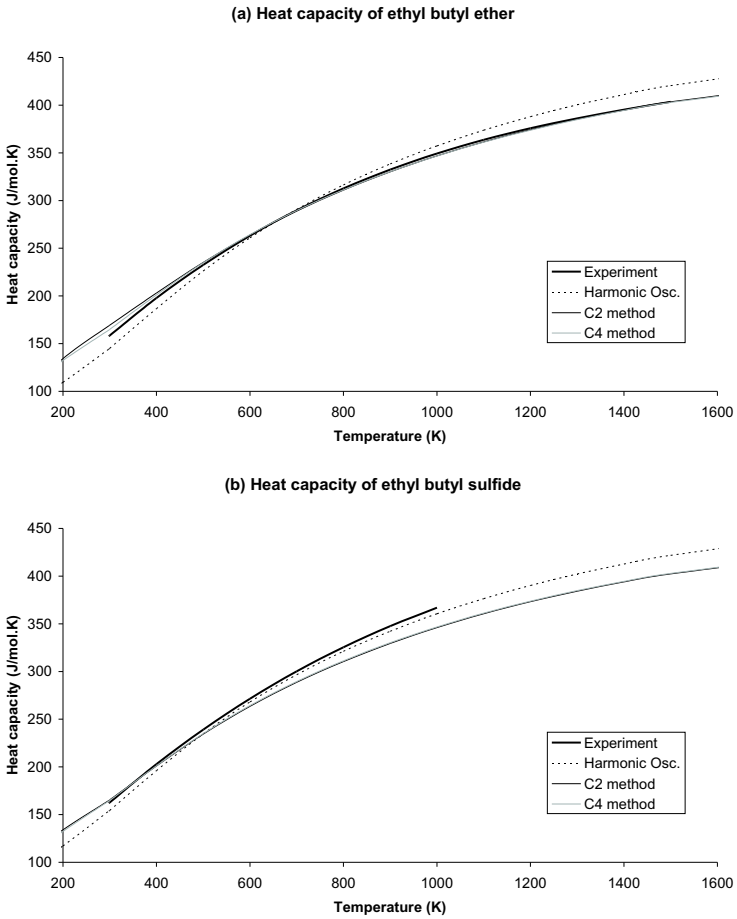

Figure 7.13: Heat capacity in J/(mol.K) of (a) ethyl butyl ether and (b) ethyl butyl sulfide.

7.5.2 Sulfur compounds

Entropy and heat capacity values for the selected set of thiols and sulfides are presented in Table 7.2. When available the results of Guthrie's work [39] are also reported.

The agreement of the calculated entropy values with experiment is satisfactory but not of the same level as for alcohols and ethers. While the HO results still underestimate the experimental values significantly, the 1D-HR predictions are close to experiment, except for some smaller sulfides. For dimethyl sulfide, methyl ethyl sulfide and diethyl sulfide the HO values are already reproducing the entropy quite well, and as a result the 1D-HR and 2D-HR predictions now exceed the experimental data. Both models predict almost the same entropy values, the differences are small compared with the corrections obtained in alcohols and ethers. Anyway, the best overall agreement is given by the 1D-HR approach and this conclusion has already been made in the study of n-alkanes [16]. The reasons are probably the same: cancellation effects by coincidence.

The analysis of the heat capacities reveals some interesting features. For higher temperatures, the HO approximation will normally provide an upper limit for the heat capacities, as the contribution for each activated mode will be R, while for the HR modes it will tend to $R/2$. This rule indicates that the HO models are expected to always overestimate the heat capacity at high temperatures. This rule is not systematically respected in Table 7.2. For the larger molecules (such as 1-butanethiol) the experimental heat capacities are larger than those predicted in the HO approximation ! This is a very strong evidence of an inappropriate level of theory to describe the vibrational modes with a higher activation temperature.
As the HR model lowers the heat capacity values by $R/2$ (at high temperatures) for each internal rotation present, the 1D and 2D-HR predictions will be worse than the HO values. This situation is shown in Figure 7.13(b). This failure in reproducing the correct behavior of the heat capacity in sulfides lies in the presence of low vibrational modes in sulfides. Contrary to ethers and n-alkanes, now low temperature bending modes are appearing resulting from the heavy S atom and the long CS bonds. They are responsible for higher moments of inertia ($I \sim r^2 = |CS|^2$) and hence lower HO frequencies ($\sim (\frac{ddV}{I})^{1/2}$). As the vibrational temperatures originating from these bending modes are of the same magnitude of the vibrational temperatures of internal rotations, they are

(Table 7.2)

	basis	ref. conf.	S(298.15K)	C(100K)	C(200K)	C(298.15K)	C(400K)	C(600K)	C(800K)	C(1000K)	C(1500K)
ethanethiol											
exp			296,02	53,33	62,93	74,37	87,26	112,27	133,05	147,53	168,32
HO	B2	HSg	284,63	41,94	56,21	70,94	87,09	114,13	134,29	149,59	173,75
1D-HR	B2	HSg	293,45	45,49	59,71	72,54	87,04	111,50	129,90	144,07	166,84
dimethyl sulfide											
exp			285,85		62,10	75,22	88,51	112,45	132,23	147,24	169,79
HO	B2		284,56	46,11	58,45	72,18	87,78	114,06	133,69	148,71	172,86
1D-HR	B2		292,79	47,57	61,14	73,18	86,47	109,72	127,83	142,05	165,32
1-propanethiol											
exp			336,50		76,98	96,86	116,84	152,34	180,97	202,02	232,71
HO	B2	HSgt	317,39	52,60	71,60	91,63	114,38	152,83	181,28	202,64	236,04
1D-HR	B2	HSgt	335,34	61,77	78,95	95,92	115,96	150,16	175,74	195,23	226,22
methyl ethyl sulfide											
exp			333,15			95,04	116,64	152,18	179,70	200,51	
HO	B2	St	323,62	55,44	73,09	92,44	114,64	152,36	180,36	201,51	235,00
1D-HR	B2	St	341,42	57,27	76,15	93,91	113,79	147,70	173,26	192,90	224,51
1-butanethiol											
exp			375,20		95,35	120,58	146,44	193,67	233,32	263,87	310,80
HO	B2	HSgtt	348,69	62,43	86,20	111,84	141,30	191,30	228,14	255,61	298,30
1D-HR	B2	HSgtt	373,17	76,53	100,35	120,79	145,62	188,94	221,56	246,35	285,59
methyl propyl sulfide											
exp			371,68			117,29	145,28	191,66	227,95	255,74	
HO	B1	Stt	355,85	65,50	87,73	112,15	140,68	189,73	226,17	253,56	296,63
	B2	Sgt	353,75	64,28	87,82	113,10	142,10	191,26	227,49	254,66	297,32
1D-HR	B1	Stt	375,44	73,05	96,19	117,21	142,03	185,33	218,12	243,21	283,34
	B2	Sgt	374,91	69,79	94,35	117,76	143,57	187,07	219,56	244,36	284,02
2D-HR	B1	Stt	376,67	72,85	95,65	117,09	142,11	185,56	218,41	243,52	283,65
	B2	Sgt	376,21	70,76	94,42	116,84	142,57	186,59	219,50	244,53	284,38
diethyl sulfide											
exp			368,00		95,66	120,11	145,36	191,60	230,12	259,29	304,20
HO	B2	tSt	351,59	64,84	87,76	112,75	141,58	190,75	227,10	254,37	297,17
1D-HR	B2	tSt	378,55	67,57	90,86	114,49	141,21	185,95	218,97	244,00	283,87
2D-HR	B2	tSt	378,29	67,86	91,21	114,56	141,23	186,07	219,19	244,30	284,23
1-pentanethiol											
exp			415,39			141,78	176,13	233,85	279,75	314,90	360,05
HO	B2	HSgttt	380,35	72,63	100,99	132,16	168,29	229,82	275,03	308,62	360,60
1D-HR	B2	HSgttt	417,48	91,15	122,22	146,06	175,56	227,93	267,55	297,62	345,05

(Table 7.2 continued)

	basis	ref. conf.	S(298.15K)	C(100K)	C(200K)	C(298.15K)	C(400K)	C(600K)	C(800K)	C(1000K)	C(1500K)
methyl butyl sulfide											
exp			411,90			140,67	175,04	232,69	278,55	314,08	
HO	B2	Sgtt	385,95	74,64	102,60	133,43	169,11	229,80	274,40	307,68	359,62
1D-HR	B2	Sgtt	414,98	84,75	116,19	142,99	173,42	225,94	265,47	295,57	343,46
Ref.[39]			414,47								
ethyl propyl sulfide											
exp			414,12			139,02	173,84	232,43	279,18	315,44	
HO	B2	tSgt	387,43	73,50	102,37	133,34	168,97	229,60	274,19	307,48	359,47
1D-HR	B2	tSgt	415,95	81,74	110,60	139,00	171,23	225,37	265,31	295,51	343,42
Ref.[39]			405,76								
1-hexanethiol											
exp			454,70		130,54	167,69	205,10	271,82	326,01	366,24	425,84
HO	B2	HSgtttt	411,60	82,83	115,81	152,51	195,34	268,39	321,96	361,65	422,89
	B2	*HSttttt*	416,92	85,18	116,56	152,69	195,36	268,35	321,92	361,62	422,87
1D-HR	B2	HSgtttt	457,18	105,62	143,46	170,88	205,22	266,77	313,45	348,81	404,46
	B2	*HSttttt*	457,02	105,93	144,42	171,15	205,01	266,28	312,99	348,45	404,27
2D-HR	B2	*HSttttt*	460,64	113,25	140,64	168,85	204,98	267,72	314,68	350,14	405,74
Ref.[39]			457,73								
methyl pentyl sulfide											
exp			451,18			163,50	204,14	271,71	324,83	365,62	
HO	B2	Sgttt	418,80	85,19	117,53	153,85	196,20	268,39	321,35	360,73	421,93
1D-HR	B2	Sgttt	450,18	99,44	137,92	168,29	203,47	265,05	311,56	346,91	402,96
Ref.[39]			453,67								
ethyl butyl sulfide											
exp			453,39			161,85	202,96	271,46	325,47	367,00	
HO	B2	tSgtt	418,56	83,73	117,12	153,62	195,93	268,09	321,07	360,48	421,76
1D-HR	B2	tSgtt	453,89	96,29	132,22	164,11	201,03	264,23	311,22	346,72	402,86
dipropyl sulfide											
exp			448,80			161,10	202,29	272,16	328,47	372,46	
HO	B1	ttStt	417,17	85,39	117,36	152,75	194,46	266,36	319,49	359,12	420,86
	B2	tgSgt	412,56	82,17	117,07	154,06	196,50	268,54	321,36	360,65	421,80
	B2	*ttStt*	418,67	85,81	117,78	153,63	195,79	267,93	320,95	360,40	421,73
1D-HR	B1	ttStt	444,99	99,21	130,68	161,25	198,17	261,90	309,36	345,21	401,92
	B2	tgSgt	451,89	96,47	129,34	162,75	200,89	264,80	311,79	347,19	403,12
	B2	*ttStt*	447,81	99,97	129,01	160,49	198,23	262,66	310,27	346,11	402,61
2D-HR	B1	ttStt	452,33	100,59	129,38	160,49	197,99	262,25	309,93	345,93	402,77
	B2	*ttStt*	449,76	96,71	127,27	160,59	199,14	263,84	311,37	347,13	403,52
Ref.[39]			450,91								

Table 7.2: Thermodynamic properties of thiols and sulfides

heavily mixed. Visual study of the normal modes gives a strong indication of highly mixed modes.

Due to this multitude of low frequency modes, the sulfide results become more sensitive to the considered level of theory and that basisset B2 fails in predicting a correct reproduction of the heat capacities in sulfides. This suggestion of B2 being a less suitable level of theory for studying sulfides, is reenforced by the results of Ref.[18], where the energy differences of the conformers of methyl propyl sulfide were found to largely depend on the used basisset, while for methyl propyl ether these differences are almost not varying for both basis sets.

7.6 Summary

In this chapter the thermodynamic properties –entropy and heat capacity– of alcohols/thiols and ethers/sulfides have been the subject of a thorough investigation. In these molecules several internal rotations are present. These rotations have a tendency to generate multiple conformers with similar energies, and may exhibit, depending on the level of theory, a global potential energy minimum at a conformation different from the all-trans geometry. Both properties are different from n-alkanes in which there is a distinct energy minimum at the all-trans conformation. It was therefore difficult to predict if the 1D-HR approach would be able to reproduce the experimental data on entropy and heat capacity with the same kind of accuracy as for n-alkanes.

It seems that despite the quite different internal rotation profiles the 1D-HR method is indeed capable of reproducing entropy values close to experiment. The 2D-HR method, although theoretically more evolved, seems to slightly overestimate the entropy.
The reproduction of the heat capacity on the other hand is more complicated as it is very sensitive to the used level of theory in particular when smooth potential energy surfaces are appearing with broad valleys and low barriers. This is confirmed by the satisfactory reproduction of heat capacities in alcohols and ethers, but the failure of the hindered rotor model in predicting reliable values in thiols and sulfides.

The general conclusion is that the 1D-HR approach is a very satisfactory model to describe thermodynamic properties of the presented single chain molecules: primary alcohols and thiols, and ethers and sulfides.

Chapter 8

Applicability of the hindered rotor scheme to the puckering mode in four-membered rings

This chapter is based on Ref.[21]:

Vansteenkiste, P.; Van Speybroeck, V.; Verniest, G.;
De Kimpe, N. and Waroquier, M.
J. Phys. Chem. A **2006**, *110*, 3838

Abstract

The hindered rotor scheme, originally developed for internal rotors in flexible chains [14] is extended to puckering motions in four-membered rings. The applicability of the approach is tested to a variety of heterocyclic compounds for which the partition function, entropy and heat capacity is calculated. The entropy may be substantially altered by a correct description of the puckering mode. The equilibrium puckering angle ranges between 0° and 30° depending on the hetero-substitution X (CH_2, O, S, NH, PH, C=O, C=S, C=NH, C=PH) in the four-membered ring.

8.1 Introduction

Strained cyclic molecules are of fundamental nature in heterocyclic chemistry as many biological processes are directed by compounds bearing a heterocyclic moiety. These small cyclic compounds have beside the standard vibrational modes also skeletal motions which involve the entire backbone of the molecule. These are the so-called ring vibrations. The potential energy associated with these ring vibrations is not purely harmonic in nature, but can exhibit various minima leading to a number of stable ring conformers. They show large similarities with internal rotations in flexible chains, apart from the fact that they are constrained. It is now generally accepted in literature, that the Harmonic Oscillator approximation (HO) fails for the description of the thermodynamic quantities of such flexible molecules, exhibiting a number of torsional modes about single bonds. The one-dimensional hindered rotor (1D-HR) scheme (e.g. [58, 44, 35, 2, 14, 16]) is a conceptually simple but accurate model to overcome this problem. This approach is nowadays used by many authors for treating internal rotations. The number of theoretical works on the description of low vibrational modes in cyclic molecules and their influence on the partition function is far more limited. A study of Katzer and Sax on the thermochemical properties of structurally related silicon hydrides [53] revealed that the impact of ring puckering can become very important in four- and five- membered rings.

The aim of this chapter is to extend the Hindered Rotor scheme to ring vibrations which are characterized by a strongly anharmonic potential. The partition function of this specific mode is manually constructed by calculating the energy levels in the puckering potential. The approach is tested on four-membered rings of the structure as given in Scheme 1:

All these molecules with X different from CH_2 have potential applications in heterocyclic chemistry, while the cyclobutanone derivatives have been shown to have a large application in various domains [127].

Experimental studies, employing various techniques, on the spectra of numerous cyclic molecules (Refs.[128, 129, 130, 131, 132, 133, 134, 135, 136, 137, 138, 139, 140, 141, 142, 143, 144], and references therein) provide extensive information on the ring puckering of four-membered rings. Apparently, for many of these compounds, the equilibrium structure does not correspond to the most symmetrical geometry, being the planar conformation, but is mainly determined by the balance of two opposing forces [145]. Minimizing Bayer or

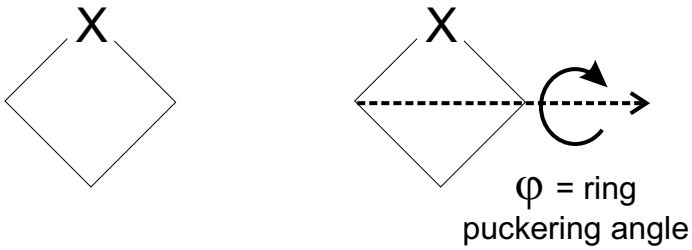

1 X= CH_2: cyclobutane
2 O: oxetane
3 S: thietane
4 NH: azetidine
5 PH: phosphetane
6 C=O: cyclobutanone
7 C=S: cyclobutanethione
8 C=NH: cyclobutylideneamine
9 C=PH: cyclobutylidenephosphine

Scheme 1

angle strain results in a planar form whereas the torsional or Pitzer strain is lower in a puckered geometry.

Based on minor assumptions, the potential energy barrier between the equilibrium and planar structure can be determined from the experimental spectrum. The geometries on the other hand require more detailed information, and are somewhat harder to assess. This is best illustrated by the study of cyclobutane, where the coupling of the ring puckering and CH_2 rocking motion is crucial for determining the equilibrium geometry [129].

In addition to these experimental studies, many computational ab initio studies have been performed [136, 137, 138, 139, 140, 141, 142] with the principal aim to reproduce the puckering barrier and equilibrium angle. The latter quantities seem hard to reproduce and require high post–Hartree-Fock levels of theory [137], while present DFT and MP2 studies in general failed to come close to the experimentally determined values. As the theoretical predictions are susceptible to good predictions of the geometrical features and puckering potential, a validation of the used electronic level of theory will be given.

8.2 Theoretical models

The molecular partition function associated with the internal degrees of freedom is systematically evaluated following the standard procedure within the Harmonic Oscillator approximation (HO). The latter assumes only small variations around the equilibrium configuration which may be described by a quadratic potential energy surface. Nowadays it is well known that the HO approximation fails in an accurate reproduction of the partition function of molecules that have internal modes in the low vibrational spectrum that do not correspond with pure vibrations. Among them, internal rotations about single bonds are certainly the most known and have been widely studied. The one-dimensional Hindered Rotor scheme (1D-HR) has been put forward as a computationally attractive and accurate scheme for treating internal rotations beyond the HO approximation [16]. In this approach, the global rotation and the internal rotations are decoupled and each internal rotation is described in one dimension ignoring the coupling between adjacent torsional modes. The reduced moment of inertia is kept fixed at the value of some reference geometry, often taken as the most stable configuration.

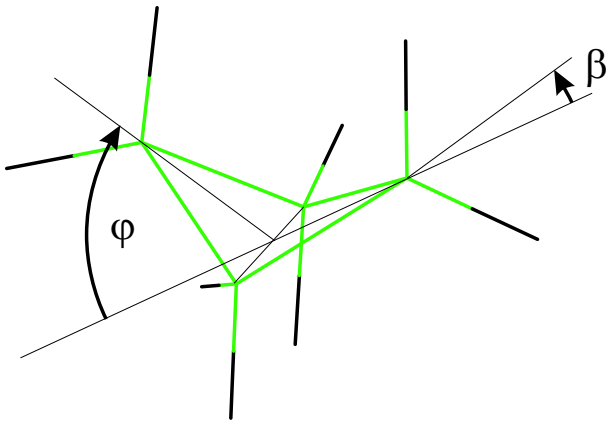

Figure 8.1: Schematic representation of cyclobutane, defining the puckering pseudorotation. Also the CH_2 rocking angle β is defined.

In this chapter a similar methodology is followed for large amplitude vibrations that correspond to ring inversions. In this case the rotation axes connect two non-bonded atoms as schematically shown in Figure 8.1 for cyclobutane. The frequency calculation gives all normal modes of the molecule and enables

one to select those vibrational modes that correspond with pseudo-rotations. For the four-membered rings under study, only one ring puckering vibration is present, but for larger cyclic systems this number increases.
The shape of the potential function associated with the ring puckering depends on the structural features inhibiting the ring vibration. This function is calculated along the lines of Refs.[14, 16] by pointwise geometry optimizations at fixed out of plane angles and thereby relaxing all other degrees of freedom.
In order to evaluate the new molecular partition function, one has to replace the harmonic oscillator contribution to the partition function as obtained from the standard quantum chemical packages by a manually constructed partition function, based on the second order derivative of the potential energy along the puckering angle and combined with its reduced moment of inertia. The need of this procedure was established in earlier work of the authors [146, 22].

The ring puckering partition function Q_{1D} can be obtained quantum mechanically or classically dependent on the temperature range of interest. For low temperatures (below 400K) a quantum mechanical treatment is needed and one has to solve the one-dimensional Schrödinger equation

$$\left[-\frac{\hbar^2}{2I^{red}}\frac{\partial^2}{\partial\phi^2} + V(\phi)\right]\psi_k(\phi) = \epsilon_k\psi_k(\phi) \tag{8.1}$$

The quantity I^{red} represents the generalized reduced moment of inertia [16, 5] and $V(\phi)$ is the potential associated with the pseudo-rotation. The Schrödinger equation is solved by the numerical procedure as outlined in Ref.[2], yielding all rotational energy eigenvalues ϵ_k required for the evaluation of the partition function of the ring vibration defined by

$$Q_{1D}^{HR} = \frac{1}{\sigma}\sum_k g_k e^{-\frac{\epsilon_k}{kT}} \tag{8.2}$$

with σ the symmetry number of the pseudo-rotational top, and g_k the degeneracy of the energy level k.
For temperatures above 500 K, the quantum mechanical and classical partition function are expected to converge. The classical partition function is obtained as an integral :

$$Q_{1D}^{HR} = K(T)\int_{-\pi}^{\pi} \mathrm{d}\varphi\ \sqrt{I^{red}}\ e^{-\beta V^{1D}(\varphi)} \tag{8.3}$$

with $K(T) = \sqrt{\frac{2\pi k_B T}{\hbar^2}}$. These results can be enhanced by the use of the Pitzer-Gwinn correction factor [15], extending the validity of the classical approach

to lower temperatures.

Once the molecular partition function is known, the entropy and heat capacity can be readily evaluated :

$$S = R\left(\ln Q_{tot} + T\left(\frac{\partial \ln Q_{tot}}{\partial T}\right)\right) \tag{8.4}$$

$$C = RT\left(2\frac{\partial \ln Q_{tot}}{\partial T} + T\frac{\partial^2 \ln Q_{tot}}{\partial T^2}\right). \tag{8.5}$$

8.3 Results and discussion

Level of theory study on cyclobutane 1, azetidine 4 and thietane 3. An appropriate level of theory for the subsequent study must be selected. This is done on the basis of a brief level of theory study on cyclobutane, azetidine and thietane for which experimental data are available [128, 129, 132, 133, 134]. All ab initio calculations were performed using the Gaussian03 software package [13] with the 6-31+G(d,p) basis set which is a valuable compromise between computational cost and accuracy [147]. A variety of Density Functional Theory (DFT) based methods are tested which can be divided as follows: pure DFT functionals (BP86, BLYP), hybrid DFT (HDFT) functionals (B3LYP, PBE1PBE, mPW1PW91, mPW1k) and hybrid meta DFT (HMDFT) functionals (B1B95, BB1k, mPW1B95, mPWB1k). For an overview of diverse DFT functionals reference is given to Ref.[148] and references therein.

Cyclobutane is by far the most investigated molecule and this species is used as a starting point for our level of theory study. A summary of the experimental history on this molecule is given in Ref.[137], while our results are compared with the experimental values of Egawa et al. [129]. Table 8.1 contains the barrier height V_0 and several structural parameters of the equilibrium geometry, i.e. the puckering angle φ_{min} at the energetically favored geometry and the rocking angle β, defined as the angle between the $\widehat{HCH}$ bisector and the bisector of the corresponding $\widehat{CCC}$ angle (Figure 8.1). Also the coupling parameter $\delta = \beta/\varphi$ is reported as frequently referred to in other literature works. The two most significant quantities are the barrier height V_0 between the equilibrium D_{2h} structure and the planar D_{4v} conformation, and the puckering angle φ_{min}. The experimental value of V_0 is 6.10 kJ/mol. DFT methods using pure functionals (BP86 and BLYP) fail in reproducing accurately this energy barrier whereas the hybrid meta DFT functionals perform well.
Further comparison with the experimental puckering angle φ_{min} [27.9°±1.6°] learns that HMDFT methods slightly overestimate the puckering angle, whereas HDFT methods give the most accurate value for this angle. Comparison of the calculated bond lengths (not shown) with experiment reveals that the functionals optimized for kinetics (mPW1k, BB1k, mPWB1k) are unable to produce acceptable values for the bond lengths. The coupling parameter δ is about 0.16 for all calculations, while experiment suggests 0.22. Also azetidine is well investigated by the experiment [134] and is characterized by a single well potential. The best performing functionals for azetidine are again the B1B95 and

	Cyclobutane 1				Azetidine 4	Thietane 3	
	V_0 (kJ/mol)	φ_{min}	β	δ	φ_{min}	V_0 (kJ/mol)	φ_{min}
DFT:							
BP86	4.29	27.1	4.3	0.16	28.4	2.06	23.8
BLYP	3.20	25.2	4.0	0.16	27.1	1.57	22.1
HDFT:							
B3LYP	3.69	25.7	4.1	0.16	26.6	1.53	22.0
PBE1PBE	5.11	27.9	4.5	0.16	28.2	2.12	23.9
mPW1PW91	4.73	27.4	4.4	0.16	27.8	1.88	23.1
mPW1k	5.11	27.8	4.5	0.16	27.4	1.84	23.0
HMDFT:							
B1B95	5.84	29.3	4.7	0.16	29.3	2.71	25.4
BB1K	6.33	29.7	4.8	0.16	29.1	2.71	25.3
mPW1B95	6.35	29.7	4.8	0.16	29.4	2.85	25.8
mPWB1k	6.55	30.0	4.8	0.16	29.2	2.84	25.6
post-HF:							
MP2/6-311+G(d,p) [139](b)					32.36		
CCSD(T)/cc-pVQZ [137]	6.53	29.6	5.7	0.19			
CBS-limits:							
B3LYP [137]	3.59	26					
MP2 [137]	8.09	32					
Experimental	6.10 ± 0.02	27.9 ± 1.6	6.2 ± 1.2	0.22 ± 0.05	29.7 ± 1.4	3.28 ± 0.02	26 ± 2

Left: Summary of the level of theory analysis on cyclobutane, showing the barrier height V_0, and the geometrical parameters of the potential minimum structure: the puckering angle φ_{min}, β, along with the derived coupling parameter $\delta = \beta/\varphi$. Experimental values are obtained from Ref.[129].
Middle: Summary of the level of theory analysis on azetidine, showing the puckering angle φ_{min}. Experimental values are obtained from Ref.[134](c).
Right: Summary of the level of theory analysis on thietane showing the barrier height V_0 and equilibrium puckering angle φ_{min}. Experimental values are obtained from Ref.[132].
Bond lengths are in Å, while (dihedral) angles are in degree.

Table 8.1: Summary of the level of theory analysis on cyclobutane **1**, azetidine **4** and thietane **3**.

mPW1B95 functionals. The results for thietane show that only hybrid meta DFT functionals give acceptable accuracy for the barrier height and puckering angle (cfr. Table 8.1).
During the further course of this chapter the mPW1B95 functional is used for thermodynamic analysis of all four-membered heterocyclic and carbonyl compounds.

In addition to the DFT level of theory study, we present some post–Hartree-Fock and CBS-limit results on cyclobutane and oxetane, as reported in references [139](b) and [137]. It can be concluded that MP2 does not perform well for these systems, whereas the very time-consuming CCSD(T) level is excellent. However, the computational efficient mPW1B95 method gives comparable accuracy as the CCSD(T) method.

Ring puckering potentials The shape of the potential (fig.8.2) associated with the ring inversion is determined by the puckering angle at the equilibrium and the barrier to inversion. These quantities together with important bond lengths and bond angles are given in table 8.2 for the studied molecules. Two types of potentials occur: a symmetrical double minimum or an asymmetrical shape. Azetidine (**4**) and phosphetane (**5**) exhibit an asymmetrical single and double well potential, respectively. Azetidine has only one minimum with the NH bond in equatorial position (positive values of φ), whereas for phosphetane the conformer with the PH bond in axial position (negative values of φ) is lowest in energy [142]. The lone-pair of phosphorus is much more spread out than of nitrogen and orients itself in equatorial position, away from the ring structure.

Azetidine is a nice example of the interplay between theory and experiment. Originally an asymmetric double well potential function was proposed with a stable equatorial and axial conformer [134](a). On the basis of suggestions of theory, the experiments were re-evaluated. It was concluded that the axial conformer is unstable and that the potential has only one single minimum which corresponds to a puckered conformation with the N-H bond in the pseudo-equatorial orientation. The origin of the asymmetry must be traced back to the pyramidal nitrogen atom. All other molecules under study here, i.e. cyclobutane, oxetane, thietane, cyclobutanone, thiocyclobutanone, cyclobutylideneamine, and cyclobutylidenephosphine have a symmetrical double well potential function. The barrier height and the puckering angle can be

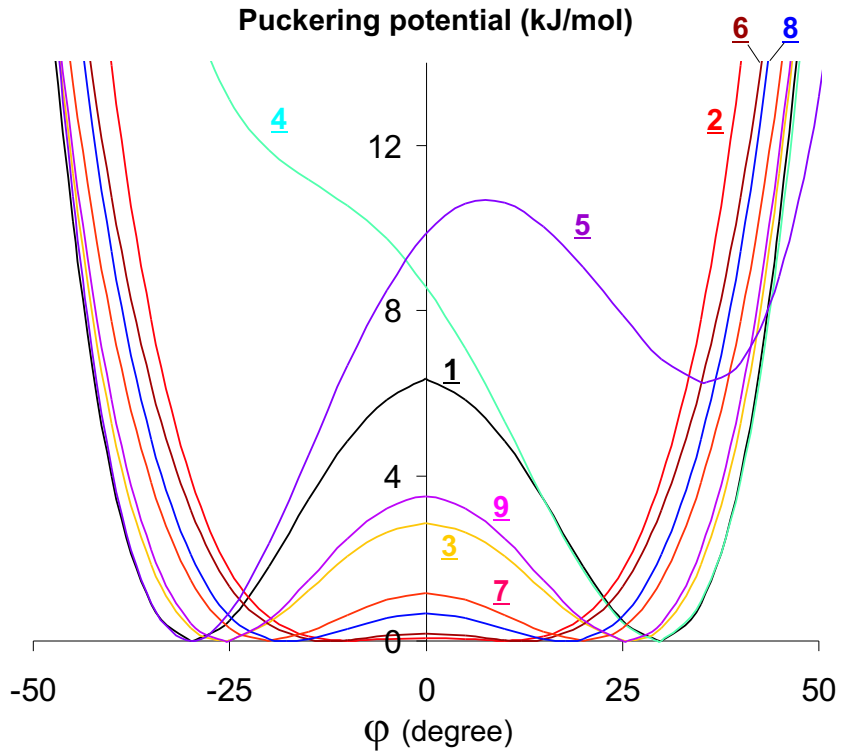

Figure 8.2: Potential energy profiles of cyclobutane **1**, oxetane **2**, thietane **3**, azetidine **4**, phosphetane **5**, cyclobutanone **6**, cyclobutanethione **7**, cyclobutylideneamine **8**, and cyclobutylidenephosphine **9**.

rationalized to a large extent using the concept of competing angle and torsional strain. Cyclobutane has the highest barrier to ring inversion as it has four pairs of eclipsing hydrogen atoms in the planar ring conformation. The hetero-element in the four-membered ring has a major influence on the puckering angle and barrier height as can be illustrated by comparing thietane and oxetane. The former compound is characterized by large carbon-sulfur bonds and a larger bond angle between the carbons (95.7°) in order to minimize the angle strain but as a consequence a larger puckering (25.8°) is observed. Cyclobutanone represents an example of an extremely fine balance between angle and torsional strain. Because of the sp^2 hybridization of the carbon atom at the carbonyl group, angle strain will increase more rapidly with ring puckering than in the other molecules. This is counterbalanced by torsional strain of three eclipsing methylene groups resulting in a nearly vanishing barrier to ring

	V_0 (kJ/mol)	φ_{min}	$\|C-C\|$	$\|C-X\|$ $(X=C,O,S,N)$	$\|C=X\|$ $(X=O,S,N)$	$\widehat{CCC}$
cyclobutane 1	6.35	29.7	1.534	1.534	-	91.9
oxetane 2	0.06	9.8	1.530	1.433	-	84.2
thietane 3	2.85	25.8	1.531	1.834	-	95.7
azetidine 4	-	29.4	1.469	1.535	-	85.4
phosphetane 5	-	**-30.0**	1.533	1.880	-	96.1
cyclobutanone 6	0.18	12.2	1.546	1.521	1.199	90.6
cyclobutanethione 7	1.16	20.1	1.544	1.508	1.609	88.8
cyclobutylideneamine 8	0.68	17.7	1.546 1.546	1.509 1.519	1.260	89.7
cyclobutylidenephosphine 9	3.49	25.7	1.543 1.544	1.511 1.509	1.671	88.3

Table 8.2: Main parameters of the equilibrium geometry of the selected molecules, and barrier height V_0 in kJ/mol calculated at the mPW1B95/6-31+G(d,p) level of theory. The second lines for cyclobutylideneamine and cyclobutylidenephosphine refer to the bonds on the side of the NH or PH orientation. Bond lengths are in Å, while (dihedral) angles are in degree.

inversion.

Frequency Spectrum The vibrational analysis learns that all four-membered rings possess one low lying frequency, i.e. below 250 cm^{-1}, that corresponds to the ring puckering vibration. The frequency of the latter mode is at least four times smaller than the next normal mode in the vibrational spectrum. This motivates the treatment as a one-dimensional problem. Once however substituted cyclobutanes containing a number of heavy elements in the side chain are considered, a one-dimensional approach could be insufficient. This item may be interesting for future research.

Molecular Partition Functions In figure 8.3, the ratio of the molecular partition functions calculated in the HR and HO approximation are shown. Depending on the X (cfr. Scheme 1) in the four-membered ring the partition function is reduced or enhanced by approximately a factor of two. We will now rationalize these results on the basis of a detailed study of the quantum mechanical energy levels in the puckering potential of cyclobutane, oxetane and azetidine which are shown in figure 8.4. Additionally the values for the partition function of the puckering mode is given in the HO and HR approximation. The partition function is largely affected by the density of states in the low-energy spectrum. In this case the classical evaluation of the partition function is also justified. When the puckering is treated as a vibrational mode in the HO approximation, the energy levels are equidistant and the inter-level energy spacing is determined by the force constant of the harmonic oscillator

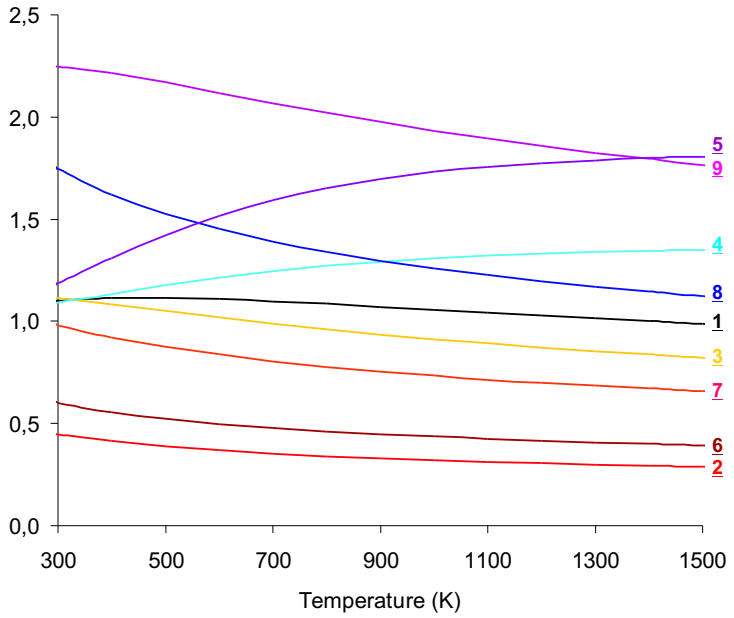

Figure 8.3: The ratio of the HR partition functions with the HO partition functions for all four-membered ring compounds studied: cyclobutane **1**, oxetane **2**, thietane **3**, azetidine **4**, phosphetane **5**, cyclobutanone **6**, cyclobutanethione **7**, cyclobutylideneamine **8**, and cyclobutylidenephosphine **9**.

potential at the equilibrium puckering angle. In the case of cyclobutane the low energy levels are (nearly) doubly degenerate due to the two energy wells which are separated by an energy barrier of 6.25 kJ/mol. An important aspect which must be taken into account for calculating the partition function is the symmetry number of the puckering mode. For cyclobutane this number amounts to two due to the symmetrical shape of the potential function and due to indistinguishable stable conformers at $+30°$ and $-30°$ of the puckering angle; both conditions are needed to allow the use of a symmetry number. The global effect is only a slight increase of the partition function, due to the compensating effect of the double degeneracy and the symmetry number. For oxetane the partition function decreases by approximately two in the HR approximation. The energy levels are only slightly altered but the major effects originate from the symmetry number of two. For azetidine, the puckering potential is not symmetric and only a slight increase of the partition function is noticed.

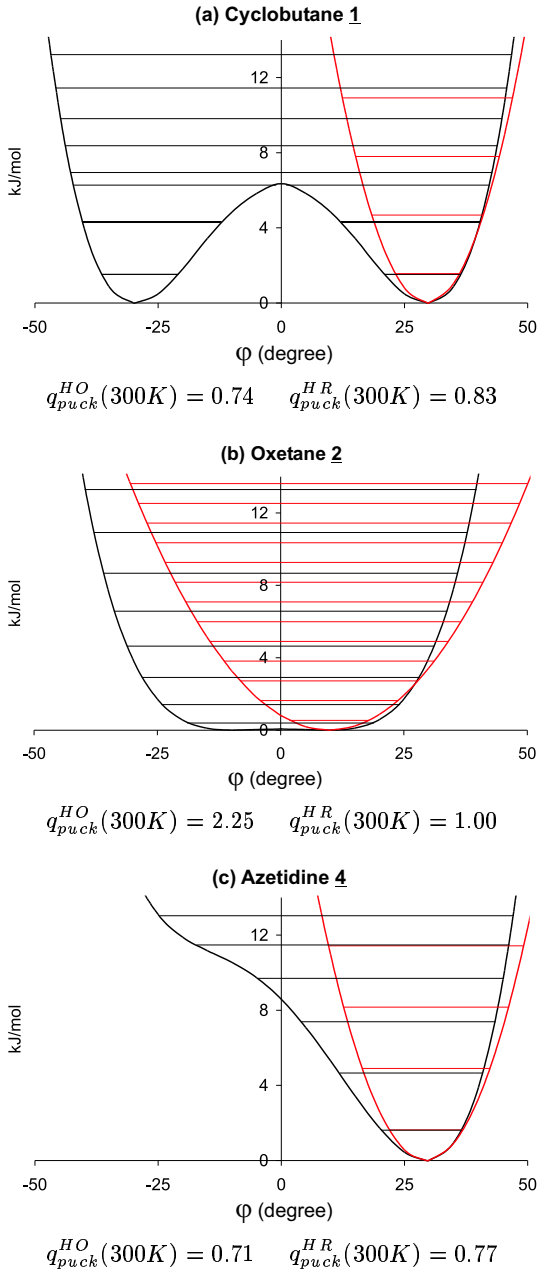

Figure 8.4: Energy levels in the HO (red) and 1D-HR (black) approach for (a) cyclobutane **1**, (b) oxetane **2**, and (c) azetidine **4**.

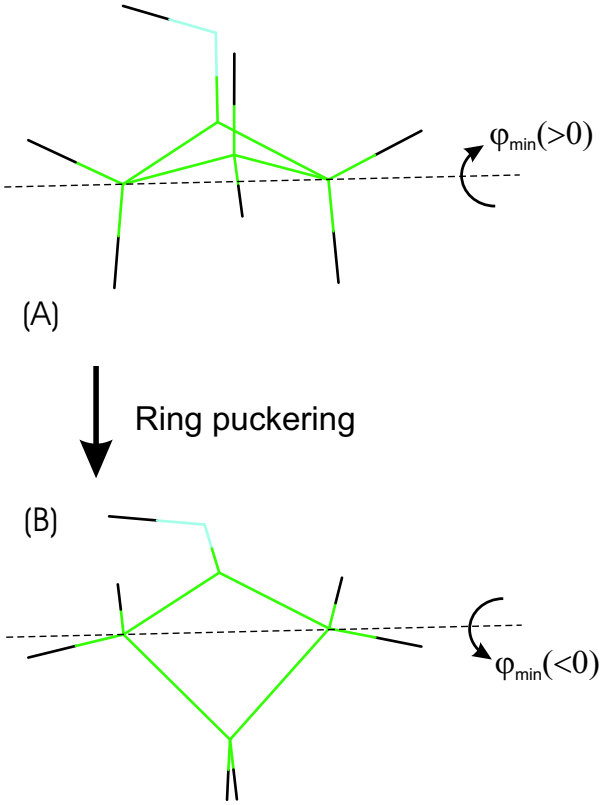

Figure 8.5: Two possible distinct conformers (A,B) accessible through ring puckering. Starting from A, conformer B cannot be reached using global rotation only.

To understand the results of cyclobutylideneamine (**8**) and cyclobutylidenephosphine (**9**) (Fig.8.3) one important remark needs to be made about the symmetry number of the puckering mode. Also for these molecules the ring inversion is characterized by a double symmetrical well potential, but the conformers at positive and negative values of the puckering angle are now geometrically different. The N-H (P-H) bond of the imine (phosphine) moiety is either oriented to the front or the back of the molecule, as schematically shown in figure 8.5. In this case no symmetry number may be applied. This explains the large influence of the HR model on the partition function for these molecules as in the HO approach only half of the conformers is taken into account.

Thermodynamic quantities Some results for the entropy and heat capacity are listed in Table 8.3 in the HO and HR approximation together with the experimental values when available. The heat capacity is nearly unaffected by the method for constructing the partition function. The origin must be traced back to the large separation between the lowest and next lowest frequency mode in the vibrational spectrum. It is generally known that for the heat capacity not only low frequencies are important but also a range of intermediate modes. The latter are not present for the studied molecules resulting in a good performance of the HO approximation for the heat capacity. The heat capacity of phosphetane (**5**) (at 298.15K) is somewhat more affected, due to the presence of the second conformer which is not described in the HO approach.
The entropy is more affected, e.g. in case of oxetane a correction of 9 J/mol/K is observed bringing the prediction closer to the experiment.

The ab initio results of Table 8.3 are calculated using the selected mPW1B95 /6-31+G(d,p) level of theory. The selection of this level was based on its capability of reproducing the correct geometry and potential barrier height. It is now instructive to examine the influence of other ab initio levels in reproducing the entropy. For this purpose the entropy of cyclobutane and oxetane, for which experimental estimates are available, are calculated with the B3LYP, PBE1PBE and B1B95 functionals (all combined with the 6-31+g(d,p) basis set). Results are given in Table 8.4. The correction due to 1D-HR can be very large and may strongly vary depending on the level of theory. In oxetane the 1D-HR corrections with respect to HO fluctuate from 9 to 22 J/mol/K. The final 1D-HR predictions of the entropies, however, are all close to each other and are in reasonable agreement with experiment.

mPW1B95	S(298,15K)	C(298,15K)	C(600K)
cyclobutane 1			
exp. (Ref.[23])	265.39	73.35	140.00
HO	262.43	68.46	140.86
1D-HR	263.70	68.34	138.89
oxetane 2			
exp. (Ref.[23])	265.26	61.99	119.60
exp. (Ref.[24])	-	61.50	121.31
HO	278.63	61.36	119.87
1D-HR	269.61	59.07	117.61
thietane 3			
exp. (Ref.[23])	-	69.24	127.23
HO	283.94	68.05	125.76
1D-HR	284.30	65.94	123.08
azetidine 4			
exp.	-	-	-
HO	271.46	64.55	130.20
1D-HR	273.10	66.76	131.39
phosphetane 5			
exp.	-	-	-
HO	285.32	75.37	140.50
1D-HR	289.28	80.62	141.32
cyclobutanone 6			
exp. (Ref.[24])	-	74.31	139.91
HO	298.43	78.42	142.11
1D-HR	291.94	76.17	140.00
cyclobutanethione 7			
exp.	-	-	-
HO	305.84	81.16	144.99
1D-HR	304.04	78.60	142.53
cyclobutylideneamine 8			
exp.	-	-	-
HO	296.78	80.84	151.73
1D-HR	299.32	78.26	149.31
cyclobutylidenephosphine 9			
exp.	-	-	-
HO	308.14	87.54	158.09
1D-HR	314.70	85.87	155.62

Table 8.3: Experimental and calculated values of entropy S and heat capacity C at temperatures defined between brackets. All units in J/mol/K.

S(298,15K)	mPW1B95	B3LYP	PBE1PBE	B1B95
cyclobutane 1				
exp. (Ref.[23])	265.39	265.39	265.39	265.39
HO	262.43	263.66	262.99	262.93
1D-HR	263.70	264.59	264.14	264.14
oxetane 2				
exp. (Ref.[23])	265.26	265.26	265.26	265.26
HO	278.63	283.18	284.91	280.19
1D-HR	269.61	261.21	269.79	270.13

Table 8.4: Experimental and calculated values of entropy S at 298.15K for different levels of theory with the 6-31+G(d,p) basis set. All units in J/mol/K.

8.4 Conclusion

In this chapter we have adapted the Hindered Rotor approach for flexible chains to four-membered rings. The latter molecules exhibit one low vibrational mode which corresponds to the puckering vibration. The puckering potentials may vary largely in terms of the hetero-element that is introduced in the ring. Most molecules are characterized by a double well symmetrical potential except azetidine and phosphetane. Depending on the system of interest the partition function may be doubled or halved. The symmetry of the ring inversion and the shape of the potential determine the final result. The entropy undergoes the largest influence of treating the puckering mode in the HR model whereas the heat capacity is nearly unaffected.
We found that the thermodynamic properties are only affected to a minor extent by the level of theory, provided the 1D-HR model is used.

Chapter 9

The extended hindered rotor model

This chapter is based on Ref.[22]:

Vansteenkiste, P.; Van Neck, D.; Van Speybroeck, V.
and Waroquier, M.
J. Chem. Phys. **2006**, *124*, Art. No. 044314

Abstract

Large-amplitude motions, particularly internal rotations, are known to affect substantially thermodynamic functions and rate constants of reactions in which flexible molecules are involved. Up to now all methods for computing the partition functions of these motions rely on the Pitzer approximation of more than 50 years ago, in which the large-amplitude motion is treated in complete independence of the other (vibrational) degrees of freedom. In this chapter an extended hindered-rotor model (EHR) is developed in which the vibrational modes, treated harmonically, are correctly separated from the large-amplitude motion, and in which relaxation effects (the changes in the kinetic energy matrix and potential curvature) are taken into account as one moves along the large-amplitude path. The model also relies on a specific coordinate system in which the Coriolis terms vanish at all times in the Hamiltonian. In this way an increased level of consistency between the various internal modes is achieved, as compared to the more usual hindered-rotor (HR) description. The method is illustrated by calculating the entropies and heat capacities on 1,3-butadiene and 1-butene (with respectively one and two internal rotors) and the rate constant for the addition reaction of a vinyl radical to ethene. We also discuss various variants of the one-dimensional hindered rotor (1D-HR) scheme existing in the literature, and its relation with the EHR model. It is argued why in most cases the HR approach is already quite successful.

9.1 Introduction

In standard ab initio calculations the molecular partition function, from which all thermodynamic molecular properties can be derived, is constructed using the independent harmonic oscillator (HO) approximation. This description is adequate when only small deviations from the equilibrium geometry are relevant (*i.e.* low temperatures, or steep potentials). Basically the HO model only needs information which can be derived from the equilibrium geometry. The low vibrational spectrum of most molecules is characterized by some large-amplitude vibrations that give rise to large deviations from the equilibrium configuration. Among them internal rotations (IR) about single bonds are certainly the most important. They have been the subject of extensive studies in the literature since decades. As the shape of the rotational potential gives rise to various stable conformers, the consideration of a quadratic form of the potential (as harmonic oscillator) is no longer meaningful and can lead to partition functions which largely deviate from the real ones. Instead of the HO-approach one often applies a variant of the hindered rotor model (HR).

This HR model is usually implemented in one dimension (1D-HR). The potential energy becomes a function in the selected coordinate, and may generate multiple local energy minima (conformers). Initially this potential energy was calculated as a rigid rotation, but nowadays it is obtained from a potential energy scan in which the geometry is allowed to relax. The kinetic energy is completely determined by the moments of inertia, but the method of calculating the latter varies in different approximative schemes.
The simplest approximation was suggested by Pitzer [26, 15, 27, 28, 29, 30] and has become a method of general use for one-dimensional treatment of internal rotors. Only the coupling with the overall rotation is taken into account, and neither relaxation effects nor coupling with other internal modes are involved. The calculation of the moments of inertia is based on the reference geometry, and it is further assumed that these moments remain fixed along the large-amplitude path. Despite the apparent inconsistency between the kinetic energy (with fixed moments of inertia) and the variable potential energy, this method led to good predictions for the entropy and heat capacity of n-alkanes [14].
Pitzer also suggested a multidimensional treatment of the rotors. We applied this scheme (nD-HR) for pentane and hexane [16, 17] making use of the classical expression for the partition function as elaborated by Eidinoff and Aston

[71]. At this stage the reduced moments of inertia are constructed from the full kinetic energy matrix of the overall rotation and subsequent internal rotors, and represent functions of the rotational angles. This scheme represents a step forward in a more advanced and consistent description of IR's as the coupling between the overall rotation and internal rotors is taken into account, but coupling between the internal rotations and the other vibrations in the molecule is still ignored.
An overview of the several possibilities to construct (reduced) moments is given by East and Radom [5].

Although the HR method can easily be implemented, this procedure still has some practical drawbacks [6]. For the calculation of molecular properties all vibrational modes are needed, whereas the HR method is applied only to some specific large amplitude motions and thus does not provide a full description. The other vibrational modes are still treated with the HO method. Usually one replaces the harmonic modes corresponding with the internal rotation by its HR description, but the identification of these HO-modes may be problematic for larger molecules since most of the low vibrational normal modes are mixtures of several internal rotations and other vibrations. A good illustration is the propagation kinetics of polyethylene in which large alkyl chains are involved (Scheme 1). In these long chain molecules no clear identification

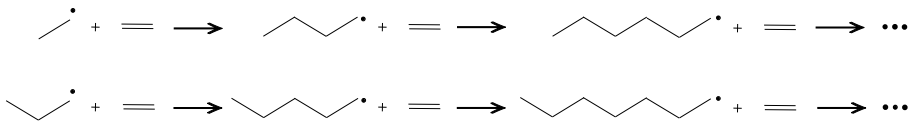

Scheme 1

of separate internal rotations is possible, due to a strong mixing among torsional modes and other skeletal vibrations [146]. It was shown that the 1D-HR model fails dramatically when used in conjunction with the HO frequencies obtained as output of a standard ab initio calculation. The propagation rate constant diverges for an increasing length of the alkyl chain, whereas all experiments point to a convergent behavior. The problem can be solved in a computationally attractive way by using one-dimensional HO predictions q_{HO}^{1D} that are obtained using the second derivative of the rotational potential at the equilibrium position along the 1D path of the torsional angle. However, the method is still not fully consistent, in the sense that the normal mode found

by solving the complete multi-dimensional normal mode problem differs from the one-dimensional solution.
In Ref.[6] of Ayala and Schlegel, a method is presented for the identification and treatment of internal rotations in a normal mode vibrational analysis. A commonly committed error is that normal modes are inspected in terms of Cartesian coordinates instead of internal coordinates, frequently yielding wrong information. Ayala and Schlegel proposed a method for correcting for these effects. They construct a projector that removes all internal coordinates corresponding to bond stretches and bond angles, leaving only bond torsions (IR's). Then the normal mode problem is solved yielding the projected vibrational frequencies and corresponding HO partition functions. Replacing these last values by those predicted by the IR's, an important correction is obtained for the partition function, and a valuable step is made in a consistent treatment of IR's and their impact on thermodynamic properties.
To some extent this model removes the inconsistency involved in the commonly used correction factor q_{HR}^{1D}/q_{HO}^{mD} for the partition function, where q_{HO}^{mD} corresponds to the normal mode found by solving the complete multi-dimensional normal mode problem. This can give rise to large inaccuracies since the multi-dimensional solution differs from the one-dimensional mode: $q_{HO}^{1D} \neq q_{HO}^{mD}$. The determination of the one-dimensional HO prediction q_{HO}^{1D} of the partition function of the vibrational mode which is replaced by an IR, also requires the calculation of the *effective* moment of inertia, more specifically the same moment as for the evaluation of q_{HR}^{1D}.
Clearly, it should be useful to have a method that treats all low vibrational modes without inconsistencies or the need of *ad hoc* factors.

In addition to the problem of the large-amplitude vibrations, much attention has been devoted to include rotational-vibrational coupling within the same framework. These approaches focus on the calculation of energy levels and are all based on the work of Watson [149]. In particular we mention the work of Bowman and co-workers [150] and Gerber and co-workers [151]. In these procedures, the Coriolis coupling terms add crucially to the complexity of the description, and are usually ignored.
In 1989 Jellinek and Li emphasized the problem of separability of the global rotation and internal motion and proposed an exact description in which there exists a complete instantaneous separation of energies such that the Coriolis term in the Hamiltonian is zero at all times [152]. Our implementation as proposed in the current chapter turns out to coincide with the principles of the

Jellinek description. A general Z-matrix-like internal coordinate system (3N-6 variables) is introduced and connected with the global variables (translation, global rotation) by imposing appropriate conditions. These are **conservation of momentum and angular momentum** under internal reorganization.

In practice, one needs to introduce two body-fixed frames:

(i) frame (1) coinciding with the center of mass (at all times) and representing the global motion, and

(ii) frame (2) attached to the reference atoms chosen for determining the internal coordinates.

Frame (1) is defined in such a way that the atomic velocities in this frame do not contribute to the total linear and angular momentum of the system. The resulting classical description of the kinetic energy will be derived in the next section.

In the second part of the theory, an extended HR description (EHR) is introduced which is based on the exact (classical) kinetic energy description in combination with an appropriate approximation of the potential energy for one internal rotor. The rotational potential is written as a one-dimensional function $V^{HR}(\varphi)$, as usually done in the standard HR model, but in the other 3N-7 coordinates (orthogonal to the large-amplitude path) a quadratic approximation is used resulting in a φ-dependent Hessian for the vibrational degrees of freedom. Since our main interest goes to the accurate determination of thermodynamic and kinetic quantities derived from the partition function, the whole scheme is solved classically except for the small-amplitude vibrations that are treated quantum mechanically. The classical solution implies that the traditional interpretation of the energy levels is given up.
The proposed EHR model has the merit of a consistent treatment of the harmonic oscillator and hindered rotor description, integrated in one unified model, and also fully incorporates the variation of the geometry by means of variable (internal and principal) moments of inertia for **all** modes.
In this chapter we also examine how the global partition function in the 1D-HR scheme is related to its EHR counterpart, and why the former yields good results in most of the cases.
The EHR model will be validated on its capability of reproducing thermodynamic quantities such as entropy and heat capacity in 1,3-butadiene in which only one rotor is present and for which experimental data are available. The EHR model is easily extended to multiple internal rotors. This is demonstrated

on 1-butene, in which two internal rotors are present.
Another quantity of interest is the frequency factor of the reaction rate. The reaction rate is directly proportional to the partition function of the transition state. In the case if addition reactions *e.g.*, the rate is sensitive to the details of the description of the additional internal rotation about the forming bond. The importance of internal rotations in the transition state is well documented in the literature for addition reactions of radicals to olefins [2, 44, 35]. In this chapter we demonstrate the impact of the coupling with the other vibrational modes on the addition of a vinyl radical to ethene.

9.2 Theory

9.2.1 Classical kinetic energy

In order to derive the classical kinetic energy for a molecule with N atoms, one needs to introduce appropriate variables of motion. In a Z-matrix-like formulation, it is possible to define $n = 3N - 6$ internal coordinates θ_i, describing the internal structure of the molecule related to a frame B' that is determined by the three first atoms. The absolute position of atom 1 is taken as the origin $O_{B'}$, while the vector $\vec{r}_{12}$ between atom 1 and atom 2 determines the $X_{B'}$-axis, and the component of $\vec{r}_{23}$ perpendicular to this axis determines the $Y_{B'}$-axis. In this way, the coordinates of atom A in the space-fixed frame S are described by the vector:

$$\vec{r}_A^{(S)} = \vec{r}_{O_{B'}}^{(S)} + \bar{R}_{B'S} \cdot \vec{r}_A^{(B')}(\theta_i) \tag{9.1}$$

where $\bar{R}_{B'S}$ is the rotational tensor between the orientation of the axes in frame B' and S. It is convenient to introduce an additional frame B, that at a given time ($t = 0$) coincides with the center of mass (CM) and is oriented along the principal axes of the molecule, but with as yet unspecified dynamics. The coordinates in frame S can be expressed as

$$\begin{aligned} \vec{r}_A^{(S)} &= \vec{r}_{O_B}^{(S)} + \bar{R}_{BS} \cdot \vec{r}_A^{(B)} \\ &= \vec{r}_{O_B}^{(S)} + \bar{R}_{BS} \cdot \left(\vec{r}_{O_{B'}}^{(B)} + \bar{R}_{B'B} \cdot \vec{r}_A^{(B')}(\theta_i) \right), \end{aligned} \tag{9.2}$$

and the velocity of atom A in the S-frame becomes:

$$\begin{aligned} \dot{\vec{r}}_A^{(S)} &= \dot{\vec{r}}_{O_B}^{(S)} + \dot{\bar{R}}_{BS} \cdot \vec{r}_A^{(B)} \\ &\quad + \bar{R}_{BS} \cdot \left(\dot{\vec{r}}_{O_{B'}}^{(B)} + \dot{\bar{R}}_{B'B} \cdot \vec{r}_A^{(B')} + \bar{R}_{B'B} \cdot \dot{\vec{r}}_A^{(B')} \right). \end{aligned} \tag{9.3}$$

The velocity of atom A in the B'-frame has the generic form

$$\dot{\vec{r}}_A^{(B')} = \sum_i \frac{\partial \vec{r}_A^{(B')}}{\partial \theta_i} \dot{\theta}_i = \sum_i \vec{U}_i^{(B')}(A)\, \dot{\theta}_i. \tag{9.4}$$

For practical calculations, the n internal coordinates in the Z-matrix formalism can be divided into three classes: dihedral angle, bond angle or bond length.

(i) The first two classes correspond with rotations about an axis lying along a bond (changes in dihedral), or about an axis perpendicular to the plane formed by two bonds (changes in bond angle). The velocity (in frame

B') of atom A subject to these two rotations can be expressed in terms of an angular velocity $\vec{\omega}_i$ as follows:

$$\begin{aligned} \vec{U}_i^{(B')}(A)\,\dot{\theta}_i &= \vec{\omega}_i^{\,(B')} \times \left(\vec{r}_A^{\,(B')} - \vec{r}_{O_i}^{\,(B')}\right) \\ &= \bar{\chi}^{(B')}(A - O_i) \cdot \vec{\omega}_i^{\,(B')} \end{aligned} \tag{9.5}$$

where O_i is the origin of the rotation (lies on the $\vec{\omega}_i$-axis), and $\bar{\chi}^{(B')}$ represents a tensor with matrix representation

$$\bar{\chi}^{(B')}(A - O_i) = \tag{9.6}$$

$$\begin{bmatrix} 0 & +(z_A^{(B')} - z_{O_i}^{(B')}) & -(y_A^{(B')} - y_{O_i}^{(B')}) \\ -(z_A^{(B')} - z_{O_i}^{(B')}) & 0 & +(x_A^{(B')} - x_{O_i}^{(B')}) \\ +(y_A^{(B')} - y_{O_i}^{(B')}) & -(x_A^{(B')} - x_{O_i}^{(B')}) & 0 \end{bmatrix}$$

for any atom A submitted to this rotation. It is equal to zero for any other atom A. The unit vector of the angular velocity $\vec{\omega}_i^{\,(B')} = \vec{e}_{\omega_i}^{\,(B')}(\theta_1, \ldots, \theta_n)\,\dot{\theta}_i$ depends on the internal geometry.

(ii) The third class of internal coordinates corresponds to a bond stretch, and results in a constant contribution to the velocity

$$\vec{U}_i^{(B')}(A)\,\dot{\theta}_i = \vec{v}_i^{\,(B')} = \vec{e}_{v_i}^{\,(B')}(\theta_1, \ldots, \theta_n)\,\dot{\theta}_i. \tag{9.7}$$

Note that $\vec{U}_i^{\,(B')}(A)$ represents a vector and that a transformation to any other frame is accordingly given by: $\vec{U}_i^{(S)}(A) = \bar{R}_{B'S} \cdot \vec{U}_i^{(B')}(A)$.

The time-derivatives of the rotation tensors appearing in Eq.(9.3) can be reformulated, using $\bar{\chi}$ tensors, as

$$\dot{\bar{R}}_{BS} \cdot \vec{r}_A^{\,(B)} = \bar{\chi}^{(S)}(A - O_B) \cdot \vec{\omega}^{\,(S)} \tag{9.8}$$

$$\dot{\bar{R}}_{B'B} \cdot \vec{r}_A^{\,(B')} = \bar{\chi}^{(B)}(A - O_{B'}) \cdot \vec{\nu}^{\,(B)} \tag{9.9}$$

where we introduced two rotation vectors $\vec{\omega}^{\,(S)}$ and $\vec{\nu}^{\,(B)}$ controlling the rotation of frame B relative to S, and of frame B' relative to B.
The velocity of atom A can now be written as

$$\dot{\vec{r}}_A^{\,(S)} = \dot{\vec{r}}_{O_B}^{\,(S)} + \bar{\chi}^{(S)}(A - O_B) \cdot \vec{\omega}^{\,(S)} + \bar{R}_{BS} \cdot \dot{\vec{r}}_A^{\,(B)}, \tag{9.10}$$

$$\dot{\vec{r}}_A^{\,(B)} = \dot{\vec{r}}_{O_{B'}}^{\,(B)} + \bar{\chi}^{(B)}(A - O_{B'}) \cdot \vec{\nu}^{\,(B)} + \sum_i \vec{U}_i^{(B)}(A)\,\dot{\theta}_i. \tag{9.11}$$

In this expression the relative motion of B and B' is described by the vectors $\dot{\vec{r}}_{O_{B'}}^{\,(B)}$ and $\vec{\nu}^{\,(B)}$, and can be eliminated by imposing suitable conditions on the

B-frame. Apart from the initial conditions at $t = 0$, the dynamics of the B-frame is at this point still unspecified. In the simple case of a rigid body frame B' is fixed to B and the angular velocity $\vec{\nu}^{(B)}$ disappears. Only one contribution remains (terms with $\vec{\omega}^{(S)}$) describing the overall rotation of the molecule. In the present case of a nonrigid molecule, we still would like frame B to refer exclusively to the overall rotation (and translation), by imposing certain conditions on its dynamics. In particular, we impose that total momentum and angular momentum of the molecule are vanishing in frame B:

$$\sum_A m_A \dot{\vec{r}}_A^{(B)} = 0 \tag{9.12}$$

$$\sum_A m_A \vec{r}_A^{(B)} \times \dot{\vec{r}}_A^{(B)} = 0. \tag{9.13}$$

In addition to these constraints we assume that the origin of frame B coincides at $t = 0$ with the CM. The first condition (9.12) leads to $\vec{r}_{CM}^{(B)} = \sum_A m_A \vec{r}_A^{(B)}/M = 0$ for all times t and ensures that the origin of frame B remains in the CM. From Eq.(9.2) it then follows that $\vec{r}_{O_B}^{(S)} = \vec{r}_{CM}^{(S)}$. Deriving the CM velocity from Eq.(9.11),

$$\begin{aligned} M\dot{\vec{r}}_{CM}^{(S)} &= \sum_A m_A \dot{\vec{r}}_A^{(S)} \\ &= M\dot{\vec{r}}_{O_B}^{(S)} + \bar{\chi}^{(S)} \left(\sum_A m_A \vec{r}_A^{(S)} - M\vec{r}_{O_B}^{(S)} \right) \cdot \vec{\omega}^{(S)} \\ &\quad + \bar{R}_{BS} \cdot \left[M\dot{\vec{r}}_{O_{B'}}^{(B)} + \bar{\chi}^{(B)} \left(\sum_A m_A \vec{r}_A^{(B)} - M\vec{r}_{O_{B'}}^{(B)} \right) \cdot \vec{\nu}^{(B)} \right. \\ &\quad \left. + \sum_i \sum_A m_A \vec{U}_i^{(B)}(A) \dot{\theta}_i \right] \end{aligned} \tag{9.14}$$

it is clear that condition (9.12) is equivalent with

$$\dot{\vec{r}}_{O_{B'}}^{(B)} = -\bar{\chi}^{(B)}(-O_{B'}) \cdot \vec{\nu}^{(B)} - \frac{1}{M} \sum_i \left(\sum_A m_A \vec{U}_i^{(B)}(A) \right) \dot{\theta}_i \tag{9.15}$$

Defining, for each internal coordinate, $\vec{W}_i^{(B)} = \sum_A m_A \vec{U}_i^{(B)}(A)$, one may rewrite the velocity of atom A as

$$\begin{aligned} \dot{\vec{r}}_A^{(S)} &= \dot{\vec{r}}_{CM}^{(S)} + \bar{\chi}^{(S)}(A - CM) \cdot \vec{\omega}^{(S)} + \bar{R}_{BS} \cdot \dot{\vec{r}}_A^{(B)} \\ \dot{\vec{r}}_A^{(B)} &= \bar{\chi}^{(B)}(A) \cdot \vec{\nu}^{(B)} + \sum_i (\vec{U}_i^{(B)}(A) - \frac{1}{M} \vec{W}_i^{(B)}) \, \dot{\theta}_i. \end{aligned} \tag{9.16}$$

This means that the 'freedom' of rotation of frame B' relative to B is restricted to rotation axes through the origin of B or, equivalently, the center of mass. Also, there is a correction to $\vec{U}_i$ in order to keep the center of mass at O_B.

The remaining unknown quantity $\vec{\nu}^{(B)}$ is determined by the angular momentum condition (9.13). Using the $\bar{\chi}$ tensor formulation, this constraint is rewritten as:

$$\sum_A m_A \vec{r}_A^{(B)} \times \dot{\vec{r}}_A^{(B)} = -\sum_A m_A \bar{\chi}^{(B)}(A) \cdot \dot{\vec{r}}_A^{(B)} = 0. \tag{9.17}$$

Replacing $\dot{\vec{r}}_A^{(B)}$ with Eq.(9.16), we get

$$\sum_A m_A \bar{\chi}^{(B)}(A) \cdot \left(\bar{\chi}^{(B)}(A) \cdot \vec{\nu}^{\,(B)} \right) = \tag{9.18}$$
$$-\sum_i \sum_A m_A \bar{\chi}^{(B)}(A) \cdot (\vec{U}_i^{(B)}(A) - \frac{1}{M} \vec{W}_i^{(B)})\, \dot{\theta}_i.$$

This leads to the determination of the angular velocity $\vec{\nu}^{\,(B)}$ in terms of the inertial tensor $\bar{I}$,

$$\vec{\nu}^{\,(B)} = -\sum_i \left(\bar{I}^{(B)} \right)^{-1} \cdot \vec{X}_{0i}^{(B)}\, \dot{\theta}_i, \tag{9.19}$$

with

$$\begin{aligned} \bar{X}_{00}^{(B)} &= \sum_A m_A \bar{\chi}^{(B)}(A) \cdot \bar{\chi}^{(B)}(A) = \bar{I}^{(B)} \\ \vec{X}_{0i}^{(B)} &= \sum_A m_A \bar{\chi}^{(B)}(A) \cdot \vec{U}_i^{(B)}(A). \end{aligned}$$

The final expression for the velocity of atom A reads

$$\begin{aligned} \dot{\vec{r}}_A^{(S)} &= \dot{\vec{r}}_{CM}^{(S)} + \bar{\chi}^{(S)}(A - CM) \cdot \vec{\omega}^{\,(S)} \\ &+ \sum_i \left(\vec{U}_i^{(S)}(A) - \frac{1}{M} \vec{W}_i^{(S)} - \bar{\chi}^{(S)}(A - CM) \cdot \left(\bar{I}^{(S)} \right)^{-1} \cdot \vec{X}_{0i}^{(S)} \right) \dot{\theta}_i \end{aligned} \tag{9.20}$$

An interesting feature to note is that the B-frame turns out to coincide exactly with the frame introduced by Jellinek [152] but based upon different grounds. It is easy to show, *e.g.*, that by virtue of Eqs.(9.13) and (9.16), the total angular momentum with respect to the CM,

$$\begin{aligned} \vec{L}^{(S)} &= \sum_A m_A (\vec{r}_A^{(S)} - \vec{r}_{CM}^{(S)}) \times (\dot{\vec{r}}_A^{(S)} - \dot{\vec{r}}_{CM}^{(S)}) \\ &= \sum_A m_A (\vec{r}_A^{(S)} - \vec{r}_{CM}^{(S)}) \times [\vec{\omega}^{(S)} \times (\vec{r}_A^{(S)} - \vec{r}_{CM}^{(S)})] = \bar{I}^{(S)} \cdot \vec{\omega}^{(S)} \end{aligned} \tag{9.21}$$

is at each instant the same as that of a rigid body with inertial tensor $\bar{I}$ and angular velocity $\vec{\omega}^{(S)}$.
The kinetic energy $T = \frac{1}{2}\sum_A m_A \dot{\vec{r}}_A^{(S)} \cdot \dot{\vec{r}}_A^{(S)}$ can now be worked out as:

$$\begin{aligned} T &= \frac{1}{2}\vec{\omega}\cdot\bar{I}\cdot\vec{\omega} + \frac{M}{2}(\dot{\vec{r}}_{CM})^2 \\ &\quad + \frac{1}{2}\sum_i\sum_j \dot{\theta}_i\dot{\theta}_j \Big(X_{ij} - \vec{W}_i\cdot\frac{1}{M}\vec{W}_j - \vec{X}_{0i}\cdot\bar{I}^{-1}\cdot\vec{X}_{0j} \\ &\quad - \frac{1}{M}\vec{W}_i\cdot\vec{W}_j + \frac{M}{M^2}\vec{W}_i\cdot\vec{W}_j + \frac{1}{M}\vec{W}_i\cdot M\bar{\chi}(CM-CM)\cdot\bar{I}^{-1}\cdot\vec{X}_{0j} \\ &\quad - \vec{X}_{0i}\cdot\bar{I}^{-1}\cdot\vec{X}_{0j} + \vec{X}_{0i}\cdot\bar{I}^{-1}\cdot M\bar{\chi}(CM-CM)\cdot\frac{1}{M}\vec{W}_j \\ &\quad + \vec{X}_{0i}\cdot\bar{I}^{-1}\cdot\bar{I}\cdot\bar{I}^{-1}\cdot\vec{X}_{0j}\Big) \\ &\quad + M\dot{\vec{r}}_{CM}\cdot\bar{\chi}(CM-CM)\cdot\vec{\omega} \\ &\quad + M\dot{\vec{r}}_{CM}\cdot\sum_i\left(\frac{1}{M}\vec{W}_i - \frac{1}{M}\vec{W}_i - \bar{\chi}(CM-CM)\cdot\bar{I}^{-1}\cdot\vec{X}_{0i}\right)\dot{\theta}_i \\ &\quad + \vec{\omega}\cdot\sum_i\left(\vec{X}_{0i} - \bar{\chi}(CM-CM)\cdot\vec{W}_i - \bar{I}\cdot\bar{I}^{-1}\cdot\vec{X}_{0i}\right)\dot{\theta}_i \end{aligned} \tag{9.22}$$

with the additional definition

$$X_{ij} = \sum_A m_A \vec{U}_i(A)\cdot\vec{U}_j(A). \tag{9.23}$$

In the above expression many contributions cancel each other, and the final result is simply

$$\begin{aligned} T &= \frac{1}{2}\vec{\omega}\cdot\bar{I}\cdot\vec{\omega} + \frac{M}{2}(\dot{\vec{r}}_{CM})^2 \\ &\quad + \frac{1}{2}\sum_i\sum_j\left(X_{ij} - \vec{W}_i\cdot M^{-1}\,\vec{W}_j - \vec{X}_{0i}\cdot\bar{I}^{-1}\cdot\vec{X}_{0j}\right)\dot{\theta}_i\dot{\theta}_j \end{aligned} \tag{9.24}$$

Note that no Coriolis contributions (terms of the form $\vec{\omega}\dot{\theta}_i$) are present in Eq.(9.24), and that all quantities involved are rotational scalars. In particular the coefficients of the $\dot{\theta}_i\dot{\theta}_j$ terms only depend on the geometry, *i.e.* on the internal coordinate vector $\Theta = (\theta_1, .., \theta_n)^T$. In matrix form, the internal part of the kinetic energy can therefore be written as

$$T_{int} = \frac{1}{2}\dot{\Theta}^T A_\Theta(\theta_1, \ldots, \theta_n)\dot{\Theta}. \tag{9.25}$$

The expression of the kinetic energy [Eq.(9.24)] shows a separation between the internal motions and the overall rotation and translation. It can be argued that

this is the only meaningful definition of internal motion when large-amplitude deviations from the equilibrium geometry are present. The drawback, of course, lies in the fact that $\vec{\omega}$ is a function of both the positions and velocities of the atoms, and cannot be defined as the time derivative of some generalized coordinate.

If one considers systems at definite angular momentum, the centrifugal term $\vec{\omega} \cdot \bar{I} \cdot \vec{\omega}/2 = \vec{L} \cdot (\bar{I})^{-1} \cdot \vec{\omega}/2$ can be taken as an additional potential influencing the internal motion. For the present applications to partition functions and thermodynamic properties we will only take the average effect of the centrifugal term into account in the total partition function. For the contribution of the internal modes we further concentrate on the system with $\vec{L} = 0$.

9.2.2 Extended hindered rotor model (EHR)

To illustrate the utility and efficiency of the extended hindered rotor model (EHR) we further elaborate on the case of one internal rotation. The presented theory can easily be extended to multiple large-amplitude motions.
If we define $\varphi = \theta_1$ to be the dihedral angle associated with the internal rotation, the potential energy profile $V^{HR}(\varphi)$ is a function of this coordinate only. The standard procedure to obtain $V^{HR}(\varphi)$ is to perform a constrained optimization with the angle φ fixed at various values. This approach, in which all variables except φ are allowed to relax, yields the equilibrium values $\theta_i^{eq}(\varphi)$ of the other variables as a function of φ. They may differ from the values of the internal coordinates θ_i corresponding with the most stable conformation ($\varphi = 0$) and the deviations

$$\tau_i \quad = \quad \theta_i - \theta_i^{eq}(\varphi). \tag{9.26}$$

may be regarded as new coordinates. It is now a reasonable approximation to expand, for each value of φ, the potential energy variation in the vibrational coordinates τ_i up to second order,

$$V^{tot}(\varphi, \tau) = V^{HR}(\varphi) + \frac{1}{2}\tau^T H^{vib}(\varphi)\tau \tag{9.27}$$

The matrix $H^{vib}(\varphi)$ is the Hessian of the remaining vibrations as a function of φ. To the same level of approximation the kinetic matrix A_Θ in Eq.(9.25) should be evaluated along the large-amplitude path with $\theta_i = \theta_i^{eq}(\varphi)$, and depends only on φ. Using the fact that

$$\dot{\tau}_i = \dot{\theta}_i - \frac{\partial \theta_i^{eq}}{\partial \varphi}\dot{\varphi}, \tag{9.28}$$

the internal kinetic energy in the new variables becomes:

$$T_{int} = \frac{1}{2}\begin{bmatrix} \dot{\varphi} & \dot{\tau}^T \end{bmatrix} A(\varphi) \begin{bmatrix} \dot{\varphi} \\ \dot{\tau} \end{bmatrix} \tag{9.29}$$

with the transformed kinetic energy matrix given by

$$A(\varphi) = \begin{pmatrix} 1 & \frac{\partial \theta_2^{eq}}{\partial \varphi} & \dots & \frac{\partial \theta_n^{eq}}{\partial \varphi} \\ 0 & 1 & 0 & 0 \\ \vdots & 0 & \ddots & \vdots \\ 0 & 0 & \dots & 1 \end{pmatrix} A_\Theta \begin{pmatrix} 1 & 0 & \dots & 0 \\ \frac{\partial \theta_2^{eq}}{\partial \varphi} & 1 & 0 & 0 \\ \vdots & 0 & \ddots & \vdots \\ \frac{\partial \theta_n^{eq}}{\partial \varphi} & 0 & \dots & 1 \end{pmatrix} = \begin{pmatrix} A_{\varphi\varphi} & A_{\varphi\tau} \\ A_{\tau\varphi} & A_{\tau\tau} \end{pmatrix}. \tag{9.30}$$

The total energy $E_{tot} = E_{tr} + E_{rot} + E_{int}$ can now be written as

$$E_{tr} = \frac{1}{2}M\left(\dot{x}_{CM}^2 + \dot{y}_{CM}^2 + \dot{z}_{CM}^2\right) \tag{9.31}$$

$$E_{rot} = \frac{1}{2}\omega^T I(\varphi)\omega \tag{9.32}$$

$$E_{int} = \frac{1}{2}\begin{bmatrix} \dot{\varphi} & \dot{\tau}^T \end{bmatrix} A(\varphi) \begin{bmatrix} \dot{\varphi} \\ \dot{\tau} \end{bmatrix} + V^{HR}(\varphi) + \frac{1}{2}\tau^T H^{vib}(\varphi)\tau \tag{9.33}$$

$$= \frac{1}{2}\begin{bmatrix} p_\varphi & P_\tau^T \end{bmatrix} A^{-1}(\varphi) \begin{bmatrix} p_\varphi \\ P_\tau \end{bmatrix} + V^{HR}(\varphi) + \frac{1}{2}\tau^T H^{vib}(\varphi)\tau.$$

The energy contribution E_{int} arising from the internal motions has been transformed into its canonical form with generalized coordinates (φ, τ) and moments (p_φ, P_τ).

At this point we distinguish between the 'slow' internal rotation and the 'fast' vibrations (having higher frequencies), by assuming that the latter follow adiabatically the geometrical changes due to the rotational motion. The rotational variables φ, p_φ are treated classically, whereas the τ, P_τ are considered as canonically conjugate quantum mechanical operators (*i.e.* $P_{\tau_i} = -i\hbar\partial/\partial\tau_i$). In other words, E_{int} can be viewed as a quantum mechanical Hamiltonian for the vibrations, with parametric dependence on φ, p_φ.
As indicated, we will only consider the averaged effect of the centrifugal term in Eq.(9.32) on the molecular partition function. It seems physically reasonable that this can be done (at the classical level) by integrating over all possible values of angular momentum. The resulting contribution Q_{rot} to the partition function is that of a rigid body with inertial tensor $\bar{I}$, and as it is proportional to the determinant Det[I] it only depends on the internal geometry, $Q_{rot} \equiv Q_{rot}(\varphi, T)$ where T stands for the temperature.
Based on Eqs.(9.31-9.33) one can then propose the following expression for the molecular partition function (omitting the trivial translational part),

$$Q_{rot-int}(T) = \frac{1}{h}\int \mathrm{d}\varphi\, Q_{rot}(\varphi, T) dp_\varphi \mathrm{Tr}[\mathrm{e}^{-\beta E_{int}}], \tag{9.34}$$

with $\beta = 1/RT$, where the integration is over the phase space of the classical variables, and the trace is taken with respect to the Hilbert space of the τ, P_{τ_i} operators.
The trace can be evaluated exactly, since the eigenvalues of E_{int} are known. To see this, one notes that the vibrational Hamiltonian is of the generic form

$$\mathcal{H} = P_\tau^T B P_\tau + b^T P_\tau + P_\tau^T b + \tau^T C \tau \tag{9.35}$$

where the positive-definite matrices B and C, as well as the column matrix b, are constant. To find the eigenvalue spectrum we may as well work in momentum space, treating the P_i as real numbers and the $\tau_i = +i\hbar\partial/\partial P_{\tau_i}$ as operators. The terms in Eq.(9.35) which are linear in P_τ, can then be absorbed by a shift $P'_\tau = P_\tau + B^{-1}b$ in the P_{τ_i} variables, yielding

$$\mathcal{H} = P_\tau'^T B P'_\tau + \tau^T C \tau - b^T B^{-1} b. \tag{9.36}$$

The last term merely produces a constant shift in the eigenvalues, and since we still have that $\tau_i = +i\hbar\partial/\partial P'_{\tau_i}$, the Hamiltonian in Eq.(9.36) is now the standard representation of a system of HO, which can be decoupled in the usual way.

Application to Eq.(9.34) yields

$$Q_{rot-int}(T) = \int \mathrm{d}\varphi \; \mathrm{e}^{-\beta V^{HR}(\varphi)} \; Q_{rot}(\varphi, T) \prod_{i=2}^{n} Q_i^{HO}(\varphi, T) \tag{9.37}$$
$$\frac{1}{h} \int \mathrm{d}p_\varphi \; \exp\left(-\frac{\beta p_\varphi^2}{2} [(A^{-1})_{\varphi\varphi} - (A^{-1})_{\varphi\tau}[(A^{-1})_{\tau\tau}]^{-1}(A^{-1})_{\tau\varphi}] \right),$$

where the φ-dependent HO frequencies follow from $\mathrm{Det}[H^{vib} - \omega_i A_{\tau\tau}] = 0$. Also note that the subsequent p_φ integration does not need an explicit calculation of A^{-1}, since

$$(A^{-1})_{\varphi\varphi} - (A^{-1})_{\varphi\tau}[(A^{-1})_{\tau\tau}]^{-1}(A^{-1})_{\tau\varphi} = (A_{\varphi\varphi})^{-1}. \tag{9.38}$$

The same statement holds also for the case of more than one internal rotor.

The focus of this work is to compute the total partition function of a molecule. Contrary to the well-known HR model, the global rotational and vibrational part are solved for each value of φ. All vibrational degrees of freedom, except the 'isolated' internal rotation, are treated quantum mechanically, whereas the hindered rotor part and global rotation are solved classically by integration,

$$Q_{rot,int}^{EHR} = K(T) \int_0^{2\pi} \mathrm{d}\varphi \; \sqrt{A_\varphi(\varphi)} \; e^{-\beta V^{HR}(\varphi)} \; \prod_{i=2}^{n} Q_i^{HO}(\varphi, T) \; Q_{rot}(\varphi, T) \tag{9.39}$$

with $K(T) = \sqrt{\frac{2\pi k_B T}{h^2}}$.
This classical solution is valid for high T, and the extension to lower temperatures is made by applying the Pitzer-Gwinn correction $Q_\varphi^{HO-QM}/Q_\varphi^{HO-Cl}$ [15].

This leads to the final expression of the global partition function of the molecule within the scope of a consistent scheme [Extended Hindered Rotor (EHR)] in which both large and small amplitude vibrations are treated on the same footing. It is instructive to introduce a scaling factor $\kappa_{EHR}(T)$ defined as the ratio between the true EHR partition function [Eq.(9.39)] and the HO prediction as resulting from the standard ab initio programs, *e.g.* Gaussian [13] and others:

$$Q_{rot,int}^{EHR}(T) = \kappa_{EHR}(T) \; Q_{rot,int}^{HO}(T) \tag{9.40}$$

The HO expression for the total partition function consists of the product of the global rotation partition function $Q_{rot}(\varphi = 0, T)$ with the total partition

function of the internal modes in the HO approach but determined at the global energy minimum (*i.e.* $\varphi = 0$):

$$Q_{int}^{HO}(T) = \prod_{i=1}^{n} Q_i^{HO}(\varphi = 0, T). \tag{9.41}$$

This enables us to extract a closed expression for the scaling factor $\kappa_{EHR}(T)$:

$$\kappa_{EHR}(T) = c_\varphi \int_0^{2\pi} f_A(\varphi)\ f_{vib}(\varphi, T)\ e^{-\beta V^{HR}(\varphi)}\ \mathrm{d}\varphi \tag{9.42}$$

with the geometry correction factor

$$f_A(\varphi) = \sqrt{\frac{A_\varphi(\varphi)}{A_\varphi(0)} \frac{I_x(\varphi) I_y(\varphi) I_z(\varphi)}{I_x(0) I_y(0) I_z(0)}} \tag{9.43}$$

as originally introduced in Refs.[16, 17], and the vibrational correction factor:

$$f_{vib}(\varphi, T) = \frac{\prod_{i=2}^{n} Q_i^{HO}(\varphi, T)}{\prod_{i=2}^{n} Q_i^{HO}(0, T)} \tag{9.44}$$

The coefficient

$$c_\varphi = \frac{1}{Q_{\varphi,Cl}^{HO}}\ K(T) \sqrt{A_\varphi(0)} \tag{9.45}$$

can further be elaborated yielding

$$c_\varphi = \sqrt{\frac{\beta}{2\pi}} \sqrt{\left.\frac{\partial^2 V}{\partial \varphi^2}\right|_0} \tag{9.46}$$

and following closed expression for the correct EHR partition function is found:

$$\begin{aligned} Q_{rot,int}^{EHR}(T) &= Q_{rot,int}^{HO}(T) \sqrt{\frac{\beta}{2\pi}} \sqrt{\left.\frac{\partial^2 V}{\partial \varphi^2}\right|_0} \int_0^{2\pi} f_A(\varphi)\ f_{vib}(\varphi, T)\ e^{-\beta V^{HR}(\varphi)}\ \mathrm{d}\varphi \\ &= \kappa_{EHR}(T)\ Q_{rot,int}^{HO}(T) \end{aligned} \tag{9.47}$$

It turns out that the correction on the HO partition function becomes independent of the absolute value of the (reduced) moment of inertia of the internal rotation under consideration but only depends on its relative variations.

The increased consistency of the EHR approach is thus reflected in the correction factors f_A and f_{vib} solely. All additional coupling terms originating from rotational-vibrational coupling and Coriolis terms are comprised in these factors.

9.2.3 Relation between HR and EHR

It is instructive to discuss the differences between the proposed coupled-vibrational EHR scheme and the standard 1D-HR scheme.
This can best be visualized by deriving a similar expression as Eq.(9.47) within the 1D-HR description. The partition function for the specific internal rotation with torsional angle φ *including the Pitzer-Gwinn correction factor* can be expressed as:

$$Q_{\varphi}^{HR} = Q_{\varphi}^{HO-QM} \sqrt{\frac{\beta}{2\pi}} \sqrt{\left.\frac{\partial^2 V}{\partial \varphi^2}\right|_0} \int_0^{2\pi} e^{-\beta V^{HR}(\varphi)} \, \mathrm{d}\varphi \tag{9.48}$$

and Q_{φ}^{HO-QM} represents the quantum mechanical partition function for the torsional motion φ with frequency $\nu = \sqrt{\left.\frac{\partial^2 V}{\partial \varphi^2}\right|_0 / I^{red}}$ resulting from the curvature of the potential energy at the equilibrium position and the reduced moment of inertia. It should be stressed that it does not describe an eigenmode, and an inconsistency frequently encountered in the literature consists in replacing the pure HO-mode Q_1^{HO} by Q_{φ}^{HR} of Eq.(9.48), as discussed in the introduction.

In a well-implemented 1D-HR model the global partition function has the final expression:

$$\begin{aligned} Q_{rot,int}^{1D-HR}(T) &= Q_{rot,int}^{HO}(T) \sqrt{\frac{\beta}{2\pi}} \sqrt{\left.\frac{\partial^2 V}{\partial \varphi^2}\right|_0} \int_0^{2\pi} e^{-\beta V^{HR}(\varphi)} \, \mathrm{d}\varphi \\ &= \kappa_{EHR}(T) \; Q_{rot,int}^{HO}(T) \end{aligned} \tag{9.49}$$

The great similarity of Eq.(9.49) and Eq.(9.47) is not a straightforward result, as both models rely on different grounds.

The origin of the success of the 1D-HR method in most of the applications is now clear. The only difference with EHR lies in the presence of the factors $f_A(\varphi)$ and $f_{vib}(\varphi, T)$ in the integral. The value of these factors at the potential energy minimum is unity by definition, making the HR and EHR integrands equal at the reference geometry.
The presence of the $f_A f_{vib}$ factor in the integrand can only have a significant influence on κ_{EHR} when the Boltzman factor is appreciably different from zero over a large enough range of φ. This can only occur at elevated temperatures, or for small potential energy variations along the large amplitude path. As a result, the correction of the EHR values versus HR will be small in general.

In the next sections, we present three examples to illustrate the differences between HR and EHR. The aim is to show the influence of the geometry and vibrational coupling on thermodynamic and kinetic properties. As the partition function itself is not a directly measurable quantity, we have to rely on derived properties. The first two examples employ the entropy and heat capacity, while in the third example the rate constant of an addition reaction is studied. These three quantities sample partition function, and hence the scaling factor $\kappa_{(E)HR}$, in different ways. The entropy and heat capacity involve derivatives with respect to temperature:

$$S = R\left(\ln Q_{tot} + T\left(\frac{\partial \ln Q_{tot}}{\partial T}\right)\right) \tag{9.50}$$

$$C = RT\left(2\frac{\partial \ln Q_{tot}}{\partial T} + T\frac{\partial^2 \ln Q_{tot}}{\partial T^2}\right). \tag{9.51}$$

Within the formulation of transition state theory, the rate constant of a bimolecular reaction can be expressed as follows [31, 32]:

$$k(T) = \frac{k_B T}{h}\frac{(q_\ddagger/V)}{(q_A/V)(q_B/V)}e^{-\frac{\Delta E_0}{k_B T}}. \tag{9.52}$$

When an internal rotation is present in the transition state only, the reaction rate becomes proportional to the partition function of interest ($q_\ddagger$).

The role of the scaling factor $\kappa_{(E)HR}$ in the HR or EHR approach becomes clear when we refer all quantities to their HO solution:

$$S_{(E)HR} = S_{HO} + R\left(\ln \kappa_{(E)HR} + T\left(\frac{\partial \ln \kappa_{(E)HR}}{\partial T}\right)\right) \tag{9.53}$$

$$C_{(E)HR} = C_{HO} + RT\left(2\frac{\partial \ln \kappa_{(E)HR}}{\partial T} + T\frac{\partial^2 \ln \kappa_{(E)HR}}{\partial T^2}\right) \tag{9.54}$$

$$k_{(E)HR}(T) = k_{HO}(T)\ \kappa_{(E)HR}. \tag{9.55}$$

9.3 Application to 1,3-butadiene

In a first example the model is applied to 1,3-butadiene, in which only one internal rotation is present about a single CC bond. The one-dimensional hindered rotor potential is calculated along the lines of Refs.[16, 14] by pointwise geometry optimizations at fixed out of plane angles (5° increments). For each of these constrained optimizations the Hessian was calculated in internal coordinates.

All ab initio calculations were performed using the Gaussian03 software package [13] on the B3LYP/6-311g** [7, 8] level of theory. It should be stressed that the B3LYP method as used here yields highly accurate geometries for the systems under study [153, 154]. In addition this DFT functional also predicts quite reliable quantitative values for the energy barriers in n-alkanes [14]. As the primary goal of this numerical application is to test the applicability and efficiency of the proposed EHR model, the proposed level of theory is largely sufficient [154]. The most intensive computational cost lies in the construction of the full Hessian at each point of the rotational potential. The required computational time is almost double of that needed in a standard 1D-HR calculation, which is more than feasible.

The potential $V^{HR}(\varphi)$ is shown in Fig.9.1. In the vicinity of the reference

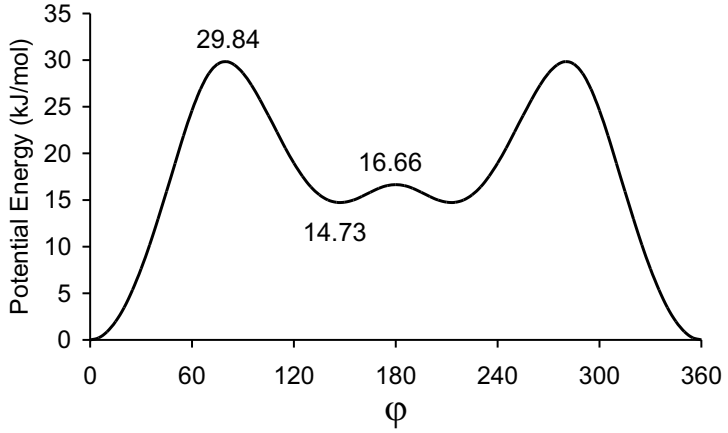

Figure 9.1: Potential energy profile of the internal rotation of 1,3-butadiene. The reference ($\varphi = 0$) is the *trans* geometry.

geometry $\varphi = 0$ the variation is very steep and results in a barrier of about

30 kJ/mol. Around the cis geometry, there is a wide plateau with two shallow minima, lying approximately 15 kJ/mol higher in energy than the reference conformation. This specific energy profile suggests the HO approach to be relatively accurate, as high energies are needed to overcome the large energy barrier towards the energy plateau in the centre. At moderate temperatures only a small amount of molecules will reside into the higher energy conformations.

9.3.1 The scaling factor $\kappa_{EHR}(T)$

The difference of the EHR scaling factor [Eq.(9.42)] versus the HR approach [Eq.(9.49)] is completely determined by two correction factors: the geometry factor $f_A(\varphi)$ and the vibrational correction factor $f_{vib}(\varphi, T)$ arising from the other $3N-7$ degrees of freedom.

(i) **The geometry factor** $f_A(\varphi)$ depends on the variation of the moments of inertia arising from both global and internal rotation. The global moments of inertia I_x, I_y and I_z turn out to vary very slowly [16]. The behavior of the geometry factor in terms of the torsional angle is thus mostly determined by the reduced moment of inertia $A_\varphi(\varphi)$ [$=A_{\varphi\varphi}$ in Eq.(9.30)] associated with the internal rotation in the EHR model. The explicit structure of $A_{\varphi\varphi}$ suggests that its magnitude is largely influenced by the relaxation effects, in other words by the changes of the 3N-7 other internal degrees of freedom from their equilibrium positions with varying torsional angle φ. To estimate these effects, the variation of the dihedral angles and bond angles along the internal rotation path in case of 1,3-butadiene is visualized in Fig.9.2(a) and 9.2(b). The bond lengths are not shown as they change little. The largest relaxation values are noticed for the dihedrals (maximum 10°), while the bond angles show rather small variations (maximum 3°). Anyway, the sum of the derivatives of all (3N-7) internal coordinates with respect to the torsional angle [displayed in Fig.9.2(c)] shows large fluctuations, and this is the determinative factor in the evaluation of the final EHR moment of inertia [Eq.(9.30)], and its difference with the 1D-HR reduced moment of inertia. This is best visualized in Fig.9.2(d). The dotted line gives the behavior of the A_{θ_1,θ_1} element of the matrix A_Θ [Eq.(9.30)] which coincides with the constant reduced moment I_m at the reference state.

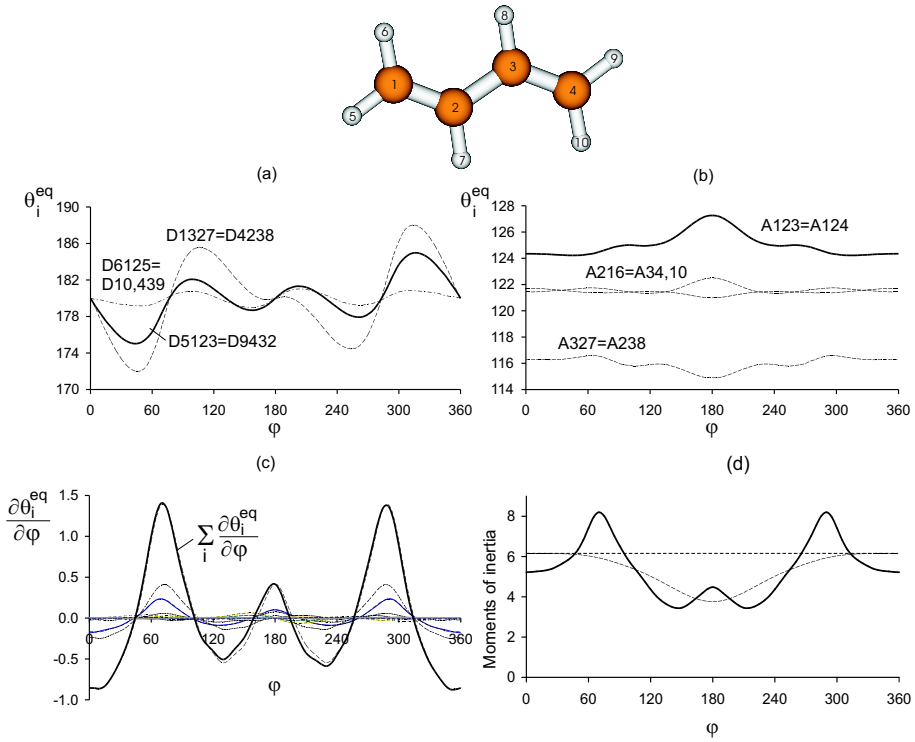

Dihedral and bond angles (in degree) are labelled according to the atom numbers as given at the top of the figure.
All moments are expressed in units $m_{au}\mathring{A}^2$.

Figure 9.2: The influence of the relaxation on the dihedral angles (a) and bond angles (b) is shown as a function of the torsional angle φ. In (c) the summation over the derivatives of the equilibrium angles and bond stretches is displayed (bold black line). Also the individual contributions are plotted. In (d) the resulting EHR moment $A_{\varphi\varphi}$ (black line) is compared to the constant HR moment $A_{\theta_1\theta_1}(\theta_1 = 0)$ and with the varying reduced moment $A_{\theta_1\theta_1}(\theta_1)$ (dotted line).

(ii) **The vibrational correction factor** $f_{vib}(\varphi, T)$ is even more important than the geometry factor. It shows a temperature dependence, and since thermodynamic functions contain derivatives of the partition function with respect to temperature, this vibrational factor may significantly alter the behavior of the thermodynamic functions. $f_{vib}(\varphi, T)$ [Eq.(9.44)] is the correction factor arising from the coupling of the IR with the remaining vibrational modes and hence is inherent to the EHR model. These modes are described within the HO approach and as the vibrational partition function is of the form:

$$Q^{HO} = \frac{e^{-\frac{\Theta^{HO}}{2T}}}{1 - e^{-\frac{\Theta^{HO}}{T}}}, \tag{9.56}$$

the lowest vibrational temperatures will generate the largest contributions to $\prod_{i=2}^{n} Q_i^{HO}(\varphi, T)$. In Fig.9.3 the fluctuations of the vibrational temperatures Θ_i^{HO} for the vibrational modes are plotted (up to 2000K) and the most pronounced variations are situated near $\varphi \approx 70°$ and 290° which is immediately reflected in the behavior of f_{vib} [Fig.9.4(a)].

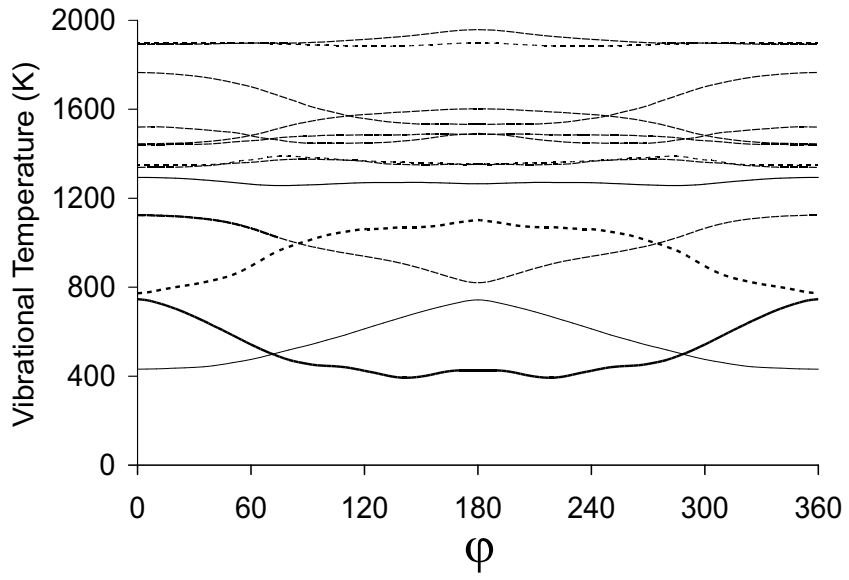

Figure 9.3: Vibrational temperatures ($\Theta_i = \frac{h\nu_i}{k_B}$) variation of the lowest (up to 2000K) HO modes in terms of the internal rotation coordinate φ.

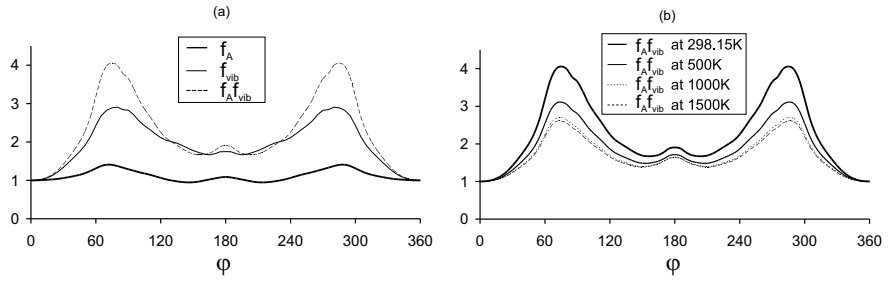

Figure 9.4: (a) Variation of the two correction factors f_A and f_{vib} as a function of the torsional angle φ at $T = 298.15K$. (b) Variation of the global correction factor $f_A f_{vib}$ at different temperatures $T = 298.15K, 500K, 1000K, 1500K$.

Apparently the shape of the total scaling factor $f_A f_{vib}$ is mainly determined by the vibrational correction factor f_{vib}. For higher temperatures the shape of the function is maintained but the maxima of the scaling factor are systematically decreasing [Fig.9.4(b)]. For very high temperatures the vibrational factor f_{vib} converges to its classical limit. In view of the temperature dependence of f_{vib} we expect the largest corrections on thermodynamic quantities in the lower and intermediate temperature regime. In this particular example validation of the EHR model takes place at the level of the global partition function Q which comprises complete integration over the dynamics. The scaling factor $\kappa_{EHR}(T)$, representing the ratio of the EHR prediction with respect to the HO reference, is given in Fig.9.5(a). The presence of one hindered rotor in 1,3-butadiene does not give rise to high values of the scaling factor. This is also mainly due to the steep potential around the reference geometry. At room temperature the EHR model predicts a scaling of 1.06, compared to 1.02 in the standard 1D-HR approach.

9.3.2 Reproduction of thermodynamic quantities

Experimental validation of EHR is possible with the predicted thermodynamic functions: entropy and heat capacity. In Table 9.1(a) we display the results for these properties in the HO, HR and EHR models together with the experimental values. The latter are taken from compilations of thermochemical reference data of C.L. Yaws [23] and NIST [24]. These reference data often result from fitting measured data from various sources, making the overall accuracy at any single temperature hard to assess. The quoted heat capacities in the compila-

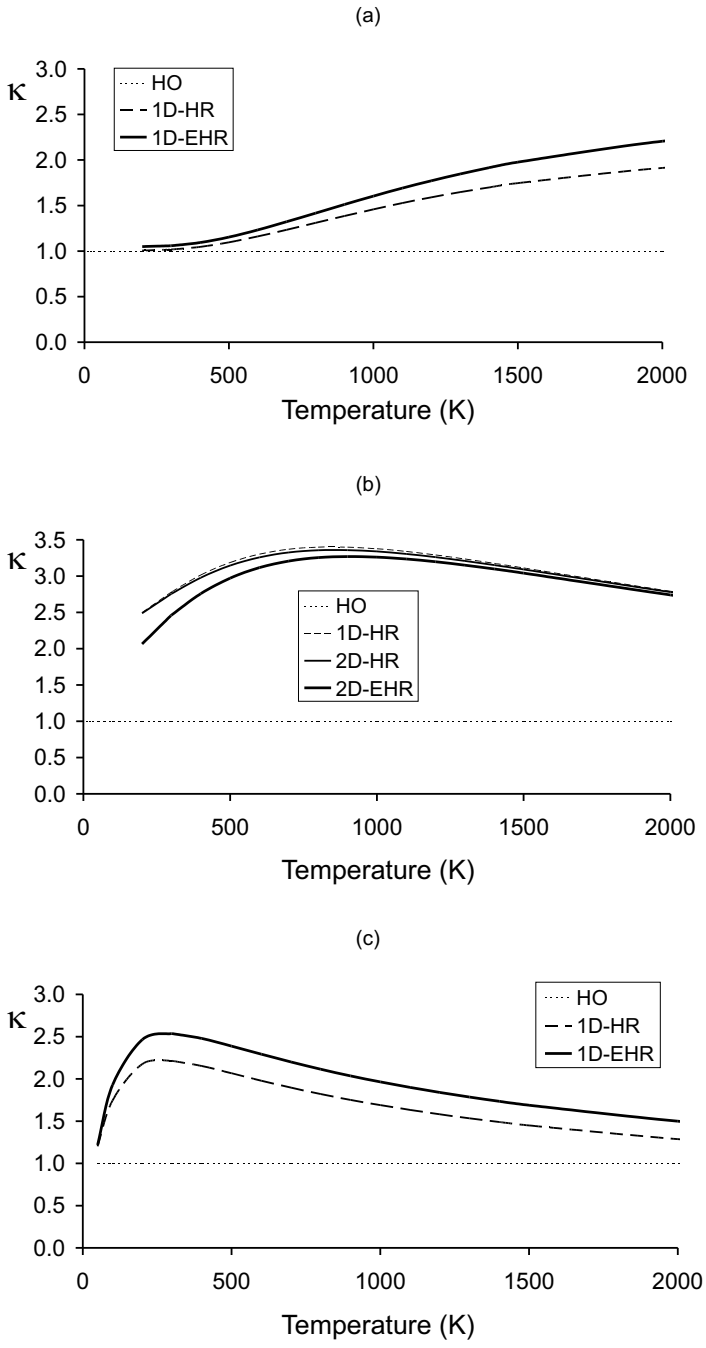

Figure 9.5: Scaling factors $\kappa(T)$ for the global partition function in (a) 1,3-butadiene, (b) 1-butene and (c) the transition state for the addition reaction of a vinyl radical to ethene.

tions [23] and [24], *e.g.*, can differ by about 2 J/mol/K. One should therefore attach more significance to systematic trends over a wide temperature range, as explained below in connection with Table 9.1(b) and Figure 9.7.

(a)	S(298.15K)	C(100K)	C(298,15K)	C(400K)	C(600K)	C(1000K)	C(1500K)
ref.[23]	278.74	39.77	81.37	101.31	135.02	175.43	195.87
ref.[24]		41.31	79.81	103.44	136.51	173.10	197.54
HO	276.42	40.88	74.33	94.87	127.63	167.79	194.52
1D-HR	277.06	40.98	76.57	99.82	134.69	171.27	194.38
1D-EHR	277.72	41.64	78.00	101.65	136.80	172.62	195.04

(b)	RMS of C(100K → 1500K)		MAD of C(100K → 1500K)	
	ref.[23]	ref.[24]	ref.[23]	ref.[24]
HO	6.11	5.90	5.40	5.31
1D-HR	2.84	2.35	2.30	2.17
1D-EHR	2.06	1.31	1.69	1.05

Level of theory: B3LYP/6-311g**.
All values are given in J/mol/K.

Table 9.1: (a) Comparison of entropy and heat capacity of the different models with two sets of reference values [23, 24] in 1,3-butadiene. (b) RMS and MAD deviations of the calculated heat capacities from experiment for the entire temperature range.

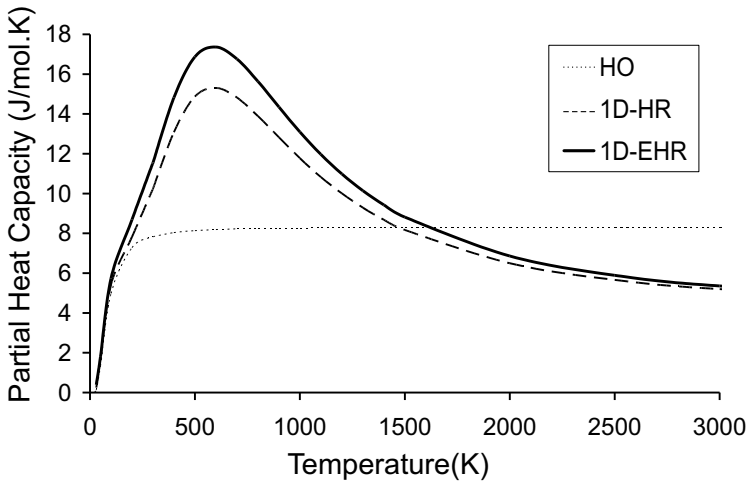

Figure 9.6: Partial heat capacity of the internal rotation in 1,3-butadiene in the HO, HR and EHR model.

Corrections for the entropy arising from the hindered rotor in this specific molecule are expected to be small due to the steep walls of the potential energy around the reference geometry, making the population of the other conformers than *trans*-butadiene less probable. Nevertheless, the entropy correction in the EHR model is almost twice as large as the prediction in the 1D-HR model. In molecules with floppier internal rotations, as n-alkanes, the corrections for hindered rotors are much larger as confirmed in Ref.[14].

The heat capacities are more sensitive to the specific model used for the internal motions. To get an idea about the nature, origin and magnitude of the anharmonic correction to the heat capacity, we plot the contribution to the heat capacity for the specific internal rotation in Fig.9.6 as a function of temperature. The heat capacities in the HO model converge to a value of R for higher temperatures whereas the (E)HR predictions tend to R/2. In the lower temperature regime -the extent of this region is determined by the specific temperature- the IR rotor predictions lie above the HO values. These results are completely in agreement with the results of Katzer and Sax [53] who studied the impact of anharmonic molecular vibrations in the thermochemistry of silicon hydrides. Also note that the standard anharmonic oscillator correction (using local information about the third order derivatives at the equilibrium point) does not lead to a significant improvement over the HO, as we have checked explicitly for the applications in this section and the next.

In Fig.9.7(a) and (b) the absolute deviations of the heat capacities from the reference values (Ref.[23] and Ref.[24] respectively) are visualized in terms of the temperature. The HO model systematically underestimates the experimental values at all temperatures, but the deviations are less pronounced for higher temperatures. As shown in Table 9.1(b), the mean absolute deviation (MAD) from both sets of reference values is more than 5 J/mol/K, while the maximal deviation amounts to about 9J/mol/K.
Changing the HO to a rotational description leads to a substantial improvement and a MAD of less than half the HO value, within the range of acceptable results. However, it is clear that a further systematic and significant improvement is present when going from HR to EHR.

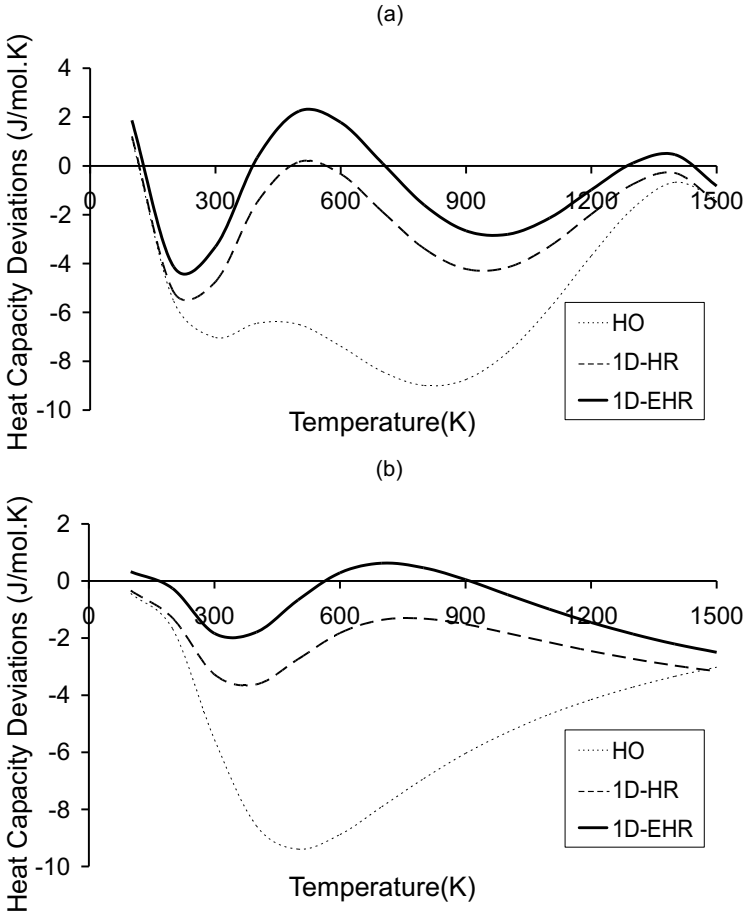

Figure 9.7: Deviations from reference values of the heat capacity calculated in the HO, HR and EHR approach: (a) compared to Ref.[23], (b) compared to Ref.[24].

9.4 Application to 1-butene

In a second example the EHR model is applied to 1-butene, in which two internal rotations are present about single C-C bonds. The theory is easily extended to multiple large-amplitude motions. We are not going into detail, since it is a straightforward extension of the presented theory. The only inconvenience in the numerical application of 2D-EHR is that in a proper EHR model the coupling of the two internal rotations should be strictly taken into account. This causes some increase of the computation time as two-dimensional rotational potential surfaces should be constructed following the lines explained in refs. [16, 17]. The search for a proper 1D treatment of the two coupled internal rotations within EHR will certainly enlarge the utility and efficiency of the EHR model. Suitable one-dimensional approximation schemes need to be investigated and are requisite for high-dimensional nD-EHR applications ($n > 3$). This work is in progress.

The scaling factors $\kappa(T)$ in the various schemes, shown in Fig.9.5(b), are noticeably higher than in the case of 1,3-butadiene. The largest correction is predicted by the standard 1D-HR model. Coupling of the two rotations (2D-HR) has only little effect, but an exact treatment of the two internal rotations within the EHR model manifestly reduces the scaling factor. This result gives an indication that the coupling of the IR's with the other vibrational modes in the molecule can give rise to substantial deviations from the standard treatment. It can lead to an increase of the partition function (1,3-butadiene) or a decrease (1-butene). At room temperature an exact EHR calculation causes an enhancement of the total partition function with a factor 2.45, while in standard hindered rotor models this factor is larger (2.75 - 2.78). This deviation is apparently not manifested to the same extent in the reproduction of the thermodynamic functions. The entropy predictions are quite close to the experiment for all schemes handling the hindered rotors, and the same behavior is noticed for the heat capacities with little preference for the 2D-EHR model (see Table 9.2). Concluding, the numerical applications demonstrate that the EHR model, which represents an almost exact treatment of the internal modes in a molecular system, gives nearly similar thermodynamic functions as those predicted by the simple 1D-HR approach. The authors showed in previous work that the 1D-HR also performs well in the description of multiple (coupled) internal rotations (2D-HR and 3D-HR) [16].

	S(298.15K)	C(200K)	C(298,15K)	C(400K)	C(600K)
Ref.[23]	307.83	67.55	88.41	109.22	145.84
Ref.[24]		65.19	85.56	108.48	146.75
HO	296.97	62.41	82.64	106.30	146.61
1D-HR	307.80	65.46	85.30	107.48	144.68
2D-HR	307.62	65.37	85.27	107.57	144.87
2D-EHR	308.12	66.20	85.93	108.08	145.21

Level of theory: B3LYP/6-311g**.
All values are given in J/mol/K.

Table 9.2: Comparison of entropy and heat capacity of the different models with experiment [23, 24] in 1-butene.

9.5 Application to reaction kinetics

To underline the utility and applicability of the EHR model in predicting accurate reaction kinetic parameters, we study in this section a particular reaction as an example. More precisely the rate constant of the addition of the vinyl radical to ethene is investigated:

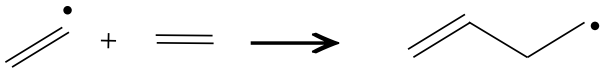

Scheme 2

Within the formulation of transition state theory, the rate constant of a bimolecular reaction can be expressed as follows [31, 32]:

$$k(T) = \frac{k_B T}{h} \frac{(q_\ddagger / V)}{(q_A/V)(q_B/V)} e^{-\frac{\Delta E_0}{k_B T}} \tag{9.57}$$

where k_B represents the Boltzmann constant, T stands for the absolute temperature, h is Planck's constant and V is the reference volume in which the translational part of the partition function is evaluated. The molecular partition functions q_A and q_B relate to the two reactants and $q_\ddagger$ is the molecular partition function of the transition state. ΔE_0 represents the molecular energy difference at absolute zero between the activated complex and the reactants, with inclusion of the zero point vibrational energies. The frequency factor figuring in the Arrhenius rate law reflects any changes in the molecular partition functions of reactants and products [44, 35].

For the reaction under study, only one internal rotation is present in the transition state, *i.e.* a torsion about the forming bond (mode 2 in Fig.9.8). Of particular importance in the calculation of the frequency factor are the so-called transitional modes in the transition structure of the reaction. They arise from the loss of three transitional and three rotational degrees of freedom when the reactants combine to form the transition state. The six transitional modes for the vinyl radical addition to ethene are schematically shown in Fig.9.8. One of these transitional modes corresponds to the reaction coordinate and is characterized by an imaginary frequency. For a radical addition reaction the latter merely corresponds to the $C-C$ stretch vibration of the forming carbon-carbon bond. Mode 3 and 5 corresponds to a symmetric and antisymmetric bending

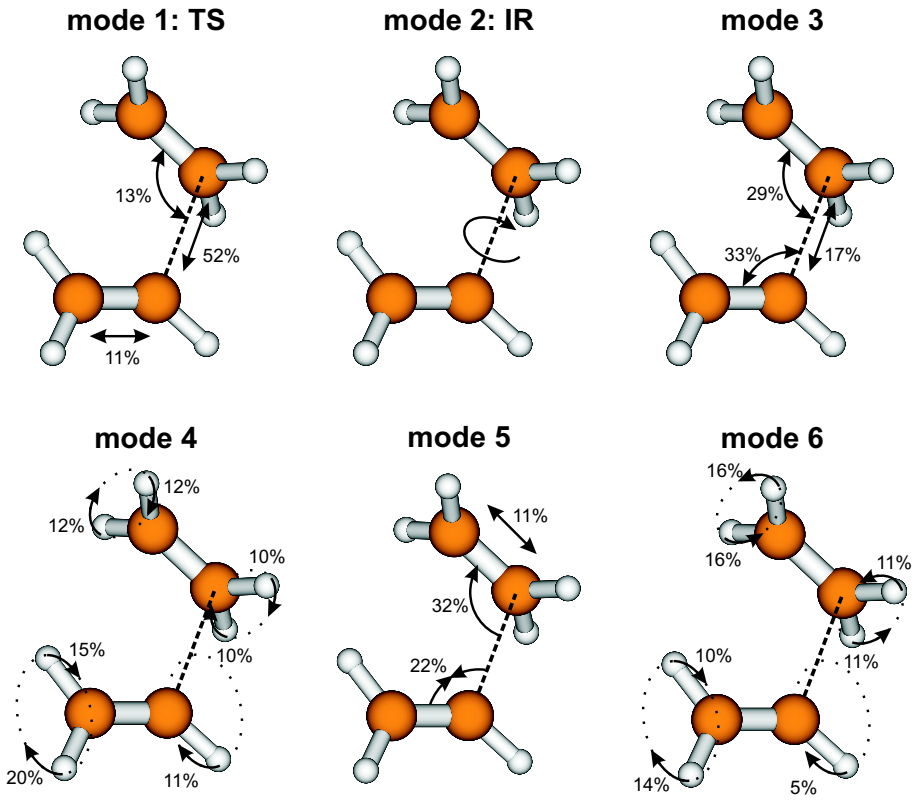

Figure 9.8: Schematic representation of the six transitional modes in the transition state for the addition of a vinyl radical to ethene.

of the two reactant species whereas ν_4 and ν_6 correspond to a symmetric and asymmetric variation of the dihedrals of the hydrogen atoms attached to the carbon backbone with respect to the forming bond.

All normal modes will slightly change in going from reactants to transition state, but due to the specific structure of the ratio $q_\ddagger/(q_A)(q_B)$, small changes occurring in the non-transitional modes will approximately cancel. On the other hand the contributions from the transitional modes will not cancel with respect to any internal mode present in the reactants. The sensitivity of the calculated frequency factor to the model used to treat the one internal rotation may thus be reflected in the contributions arising from the transitional modes. Fig.9.9 shows the variation of the vibrational frequencies of the translational modes in terms of the dihedral angle of the rotation about the forming C-C

bond. The variations in the vibrational modes are significant, *i.e.* of the order

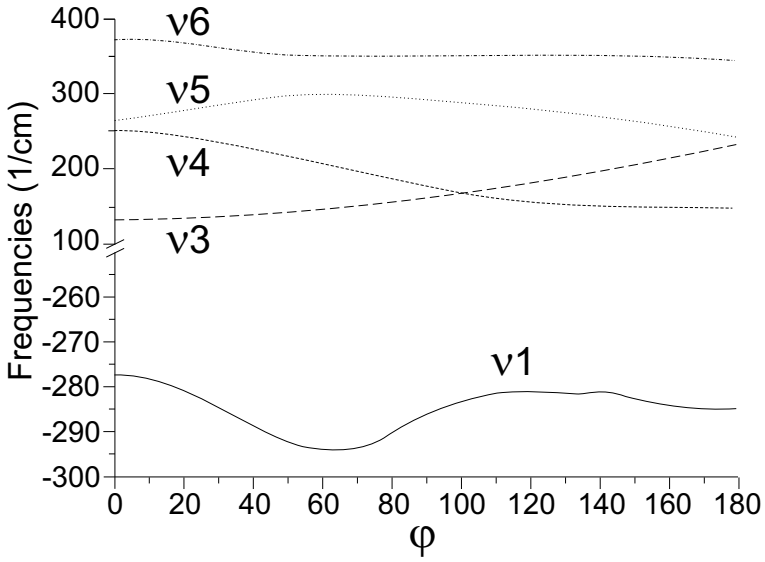

Figure 9.9: Variation of the vibrational frequencies (cm^{-1}) of the transitional modes in terms of the dihedral angle of the rotation about the forming C-C bond

of 100 cm^{-1}. It is generally known that the transitional modes corresponding to the rotation about the forming bond and the bending of the reactant species are important for a radical addition reaction, but the EHR results apparently point towards the importance to incorporate correctly the coupling between the various modes [2, 44, 35]. The impact of the coupling is nicely reflected in the scaling factor κ that amounts to about 2.5 in the 1D-EHR model and 2.0 in the standard 1D-HR scheme [see Fig.9.5(c)]. As the Arrhenius frequency factor is directly linked to the molecular partition functions, any change in the latter will directly be reflected in the value of A. The Arrhenius plots for the given reaction are shown in Fig.9.10. The values for the kinetic parameters, obtained in the temperature range of 300-600 K, are also given for the various approaches.

The activation energy is merely unaffected by any HR scheme in correspondence with previous literature work on this item [2, 34]. By taking into account the internal rotation in the transition state, the pre-exponential factor is approximately doubled. The EHR model induces a slight shift (ca. 17%) in the Arrhenius plot towards higher values.

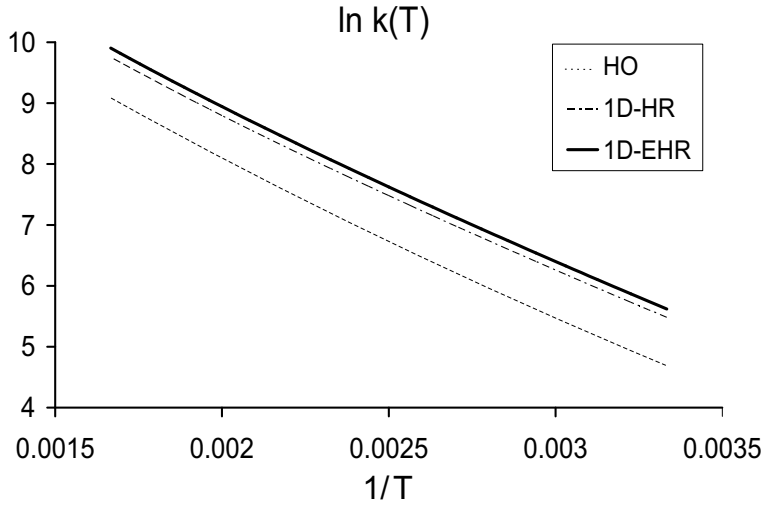

	HO	1D-HR	1D-EHR
E_a (kJ/mol)	21.98	21.40	21.46
A (m^3/mol/s)	6.48 E5	1.16 E6	1.36 E6

Figure 9.10: Arrhenius plot of k(T) for the addition of the ethyl radical to ethene.

We also checked that using a different functional (mPW1B95 [155], shown to give both reliable geometries and reaction barriers [148]) leads to the same qualitative difference between HR and EHR, *i.e.* the activation energy remains constant, whereas the pre-exponential factor increases. More extensive studies on a large database of radical addition reactions are planned to draw definite conclusions about the extent of coupling between various transitional modes and the effect on the kinetic parameters.

9.6 Summary

In this chapter we have introduced a new model that treats all internal motions, *i.e.* both large and small amplitude vibrations in the molecule, in a unified model. This scheme goes beyond the conventional separability assumption between global and internal motions and between large-amplitude motions and other vibrational degrees of freedom. The approach relies on the introduction of a specific internal coordinate system, in which the global and internal motion can be separated instantaneously at all times such that the Coriolis terms become zero.

This approach has been elaborated in detail for the case where one internal rotation is present leading to the Extended Hindered Rotor (EHR) model in which the relaxation of the other 3N-7 degrees of freedom are taken into account both in the description of the potential energy and kinetic energy. The finally obtained partition function can be written in its standard harmonic oscillator form but multiplied by a scaling factor $\kappa_{EHR}(T)$ which accounts for all additional coupling with the small amplitude vibrations. The method is validated by means of the reproduction of thermodynamic and kinetic properties. As first example 1,3-butadiene is taken, since only one internal rotation is present. Due to the specific form of the internal rotation potential the largest effect is found on the heat capacity, bringing its value to an improved agreement over the whole temperature range as compared to the HR description.

The EHR method is easily extended to more hindered rotors. As second example 1-butene with two internal rotations has been investigated. It has been shown that the coupling between the internal rotors and the other vibrations of the molecule causes a substantial reduction of the global partition function compared with the standard 1D-HR model. The applicability of the EHR model to multiple internal rotors enhances the utility of the model. It also gives a reliable alternative to the simple standard 1D-HR approach in molecules where the last method fails. The applicability on reaction kinetics is studied as well: the addition of the vinyl radical to ethene is taken as third example. Any change in the partition function is directly reflected in the pre-exponential factor. It is found that the largest influence is already involved in the 1D-HR scheme with respect to the harmonic oscillator approach, whereas the EHR model causes an additional slight enhancement of the frequency factor.

Finally, we investigated the origin of the success of a well-implemented HR model through its relation with the EHR description.

Chapter 10

General conclusions and perspectives

In this PhD thesis, we have developed and refined a computationally attractive procedure (1D-HR) to calculate total molecular partition functions in an accurate way. On the basis of the standard Harmonic Oscillator model the large amplitudes motions taking place in the molecule are systematically separated from the other vibrations and their corresponding 1D-HR partitions functions replace those obtained in the HO approximation. This 1D-HR model has shown its adequacy in treating flexible molecules. The basic ideas of this method were previously already well known (as 'Hindered Rotor'), and are commonly used to calculate various properties of molecules. These HR corrections turn out to drastically alter the standard HO predictions and to yield ab initio estimates that are often closer to the experimental values.

In the literature, many variants of the hindered rotor model are in use, and for the reader it was always difficult to unravel the precise details of the HR-model under consideration: the construction of the kinetic and potential energy in the one-dimensional model is submitted to several approaches. Still, all existing variants of the 1D-HR model predict corrections which all tend toward a better experimental agreement. Their satisfactory predictive properties lie primarily on the basis of the acceptance of the various HR methods, but a strong theoretical 'backbone' explaining the overall success of this simple model was missing. This thesis, however, succeeded in illuminating the *theoretical origins* of the HR's success, as well as in providing improvements to the model.

We have shown that, for molecules with multiple internal rotations, the one-dimensional approximation of both potential and kinetic energy (through use of the reduced moments of inertia) introduces two opposite corrections. The resulting cancellation of errors leads to excellent predictions. Initially, it was still unclear whether this cancellation was fortuitous or a result of some underlying theoretical mechanism.

This conundrum was solved through an entirely new approach: the 'Extended Hindered Rotor' (EHR) model. This method incorporates all possible coupling effects of the potential and kinetic energy terms. The inherent consistency leads to an almost exact description of floppy molecules exhibiting both large amplitude motions and regular vibrations. A downside of this procedure is the intense computational effort needed to calculate the coupled large amplitude paths. This restricts the use of this method to a maximum of two large amplitude (EHR) variables. As a result, the 'pure' ($\equiv$ multi-dimensional) EHR method is not applicable as a standard approach, unless some kind of one-dimensional approximation without major loss of accuracy could be introduced. Nevertheless, EHR is undoubtedly the ideal reference for validation of approximative methods.

Inspection of the analytical expressions of EHR [Eq.(1.13)] and 1D-HR [Eq. (1.17)] reveals why 1D-HR performs so well. The cancellation of errors in the 1D-HR approach for linear molecules is no coincidence, but a structural property. Theoretical comparison with the exact EHR reference allows us to predict in which particular cases erroneous results can be expected.

Amongst others, heavily branched molecules are not adequately described by 1D-HR, due to strong kinetic coupling effects. Sulfides, or other molecules that exhibit specific potential energy variations with multiple low energy conformers, are also problematic for the 1D-HR treatment. In both cases, there are several low vibrational modes, which do not correspond to large amplitude vibrations. Any presence of such modes should be considered as a possible case where 1D-HR may fail.

The application of the EHR model was tested on three small molecular systems through calculation of thermodynamic and kinetic properties.

This PhD thesis has made an important contribution to the accurate prediction of macroscopic quantities, derived from the molecular partition function constructed from first principles.

The main part of the research presented here has been published in seven A1 papers (see appendix B). It also gave rise to a freely distributed software pro-

gram 'HRpublic' among academic users. It can be requested through the CMM group's web-site [4]. This program is now used by several international research groups.

However, this it not the end: many challenges and unresolved issues remain. The possible applications of EHR go far beyond those implied in this thesis. The EHR description is mainly suited for molecular systems for which 1D-HR is bound to fail. For large molecules, however, the increase in computational cost must be considered. Continued efforts are required to study the impact of (heavy) side branches on the molecular partition function and derived quantities. Adaptations to the EHR formalism have to be devised for *e.g.* "skeleton" vibrations in linear molecules and coupled ring puckering in cyclic systems. For this type of problems, only small extensions to the EHR theory are required: the theory and associated software are general enough to accommodate these additions with minimal effort.

The main concept of EHR is the separation of small and large amplitude variables into two separate descriptions (HO or HR) within a single consistent model, in which no coupling terms are ignored. This procedure could also be applied to separate chemical active coordinates from the less interesting 'background' modes. For instance, in acid-base reactions in zeolites, or enzyme catalysis, the systems are too extended to use pure ab initio methods, and have to be described with hybrid methods such as QM/MM. Introduction of a EHR-like separation procedure could in principle circumvent the problems involved in calculating vibrational modes within the QM/MM description.

Bibliography

[1] McQuarrie, D. A. *Statistical Thermodynamics*, University Science Books, Mill Valley, **1973**

[2] Van Speybroeck, V.; Van Neck, D.; Waroquier, M.; Wauters S.; Saeys M.; Marin, G. B. *J. Phys. Chem. A* **2000**, *104*, 10939

[3] Van Speybroeck, V. *PhD. thesis: Ab initio static and dynamic molecular methods: a useful tool in the study of chemical reactions*, Ghent University, Ghent, **2001**

[4] http://molmod/

[5] East, A. L. L.; Radom, L. *J. Chem. Phys.* **1997**, *106*, 6655

[6] Ayala, P. Y. and Schlegel, H. B. *J. Chem. Phys.* **1998**, *108*, 2314

[7] Becke, A. D. *J. Chem. Phys.* **1993**, *98*, 5648

[8] Krishnan, R.; Binkley, J. S.; Seeger, R.; Pople, J. A. *J. Chem. Phys.* **1980**, *72*, 650

[9] An example of a reference work:
Parr, R.G.; Yang, W. *Density Functional Theory of Atoms and Molecules*; Oxford University Press: New York, 1989.

[10] Hohenberg, P.; Kohn, W. *Phys. Rev.* **1964**, *136*, 864

[11] http://www.gaussian.com

[12] *Gaussian 98*, M. J. Frisch, G. W. Trucks, H. B. Schlegel, G. E. Scuseria, M. A. Robb, J. R. Cheeseman, V. G. Zakrzewski, J. A. Montgomery, Jr. R. E. Stratmann, J. C. Burant, S. Dapprich, J. M. Millam, A. D. Daniels, K. N. Kudin, M. C. Strain, O. Farkas, J. Tomasi, V. Barone,

M. Cossi, R. Cammi, B. Mennucci, C. Pomelli, C. Adamo, S. Clifford, J. Ochterski, G. A. Petersson, P. Y. Ayala, Q. Cui, K. Morokuma, D. K. Malick, A. D. Rabuck, K. Raghavachari, J. B. Foresman, J. Cioslowski, J. V. Ortiz, A. G. Baboul, B. B. Stefanov, B. Liu, A. Liashenko, P. Piskorz, I. Komaromi, R. Gomperts, R. L. Martin, D. J. Fox, T. Keith, M. A. Al-Laham, C. Y. Peng, A. Nanayakkara, C. Gonzalez, M. Challacombe, P. M. W. Gill, B. Johnson, W. Chen, M. W. Wong, J. L. Andres., C. Gonzalez, M. Head-Gordon, E. S. Replogle, J. A. Pople, Gaussian, Inc., Pittsburgh PA, **1998**

[13] *Gaussian 03*, M. J. Frisch, G. W. Trucks, H. B. Schlegel, G. E. Scuseria, M. A. Robb, J. R. Cheeseman, J. A. Montgomery, Jr., T. Vreven, K. N. Kudin, J. C. Burant, J. M. Millam, S. S. Iyengar, J. Tomasi, V. Barone, B. Mennucci, M. Cossi, G. Scalmani, N. Rega, G. A. Petersson, H. Nakatsuji, M. Hada, M. Ehara, K. Toyota, R. Fukuda, J. Hasegawa, M. Ishida, T. Nakajima, Y. Honda, O. Kitao, H. Nakai, M. Klene, X. Li, J. E. Knox, H. P. Hratchian, J. B. Cross, V. Bakken, C. Adamo, J. Jaramillo, R. Gomperts, R. E. Stratmann, O. Yazyev, A. J. Austin, R. Cammi, C. Pomelli, J. W. Ochterski, P. Y. Ayala, K. Morokuma, G. A. Voth, P. Salvador, J. J. Dannenberg, V. G. Zakrzewski, S. Dapprich, A. D. Daniels, M. C. Strain, O. Farkas, D. K. Malick, A. D. Rabuck, K. Raghavachari, J. B. Foresman, J. V. Ortiz, Q. Cui, A. G. Baboul, S. Clifford, J. Cioslowski, B. B. Stefanov, G. Liu, A. Liashenko, P. Piskorz, I. Komaromi, R. L. Martin, D. J. Fox, T. Keith, M. A. Al-Laham, C. Y. Peng, A. Nanayakkara, M. Challacombe, P. M. W. Gill, B. Johnson, W. Chen, M. W. Wong, C. Gonzalez, and J. A. Pople, Gaussian, Inc., Wallingford CT, **2003**

[14] Vansteenkiste, P.; Van Speybroeck, V.; Marin, G. B. and Waroquier, M. *J. Phys. Chem. A* **2003**, *107*, 3139

[15] Pitzer, K. S.; Gwinn, W. D. *J. Chem. Phys.* **1942**, *10*, 428

[16] Van Speybroeck, V.; Vansteenkiste, P.; Van Neck, D.; Waroquier, M. *Chem. Phys. Lett.* **2005**, *402*, 479

[17] Vansteenkiste, P.; Van Speybroeck, V.; Pauwels, E.; Waroquier, M. *Chem. Phys.* **2005**, *314*, 109

[18] Vansteenkiste, P.; Pauwels, E.; Van Speybroeck, V.; Waroquier, M. *J. Phys. Chem. A* **2005**, *109*, 9617

[19] Tasi, G.; Mizukami, F.; Palinko, I.; Csontos, J.; Gyorffy, W.; Nair, P.; Maeda, K.; Toba, M.; Niwa, S.; Kiyozumi, Y.; Kiricsi, I. *J. Phys. Chem. A* **1998**, *102*, 7698

[20] Vansteenkiste, P.; Verstraelen, T.; Van Speybroeck, V.; Waroquier, M. *Chem. Phys.* **2006**, submitted

[21] Vansteenkiste, P.; Van Speybroeck, V.; Verniest, G.; De Kimpe, N.; Waroquier, M. *J. Phys. Chem. A* **2006**, *110*, 3838

[22] Vansteenkiste, P.; Van Neck, D.; Van Speybroeck, V.; Waroquier, M. *J. Chem. Phys.* **2006**, *124*, Art. No. 044314

[23] Yaws, C. L. *Chemical Properties Handbook*, McGraw-Hill Handbooks, **1999**

[24] N.I.S.T. Chemistry Webbook: http://webbook.nist.gov/chemistry/

[25] http://www.gaussian.com/g_whitepap/vib.htm

[26] Pitzer, K. S. *J. Chem. Phys.* **1940**, *8*, 711

[27] Pitzer, K. S. *J. Chem. Phys.* **1946**, *14*, 239

[28] Kilpatrick, J. E. and Pitzer, K. S. *J. Chem. Phys.* **1949**, *17*, 1064

[29] Herschbach, D. R.; Johnston, H. S.; Pitzer, K. S.; Powell, R. E. *J. Chem. Phys.* **1956**, *25*, 736

[30] Li, J. C. M. and Pitzer, K. S. *J. Phys. Chem.* **1956**, *60*, 466

[31] Laidler, K. J. *Chemical Kinetics* ; ed. by Harper Collins Publishers, Inc, **1987**

[32] Mc Quarrie, D. A. and Simon, J. D. *Physical Chemistry - A molecular approach*, University Science Books, Sausalito, California, **1997**

[33] Van Speybroeck, V.; Borremans, Y.; Van Neck, D.; Waroquier, M.; Wauters, S.; Saeys, M.; Marin, G.B. *J. Phys. Chem. A* **2001**, *105*, 7713

[34] Van Speybroeck, V.; Van Neck, D.; Waroquier, M. *J. Phys. Chem. A* **2002**, *106*, 8945

[35] Heuts, J. P. A.; Gilbert, R. G.; Radom, L. *J. Phys. Chem.* **1996**, *100*, 18997

[36] Lide, D. R.; Frederikse, H. P. R. *CRC Handbook of Chemistry and Physics, 74th edition*, CRC Press inc., Boca Raton, **1995**

[37] Entropy and Entropy of Formation of Gas, http://www.knovel.com/

[38] Stull, D. R.; Westrum, E. F.; Sinke, G. C. *The Chemical Thermodynamics of Organic Compounds*, John Wiley & Sons, New York, **1969**

[39] Guthrie, J. P. *J. Phys. Chem. A* **2001**, *105*, 8495

[40] Wong, M. W.; Radom, L. *J. Phys. Chem. A* **1998**, *102*, 2237

[41] Parker, C. L.; Cooksy, A. L. *J. Phys. Chem. A* **1998**, *102*, 6186

[42] Lynch, B. J.; Fast, P. L.; Harris, M.; Truhlar, D. G. *J. Phys. Chem. A* **2000**, *104*, 4811

[43] Smith, G. D. and Jaffe, R. L. *J. Phys. Chem.* **1996**, *100*, 18718

[44] Heuts, J. P. A.; Gilbert, R. G.; Radom, L. *Macromolecules* **1995**, *28*, 8771

[45] Raghavachari, K. *J. Chem. Phys.* **1984**, *81*, 1383

[46] Wiberg, K. B.; Murcko, M. A. *J. Am. Chem. Soc.* **1988**, *110*, 8029

[47] Tsuzuki, S.; Schäfer, L.; Goto, H.; Jemmis, E. D.; Hosoya, H.; Siam, K.; Tanabe, K.; Osawa, E. *J. Am. Chem. Soc.* **1991**, *113*, 4665

[48] Mirkin, N. G.; Krimm, S. *J. Phys. Chem.* **1993**, *97*, 13887

[49] Frey, R. F.; Cao, M.; Newton, S. Q.; Schaefer, L. *J. Mol. Struct. (THEOCHEM)* **1993**, *285*, 99

[50] Herrebout, W. A.; van der Veken, B. J.; Wang, A.; Durig, J. R. *J. Phys. Chem.* **1995**, *99*, 578

[51] Koglin, E.; Meier R. J. *Chem. Phys. Letters* **1999**, *312*, 284

[52] Scott, D. W. *J. Chem. Phys.*, **1974**, *60*, 3144

[53] Katzer, G. and Sax, A. F. *J. Phys. Chem. A* **2002**, *106*, 7204

[54] (a) Mizushima, S. *Structure of Molecules and Internal Rotation*, Academic, New York, **1954**
(b) Orville-Thomas, W. J. *Internal rotation in molecules*, Wiley, London,

1974
(c) Lister, D. G.; MacDonald, J. N.; Owen, N. L. *Internal rotation and Inversion*, Academic, London, **1978**

[55] (a) Wilson, E. B. *J. Adv. Chem. Phys.* **1959**, *2*, 367
(b) Lowe, J. P. *Prog. Phys. Org. Chem.* **1968**, *6*, 1
(c) Förster, H. and Vögtle, F. *Angew. Chem.* **1977**, *16*, 429
(d) Long, D. A. *J. Mol. Struct.* **1985**, *126*, 9
(e) Berg, U. and Sandström, J. *Adv. Phys. Org. Chem.* **1989**, *25*, 1
(f) Dale, J. *Tetrahedron* **1996**, *22*, 3373

[56] (a) Slanina, Z. *J. Phys. Chem.* **1982**, *86*, 4782
(b) Slanina, Z. *Ber. Busen-Ges. Phys. Chem.* **1983**, *87*, 28
(c) Slanina, Z. *J. Phys. Chem.* **1986**, *90*, 2957

[57] (a) Pan, H. *J. Phys. Chem.* **1987**, *87*, 4846
(b) Pan, H. *Chem. Phys. Lett.* **1988**, *155*, 35
(c) Bhattacharyya, K. *Chem. Phys. Lett.* **1989**, *159*, 40
(d) Yorish, V. S. *Chem. Phys. Lett.* **1994**, *219*, 279

[58] Truhlar, D. G. *J. Comp. Chem.* **1991**, *12*, 266

[59] DeTar, D. F. *J. Phys. Chem. A* **1998**, *102*, 5128

[60] Robertson, S.H. and Wardlaw, D.M. *Chem. Phys. Lett.* **1992**, *199*, 391

[61] Gang, J; Pilling, M. J.; Robertson, S. H. *J. Chem. Soc., Faraday Trans.* **1996**, *92*, 3509

[62] Gang, J.; Pilling, M. J.; Robertson, S.H. *J. Chem. Soc.* **1997**, *93*, 1481

[63] Vivian, J. T.; Lehn, S. A.; Frederick, J. H. *J. Chem. Phys.* **1997**, *107*, 6646

[64] Goldstein, M.; Poole, C.; Safko, I. *Classical Mechanics*, Addison Wesley, **2002**

[65] Smeyers, Y. G. and Bellido, M. N. *Int. J. Quantum Chem.* **1981**, *19*, 553

[66] Moule, D. C.; Smeyers, Y. G.; Senent, M. L.; Clouthier, D. J.; Karolczak, J.; Judge, R. H. *J. Chem. Phys.*, **1991**, *95*, 3137

[67] Smeyers, Y. G.; Senent, M. L.; Botella, V; Moule, D. C. *J. Chem. Phys.*, **1993**, *98*, 2754

[68] Vivier-Bunge, A.; Uc, V. H.; Smeyers, Y. G. *J. Chem. Phys.* **1998**, *109*, 2279

[69] Sumathi, R.; Carstensen, H. H.; Green, W. H. *J. Phys. Chem. A* **2001**, *105*, 6910

[70] Sumathi, R.; Carstensen, H. H.; Green, W. H. *J. Phys. Chem. A* **2001**, *105*, 8969

[71] Eidinoff, M. L. and Aston, J. G. *J. Chem. Phys.* **1946**, *3*, 379

[72] Prudente, F. V.; Riganelli, A.; Varandas, A. J. C. *J. Phys. Chem. A* **2001**, *105*, 5272

[73] Mencarelli, P. *J. Chem. Ed.* **1995**, *72*, 511

[74] Tsuzuki, S.; Uchimaru, T.; Tanabe, K. *Chem.Phys.Lett.* **1995**, *246*, 9

[75] Salam, A. and Deleuze, M. S. *J. Chem. Phys.* **2002**, *116*, 1296

[76] Messerly, G. H. and Kennedy, R. M. *J. Am. Chem. Soc.* **1940**, *62*, 2988

[77] Messerly, J. F.; Guthrie, G. B.; Todd, S. S.; Finke, H. L. *J.Chem.Eng.Data* **1967**, *12*, 338

[78] Huffman, H. M.; Gross, M. E.; Scott, D. W.; McCullough, J. P. *J.Phys.Chem.* **1961**, *65*, 495

[79] Scott, D. W.; McCullough, J. P.; Williamson, K. D.; Waddington, G. *J. Am. Chem. Soc.* **1951**, *73*, 1707

[80] Waddington, G.; Smith, J. C.; Scott, D. W.; Huffman, H. M. *J. Am. Chem. Soc.* **1949**, *71*, 3902

[81] Poling, B. E.; Prausnitz, J. M.; O'Connell, J. P. *The properties of gases and liquids*, Mc.Graw-Hill

[82] Greene, T. W.; Wuts, P. G. M. *Protective Groups in Organic Synthesis*, Wiley, New York, **1999**

[83] Kallend, A. S. *Trans. Faraday Soc.* **1967**, *63*, 2442

[84] Halstead, C. J. and Jenkins, D. R. *Trans. Faraday Soc.* **1969**, *65*, 3013

[85] Durie, R. A.; Johnson, G. M.; Smith, M. Y. *Combust. Flame* **1971**, *17*, 197

[86] Wayne, R. P. *Chemistry of Atmospheres*, Oxford Science Publications, Clarendon Press, Oxford, **1985**

[87] Wine, P. H.; Kreutter, N. M.; Gump, C. A.; Ravishankara, A. R. *J. Phys. Chem.* **1981**, *85*, 2660

[88] Friedl, R. R.; Brune, W. H.; Anderson, J. G. *J. Phys. Chem.* **1985**, *89*, 5505

[89] Wang, N. S.; Howard, C. J. *J. Phys. Chem.* **1990**, *94*, 8787

[90] (a) Franzen, S. *Chem. Phys. Lett.* **2003**, *381*, 315
(b) Barrena, E.; Palacios-Lidon, E.; Munuera, C.; Torrelles, X.; Ferrer, S.; Jonas, U.; Salmeron, M.; Ocal, C. *J. Am. Chem. Soc.* **2004**, *126*, 385

[91] Zhu, Z; Srivastava, A.; Osgood, R. M. Jr. *J. Phys. Chem. B* **2003**, *107*, 13939

[92] Perdew, J. P. and Yang, Y. *Phys. Rev. B* **1992**, *45*, 13244

[93] (a) Bauschlicher, C. W. Jr.; Partridge, H. *Chem. Phys. Lett.* **1995**, *240*, 533
(b) Ventura, O. N.; Kieninger, M. *Chem. Phys. Lett.* **1995**, *245*, 488
(c) Ignatyev, I. S.; Xie, Y.; Allen, W. D.; Schaefer, H. F. III *J. Chem. Phys.* **1997**, *107*, 141

[94] Denis, P. A.; Ventura, O. N. *Int. J. Quantum Chem.* **2000**, *80*, 439

[95] (a) Ventura, O. N.; Cachau, R. E.; Kieninger, M. *Chem. Phys. Lett.* **1999**, *301*, 331
(b) Denis, P. A.; Ventura, O. N. *Chem. Phys. Lett.* **2001**, *344*, 221

[96] (a) Scott, A. P.; Radom, L. *J. Phys. Chem.* **1996**, *100*, 16502
(b) Lynch, B. J.; Truhlar, D. G. *J. Phys. Chem. A* **2001**, *105*, 2936

[97] Wang, L.; Zhang, J. *Chem. Phys. Lett.* **2002**, *356*, 490

[98] Tozer, D. J. *Chem. Phys. Lett.* **1999**, *308*, 160

[99] Kakar, R. K.; Quade, C. R. *J. Chem. Phys.* **1980**, *72*, 4300

[100] Durig, J. R.; Bucy, W. E.; Wurrey, C. J.; Carreira, L. A. *J. Phys. Chem.* **1975**, *79*, 988

[101] Fang, H. L.; Swofford, R. L. *Chem. Phys. Lett.* **1984**, *105*, 5

[102] Senent, M. L.; Smeyers, Y. G.; Dominguez-Gomez, R.; Villa, M. *J. Chem. Phys.* **2000**, *112* 5809

[103] Weibel, J. D.; Jackels, C. F. ; Swofford, R. L. *J. Chem. Phys.* **2002**, *117*, 4245

[104] Takahashi, K.; Sugawara, M.; Yabushita S. *J. Phys. Chem. A* **2003**, *107*, 11092

[105] (a) Tsuzuki, S; Uchimaru, T.; Tanabe, K. *J. Mol. Struct. (THEOCHEM)* **1996**, *366*, 89
(b) Oyanagi, K. and Kuchitsu, K. *Bull. Chem. Soc. Jpn.* **1978**, *51*, 2237

[106] (a) Kitagawa, T.; Miyazawa, T. *Bull. Chem. Soc. Jpn.* **1968**, *41*, 1976
(b) Durig, J. R.; Compton, D. A. C. *J. Chem. Phys.* **1978**, *69*, 4713
(c) Chen, C.; Bozzelli, J. W. *J. Phys. Chem. A* **2003**, *107*, 4531

[107] (a) Sakakibara, M.; Matsuura, H.; Harada, I.; Shimanouchi, T. *Bull. Chem. Soc. Jpn.* **1977**, *50*, 111
(b) Durig, J. R.; Rollins, M. S.; Phan, H. V. *J. Mol. Struct.* **1991**, *263*, 95
(c) Hayashi, M.; Adachi, M.; Nakagawa, J. *J. Mol. Spectrosc.* **1981**, *86*, 129
(d) Adachi, M.; Nagagawa, J.; Hayashi, M. *J. Mol. Spectrosc.* **1982**, *91*, 381

[108] Kanesaka, I.; Snyder, R. G.; Strauss, H. L. *J. Chem. Phys.* **1986**, *84*, 395

[109] (a) Plusquellic, D. F.; Suenram, R. D.; Mate, B.; Jensen, J. O.; Samuels, A. C. *J. Chem. Phys.* **2001**, *115*, 3057
(b) Kuze, N.; Kuroki, N.; Takeuchi, H.; Egawa, T.; Konaka, S. *J. Mol. Struct.* **1993**, *301*, 81
(c) Hayashi, M.; Adachi, M. *J. Mol. Struct.* **1982**, *78*, 53

[110] DeTar, D. F. *J. Phys. Chem. A* **1999**, *103*, 7055

[111] DeTar, D. F. *J. Phys. Chem. A* **2001**, *105*, 2073

[112] Aubanel, E. E.; Robertson, S. H.; Wardlaw, D. M. *J. Chem. Soc.* **1991**, *87*, 2291

[113] Robertson, S. H.; Wagner, A. F.; Wardlaw, D. M. *J. Chem. Phys.* **1995**, *103*, 2917

[114] Robertson, S. H.; Wagner, A. F.; Wardlaw, D. M. *Faraday Discuss. Chem. Soc.* **1995**, *102*, 65

[115] Robertson, S. H.; Wagner, A. F.; Wardlaw, D. M. *J. Chem. Phys.* **2000**, *113*, 2648

[116] Robertson, S. H.; Wagner, A. F.; Wardlaw, D. M. *J. Phys. Chem. A* **2002**, *106*, 2598

[117] Robertson, S. H.; Wagner, A. F.; Wardlaw, D. M. *J. Chem. Phys.* **2002**, *117*, 593

[118] Senent, M. L. and Smeyers, Y. G. *J. Chem. Phys.* **1996**, *105*, 2789

[119] Senent, M. L.; Moule, D. C.; Smeyers, Y. G. *Can. J. Phys.* **1995**, *73*, 425

[120] Senent, M. L.; Moule, D. C.; Smeyers, Y. G. *J. Chem. Phys.* **1995**, *102*, 5952

[121] Senent, M. L.; Moule, D. C.; Smeyers, Y. G. *J. Phys. Chem.* **1995**, *99*, 7970

[122] Senent, M. L.; Smeyers, Y. G.; Moule, D. C. *J. Phys. Chem. A* **1998**, *102*, 6730

[123] Senent, M. L.; Dominguez-Gómez, R. *Chem. Phys. Lett.* **2002**, *351*, 251

[124] (a) Kjaergaard, H. G.; Henry, B. R.; Tarr, A. W. *J. Chem. Phys.* **1991**, *94*, 5844
(b) Wang, L. and Zhang, J. *J. Mol. Struct. (THEOCHEM)* **2001**, *543*, 167
(c) Salai Cheettu Ammal, S.; Ananthavel, S. P.; Chandrasekhar, J.; Venuvanalingam, P. *Chem. Phys. Lett.* **1996**, *248*, 153
(d) Jursic, B. S. *Chem. Phys. Lett.* **1998**, *295*, 447
(e) Hermida-Ramón, J. M.; Ríos, M. A. *Theor. Chem. Acc.* **2000**, *105*, 1
(f) Atadinç, F.; Selçuki, C.; Sari, L.; Aviyente, V. *Phys. Chem. Chem. Phys.* **2002**, *4*, 1797
(g) Andersen, A.; Carter, E. A. *J. Phys. Chem. A* **2003**, *107*, 9463
(h) Van den Kerkhof, T.; Bouwen, A.; Goovaerts, E.; Herrebout, W. A.; van der Veken, B. J. *Phys. Chem. Chem. Phys.* **2004**, *6*, 358

[125] Block, D. A.; Armstrong, D. A.; Rauk, A *J. Phys. Chem. A* **1999**, *103*, 3562

[126] Chao, J. *J. Phys. Chem. Ref. Data* **1986**, *15*, 1369

[127] (a) Bellus, D. and Ernst, B. *Angew. Chem. Int. Ed.* **1998**, *27*, 797
(b) de Meijere, A. *Houben-Weyl Methods in Organic Chemistry Vol. E17e and E17f (4th Ed.): Carbocyclic Three- and Four-Membered Ring Compounds*, Georg Thieme Verlag, Stuttgart, New York, **1997**

[128] (a) Dunitz, J. D. and Schomaker, V. *J. Chem. Phys.* **1952**, *20*, 1703
(b) Meiboom, S. and Snyder, L. C. *J. Chem. Phys.* **1970**, *52*, 3857
(c) Cremer, D. *J. Am. Chem. Soc.* **1976**, *99*, 1307

[129] Egawa, T.; Fukuyama, T.; Yamamoto, S.; Takabayashi, F.; Kambara, H.; Ueda, T.; Kuchitsu, K. *J. Chem. Phys.* **1987**, *86*, 6018

[130] (a) Rathjens, G. W. Jr.; Gwinn, W. D. *J. Am. Chem. Soc.* **1953**, *75*, 5629
(b) Rathjens, G. W. Jr.; Freeman, N. K.; Gwinn, W. D.; Pitzer, K. S. *J. Am. Chem. Soc.* **1953**, *75*, 5634

[131] (a) Danti, A.; Lafferty, W. J.; Lord, R. C. *J. Chem. Phys.* **1960**, *33*, 294
(b) Chan., S. I.; Zinn, J.; Gwinn, W. D. *J. Chem. Phys.* **1960**, *33*, 295
(c) Chan., S. I.; Zinn, J.; Fernandez, J.; Gwinn, W. D. *J. Chem. Phys.* **1960**, *33*, 1643
(d) Chan., S. I.; Zinn, J.; Gwinn, W. D. *J. Chem. Phys.* **1961**, *34*, 1319
(e) Chan., S. I.; Borgers, T. R.; Russel, J. W.; Strauss H. L.; Gwinn, W. D. *J. Chem. Phys.* **1966**, *44*, 1103
(f) Ueda, T. and Shimanouchi, T. *J. Chem. Phys.* **1967**, *47*, 5018
(g) Jokisaari, J. and Kauppinen, J. *J. Chem. Phys.* **1973**, *59*, 2260

[132] (a) Harris, D. O.; Harrington, H. W.; Luntz, A. C.; Gwinn, W. D. *J. Chem. Phys.* **1966**, *44*, 3467
(b) Karakida, K. and Kuchitsu, K. *Bull. Chem. Soc. Jpn.* **1975**, *48*, 1691

[133] (a) Durig, J. R. and Lord, R. C. *J. Chem. Phys.* **1966**, *45*, 61
(b) Borgers, T. R. and Strauss H. L. *J. Chem. Phys.* **1966**, *45*, 947

[134] (a) Carriera, L. A. and Lord, R. C. *J. Chem. Phys.* **1969**, *51*, 2735
(b) Bocian, D. F.; Schick, G. A.; Birge, R. R. *J. Chem. Phys.* **1981**, *75*, 2626
(c) Günther, H.; Schrem, G.; Oberhammer, H. *J. Mol. Spectrosc.* **1984**, *104*, 152

[135] Scharpen, L. H. and Laurie, V. W. *J. Chem. Phys.* **1968**, *49*, 221

[136] (a) Wright, J. S. and Salem, L. *J. Am. Chem. Soc.* **1971**, *94*, 322
(b) Barfield, M. *J. Am. Chem. Soc.* **1993**, *115*, 6916
(c) Sorescu, D. C.; Thompson, D. L.; Raff, L. M. *J. Chem. Phys.* **1994**, *101*, 3729
(d) Fisher, G.; Purchase, R. L.; Smith, D. M. *J. Mol. Struct.* **1997**, *405*, 159
(e) Henseler, D. and Hohlneicher, G. *J. Phys. Chem. A* **1998**, *102*, 10828

[137] Glendening E. D. and Halpern, A. M. *J. Phys. Chem. A* **2005**, *109*, 635

[138] Sellers, H.; Almlöf, J.; Saebø, S. *J. Phys. Chem.* **1987**, *91*, 4216

[139] (a) Dutler, R.; Rauk, A.; Shaw, R. A. *J. Phys. Chem.* **1990**, *94*, 118
(b) López, J. C.; Blanco, S.; Lesarri, A.; Alonso, J. L. *J. Chem. Phys.* **2001**, *114*, 2237

[140] Gutsev, G. L. and Adamowicz, L. *J. Phys. Chem.* **1995**, *99*, 13412

[141] Mastryukov, V. S. and Boggs, J. E. *J. Mol. Struct.*(THEOCHEM) **1995**, *338*, 235

[142] Bachrach, S. M. *J. Phys. Chem.* **1989**, *99*, 7780

[143] Palafox, M. A.; Núñez, J. L.; Gil, M. *J. Phys. Chem.* **1995**, *99*, 1124

[144] Palafox, M. A.; Iza, N.; Gil, M.; Núñez, J. L. *Int. J. Quant. Chem.* **2002**, *89*, 25

[145] (a) Laane, J. *J. Phys. Chem.* **1991**, *95*, 9246
(b) Legon, A. C. *Chem. Rev.* **1980**, *80*, 231
(c) Cremer, D. *J. Am. Chem. Soc.* **1977**, *99*, 1307

[146] Van Cauter, K.; Van Speybroeck, V.; Vansteenkiste, P.; Reyniers, M. F.; Waroquier, M. *Chem. Phys. Chem.* **2006**, *7*, 131

[147] (a) Lynch, B. J.; Zhao, Y.; Truhlar, D. G. *J. Phys. Chem. A* **2003**, *107*, 1384
(b) Carbonniere, P.; Lucca, T.; Pouchan, C.; Rega, N.; Barone, V. *J. Comp. Chem.* **2004**, *26*, 384

[148] Zhao, Y.; Truhlar, D. G. *J. Phys. Chem. A* **2005**, *109*, 5656

[149] Watson, J. K. G. *Mol. Phys.* **1968**, *15*, 479

[150] (a) Carter, S.; Pinnavaia, N.; Handy, N. C. *Chem. Phys. Lett.* **1995**, *240*, 400
(b) Carter, S.; Bowman, J. M.; Harding, L. B. *Spectrochim. Acta A* **1997**, *53*, 1179
(c) Carter, S.; Culik, S. J.; Bowman, J. M. *J. Chem. Phys.* **1997**, *107*, 10458
(d) Carter, S. and Bowman, J. M. *J. Chem. Phys.* **1998**, *108*, 4397
(e) Carter, S.; Bowman, J. M.; Handy, N. C. *Theor. Chem. Acc.* **1998**, *100*, 191
(f) Carter, S. and Handy, N. C. *J. Chem. Phys.* **2000**, *113*, 987
(g) Tew, D. P.; Handy, N. C.; Carter, S. *Mol. Phys.* **2001**, *99*, 393
(h) Tew, D. P.; Handy, N. C.; Carter, S. *Phys. Chem. Chem. Phys.* **2001**, *3*, 1958
(i) Tew, D. P.; Handy, N. C.; Carter, S.; Irle, S.; Bowman, J. M. *Mol. Phys.* **2003**, *101*, 3513

[151] (a) Roitberg, A.; Gerber, R. B.; Elber, R.; Ratner, M. A. *Science* **1995**, *268*, 1319
(b) Norris, L.; Ratner, M. A.; Roitberg, A.; Gerber, R. B. *J. Chem. Phys.* **1996**, *105*, 11261
(c) Jung, J. O. and Gerber, R. B. *J. Chem. Phys.* **1996**, *105*, 10332
(d) Roitberg, A.; Gerber, R. B.; Elber, R.; Ratner, M. A. *J. Phys. Chem. B* **1997**, *101*, 1700

[152] Jellinek, J. and Li, D. H. *Phys. Rev. Lett.* **1989**, *62*, 241

[153] (a) Kohn, W.; Becke, A. D.; Parr, R. G. *J. Phys. Chem.* **1996**, *100*, 12974
(b) Coote, M. L. *J. Phys. Chem. A* **2004**, *108*, 3865

[154] Wong, B. M. and Green, W. H. *Mol. Phys.* **2005**, *103*, 1027

[155] Zhao, Y. and Truhlar, D. G. *J. Phys. Chem. A* **2004**, *108*, 6908

Appendix A

Physical constants and abbreviations

Table A.1: Physical Constants

Constant and Symbol		SI Value
Speed of light in vacuum	c	2.99792458×10^{8} m/s
Proton charge	e	1.602177×10^{-19}C
Permittivity of vacuum	ϵ_0	$8.8541878 \times 10^{-12} C^2/N - m^2$
Avogrado Constant	N_A	$6.02214 \times 10^{23} mol^{-1}$
Electron rest mass	m_e	9.10939×10^{-31} kg
Proton rest mass	m_p	1.672623×10^{-27} kg
Neutron rest mass	m_n	1.674929×10^{-27} kg
Planck constant	h	6.62608×10^{-34} J s
Faraday constant	F	96485.3 C/mol
Permeability of vacuum	μ_0	$4\pi \times 10^{-7} NC^{-2}s^2$
Bohr radius	a_0	$5.291772 \times 10^{-11} m$
Bohr magneton	β_e	9.27402×10^{-24} J/T
Nuclear magneton	β_N	5.05079×10^{-27} J/T
Electron g value	g_e	2.0023193044
Proton g value	g_p	5.585695
Gas constant	R	8.3145 J/mol.K
Boltzmann constant	k_B	1.38066×10^{-23} J/K
Gravitational constant	G	$6.673 \times 10^{-11} m^3/kg.s^2$

Table A.2: Energy Conversion Factors

1 erg=10^{-7} J
1 cal=4.184 J
1 eV=1.602177×10^{-19} J = 1.602177×10^{-12} erg = 23.0605 kcal/mol
1 hartree = 4.35975×10^{-18} J = 27.2114 eV=627.510 kcal/mol

Table A.3: Atomic Units and their SI equivalents

Quantity	Atomic Units	SI Value
Mass	m=1 (electron mass)	9.1091×10^{-31} kg
Charge	$\|e\|$=1 (electron charge)	1.6021×10^{-19} C
Angular momentum	$\hbar$=1	1.0545×10^{-34} J.s
Permittivity	$\kappa_0 = 4\pi\epsilon_0 = 1$	$1.1126 \times 10^{-10} C^2.J^{-1}.m^{-1}$
Length	$\kappa_0\hbar^2/me^2 = a_0 = 1$ (bohr) (Bohr radius)	5.29177×10^{-11} m
Energy	$me^4/\kappa_0^2\hbar^2 = e^2/\kappa_0 a_0 = 1$ (1 hartree = twice the ionization energy of atomic hydrogen)	4.35944×10^{-18} J
Time	$\kappa_0^2\hbar^3/me^4 = 1$ period of an electron in the first Bohr orbit)	$2.41889 \times 10^{-17} s$
Speed	$e^2/\kappa_0\hbar = 1$ (speed of an electron in the firs Bohr orbit)	$2.18764 \times 10^6 m.s^{-1}$
Electric Potential	$me^3/\kappa_0^2\hbar^2 = e/\kappa_0 a_0 = 1$ (potential energy of an electron in the first Bohr orbit)	27.211 V
Magnetic dipole moment	$e\hbar/m = 1$ (twice a Bohr magneton)	$1.85464 \times 10^{-23} J.T^{-1}$

Table A.4: Abbreviations and symbols

HO	Harmonic Oscillator
HR	Hindered Rotor
EHR	Extended Hindered Rotor
PES	Potential Energy Surface
HF	Hartree-Fock
DFT	Density Functional Theory
Q	partition function
$\kappa_{(E)HR}$	scaling factor: $\frac{Q_{tot}^{(E)HR}}{Q_{tot}^{HO}}$
S	entropy
C	heat capacity
$k(T)$	reaction rate
V	potential energy
T	kinetic energy
A	kinetic energy matrix
I^{red}	reduced moment of inertia
f_A	geometry correlation function, geometry factor
f_{vib}	vibrational correction factor
t	trans conformer
g	gauche conformer
x	distorted gauche conformer

Appendix B

List of Publications

Updated March 2006

Publications in International Peer-Reviewed Journals

1. Vansteenkiste, P.; Van Speybroeck, V.; Marin, G. B. and Waroquier, M.
Ab Initio Calculation of Entropy and Heat Capacity of Gas-Phase n-Alkanes Using Internal Rotations
J. Phys. Chem. A **2003**, *107*, 3139

2. Van Speybroeck, V.; Vansteenkiste, P.; Van Neck, D.; Waroquier, M.
Why does the uncoupled hindered rotor model work well for the thermodynamics of n-alkanes?
Chem. Phys. Lett. **2005**, *402*, 479

3. Vansteenkiste, P.; Van Speybroeck, V.; Pauwels, E.; Waroquier, M.
How should we calculate multi-dimensional potential energy surfaces for an accurate reproduction of partition functions?
Chem. Phys. **2005**, *314*, 109

4. Vansteenkiste, P.; Pauwels, E.; Van Speybroeck, V.; Waroquier, M.
Rules for Generating Conformers and Their Relative Energies in n-Alkanes with a Heteroelement O or S: Ethers and Alcohols, or Sulfides and Thiols
J. Phys. Chem. A **2005**, *109*, 9617

5. Van Cauter, K.; Van Speybroeck, V.; Vansteenkiste, P.; Reyniers, M. F.; Waroquier, M.
Ab Initio Study of Free-Radical Polymerization: Polyethylene Propagation Kinetics
Chem. Phys. Chem. **2006**, *7*, 131

6. Vansteenkiste, P.; Van Neck, D.; Van Speybroeck, V.; Waroquier, M.
An extended hindered-rotor model with incorporation of Coriolis and vibrational-rotational coupling for calculating partition functions and derived quantities
J. Chem. Phys. **2006**, *124*, Art. No. 044314

7. Vansteenkiste, P.; Van Speybroeck, V.; Verniest, G.; De Kimpe, N.; Waroquier, M.
Applicability of the Hindered Rotor Scheme to the Puckering Mode in Four-Membered Rings
J. Phys. Chem. A **2006**, *110*, 3838

Poster Presentations

Research results were presented as poster presentations on several international conferences.